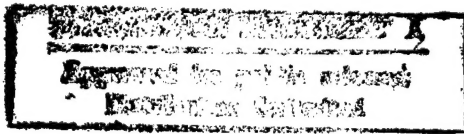



REPORT DOCUMENTATION PAGE			Form Approved OMB No. 0704-0188	
Public reporting burden for this collection of information is estimated to average 1 hour per response, including the time for reviewing instructions, searching existing data sources, gathering and maintaining the data needed, and completing and reviewing the collection of information. Send comments regarding this burden estimate or any other aspect of this collection of information, including suggestions for reducing this burden, to Washington Headquarters Services, Directorate for Information Operations and Reports, 1215 Jefferson Davis Highway, Suite 1204, Arlington, VA 22202-4302, and to the Office of Management and Budget, Paperwork Reduction Project (0704-0188), Washington, DC 20503.				
1. AGENCY USE ONLY (Leave blank)		2. REPORT DATE 11 September 1998		3. REPORT TYPE AND DATES COVERED
4. TITLE AND SUBTITLE THE USE OF SATELLITE MICROWAVE RAINFALL MEASUREMENTS TO PREDICT EASTERN NORTH PACIFIC TROPICAL CYCLONE INTENSITY			5. FUNDING NUMBERS	
6. AUTHOR(S) DEREK A. WEST				
7. PERFORMING ORGANIZATION NAME(S) AND ADDRESS(ES) OHIO STATE UNIVERSITY			8. PERFORMING ORGANIZATION REPORT NUMBER 98-029D	
9. SPONSORING/MONITORING AGENCY NAME(S) AND ADDRESS(ES) THE DEPARTMENT OF THE AIR FORCE AFIT/CIA, BLDG 125 2950 P STREET WPAFB OH 45433			10. SPONSORING/MONITORING AGENCY REPORT NUMBER	
11. SUPPLEMENTARY NOTES				
12a. DISTRIBUTION AVAILABILITY STATEMENT Unlimited distribution In Accordance With 35-205/AFIT Sup 1			12b. DISTRIBUTION CODE	
13. ABSTRACT (Maximum 200 words)				
 				
14. SUBJECT TERMS			15. NUMBER OF PAGES 182	
			16. PRICE CODE	
17. SECURITY CLASSIFICATION OF REPORT	18. SECURITY CLASSIFICATION OF THIS PAGE	19. SECURITY CLASSIFICATION OF ABSTRACT	20. LIMITATION OF ABSTRACT	

19980915 026

THE USE OF SATELLITE MICROWAVE RAINFALL MEASUREMENTS TO
PREDICT EASTERN NORTH PACIFIC TROPICAL CYCLONE INTENSITY

DISSERTATION

Presented in Partial Fulfillment of the Requirements for

the Degree Doctor of Philosophy in the Graduate

School of The Ohio State University

By

Derek A. West, M.S.

* * * * *

The Ohio State University

1998

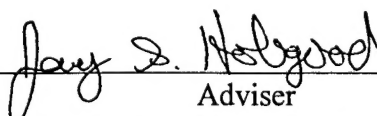
Dissertation Committee:

Dr. Jay Hobgood, Adviser

Dr. John Rayner

Dr. Carolyn Merry

Approved by



Adviser
Atmospheric Sciences Graduate Program

ABSTRACT

This dissertation examined the potential use of satellite passive-microwave rainfall measurements derived from Special Sensor Microwave/Imager (SSM/I) radiometers onboard the Defense Meteorological Satellite Program (DMSP) constellation of polar-orbiting satellites to improve eastern North Pacific Ocean tropical cyclone intensity specifying and forecasting techniques. Relationships between parameters obtained from an operational SSM/I-based rainfall-measuring algorithm and current intensity and ensuing 12-, 24-, 36-, 48-, 60-, and 72-hour intensity changes from best-track data records were examined in an effort to identify statistically significant rainfall-related specifiers of current intensity and predictors of future intensity changes.

Correlations between rainfall parameters and current intensity and future intensity changes were analyzed using tropical cyclone data from seven years, 1991 to 1997. Stratifications based upon current intensity, prior 12-hour rate of intensity change, climate, translation speed, landfall, and synoptic-scale environmental-forcing variables were studied to understand factors that may affect a statistical relationship between rainfall parameters and current intensity and future intensity changes. The predictive skill of statistically significant rainfall parameters was assessed by using independent tropical cyclone data from 1994 and 1995. In addition, case studies on individual tropical

cyclones were conducted to gain insight on predictive performance and operational implementation issues.

Impacts of these statistically significant rainfall parameters on a multiple-linear-regression-based eastern North Pacific tropical cyclone intensity-change forecasting method under development at The Ohio State University were studied. The overall goal was to determine if SSM/I-rainfall parameters could add predictive skill to an objective tropical cyclone intensity-change forecast guidance product. The guidance product's skill in predicting intensity change was assessed by statistically comparing its predicted 12-, 24-, 36-, 48-, 60-, and 72-hour intensity-change forecast errors with those from a homogeneous sample of official National Hurricane Center (NHC) forecast advisories, currently operational statistical intensity-change forecast guidance, and forecast guidance products developed by previous research at The Ohio State University.

Low (i.e., $r \sim 0.3-0.4$), but significant, correlations between rainfall parameters and future intensity changes were found. By combining these significantly correlated rainfall parameters with climatic and persistence variables, weekly sea surface temperatures (SST), and global-NWP-model data, multiple-linear-regression models to predict future intensity changes were developed. The resulting rain-related forecast models explained about 60 percent of the variance of intensity change at all 12-hour forecast intervals between 12 and 72 hours into the future. A homogeneous comparison of up to 46 cases at the 12- and 24-hour forecast intervals and at least 25 cases at the 72-hour forecast interval found that a combination of persistence, climatic, weekly SST, and rainfall data outperformed: official NHC forecast advisories; statistical hurricane intensity

forecasting (SHIFOR) operational guidance; the climatic and persistence method of Hobgood; and, Petty's method using climatic, persistence, weekly SST, and global-NWP-model data. Mean absolute forecast errors for the best rain-related forecast model were 2.8 and 5.0 m s⁻¹ for the 12- and 24-hour forecast intervals, respectively. The corresponding mean relative absolute forecast errors were 3 and 14 percent less than official NHC forecast advisories. This research demonstrated that satellite passive-microwave rainfall information could improve eastern North Pacific tropical cyclone intensity-change forecast guidance products for the 12- and 24-hour forecast intervals.

Additional results were also found. The percentage of coverage of the tropical cyclone's inner-core region by convective rainfall was moderately (i.e., $r \sim 0.6$) correlated with current tropical cyclone intensity. The accuracy of center fixes by SSM/I was found to be much better than center-fix accuracies reported in previous studies that used data from other satellite systems. SSM/I observations of rainfall were able to monitor the convective ring cycle of strong hurricanes. A diurnal variation of convective rainfall decreased with increasing tropical cyclone intensity.

Dedicated to Mom, Dad, Grandma, Andy, and Phil

ACKNOWLEDGMENTS

I wish to thank my adviser, Dr. Jay Hobgood, for intellectual support, encouragement, and enthusiasm which made this dissertation possible and for his patience in correcting both my stylistic and scientific errors. Members of my Advisory and Dissertation Committees (i.e., Dr. John Rayner, Dr. Carolyn Merry, and Dr. Jeffery Rogers) provided constructive criticism of my research efforts. Many thanks go out to my fellow graduate students and friends. Dr. Kevin Petty, Mr. Kenneth Yetzer, Mr. Chung-Chieh Wang, Mr. Maurice McHugh, Mr. Kevin Weakley, and others gave many hours of help, support, and insightful discussions. Department of Geography computer support technicians Mr. James DeGrand, Mr. Sang-Ki Hong, and Mr. Jens Bledvad aided my research efforts. Special thanks go to those that helped me obtain PV~WAVE® software to conduct data display and analysis (i.e., Dr. Larry Brown and Mr. Geoff Hulse). Mr. John Snowden of the Center for Mapping helped me with understanding the use of 8-mm tape drives. Mr. Richard Cullather of the Byrd Polar Research Center provided some ECMWF data in an easy-to-use format. Also, I would like to thank the entire staff of the interlibrary loan office at The Ohio State University for helping me to obtain relevant references.

The United States Air Force gave me the opportunity to conduct this research via an assignment to the Air Force Institute of Technology's Civilian Institutions (AFIT/CI) Program. Major Tom Neu, Captain James Ulman, and Mrs. Mary Ellen Ogle provided great program-manager support considering my often and unique requests for assistance. An American Meteorological Society travel scholarship that helped defray the costs of presenting my research at a symposium on tropical cyclone intensity change is appreciated. My research efforts were aided tremendously by the professional staff of the Air Force Weather Technical Library (AFWTL). The AFWTL staff (i.e., Mr. Charles Travers, Mr. David Pigors, SSgt Tosha French, and Mr. Gary Swanson) provided me with hard-to-obtain reference materials crucial to this research. Mr. Tom Ross, Ms. Debbie Wolfe, and Mr. Stu Gibeau of the Air Force Combat Climatology Center (AFCCC, OL-A) collocated at the National Climatic Data Center (NCDC) in Asheville, North Carolina, provided me with important data in an easy-to-use format and a timely manner.

Naval Research Laboratory personnel in Monterey, California (NRL-MRY), provided a great deal of the data and a powerful software program (TROPX) used during this research. Mr. Jeffery Hawkins, Dr. Joseph Turk, Mr. Kim Richardson, Mr. Charles "Buck" Sampson, Mr. Thomas Lee, Mr. Roland Nagle, and Mr. Vince Hickey all went out of their way to assist and guide me. Ms. Marla "MJ" Helveston modified TROPX to produce the rain-rate data and generated several figures for this "Fly-boy's" dissertation. Mr. Don Boucher and Ms. Arlene Kishi of Hughes Aerospace Corporation; Dr. Mark DeMaria, Mr. Colin McAdie, and Dr. Steve Lyons of NHC/TPC; Dr. Frank Marks, Dr.

Hugh Willoughby, Mr. James Franklin, and Mr. Sam Houston of HRD/NOAA; Major Roger Edson and Mr. Frank Wells of JTWC; Lieutenant Colonel Joel Martin and Mr. Paul McCrone of AFWA; Dr. Russell Elsberry of the Naval Postgraduate School; Dr. Grant Petty of Purdue University; Mr. Daniel Cecil of Texas A&M University; Dr. Marie Colton of ONR; and, Mr. Ralph Ferraro and Ms. Nancy Everson of NESDIS/NOAA all provided excellent advice, discussion, and assistance. Marshall Space Flight Center (MSFC/DAAC) in Huntsville, Alabama, provided me with some SSM/I data. Colonel Judd Staley and Mr. Robert Dumont (OFCM); Dr. K. Abe (WMO); Dr. William Gray and Mrs. Barbara Brumit (CSU); Mr. Gerald Felde (AFRL); Dr. Marja Bister (MIT); and, Mr. Gene Poe and Mr. Glenn Sandlin (NRL-DC) provided me very useful reference materials.

Mr. John Pavone (CARCAH) and Lieutenant Colonel Doug Niolet (AFRC) made it possible for me to fly onboard a 53rd WRS "Hurricane Hunters" WC-130H aircraft into the historic eastern North Pacific Hurricane Linda (1997). While onboard, the aircrew (especially, Captain Dan Darbe, aerial reconnaissance weather officer) treated me just like another part of the team. This flight was a memorable and insightful portion of my dissertation research. The flight and the data obtained from it are greatly appreciated. John, thanks for "paying for my books"! Jeff, thanks for putting the wheels in motion.

Lastly, Ms. Jennifer Diederich was a constant source of emotional support, friendship, humor, faith, and encouragement during my doctoral studies and the conduct of this research. Lord, thank you for the intellectual ability and academic endurance required during this journey. Deeds, not words.

VITA

January 3, 1969 Born - Macon, Georgia

1991 B.S., Psychology, United States Air Force
Academy, Colorado

1993 M.S., Atmospheric Sciences, The Ohio State University

1993-1995 Officer-in-Charge, Special Operations Weather Team,
16th Special Operations Wing, Hurlburt Field, Florida

1995-present Captain, Air Force Institute of Technology with duty at
The Ohio State University

FIELDS OF STUDY

Major Field: Atmospheric Sciences

TABLE OF CONTENTS

	<u>Page</u>
Dedication.....	v
Acknowledgments.....	vi
Vita.....	ix
List of Tables.....	xiii
List of Figures.....	xv
List of Acronyms.....	xxi
 Chapters:	
1. Introduction.....	1
1.1 Defining the Problem.....	1
1.2 Impacts of the Problem.....	4
1.3 Application of Satellite Remote Sensing to the Problem.....	5
1.4 Goals of this Research.....	7
1.5 Summary.....	11
2. Relevant Literature Review.....	12
2.1 Current State of Tropical Cyclone Intensity Forecasting in the Eastern North Pacific.....	12
2.2 Role of Latent Heat Release in Intensity Change.....	13
2.3 Satellite Passive-microwave Measurements of Rainfall.....	14
2.4 Rainfall Algorithm Used in this Research.....	21
2.5 Satellite Passive-microwave Measurements Related to Tropical Cyclone Intensity.....	24
2.6 Factors Related to Current Intensity and Future Intensity Change.....	33

	<u>Page</u>
2.7 Statistical Prediction of Eastern North Pacific Tropical Cyclone Intensity Change.....	35
3. Data and Methodology.....	38
3.1 NHC Postanalysis Best-track and Operational, Weekly SST, and ECMWF Model Data.....	38
3.2 DMSP Constellation of Satellites.....	42
3.3 SSM/I Instrument Specifications.....	43
3.4 SSM/I-related Data.....	45
3.5 Querying Data Library for SSM/I Orbits with Coverage of Tropical Cyclones.....	47
3.6 Processing SSM/I Orbits with Coincidental Coverage of Tropical Cyclones.....	48
3.7 Locating the Tropical Cyclone Center.....	49
3.8 Determining if SSM/I Coverage is Adequate.....	49
3.9 Applying the Operational Rainfall Algorithm.....	50
3.10 Examining Rainfall and Intensity and Intensity-change Correlations.....	50
3.11 Developing Rainfall Parameter and Intensity-change Prediction Model.....	52
3.12 Combining Rainfall Parameters with Hobgood and Petty Prediction Models.....	59
3.13 Evaluating Intensity-change Prediction Models.....	60
3.14 Conducting Case Studies.....	61
3.15 Surveying Rainfall Characteristics of Eastern North Pacific Tropical Cyclones.....	62
3.16 Analyzing Tropical Cyclone Center-position Differences Using the SSM/I.....	62
4. Results and Discussion.....	64
4.1 Statistics Concerning Independent and Dependent Variables.....	64
4.2 Accomplishment of Primary Goal 1: Rainfall and Intensity Correlations.....	70
4.3 Accomplishment of Primary Goal 2: Stratified Rainfall and Intensity Correlations.....	72
4.4 Accomplishment of Primary Goal 3: Forecast Model Development.....	77
4.5 Accomplishment of Primary Goal 4: Forecast Error Comparisons.....	81
4.6 Accomplishment of Primary Goal 5: Case Studies.....	85
4.7 Accomplishment of Secondary Goal 1: Convective Ring Cycle Analysis.....	91

	<u>Page</u>
4.8 Accomplishment of Secondary Goal 2: Coverage by Convective Rainfall.....	91
4.9 Accomplishment of Secondary Goal 3: SSM/I Center-fix Study.....	92
4.10 Accomplishment of Secondary Goal 4: Diurnal Cycle of Convection.....	93
4.11 Accomplishment of Secondary Goal 5: Comparison of Regression Coefficients.....	94
4.12 Accomplishment of Secondary Goal 6: Contribute to NRL Research Efforts.....	96
4.13 Accomplishment of Secondary Goal 7: Present Research in Scholarly Formats.....	96
5. Conclusions and Recommendations for Future Research.....	97
5.1 Satellite-measured Convective Rainfall is Related to Tropical Cyclone Intensity.....	97
5.2 Relationships Between Rainfall and Intensity Are Affected by Other Factors.....	97
5.3 Rainfall Parameters Can Improve Statistical Intensity Forecast Guidance.....	98
5.4 SSM/I-derived Information has Utility for Observing Tropical Cyclones.....	100
5.5 Recommendations for Future Research.....	101
List of References.....	104
Figures.....	116
APPENDIX:	
Example SPSS® Output.....	175

LIST OF TABLES

<u>Table</u>	<u>Page</u>
1 Mean Absolute Official NHC Intensity Forecast Errors (^a OFCM 1997; ^b Gross and Lawrence 1996).....	12
2 Summary of Eastern North Pacific Tropical Cyclone Intensity-change Forecasting Techniques Under Development at The Ohio State University. * indicates the five forecast variables also used by Petty (1997b).....	37
3 Climatic and Persistence Predictors (Hobgood 1998a).....	41
4 Weekly SST and Global NWP Predictors (Petty 1997b; Petty and Hobgood 1998).....	41
5 Actual Intensity-change Variables from Best-Track Data.....	42
6 DMSP Orbital Characteristics. * F-10 failed on 14 November 1997.....	43
7 SSM/I-channel Resolution Information. IFOV means instantaneous field of view (FOV) and EFOV means effective FOV.....	44
8 Candidate Rainfall Parameters.....	51
9 Summary of SSM/I orbits and tropical cyclone datasets used in this research. * Obtained from seasonal summaries: Rappaport and Mayfield (1992), Lawrence and Rappaport (1994), Avila and Mayfield (1995), Pasch and Mayfield (1996), Avila and Rappaport (1996), Rappaport and Mayfield (1997), and Lawrence (1998).....	55
10 Guidelines for Interpreting Correlation Coefficients (Hinkle <i>et al.</i> 1988).....	57
11 Descriptive Statistics for Significant Climatic and Persistence Predictors for Model Training Dataset.....	65
12 Descriptive Statistics for Significant Weekly SST and Global-NWP Predictors for Model Training Dataset.....	65

<u>Table</u>	<u>Page</u>
13 Descriptive Statistics for Significant Convective Rainfall Predictors for Model Training Dataset.....	66
14 Descriptive Statistics for Actual Intensity-change Variables for Model Training Dataset.....	66
15 Descriptive Statistics for Significant Climatic and Persistence Predictors for Model Testing Dataset.....	67
16 Descriptive Statistics for Significant Weekly SST and Global-NWP Predictors for Model Testing Dataset.....	67
17 Descriptive Statistics for Significant Convective Rainfall Predictors for Model Testing Dataset.....	68
18 Descriptive Statistics for Actual Intensity-change Variables for Model Testing Dataset.....	68
19 Statistically Significant Rainfall and Intensity Variable Correlations. * Correlation coefficients are all significant at the 0.95 level.....	71
20 Stratified Correlation Coefficients Between Intensity and Rainfall Parameters. Only those coefficients significant at the 0.95 level are bolded.....	73
21 Standardized Regression Coefficients for the Forecast Model Including Rainfall Predictors. Only those coefficients significant at the 0.95 level are displayed.....	79
22 Standardized Regression Coefficients for the Forecast Model Including Rainfall, Climatic, Persistence, and Weekly SST Predictors. Only those coefficients significant at the 0.95 level are displayed.....	79
23 Standardized Regression Coefficients for the Forecast Model Including Rainfall, Climatic, Persistence, Weekly SST, and Global-NWP Predictors. Only those coefficients significant at the 0.95 level are displayed.....	80
24 Homogeneous Comparisons of Forecast Model Performance on Testing Dataset.....	84

LIST OF FIGURES

<u>Figure</u>	<u>Page</u>
1 Interactions of synoptic-scale water and motion fields (Atlas and Thiele 1981).....	116
2 Interactions involving microwave radiation (Rao <i>et al.</i> 1990).....	117
3 Geometry describing microwave radiative transfer involving rainfall.....	118
4 Conical-scanning radiometer (Skou 1989).....	119
5 SSM/I scan geometry (Hollinger <i>et al.</i> 1990).....	120
6 SSM/I scan characteristics (Spencer <i>et al.</i> 1989).....	121
7 SSM/I spatial sampling illustrating along-scan changes (Hollinger 1989).....	122
8 Equatorial view of successive SSM/I orbits with swath widths (Hollinger 1989).....	123
9 Polar view of successive SSM/I orbits with swath widths (Hollinger 1989).....	124
10 Coverage by one SSM/I in 24 hours. Dark areas indicate data gaps (Hollinger 1989).....	125
11 Center-fixing tool in TROPX depicting 85.5-GHz horizontally polarized T_B image of Hurricane Linda (1997).....	126
12 35-panel TROPX display showing 85.5-GHz horizontally polarized T_B images of tropical cyclones observed by SSM/I and used in this present research (observations 1-35).....	127
13 35-panel TROPX display showing 85.5-GHz horizontally polarized T_B images of tropical cyclones observed by SSM/I and used in this present research (observations 36-70).....	128

<u>Figure</u>		<u>Page</u>
14	35-panel TROPX display showing 85.5-GHz horizontally polarized T_B images of tropical cyclones observed by SSM/I and used in this present research (observations 71-105).....	129
15	35-panel TROPX display showing 85.5-GHz horizontally polarized T_B images of tropical cyclones observed by SSM/I and used in this present research (observations 106-140).....	130
16	35-panel TROPX display showing 85.5-GHz horizontally polarized T_B images of tropical cyclones observed by SSM/I and used in this present research (observations 141-175).....	131
17	35-panel TROPX display showing 85.5-GHz horizontally polarized T_B images of tropical cyclones observed by SSM/I and used in this present research (observations 176-210).....	132
18	35-panel TROPX display showing 85.5-GHz horizontally polarized T_B images of tropical cyclones observed by SSM/I and used in this present research (observations 211-245).....	133
19	35-panel TROPX display showing 85.5-GHz horizontally polarized T_B images of tropical cyclones observed by SSM/I and used in this present research (observations 246-280).....	134
20	35-panel TROPX display showing 85.5-GHz horizontally polarized T_B images of tropical cyclones observed by SSM/I and used in this present research (observations 281-315).....	135
21	Regions used to calculate rainfall parameters. Radial distance for each region is indicated near the radii arrowheads. The 444-, 222-, 111-, and 56-km radii correspond to the total, core, inner-core, and central-core regions of the tropical cyclone, respectively.....	136
22	Plotted tracks of tropical cyclones from 1991 to 1997 studied in this research. Bold vertical line indicates western boundary of eastern North Pacific Ocean basin (140 °W).....	137
23	Plotted tracks of tropical cyclones from 1991 to 1997 used to develop regression models for this research. Bold vertical line indicates western boundary of eastern North Pacific Ocean basin (140°W).....	138

<u>Figure</u>	<u>Page</u>
24	Plotted tracks of tropical cyclones from 1994 and 1995 used to evaluate regression models for this research. Bold vertical line indicates western boundary of eastern North Pacific Ocean basin (140°W).....139
25	Homogeneous evaluation of forecast methods on testing dataset.....140
26	Plotted track of Hurricane Tina (1992). Tropical depression, tropical storm, and hurricane intensity stages are indicated by \times , \circ , and $*$, respectively.....141
27	15-panel TROPX display showing NESDIS/ORA rainfall algorithm applied to SSM/I observations of Hurricane Tina (1992) during 20-28 September. Current interpolated intensity is indicated in the upper-left of each panel. Satellite flight number is depicted in the lower-right of each panel.....142
28	15-panel TROPX display showing NESDIS/ORA rainfall algorithm applied to SSM/I observations of Hurricane Tina (1992) during 28 September-10 October. Current interpolated intensity is indicated in the upper-left of each panel. Satellite flight number is depicted in the lower-right of each panel..... 143
29	Temporal variation of current intensity and convective rainfall (PCP1) for SSM/I observations of Hurricane Tina (1992)..... 144
30	Temporal variation of current intensity and 850-mb equivalent potential temperature (θ_e) for Hurricane Tina (1992). MPI is included for comparison to current intensity. A reference line at 336 K is provided as a threshold between high and low values of 850-mb θ_e 145
31	Temporal variation of current intensity and absolute value of 200- to 850-mb vertical shear of the zonal horizontal wind ($U2_8$) for Hurricane Tina (1992). A reference line at 8.5 m s^{-1} is provided as a threshold between high and low values of vertical shear.....146
32	Homogeneous evaluation of forecast methods on Hurricane Tina (1992). Data not available for SHIFOR.....147
33	Plotted track of Hurricane Olivia (1994). Tropical depression, tropical storm, and hurricane intensity stages are indicated by \times , \circ , and $*$, respectively.....148

<u>Figure</u>	<u>Page</u>
34	15-panel TROPX display showing NESDIS/ORA rainfall algorithm applied to SSM/I observations of Hurricane Olivia (1994) during 22-29 September. Current interpolated intensity is indicated in the upper-left of each panel. Satellite flight number is depicted in the lower-right of each panel.....149
35	4-panel TROPX display showing two SSM/I observations of Hurricane Olivia (1994) on 24 and 26 September. Top panels are 85.5-GHz horizontally polarized T_b images. Bottom panels are NESDIS/ORA rainfall images.....150
36	2-panel graphic of composites obtained from radar onboard NOAA WP-3D aircraft flights into Hurricane Olivia (1994) during 24 to 26 September. Distance and reflectivity scales apply to both panels. Graphic adapted from image file located at http://www.aoml.noaa.gov/hrd/graphics/OlivLF_2days.GIF151
37	Temporal variation of current intensity and convective rainfall (PCP1) for SSM/I observations of Hurricane Olivia (1994).....152
38	Temporal variation of current intensity and 850-mb equivalent potential temperature (θ_e) for Hurricane Olivia (1994). MPI is included for comparison to current intensity. A reference line at 336 K is provided as a threshold between high and low values of 850-mb θ_e 153
39	Temporal variation of current intensity and absolute value of 200- to 850-mb vertical shear of the zonal horizontal wind (U2_8) for Hurricane Olivia (1994). A reference line at 8.5 m s ⁻¹ is provided as a threshold between high and low values of vertical shear.....154
40	Homogeneous evaluation of forecast methods on Hurricane Olivia (1994)..... 155
41	Plotted track of Tropical Storm Genevieve (1996). Tropical depression, tropical storm, and hurricane intensity stages are indicated by ×, ○, and *, respectively..... 156
42	15-panel TROPX display showing NESDIS/ORA rainfall algorithm applied to SSM/I observations of Tropical Storm Genevieve (1996) during 29 September-5 October. Current interpolated intensity is indicated in the upper-left of each panel. Satellite flight number is depicted in the lower-right of each panel.....157

<u>Figure</u>	<u>Page</u>
43	15-panel TROPX display showing NESDIS/ORA rainfall algorithm applied to SSM/I observations of Tropical Storm Genevieve (1996) during 6-9 October. Current interpolated intensity is indicated in the upper-left of each panel. Satellite flight number is depicted in the lower-right of each panel.....
158	
44	Temporal variation of current intensity and convective rainfall (PCP1) for SSM/I observations of Tropical Storm Genevieve (1996).....
159	
45	Temporal variation of current intensity and 850-mb equivalent potential temperature (θ_e) for Tropical Storm Genevieve (1996). MPI is included for comparison to current intensity. A reference line at 336 K is provided as a threshold between high and low values of 850-mb θ_e
160	
46	Temporal variation of current intensity and absolute value of 200- to 850-mb vertical shear of the zonal horizontal wind ($U2_8$) for Tropical Storm Genevieve (1996). A reference line at 8.5 m s^{-1} is provided as a threshold between high and low values of vertical shear.....
161	
47	Homogeneous evaluation of forecast methods on Tropical Storm Genevieve (1996).....
162	
48	Plotted track of Hurricane Linda (1997). Tropical depression, tropical storm, and hurricane intensity stages are indicated by \times , \circ , and $*$, respectively.....
163	
49	15-panel TROPX display showing NESDIS/ORA rainfall algorithm applied to SSM/I observations of Hurricane Linda (1997) during 9-14 September. Current interpolated intensity is indicated in the upper-left of each panel. Satellite flight number is depicted in the lower-right of each panel.....
164	
50	15-panel TROPX display showing NESDIS/ORA rainfall algorithm applied to SSM/I observations of Hurricane Linda (1997) during 14-17 September. Current interpolated intensity is indicated in the upper-left of each panel. Satellite flight number is depicted in the lower-right of each panel.....
165	
51	Temporal variation of current intensity and convective rainfall (PCP1) for SSM/I observations of Hurricane Linda (1997).....
166	
52	Temporal variation of current intensity and 850-mb equivalent potential temperature (θ_e) for Hurricane Linda (1997). MPI is included for comparison to current intensity. A reference line at 336 K is provided as a threshold between high and low values of 850-mb θ_e
167	

<u>Figure</u>	<u>Page</u>
53	Temporal variation of current intensity and absolute value of 200- to 850-mb vertical shear of the zonal horizontal wind (U2_8) for Hurricane Linda (1997). A reference line at 8.5 m s^{-1} is provided as a threshold between high and low values of vertical shear.....168
54	Homogeneous evaluation of forecast methods on Hurricane Linda (1997).....169
55	Central-core convective rainfall coverage stratified by time of day and tropical cyclone intensity.....170
56	Inner-core convective rainfall coverage stratified by time of day and tropical cyclone intensity.....171
57	Core convective rainfall coverage stratified by time of day and tropical cyclone intensity.....172
58	Total convective rainfall coverage stratified by time of day and tropical cyclone intensity.....173
59	Mean center-fix differences when comparing SSM/I center fixes with linearly interpolated best-track data tropical cyclone locations..... 174

LIST OF ACRONYMS

ACP: Average of convective pixels

AFWA: Air Force Weather Agency

AMS: American Meteorological Society

AROWA: Applied Research; Operational Weather Analyses

DMSP: Defense Meteorological Satellite Program

DoC: Department of Commerce

DoD: Department of Defense

ECMWF: European Centre for Medium-range Weather Forecasts

EDR: Environmental data record

EFOV: Effective field of view

ESMR: Electronically Scanning Microwave Radiometer

FOV: Field of view

IFOV: Instantaneous field of view

JTWC: Joint Typhoon Warning Center

LHR: Latent heat release

LST: Local standard time

MAE: Mean absolute error

MAIC: Mean absolute intensity change

MBE: Mean bias error

MPI: Maximum potential intensity

MRAE: Mean relative average error

NCAR: National Center for Atmospheric Research

NCDC: National Climatic Data Center

NCEP: National Centers for Environmental Prediction

NESDIS/ORA: National Environmental Satellite, Data and Information System/Office of
Research Applications

NHC/TPC: National Hurricane Center/Tropical Prediction Center

NOAA: National Oceanic and Atmospheric Administration

NPOESS: National Polar-orbiting Operational Environmental Satellite System

NRL: Naval Research Laboratory with operating locations at Monterey (MRY), District
of Columbia (DC), and Stennis Space Center (SSC)

NSIPS: NRL Satellite Image Processing System

NWP: Numerical weather prediction

OFCM: Office of the Federal Coordinator for Meteorology

OTSR: Optimum Track Ship Routing

PCP: Percentage of convective pixels

PV~WAVE®: Precision Visuals~Workstation Analysis and Visualization Environment

RA IV: Regional Association IV

RSMC: Regional Specialized Meteorological Center

SDR: Sensor data record

SHIFOR: Statistical Hurricane Intensity FORecasting

SHIPS: Statistical Hurricane Intensity Prediction Scheme

SPP: Shared Processing Program

SPSS®: Statistical Package for the Social Sciences

SSM/I: Special Sensor Microwave/Imager

SST: Sea surface temperature

T_B: Brightness temperature

TDR: Temperature data record

US: United States

UTC: Uniform time code

WACP: Weighted average of convective pixels

WMO: World Meteorological Organization

Variable names are fully explained in Tables 3, 4, 5, and 8.

CHAPTER 1

INTRODUCTION

1.1 Defining the Problem

Predictions of tropical cyclone movement and intensity are two “critical” forecast problems (Simpson and Riehl 1981). Currently, intensity forecasting is the operational tropical cyclone forecaster’s “greatest problem” requiring the development of effective objective forecast guidance (Gross and Lawrence 1996). This dissertation examined this important problem with an emphasis on improving tropical cyclone intensity prediction in the eastern North Pacific Ocean basin. Perhaps, insight gained from this basin can be extrapolated to other tropical cyclone basins.

To ensure a common vocabulary, some of the relevant terms should be defined. A *tropical cyclone* is a warm-core, nonfrontal low pressure system of synoptic scale that develops over tropical or subtropical waters and has a definite organized surface circulation (OFCM 1998). This study’s basin of interest is the Pacific Ocean west of Central America and Mexico, east of 140 degrees West longitude, north of the Equator and generally south of 35 degrees North latitude (OFCM 1998). As the World Meteorological Organization (WMO) Regional Specialized Meteorological Center

(RSMC) for Regional Association IV (RA IV), the National Hurricane Center (NHC) of the Tropical Prediction Center (TPC) in Miami, Florida, is responsible for issuing forecast and warning advisories for tropical cyclones in the eastern North Pacific (Neumann 1993). The NHC/TPC is the Department of Commerce's (DoC) National Oceanic and Atmospheric Administration (NOAA) agency empowered by US law and WMO agreements to issue public intensity forecast advisories for the eastern North Pacific (OFCM 1998).

Intensity refers to the one-minute average (time interval used in WMO RA IV) maximum low-level sustained wind speed of the tropical cyclone (Holland 1993). Tropical cyclones in the eastern North Pacific can be classified according to their intensity into the following categories. *Tropical depressions* have intensities less than 17 m s^{-1} , *tropical storm* intensities are between 17 m s^{-1} and 32 m s^{-1} , and a *hurricane's* intensity is greater than or equal to 33 m s^{-1} (OFCM 1998). An additional category, *strong hurricane*, is used for intensities greater than or equal to 50 m s^{-1} in this present research. Another accepted manner of specifying tropical cyclone intensity is by minimum central sea level pressure (in units of mb or hPa). There are strong theoretical and empirical relationships between the maximum low-level wind speed and the minimum sea level pressure of a tropical cyclone (Sampson *et al.* 1995). However, satellite-based estimates of intensity and the damage potential of tropical cyclones are most often directly related to maximum wind speed (Dvorak 1990; Simpson and Riehl 1981). Forecast advisories of future tropical cyclone intensities issued by the NHC are in terms of maximum wind speed (although, in units of knots instead of m s^{-1}), as described

above (OFCM 1998). Therefore, this study discusses tropical cyclone intensity in terms of maximum wind speed. With relevant terms defined, attention can be turned to the specific research problem.

Department of Defense (DoD) formal research into the operational prediction of tropical cyclone intensity can be traced back to the United States Navy's Project AROWA (Applied Research; Operational Weather Analyses). Professor Herbert Riehl, University of Chicago, spearheaded research on this project. In 1951, Project AROWA was tasked to develop techniques to allow, "The prediction of storm intensities and the extent of areas dangerous to surface ships and aircraft along the path of the tropical cyclone" (US Navy 1956). Progress toward the goal of predicting tropical cyclone intensity has proven to be rather slow and difficult (OFCM 1997; AMS 1993). Dr. Robert Sheets (1990), former NHC director, summarized present intensity-change prediction skill as, "sorely lacking." Research interest in this topic continues to the present time and is the source of much debate (Elsberry *et al.* 1992; Elsberry 1998; Avila 1998).

Despite producing the **highest frequency** of tropical cyclones per unit area on the globe (McBride 1995), the eastern North Pacific is the **least studied** tropical cyclone basin (Tai and Ogura 1987). This unfortunate situation is most likely due to a scarcity of conventional meteorological observations. However, the lack of data does not diminish a critical need for accurate intensity forecasts which impact several agencies and millions of people. Only lately has research been directed at understanding the specific processes affecting tropical cyclone intensity in the eastern North Pacific by scientists at The Ohio State University. Whitney and Hobgood (1997) and Whitney (1995) focused their

research on the relationship between climatic sea surface temperatures (SST) and maximum potential intensities (MPI) of tropical cyclones in this region. A comparison of MPI values derived empirically by Whitney and Hobgood (1997) with MPI values derived by the thermodynamic method of Holland (1997) is ongoing by Hobgood (1998b). Hobgood (1997 and 1998a), Petty and Hobgood (1998), and Petty (1997a and b) document just recently developed tropical cyclone intensity-change forecast guidance products for the eastern North Pacific (see Section 2.7 for more details). The guidance product constructed by Hobgood (1998a) used climatic and persistence information and the method of Petty and Hobgood (1998) used climatic, weekly SST, and global-numerical-weather-prediction-(NWP)-model information to provide objective tropical cyclone future intensity-change guidance for this often overlooked basin.

1.2 Impacts of the Problem

With nearly 6 500 km of Pacific Ocean coastline, a growing tourism industry (e.g., Acapulco alone brings in over \$1 billion per year to the Mexican economy [Economist 1998]), and a fleet of fishing vessels routinely threatened by the devastating impacts of eastern North Pacific tropical cyclones, the Mexican government requires accurate intensity forecasts to properly allocate a finite amount of resources to the associated preparation and response efforts. Commercial ships transiting the region with destinations west of the Panama Canal are often directly affected by the fury of tropical cyclones.

DoD operations in the basin include the US Navy's Third Fleet based out of San Diego, California, and Pacific Air Forces headquartered in Hawaii. Naval weather forecasters are required to tailor intensity forecasts out to 72 hours to support Optimum Track Ship Routing (OTSR) operations (Titley 1995). An incorrect intensity forecast can create a potentially dangerous situation for ships. At a recent Interdepartmental Hurricane Conference, one of the US Navy's senior weather forecasters stressed the importance of tropical cyclone intensity forecasts to naval commanders and the urgent need for improved accuracy of intensity forecasts out to at least 72 hours (Barbor 1997). Forecasters at the Air Force Weather Agency's (AFWA) Americas Region Forecast Branch also have responsibilities to support DoD operations in the eastern North Pacific.

1.3 Application of Satellite Remote Sensing to the Problem

Budgetary constraints prevent the operational use of manned aerial reconnaissance to collect *in situ* measurements from tropical cyclones in this basin. Only on rare occasions are research (or operational) flights conducted in the eastern North Pacific (OFCM 1997). Therefore, meteorological satellites have become the main source of data for the operational specification and prediction of tropical cyclone intensity (Dvorak 1990) in this otherwise data-sparse region. During a recent panel discussion, Mr. Charles "Chip" Guard, University of Guam, suggested remotely sensed rainfall measurements might lead to advances in intensity forecasting skill (Elsberry *et al.* 1992). This dissertation was a direct attempt to demonstrate the feasibility of Guard's suggestion concerning satellite-measured rainfall and possible improvements of intensity forecasts.

Three wavelength (i.e., λ) regions of the electromagnetic spectrum are operationally employed in attempts to estimate rainfall from satellites. These regions are visible (i.e., $\lambda \approx 0.4$ to $0.7 \mu\text{m}$), infrared (i.e., $\lambda \approx 10.6$ to $12.6 \mu\text{m}$), and microwave (i.e., $\lambda \approx 0.3$ to 3.0 cm). Of these spectral regions, only satellite techniques using microwave measurements can produce **physically direct** estimates of rainfall (Barrett and Beaumont 1994). This dissertation examined the potential use of satellite passive-microwave rainfall measurements [derived from Special Sensor Microwave/Imager (SSM/I) radiometers (Hollinger 1991) onboard the Defense Meteorological Satellite Program (DMSP) constellation of polar-orbiting satellites] to improve eastern North Pacific tropical cyclone intensity specifying and forecasting techniques. Relationships between parameters obtained from an operational SSM/I-based rainfall-measuring algorithm (Ferraro *et al.* 1996) and current intensity and ensuing 12-, 24-, 36-, 48-, 60-, and 72-hour intensity changes from postanalysis-determined best-track data records were examined in an effort to identify statistically significant specifiers of current intensity and predictors of future intensity change.

Latent heat released by condensation in rainfall is recognized as an important factor in tropical cyclone intensity. Previous studies using SSM/I data showed correlations between rain rate or latent heat release and intensity trends in western North Pacific (Rodgers and Pierce 1995a; Rao and MacArthur 1994) and Atlantic (Rodgers *et al.* 1994b) tropical cyclones. In this dissertation, correlations between rainfall parameters within a 444.4-km radius of the center and current intensity and future intensity changes were analyzed using eastern North Pacific tropical cyclone data from seven years, 1991 to

1997. Stratifications based upon current intensity, prior 12-hour rate of intensity change, climate, translation speed, landfall, and synoptic-scale environmental-forcing parameters from global-NWP-model data were studied to understand factors that may affect a statistical relationship between rainfall parameters and current intensity and future intensity changes. The predictive skill of statistically significant rainfall parameters was assessed by using independent tropical cyclone data from 1994 and 1995.

1.4 Goals of this Research

The overall goal of this dissertation was to determine if SSM/I-rainfall parameters could add predictive skill to an objective tropical cyclone intensity-change forecast guidance product under development at The Ohio State University. The resulting guidance product's skill in predicting intensity change was assessed by statistically comparing its ensuing 12-, 24-, 36-, 48-, 60-, and 72-hour intensity-change forecast errors with those from a homogeneous sample of official NHC forecast advisories, currently operational statistical intensity-change forecast guidance, and forecasts made by the methods derived during previous research at The Ohio State University (Hobgood 1998a; Petty and Hobgood 1998). Specific goals related to the research problem are now defined. Goals listed below are classified as primary or secondary. These goals served as benchmarks for the conduct of this research and are directly linked to the data and methodology used to achieve them.

1.4.1 Primary Goal 1

Determine if correlations between rainfall parameters derived from an operational passive-microwave algorithm and eastern North Pacific tropical cyclone current intensity and future 12- to 72-hour intensity changes from best-track data are statistically significant at the 0.95 level. That is, a rainfall parameter is considered a statistically significant specifier of intensity or predictor of intensity change, if the probability that a Pearson product-moment correlation coefficient between two variables greater than or equal to 0.3 (i.e., $r \geq 0.3$) is different from zero is greater than 95 percent.

1.4.2 Primary Goal 2

Examine significant rainfall-parameter correlations with current intensity and future intensity changes based upon stratifications in current intensity, prior 12-hour rate of intensity change, season, location, weekly SST, environmental vertical shear of the horizontal wind, translation speed, and landfall.

1.4.3 Primary Goal 3

If rainfall parameters are significantly correlated with future intensity change, attempt to include them via stepwise multiple linear regression into intensity-change prediction models for eastern North Pacific tropical cyclones already composed of climatic, persistence (Hobgood 1998a), and synoptic-scale environmental-forcing predictors (Petty and Hobgood 1998). Statistical significance level must be 0.95 for a predictor's entry into the regression-based model and 0.90 to remain.

1.4.4 Primary Goal 4

If rainfall parameters remain in the regression-based model(s), statistically compare the future 12- to 72-hour intensity-change prediction errors produced by the resulting model(s) with those errors produced by a homogeneous sample of official NHC forecast advisories, currently operational statistical intensity-change forecast guidance, and the methods of Hobgood (1998a) and Petty and Hobgood (1998). The statistical significance of differences in errors will be assessed by performing paired *t* tests at the 0.95 level. Success for rainfall parameters improving intensity-change forecasts is defined as the final model(s) producing smaller intensity-change forecast errors for each forecast period than the aforementioned methods. Also, compare the final model(s)'s intensity forecast errors against the other methods according to stratifications in current intensity.

1.4.5 Primary Goal 5

Conduct case studies on interesting individual tropical cyclones with good temporal and spatial observational coverage by SSM/I to assess forecast model performance skill and demonstrate operational implementation issues.

1.4.6 Secondary Goal 1

Determine if rainfall parameters can detect the concentric eyewall cycle described by Willoughby *et al.* (1982) and Willoughby (1990). The concentric eyewall cycle is a temporal evolution of convective rings that often occurs in strong tropical cyclones. The cycle has an important impact on tropical cyclone intensity change.

1.4.7 Secondary Goal 2

Document the convective rainfall characteristics for a substantial sample of eastern North Pacific tropical cyclones with respect to current intensity and radial distance from the center of circulation. This type of documentation has never been previously done for eastern North Pacific tropical cyclones.

1.4.8 Secondary Goal 3

Analyze the accuracy of locating tropical cyclone centers of circulation with SSM/I imagery. Stratify analysis by current intensity.

1.4.9 Secondary Goal 4

Attempt to detect a diurnal cycle in eastern North Pacific tropical cyclone convective rainfall. Examine the possible relationship between current intensity and such a cycle, if a diurnal cycle is detected. Stratify analysis by radial distance from the center.

1.4.10 Secondary Goal 5

Demonstrate the stability of climatic, persistence, and synoptic-scale environmental-forcing variables as predictors of eastern North Pacific tropical cyclone intensity change. Conduct statistical analysis of a regression-model training dataset comprised of different tropical cyclone seasons than those seasons used by Hobgood (1998a), Petty and Hobgood (1998), and Petty (1997a and b). Stable intensity-change predictors should have similar standardized regression coefficients for different tropical cyclone seasons.

1.4.11 Secondary Goal 6

Contribute to the Naval Research Laboratory (NRL) in Monterey (MR Y), California, Marine Meteorology Division's efforts to develop a neural-network-based tropical cyclone intensity specification technique (Hawkins *et al.* 1996) by processing cases of SSM/I data with coverage of tropical cyclones in the eastern North Pacific.

1.4.12 Secondary Goal 7

Present the findings of this research in a scholarly journal or DoD technical report, at appropriate technical conferences, and in electronic format on the Internet.

1.5 Summary

The research problem and associated terms were defined and specific goals were enumerated above. The main hypothesis underlying this dissertation was that satellite passive-microwave-measured rainfall, through its concomitant latent heat release, is highly correlated with tropical cyclone current intensity and future intensity changes out to 72 hours. These strong correlations ought to be useful in improving objective forecast guidance tools for the critical problems of specifying tropical cyclone current intensity and predicting future intensity changes in the eastern North Pacific. Chapters to follow will provide information on previous research relevant to this dissertation, specific information on the data and tools used to achieve the goals enumerated above, and detail the accomplishment of those goals. A final chapter will discuss the conclusions to be drawn from the results of this dissertation and make recommendations for future research on this important topic.

CHAPTER 2

RELEVANT LITERATURE REVIEW

2.1 Current State of Tropical Cyclone Intensity Forecasting in the Eastern North Pacific

Improvement of intensity forecasting is rated as a “high-priority” research objective by federal agencies involved with tropical cyclone research (OFCM 1997).

Table 1 demonstrates the current condition of intensity forecasting skill for the eastern North Pacific during two time periods of interest.

Mean Absolute Official NHC Intensity Forecast Errors for Eastern North Pacific										
Forecast Period	12 hours		24 hours		36 hours		48 hours		72 hours	
	m s ⁻¹	knots	m s ⁻¹	knots	m s ⁻¹	knots	m s ⁻¹	knots	m s ⁻¹	knots
1988-1993 ^a	--	--	6	12	--	--	9	17	10	20
1990-1994 ^b	4	7	6	12	8	16	10	19	11	22

Table 1: Mean Absolute Official NHC Intensity Forecast Errors (^aOFCM 1997; ^bGross and Lawrence 1996).

Care should be taken when viewing Table 1, because it demonstrates **mean** absolute intensity forecast errors. The errors for individual tropical cyclones can be quite large,

especially for tropical cyclones that undergo unexpected rapid intensity changes. A recent dramatic example of a large official NHC intensity forecast error occurred during Hurricane Linda (1997). Some 48- and 72-hour intensity forecast advisories issued by the NHC were in error by approximately -50 m s^{-1} (Avila 1998). It is fortunate that Linda remained well away from land, because a similar underforecast could have contributed to a disastrous underresponse in a landfalling-hurricane scenario near a heavily populated area like Acapulco. Improvement in understanding and predicting future intensity change in the eastern North Pacific (and other ocean basins) is obviously needed.

2.2 Role of Latent Heat Release in Intensity Change

In 1835, Professor James Pollard Espy proclaimed that the release of latent heat due to the condensation of water vapor into precipitation (e.g., rainfall) plays a major role in tropical cyclones (Middleton 1965). Thus, the foundation for a convection or thermal theory of tropical cyclones was laid (Khrigian 1959). Numerical modeling and observational studies have shown that latent heat release is the most important diabatic process driving tropical cyclones (Anthes 1974). Latent heat release within a tropical cyclone generates available potential energy in the form of a warm-core, low pressure center that may be converted into kinetic energy. The conversion into kinetic energy occurs when friction causes low-level winds to accelerate inward toward the tropical cyclone's center. Additionally, this conversion has been found to be most effective within about 555.5 km of the center (Anthes 1974). Therefore, tropical cyclone intensity is highly sensitive to changes in latent heat release (i.e., condensation) within this region.

It must be noted that there is currently an intense debate concerning theories of the exact mechanisms involved in the generation of available potential energy and its conversion to kinetic energy within tropical cyclones. The interested reader is referred to excellent treatments of this raging theoretical debate written by Fitzpatrick (1996) and Craig and Gray (1996).

Figure 1 schematically illustrates the interaction of the synoptic-scale water and motion fields in a tropical cyclone. Moisture (i.e., water vapor), liquid water (i.e., cloud liquid water and precipitation), and motion (i.e., horizontal and vertical) are linked in a complicated nonlinear manner via latent heat release (Atlas and Thiele 1981). A tangible indication of the amount of condensation occurring in a tropical cyclone is precipitation (i.e., rainfall). Consequently, properly measured rainfall can provide useful information for understanding the link between latent heat release and tropical cyclone intensity change.

2.3 Satellite Passive-microwave Measurements of Rainfall

Visible- and infrared-satellite rainfall estimation methods are based upon cloud-top temperatures. This limitation exists because clouds, even very thin cirrus-type, are opaque in the visible and infrared spectral regions. By contrast, cloud droplets weakly interact with microwave electromagnetic radiation. However, precipitation strongly affects microwave radiation. Therefore, rainfall can be readily sensed by satellite-based passive-microwave radiometers in a physically direct manner. In crude terms, microwave methods are able to “look through clouds and see rainfall occurring below.” The

complex interactions between microwave radiation, Earth's surface, and the atmosphere are schematically summarized in Figure 2. Space-based passive-microwave radiometers remotely sense the upwelling microwave radiation emitted, absorbed, reflected, transmitted, and scattered by the Earth-atmosphere system.

The physically direct relationship between microwave radiation and rainfall will now be illustrated. The relationship begins with Planck's Law for the radiance or brightness emitted by a blackbody:

$$B_{\nu}(T) = \frac{2h\nu^3}{c^2} \frac{1}{e^{\left(\frac{h\nu}{kT}\right)} - 1} \quad (1)$$

where $B_{\nu}(T)$ is the blackbody-emitted brightness in units of $\text{W m}^{-2} \text{sr}^{-1}$, h is Planck's Constant which is $6.6260755 \times 10^{-34} \text{ J s}$, ν is frequency measured in units of Hz, c is the speed of light in a vacuum which is $2.99792458 \times 10^8 \text{ m s}^{-1}$, k is Boltzmann's Constant which is $1.380658 \times 10^{-23} \text{ J K}^{-1}$, and T is the absolute temperature with units of K.

Throughout the microwave spectrum and troposphere, $\frac{h\nu}{kT} \ll 1$, which allows the following simple Taylor-series approximation: $e^{\left(\frac{h\nu}{kT}\right)} \approx 1 + \frac{h\nu}{kT}$. Substitution into Equation 1 yields:

$$B_{\nu}(T) \approx \frac{2h\nu^3}{c^2} \frac{1}{1 + \frac{h\nu}{kT} - 1} = \frac{2h\nu^3}{c^2} \frac{1}{\frac{h\nu}{kT}} = \frac{2\nu^2 kT}{c^2} = \frac{2kT}{\lambda^2} \quad (2)$$

The resulting Equation 2 is termed the Rayleigh-Jeans Approximation. The relative error of this approximation is less than 0.2 percent.

Radiance is beneficial for the remote sensing of rainfall, because it is conveniently independent of the distance to the rainfall, if the incidence angle and pathlength are constant. With the Rayleigh-Jeans Approximation, radiance is directly related to the absolute or kinetic temperature (i.e., available from a thermometer) of a blackbody. Since space-based radiometers measure radiance instead of blackbody temperature and a blackbody is a theoretical construct not experienced in nature, it is useful to compare the radiance of a real emitter or graybody to that of a blackbody:

$$\frac{B'_{\nu}(T)}{B_{\nu}(T)} \approx \frac{\frac{2kT'}{\lambda^2}}{\frac{2kT}{\lambda^2}} = \frac{T'}{T} = \frac{T_B}{T} \equiv \epsilon_{\nu} \quad (3)$$

The ratio in Equation 3 quantifies how efficiently a graybody emits microwave radiation as compared to a blackbody with the same absolute temperature. $B'_{\nu}(T)$ is the radiance of a graybody which is remotely sensed. T' is the absolute temperature a blackbody would have for a radiance of $B'_{\nu}(T)$. T is again the absolute temperature of the graybody. T_B is defined as the brightness temperature and is related to the absolute temperature, T , by a physical property of the graybody called emissivity or emittance, ϵ_{ν} .

$$\tau_v \equiv \frac{\text{transmitted radiance at } v}{\text{incident radiance at } v} \quad (4)$$

$$\rho_v \equiv \frac{\text{reflected radiance at } v}{\text{incident radiance at } v} \quad (5)$$

$$\alpha_v \equiv \frac{\text{absorbed radiance at } v}{\text{incident radiance at } v} \quad (6)$$

Other useful frequency-dependent properties in the discussion of microwave radiance are defined above in Equations 4 to 6, as transmittance (i.e., τ_v), reflectance (i.e., ρ_v), and absorptance (i.e., α_v). These properties are related by the following identity due to conservation of energy considerations: $\tau_v + \rho_v + \alpha_v \equiv 1$. Kirchhoff's Law states that in the case of local thermodynamic equilibrium, which is a valid assumption for Earth's atmosphere below 100 km above the Earth's surface, $\alpha_v \equiv \epsilon_v$.

An equation describing the transfers of microwave radiation illustrated in Figure 2 can be written in terms of T_B and T . Using the simplified plane-parallel geometry shown in Figure 3 and neglecting scattering, an equation for microwave radiative transfer involving rainfall is derived (Grody 1997; Kidder and Vonder Haar 1995):

$$\cos \theta \frac{dT_B}{dz} = \sigma_a (T - T_B) \quad (7)$$

where the volume absorption coefficient, σ_a , has units of m^{-1} and z is the vertical distance from the surface measured in units of m. Above the rain layer, $\sigma_a \approx 0 \text{ m}^{-1}$. Therefore, integration of Equation 7 is simplified to just the depth of the rain layer, D . Also, the

integration can be further simplified by assuming that the temperature of the rain layer, T_r , is constant. The incidence angle, θ , is measured from local vertical to the radiometer. Equation 8 shows that T_B measured at the radiometer can be represented as the sum of the four components shown graphically in Figure 3:

$$T_B \approx T_1 + T_2 + T_3 + T_4 \quad (8)$$

Each term on the right-hand side of Equation 8 is defined below:

$$T_1 = T_s \epsilon \tau^{\sec \theta} \quad (9)$$

$$T_2 = (1 - \epsilon) T_c \tau^{2 \sec \theta} \quad (10)$$

$$T_3 = (1 - \epsilon) T_r (1 - \tau^{\sec \theta}) \tau^{\sec \theta} \quad (11)$$

$$T_4 = T_r (1 - \tau^{\sec \theta}) \quad (12)$$

T_1 represents the microwave emission by the surface with temperature T_s and transmission through the atmosphere. Cosmic-microwave transmission through the atmosphere and reflection at the surface is described by T_2 . T_c is the cosmic radiometric temperature which is quite small (i.e., $T_c \approx 2.7$ K). The rain layer's downwelling microwave emission, transmission through the atmosphere, and reflection by the surface is given by T_3 . T_4 describes the upwelling microwave emission by the rain layer and

transmission through the atmosphere. Transmittance of the rain layer is approximated by: $\tau \approx e^{(-\sigma_a D)}$. Substitution of Equations 9 to 12 into Equation 8 and rearrangement of terms yields:

$$T_B \approx T_s \epsilon \tau^{\sec \theta} + (1 - \epsilon) T_c \tau^{2 \sec \theta} + T_r [1 - \epsilon \tau^{\sec \theta} - (1 - \epsilon) \tau^{2 \sec \theta}] \quad (13)$$

If the small cosmic (i.e., second right-hand side) term is neglected in Equation 13, the impact of rainfall on T_B can be simply illustrated. For a nonraining atmosphere, $\tau \approx 1$, which means $T_B \approx T_s \epsilon$. As rain rate increases, σ_a increases, τ approaches zero, and T_B converges to T_r . Therefore, T_B measurements can provide extremely useful information by their radiometric response to rainfall.

Some problems confound the otherwise simple relationship between T_B and rainfall. Over water, T_B increases rapidly with rain rate, because ϵ values for water are relatively low (i.e., $\epsilon \approx 0.5$). Thus, water provides a radiometrically cool background compared to a warm rain-layer target. However, ϵ values over land are relatively high (i.e., $\epsilon \approx 0.9$). As a result, land is a radiometrically warm background for a warm rain-layer target. Therefore, a change in T_B due to rainfall emissions over land is usually too small to detect with currently operational satellite remote sensing methods. Another problem is that T_B depends upon the product of $\sigma_a D$. However, rain rate is highly related to σ_a and independent of D . Therefore, the depth of the rain layer, D , needs to be specified in order for T_B measurements to be used for explicitly determining rain rate. Also, σ_a depends not only upon rain rate, but upon cloud liquid water and water vapor, as

well. Consequently, cloud-liquid-water and water-vapor information are also necessary to perform explicit calculations of rain rate from remotely sensed measurements of T_B .

It was shown above that by neglecting scattering and cosmic-microwave radiation, Equation 13 implies that as rain rate increases, T_B increases to a limit of T_r . However, in reality, there is a point at which increasing rain rate actually results in decreasing values of T_B . This decrease of T_B occurs because, as rain rate increases, the size of hydrometeors in the rain layer (e.g., very large rain drops, ice, graupel, and hail) increases and approaches the actual wavelength size of microwave radiation. Scattering, which can then no longer be ignored, occurs which obscures emission by the rain layer and surface and allows reflection of extremely cold cosmic-microwave radiation off the top of the rain layer into the radiometer's field of view (FOV). The resulting reduction in T_B occurs over both water and land surfaces.

The previous discussion in this section describes two regimes for satellite passive-microwave measurements of rainfall: emission and scattering. Up to a threshold rain rate governed by wavelength, **emission by rainfall over water** allows T_B measurements to be used to *calculate* rain rate. Beyond that threshold rain rate, **scattering** by large hydrometeors permits T_B measurements to be used to *infer* rain rate **over both water and land**. In general, microwave frequencies below 20 GHz are used in emission-based algorithms. At frequencies above 60 GHz, scattering effects are utilized by passive-microwave algorithms. Between these frequencies, emission and scattering effects are found. An excellent summary of the current state-of-the-art algorithms developed by researchers to calculate rain rate from passive-microwave brightness temperatures was

written by Wilheit *et al.* (1994). The algorithm used in this present research exploits both emission and scattering regimes to measure rainfall in eastern North Pacific tropical cyclones. Details of the relevant algorithm and reasons it was selected for this research are discussed below.

2.4 Rainfall Algorithm Used in this Research

An important distinction in rainfall types found in tropical cyclones is convective versus stratiform (Houze 1993). Convective precipitation occurs in cumulus and cumulonimbus clouds of the eyewall and in convective rainbands. Nimbostratus clouds in tropical cyclones produce stratiform rainfall. Tropical rain rates less than or equal to 1 mm h⁻¹ are mostly due to stratiform rainfall and those greater than 10 mm h⁻¹ are generally caused by convective rainfall (Tokay and Short 1996). Rain rates between these two values can be caused by both types of rainfall. A threshold between the two types at 6 mm h⁻¹ was proposed by Johnson and Hamilton (1988) due to land-based radar studies of squall lines. However, based upon radar studies of tropical cyclones, Willoughby (1988) and Jorgensen and Willis (1982) suggested that rain rates of 3 mm h⁻¹ and greater indicate convective rainfall. Therefore, this current research used the latter 3-mm h⁻¹ threshold for determining convective rainfall in eastern North Pacific tropical cyclones.

Processes governing convective precipitation take place above the freezing level and are termed "cold-cloud." Passive-microwave algorithms best suited for this type of precipitation measurement are those that take advantage of the pronounced scattering

effects of the resulting precipitation-sized ice particles. The “warm-cloud” processes of stratiform rainfall take place at or below the freezing level. Scattering-based algorithms are not useful in this warm-cloud regime. However, emission-based algorithms can detect stratiform rainfall over water.

Greater than 90 percent of the rainfall associated with a tropical cyclone occurs within 222.2 km of the center of circulation (Hughes 1952; Riehl 1954). Of this rainfall, approximately 90 percent of the areal coverage within this region is stratiform (Jorgensen 1984). However, due to its higher rain rates, convective rainfall contributes about 60 percent of the total rainfall (Marks 1990; Jorgensen 1984). Therefore, the measurement of both convective and stratiform rainfall is important to studies of tropical cyclone rainfall.

The rainfall algorithm chosen for this research was developed by the NOAA National Environmental Satellite, Data and Information System/Office of Research Applications (NESDIS/ORA). It was developed to determine instantaneous rain rates using brightness temperatures measured by the DMSP SSM/I (Ferraro *et al.* 1996). Specific details concerning DMSP SSM/I data will be provided in Chapter 3. There are two main components of the NESDIS/ORA over-water algorithm: scattering and emission. The scattering component relates a scattering index (Grody 1991; Ferraro *et al.* 1994) to rain rates. This scattering index is the difference between the actual vertically polarized brightness temperature at 85.5 GHz and one predicted for a scattering-free atmosphere by using the vertically polarized brightness temperatures at 19.4 and 22.2 GHz. A brightness-temperature screening process is used to prevent false rain retrievals

(e.g., sea ice). The emission component is calculated by using cloud-liquid-water values greater than 0.20 mm estimated using the vertically polarized brightness temperatures at 19.4, 22.2, and 37.0 GHz (Weng and Grody 1994). Scattering-index and cloud-liquid-water relationships with rain rate were empirically developed using coincidental ground-based radar rainfall measurements from around the world (Ferraro and Marks 1995). The range of rain rates detected by the algorithm is between 0.2 and 35.0 mm h⁻¹. Validation of the algorithm found the relative absolute error between SSM/I and radar rain rates to be 10 to 20 percent. Finally, a practical reason for using the NESDIS/ORA algorithm is that it was selected by the Shared Processing Program Algorithm Research Panel as the SSM/I-rainfall algorithm to be operationally implemented by federal agencies (Colton and Poe 1994; Ferraro *et al.* 1996). Therefore, this rainfall product is readily available to NHC/TPC forecasters via the Shared Processing Program (SPP) and the Internet just a few hours after a tropical cyclone is observed by an SSM/I-equipped DMSP satellite. Images of the NESDIS/ORA rainfall algorithm applied to SSM/I observations of tropical cyclones are routinely produced by NRL in MRY and can be viewed in near real time via the Internet (http://www.nrlmry.navy.mil/sat-bin/tc_home). In May 1998, the DMSP constellation was combined with other polar-orbiting satellites operated by NESDIS to form one National Polar-orbiting Operational Environmental Satellite System (NPOESS). This reorganization of administrative control of satellites does not affect the ability of the SPP to provide SSM/I-derived products to NHC/TPC forecasters in near real time.

2.5 Satellite Passive-microwave Measurements Related to Tropical Cyclone Intensity

Links between space-based passive-microwave measurements related to precipitation and tropical cyclone intensity have been explored for over 21 years. The first research published on this specific topic was conducted by Adler and Rodgers (1977). By examining six observations of western North Pacific tropical cyclone Nora (1972), they found latent heat release (LHR) increased as intensity increased. LHR (in units of W) within a 444.4-km radius of the tropical cyclone center was calculated with a rainfall algorithm using the 19.4-GHz horizontally polarized brightness temperatures measured by the *Nimbus-5* Electrically Scanning Microwave Radiometer (ESMR-5). Adler and Rodgers (1977) developed the following equation that relates satellite-measured rainfall to LHR:

$$LHR = L_c \rho_r \int_A R \, da \quad (14)$$

where L_c is the latent heat of condensation which is $2.501 \times 10^6 \text{ J kg}^{-1}$, ρ_r is the density of rain which is $1\,000 \text{ kg m}^{-3}$, A is the area of integration in units of m^2 , R is the rain rate obtained by an algorithm in units of mm h^{-1} , and da is the incremental area or spatial resolution of the satellite sensor in units of m^2 .

Rodgers and Adler (1981) later used 71 observations by the ESMR-5 of 21 tropical cyclones during the 1973 to 1975 seasons. 49 of the observations were for 18 western North Pacific tropical cyclones and 22 of the observations were for 3 eastern North Pacific tropical cyclones. A correlation coefficient of 0.71, significant at the 0.99 level, was found between LHR within a 444.4-km radius and current intensity. One case

study of eastern North Pacific tropical cyclone Doreen (1973) qualitatively demonstrated their finding that maximum LHR generally occurred one to two days prior to maximum intensity. This finding confirmed earlier numerical tropical cyclone prediction model results that showed maximum intensity occurred one to three days after maximum LHR (Kurihara and Tuleya 1974; Rosenthal 1978). Of further interest, Rodgers and Adler (1981) found that the three eastern North Pacific tropical cyclones were more compact and had less rainfall than those of the western North Pacific.

Encouraged by the results of Adler and Rodgers (1977) and Rodgers and Adler (1981), Hunter *et al.* (1981) made the first attempt at an objective tropical cyclone intensity forecast guidance tool including passive-microwave brightness-temperature data. They employed an eigenvector representation of the 19.4-GHz horizontally polarized brightness-temperature images from the ESMR-5 centered on 120 observations of 29 tropical cyclones from the 1973 to 1974 seasons. 25 were tropical cyclones in the western North Pacific and 4 occurred in the eastern North Pacific. By adding ESMR-5 information to climatic and persistence information from the best-track data, they increased the explained variance (i.e., r^2) of intensity by 7 percent at the 24-hour forecast period and by 16 percent at the 72-hour forecast period, when compared to using only best-track data. Their guidance product based upon best-track data and ESMR-5 predictors produced mean absolute forecast errors for the 24- and 72-hour periods that were 2 and 4 m s^{-1} , respectively, less than the mean absolute official forecast errors by the Joint Typhoon Warning Center (JTWC) for the same forecast periods and tropical cyclone seasons. The Hunter *et al.* (1981) study was the first demonstration that

quantitative passive-microwave satellite data could possibly improve tropical cyclone intensity forecasts. However, their proposed use of passive-microwave satellite data was never operationally adopted by any tropical cyclone forecasting organization. Perhaps, it failed to be operationally adopted, because the eigenvector representation of the data was too complex and obscured any physically direct relationship between the microwave satellite data and future intensity change.

With the launch of the first SSM/I in 1987, routine operational passive-microwave measurements of tropical cyclones from satellites became possible. The first researcher to quantitatively relate passive-microwave brightness temperature measurements from the SSM/I to tropical cyclone intensity was Rhudy (1989). He used 23 observations of 12 tropical cyclones in the western North Pacific and Atlantic during 1987 to 1988. LHR within a 444.4-km radius and current intensity had a correlation coefficient of 0.62, significant at the 0.99 level. 85.5-GHz vertically polarized brightness-temperature differences within a 333.3-km radius yielded correlation coefficients of 0.64 and 0.74, significant at the 0.99 level, with current and future 24-hour intensities, respectively.

Relationships between SSM/I-measured rainfall and future 24-hour intensity change were examined for 27 observations of 12 tropical cyclones in the western North Pacific and Atlantic during 1987 to 1988 (MacArthur 1991; Rao *et al.* 1991; Rao and MacArthur 1994). They found a 0.68 correlation coefficient, significant at the 0.95 level, between average volumetric rain rate (in units of $\text{mm}^3 \text{h}^{-1}$) within a 222.2-km radius and future 24-hour intensity change. Case studies of western North Pacific tropical cyclones Lynn (1987) and Dinah (1987) yielded extremely high correlations between average

volumetric rain rate within a 222.2-km radius and future 24-hour intensity change. The correlation coefficient for Lynn's seven observations was 0.97 and for Dinah's four observations it was 0.99. Overall, they found a differential effect of rainfall on future intensity change due to location of rainfall with respect to the center of circulation.

Within a 222.2-km radius from the center, rainfall had a highly positive correlation with future 24-hour intensity change. However, within the annular region between 222.2 to 444.4 km from the center, rainfall had a weakly negative correlation with future 24-hour intensity change. It was noted that if a rain-rate maximum occurred outside of the core region (i.e., beyond a 222.2-km radius), short-term weakening of intensity could be expected.

McCoy (1991) used 85.5-GHz vertically polarized brightness temperature differences between regions (i.e., outer-versus-inner and left-versus-right) within a 444.4-km radius to find a 0.61 correlation coefficient with future 24-hour intensity change. He also noted that the appearance of convective rainbands beyond 222.2 km from the center usually preceded a weakening of future 24-hour intensity. His study was based on 25 observations of western North Pacific and Atlantic tropical cyclones during 1987 to 1988. In this study, McCoy (1991) was the first researcher to suggest that SSM/I measurements might be able to monitor the convective ring or concentric eyewall cycle discussed by Willoughby *et al.* (1982 and 1984) and Willoughby (1988 and 1990). This convective ring cycle is a spatial and temporal evolution of axisymmetric convective rainfall rings that commonly occurs in strong symmetric tropical cyclones with intensities greater than or equal to 50 m s^{-1} . Often, a single vigorous circular ring of rainfall or an eyewall within

a 111.1-km radius will contract inward with a concomitant intensity increase. Sometimes concentric outer convective rings form between 111.1- and 222.2-km radii and contract around the existing eyewall. This outer convective ring causes the inner eyewall to dissipate and intensity decreases. As the outer convective ring continues to contract, it often supplants the original eyewall and intensity increases when this new eyewall contracts. The entire eyewall cycle normally takes between 12 to 36 hours to complete. Multiple concentric eyewall cycles may occur provided the tropical cyclone does not make landfall, experience excessive environmental wind shear, or travel over relatively cool ocean water.

Felde and Glass (1991) related the fractional coverage of 85.5-GHz horizontally polarized brightness temperatures less than 220 K within a tropical cyclone-centered circular area with a 55.5-km radius to current intensity from best-track data. Their study used 17 observations of 11 western North Pacific tropical cyclones during the 1987 season. The correlation coefficient between fractional coverage of intense convection, indicated by depressed 85.5-GHz brightness temperatures, and current intensity was 0.73. Also, the difference between the 19.4-GHz horizontally and vertically polarized brightness temperatures (i.e., an indication of microwave emission by rainfall) within the same 55.5-km radius yielded a 0.77 correlation coefficient with current intensity. For nine observations of intensifying tropical cyclones, the correlation coefficient increased to 0.85. For eight observations of weakening tropical cyclones, the correlation coefficient decreased to 0.70. A later study by Glass and Felde (1992) used 25 observations of 19 western North Pacific tropical cyclones during 1987 to 1988. The same 85.5-GHz

parameter described above produced a 0.93 correlation coefficient with current intensity for 15 intensifying tropical cyclones and a 0.70 correlation coefficient for 10 weakening tropical cyclones.

Alliss *et al.* (1992) conducted a case study of Atlantic tropical cyclone Hugo (1989) using nine SSM/I observations. They found SSM/I-derived rainfall parameters calculated for areas within a 444.4-km radius were highly correlated with current intensity. The highest correlation coefficient was 0.93, significant at the 0.99 level. It was suggested that Hugo's intensity changes might be related to the convective ring cycle. In a similar case study of Atlantic tropical cyclone Florence (1988) using five observations, Alliss *et al.* (1993) found the average rain rate (in units of mm h^{-1}) within a 111.1-km radius had a correlation coefficient of 0.93 with current intensity, significant at the 0.98 level. Both of these studies found that as the azimuthally averaged rainfall maximum moved inward, intensity increased.

In a previous study, this present author used 17 SSM/I observations of western North Pacific tropical cyclone Freda (1987), climatic SST, and global-NWP-model data to understand the relationships between rainfall, environmental forcing, and intensity (West 1993a and b). Changes in LHR preceded changes of intensity by about 12 to 24 hours. Moisture flux convergence in the middle troposphere initiated convective rings in the outer core (i.e., within 111.1 to 222.2 km). Interactions with upper-level troughs aided inner-core (i.e., within 111.1 km) rainfall, if vertical wind shear was weak. Changes in intensity were related to the convective ring cycle.

A case study of western North Pacific tropical cyclone Flo (1990) using seven SSM/I observations found a correlation coefficient of 0.70 between rainfall within a 111.1-km radius and current intensity (Melton 1994). Zhao (1994) used three cases of western North Pacific tropical cyclones from 1992 to relate rainfall parameters to future intensity. She studied a total of 37 SSM/I observations from 21, 7, and 9 observations of tropical cyclones Gay, Elsie, and Hunt, respectively. For intensifying tropical cyclones, the correlation coefficient between a measure of total (i.e., convective and stratiform) rainfall within a 111.1-km radius and future 12-hour intensity change was 0.71, highly significant at the 0.99 level. A convective rainfall parameter within a 222.2-km radius yielded a 0.63 correlation coefficient, significant at the 0.91 level, with 12-hour future intensity change in weakening tropical cyclones. Zhao (1994) also qualitatively found the convective ring cycle occurred in these cases and maximum rainfall occurred prior to maximum intensity.

Rodgers *et al.* (1994b) studied 18 North Atlantic tropical cyclones from 1987 to 1989 with 103 SSM/I observations. They found that more intense tropical cyclones had more rainfall. Additionally, correlations between past 12-hour trends in both LHR within a 111.1-km radius and intensity varied according to the current intensity. That is, for tropical depressions the correlation coefficient was 0.06, for tropical storms it was -0.27, and for hurricanes it was 0.78, all significant at the 0.99 level. Rodgers and Pierce (1995a) later examined western North Pacific tropical cyclones from 1987 to 1992 with 257 SSM/I observations. For 123 tropical depression observations, the correlation coefficient between past 12-hour trends in both average rain rate within a 111.1-km

radius and intensity was 0.25, for 61 tropical storm observations it was 0.51, and for 73 typhoon observations it was curiously only 0.04, all significant at the 0.99 level. The little, if any, correlation coefficient for typhoon observations was explained by Rodgers and Pierce (1995a) as the result of great variability of eyewall size in western North Pacific tropical cyclones. Additionally, a diurnal variation of rainfall within a 444.4-km radius was found for weaker tropical cyclones (i.e., less than tropical storm intensity). An early morning maximum and an evening minimum were found for these weaker tropical cyclones. For stronger tropical cyclones, especially within the inner core, no significant diurnal variation was found. These findings support the results of prior research by Hobgood (1986) that included the diurnal cycle of net radiation at the cloud tops in a numerical tropical cyclone prediction model. Finally, Rodgers *et al.* (1994b) and Rodgers and Pierce (1995a) both found that higher rain rates occurred near the center of tropical cyclones, and that the spatial and temporal change of azimuthally averaged rainfall demonstrated the convective ring cycle.

Using SSM/I, climatic SST, and global-NWP-model data, Rodgers *et al.* (1994a) and Rodgers and Pierce (1995b) examined case studies of tropical cyclones to understand environmental-forcing, rainfall, and intensity relationships. Rodgers *et al.* (1994a) used 30 SSM/I observations of 3 Atlantic tropical cyclones during 1989. Tropical cyclone Dean had 7 observations, Gabrielle had 11, and Hugo had 12. In Rodgers and Pierce (1995), 18 observations of western North Pacific tropical cyclone Bobbie (1992) were used. In both studies and all cases, the convective ring cycle played an important role in intensity change. A convective ring often formed in the outer core (i.e., between 111.1-

and 222.2-km radii) and propagated inward. Maximum intensity occurred when the ring reached the inner core (i.e., within 111.1 km of the center). The formation of outer-core convective rings usually led to short-term weakening. Environmental-forcing effects were similar to those found by West (1993a and b). In a recent case study by Rodgers *et al.* (1997), 13 SSM/I observations of LHR within a 55.5-km radius of Atlantic tropical cyclone Opal (1995) were studied to understand the rapid intensity change that occurred. Three convective bursts took place prior to a rapid intensity increase. They proposed that the rapid intensity increase was due to the massive amounts of latent heat released by the convective bursts.

Recently, Cecil (1997) related 85.5-GHz-brightness-temperature-based ice-scattering signatures within a 111.1-km radius to future 24-hour intensity for 90 SSM/I observations of western North Pacific, eastern North Pacific, and Atlantic tropical cyclones. The correlation coefficient was 0.68 for all basins. For the 17 observations of 6 eastern North Pacific tropical cyclones, the correlation coefficient improved to 0.89.

Previous studies of satellite microwave measurements of tropical cyclones indicate that parameters related to rainfall are highly correlated with tropical cyclone current intensity and future intensity changes. Used in concert with other factors related to tropical cyclone intensity, SSM/I-derived rainfall parameters ought to aid in the specification of current intensity and prediction of future intensity changes in eastern North Pacific tropical cyclones.

2.6 Factors Related to Current Intensity and Future Intensity Change

Strong correlations between rainfall parameters and tropical cyclone current intensity and future intensity change were shown in the previous section. However, there are other factors affecting tropical cyclone intensity and intensity change. A brief summary of research on these factors is reviewed below. These factors will be used in the stratified statistical analysis discussed in Section 3.10.

The current intensity of a tropical cyclone can affect the relationship between LHR and future intensity change. Studies by Shapiro and Willoughby (1982), Rodgers *et al.* (1994b), and Rodgers and Pierce (1995a) showed that as tropical cyclone intensity increases, the correlation between LHR within the core region (i.e., within 222.2 km) and future intensity change becomes stronger. This increasingly efficient relationship between LHR and intensity change for more intense tropical cyclones is attributed to increasing lower-tropospheric inertial stability.

Rate of intensity change is an important factor in understanding LHR and future intensity change. Rapid intensity changes (i.e., greater than 10 m s^{-1} over a 12-hour period) are extremely hard to forecast and cause large official intensity-change forecast errors (Elsberry *et al.* 1992; Mundell 1990 and 1991; Sampson *et al.* 1995; Avila 1998; Elsberry 1998). Mundell (1990 and 1991) found that extremely intense convection, inferred by infrared-satellite measurements, within a 666.6-km radius of the tropical cyclone center usually preceded rapid-intensification events by 12 hours.

The climatic (i.e., geographic and monthly) variability of tropical cyclone intensity characteristics was first studied by Frank and Jordan (1960). Whitney (1995)

and Whitney and Hobgood (1997) conducted a related study using 31 years of data for the eastern North Pacific. In their study, geographic stratifications were north or south of 18 degrees North latitude and east or west of 110 degrees West longitude. Significant geographic and monthly variations of intensity were found.

A necessary, but not sufficient, condition for tropical cyclone formation is a SST of at least 26 degrees Celsius ($^{\circ}\text{C}$) (Palmén 1948). Also, in the study of eastern North Pacific tropical cyclones by Whitney and Hobgood (1997), the MPI of a tropical cyclone was directly related to climatic SST.

Weak tropospheric vertical shear of the horizontal wind is another necessary, but not sufficient, condition for tropical cyclone development (Gray 1968). The vector difference of the horizontal winds at 200 and 850 mb is often used to quantify this vertical shear. In a study of western North Pacific tropical cyclones, Zehr (1992) found absolute values of 200- to 850-mb vertical shear greater than 12.5 m s^{-1} to be excessive and not conducive to tropical cyclone development. More recently, Fitzpatrick (1996 and 1998) found absolute values of 200- to 850-mb vertical shear greater than 8.5 m s^{-1} to be detrimental to tropical cyclone intensification. This present research used the latter 8.5-m s^{-1} threshold to stratify vertical shear.

Translation speeds greater than 10 m s^{-1} are not conducive to intensification (Sampson *et al.* 1995). The mean translation speed of eastern North Pacific tropical cyclones is 5 m s^{-1} (Whitney 1995; Hobgood 1998a). Tropical cyclone landfall has complex interactions with intensity change (Merrill 1987). Therefore, this proposed research will exclude data at and after landfall.

2.7 Statistical Prediction of Eastern North Pacific Tropical Cyclone Intensity Change

Recently, research in the Atmospheric Sciences Graduate Program at The Ohio State University has been directed at developing statistically based guidance for forecasting intensity change in eastern North Pacific tropical cyclones (Hobgood 1998a; Petty and Hobgood 1998; Petty 1997b). The research by Hobgood (1998a) paralleled and expanded upon similar statistical hurricane intensity forecasting (SHIFOR) research in the North Atlantic by Jarvinen and Neumann (1979). Using twelve years (i.e., 1982 to 1993) of best-track data (see Section 3.1 for details on this type of data) and climatic SST, ten predictors of future intensity change out to 72 hours were identified by Hobgood (1998a). These forecast variables are summarized in Table 2. Also shown in Table 2 is the variance of intensity change explained by these variables at each forecast period and the mean absolute intensity forecast errors for a regression model tested against independent best-track data from 1994. These errors compared favorably with mean absolute official NHC intensity forecast errors (Gross and Lawrence 1996).

Petty (1997b) and Petty and Hobgood (1998) added synoptic-scale environmental-forcing information derived from global-NWP-model data (see Section 3.1 for more details) to the statistical guidance product developed by Hobgood (1998a). That research was analogous to and went beyond that of DeMaria and Kaplan's (1994) statistical hurricane intensity prediction scheme (SHIPS) study in the North Atlantic. Additionally, Petty (1997b) and Petty and Hobgood (1998) used weekly SST, instead of climatic SST data used by DeMaria and Kaplan (1994). By combining the predictors derived from the global-NWP-model and best-track data for seven years (i.e., 1989 to 1995), a total of 16

significant predictors of intensity change were identified (Petty and Hobgood 1998). Petty's (1997b) wind-shear, thermal, moisture, and eddy-flux forecast variables are summarized in Table 2. Also shown in Table 2 is the variance of intensity change explained by these variables at each forecast period and the mean absolute intensity forecast errors for a regression model tested against independent best-track data from 1994. Similar to Hobgood (1998a), these errors compared favorably with mean absolute official NHC intensity forecast errors.

Summary of Eastern North Pacific Tropical Cyclone Intensity-change Forecasting Techniques Under Development at The Ohio State University					
Climatic and persistence forecast variables identified by Hobgood (1998a) in decreasing order of importance: 1. Latitude*; 2. Current intensity*; 3. Prior 12-hour intensity trend*; 4. Longitude; 5. Distance to land as calculated with Kaplan (1992); 6. Absolute value of the Julian date minus 237; 7. Potential intensification calculated by subtracting the current intensity from the MPI defined by Whitney and Hobgood (1997); 8. Zonal component of translation; 9. Meridional component of translation; 10. Translation speed*.					
Forecast Period					
12 hours	24 hours	36 hours	48 hours	60 hours	72 hours
Explained Variance (r^2) of Intensity Change for 1988 to 1993 regression by Hobgood (1998a)					
0.48	0.50	0.53	0.57	0.61	0.63
1994 Mean Absolute Forecast Errors ($m s^{-1}$) for Hobgood (1997)					
3	6	8	10	11	11
Synoptic-scale wind-shear, thermal, moisture, and eddy-flux forecast variables identified by Petty (1997b) in decreasing order of importance: 1. Absolute vertical wind shear between 500 and 850 mb; 2. Previous 24-hour trend of absolute vertical wind shear between 200 and 850 mb; 3. Zonal component of vertical wind shear between 200 and 850 mb; 4. Temperature difference between 500 and 850 mb; 5. Previous 24-hour trend of 700-mb equivalent potential temperature; 6. 200-mb planetary eddy flux convergence at 700-km radius; 7. Relative angular momentum at 850 mb; 8. Equivalent potential temperature difference between 700 and 850 mb.					
Explained Variance (r^2) of Intensity Change for 1989 to 1991 regression by Petty (1997b)					
0.60	0.59	0.60	0.63	0.66	0.67
1994 Mean Absolute Forecast Errors ($m s^{-1}$) for Petty (1997b)					
3	6	9	10	11	11

Table 2: Summary of eastern North Pacific tropical cyclone intensity-change forecasting techniques under development at The Ohio State University. * indicates the five forecast variables also used by Petty (1997b).

CHAPTER 3

DATA AND METHODOLOGY

3.1 NHC Postanalysis Best-track and Operational, Weekly SST, and ECMWF Model Data

Best-track data indicating postanalysis-determined tropical cyclone positions (0.1-degree increments) and intensities (2.6-m s⁻¹ increments) at six-hour intervals during each named tropical cyclone (i.e., only those tropical cyclones that reached tropical storm or hurricane intensity) from 1991 to 1997 were obtained from the NHC computer file server (<ftp://ftp.nhc.noaa.gov/pub/tracks/tracks.epa>). The data format is described by Davis *et al.* (1984). The positions and intensities for most of the tropical cyclones in the best-track data were determined by satellite techniques (Dvorak 1990). The errors associated with using the Dvorak intensity specification technique are not specifically known for the eastern North Pacific. However, in a study of North Atlantic tropical cyclones, Gaby *et al.* (1980) found the mean absolute difference (i.e., accuracy) between satellite-derived and *in situ* intensity measurements was 4 m s⁻¹ and the mean difference (i.e., bias) was -2 m s⁻¹. Similarly, in a study of western North Pacific tropical cyclones, Martin and Gray (1993) found the accuracy of satellite estimates was 10 m s⁻¹ and the bias was

5 m s⁻¹. The systematic intensity errors in the eastern North Pacific best-track data are most likely on the order of the errors found in the studies cited above.

In addition to the best-track data, operational NHC intensity forecast advisory error data for these tropical cyclones were obtained from the NHC via file transfer protocol and from the National Climatic Data Center (NCDC) on 3.5-inch computer diskettes in ASCII text format. This operational data contained errors in current intensity specification and position one might expect in real-time tropical cyclone forecasting operations at the NHC. Current operational forecasting guidance (e.g., SHIFOR) values were also contained with the operational data. To conduct realistic homogeneous comparisons of statistical forecast model performance, some of these operational data (e.g., current location, current intensity, prior 12-hour intensity trend, and translation speed) were used as input during the regression model testing phase of this research.

For the regression model training phase of this research, climatic and persistence variables were calculated from the best-track data in the same manner as Hobgood (1998a). The only exception was that the calculation of potential intensity change in this dissertation used weekly SST, instead of climatic SST data. Calculation of MPI used SST data from weekly operational analyses at the National Centers for Environmental Prediction (NCEP). These SST data were freely available from a data archive at Columbia University in sequential FORTRAN binary format (<http://ingrid.ldgo.columbia.edu/descriptions/reynoldsweekly.html>). The SST data are optimally interpolated weekly to a one-degree grid. Details concerning the SST data are described by Reynolds and

Smith (1994). SST values were extracted and MPI parameters calculated using the same FORTRAN 77 computer programs from Petty's (1997b) research.

The European Centre for Medium-range Weather Forecasts (ECMWF) global NWP model data used in this research were originally obtained from the National Center for Atmospheric Research (NCAR) data archive (<http://www.scd.ucar.edu/dss/datasets/ds111.2.html>). These model data were made available in binary format to the Atmospheric Sciences Graduate Program by the Byrd Polar Research Center at The Ohio State University. The model data were optimally interpolated every 12 hours (i.e., 0000 and 1200 Uniform Time Code [UTC]) to a 2.5-degree grid with 15 pressure levels. Synoptic-scale environmental-forcing predictors identified by Petty (1997a and b) and Petty and Hobgood (1998) were calculated using the same computer programs used in that previous research. The use of ECMWF model data to evaluate environmental forcing of tropical cyclones was previously shown to be useful by Molinari *et al.* (1992), West (1993a and b), Rodgers *et al.* (1994a), and Rodgers and Pierce (1995b).

Climatic, persistence, weekly SST, global-NWP-model-derived, and actual intensity-change variables that were calculated for this present research are summarized in Tables 3 to 5. Weekly SST data were used to calculate eastern North Pacific MPI using the following equation derived by Whitney and Hobgood (1997):

$$MPI = C_0 + C_I(SST) \quad (15)$$

where MPI is maximum potential intensity in units of m s^{-1} , C_0 is $-79.17262 \text{ m s}^{-1}$, C_I is $5.361814 \text{ m s}^{-1} \text{ }^{\circ}\text{C}^{-1}$, and SST is in units of $^{\circ}\text{C}$.

Climatic and Persistence Predictors	
Description of Predictor	Variable Name
Current latitude of tropical cyclone center of circulation ($^{\circ}$ N)	LAT
Current intensity of tropical cyclone (m s^{-1})	VMAX
Intensity change in the previous 12 hours (m s^{-1})	PVMAX12
Current longitude of tropical cyclone center of circulation ($^{\circ}$ W)	LON
Current distance to land (km)	DTL
Absolute value of current Julian date minus 237	ABSJDAY
Zonal component of prior 12-hour tropical cyclone motion (m s^{-1})	USM
Meridional component of prior 12-hour tropical cyclone motion (m s^{-1})	VSM
Prior 12-hour translation speed of tropical cyclone (m s^{-1})	CSM

Table 3: Climatic and Persistence Predictors (Hobgood 1998a).

Weekly SST and Global-NWP Predictors		
Description of Predictor	Radius of Calculation	Variable Name
Potential intensity change (MPI - VMAX) (m s^{-1})	400 km	POT
Current 500-850 mb absolute vertical shear (m s^{-1})	1 400 km	A5_8
Prior 24-h trend of 200-850 mb absolute vertical shear (m s^{-1})	1 400 km	DA2_8
Current 200-850 mb zonal component of vertical shear (m s^{-1})	1 400 km	U2_8
Current 500-850 mb temperature difference (K)	1 400 km	T5_8
Prior 24-h trend of 700 mb equivalent potential temperature (K)	1 400 km	DT_E7
Current 700-850 mb equivalent potential temperature difference (K)	1 400 km	T_E7_8
Current 200-500 mb meridional component of vertical shear (m s^{-1})	1 400 km	V2_5
Current areal relative angular momentum at 850 mb ($\text{m}^4 \text{s}^{-1}$)	800 km	RAM
Current 850 mb equivalent potential temperature (K)	1 400 km	T_E8
Current relative eddy angular flux convergence (m s^{-2})	1 400 km	R1400

Table 4: Weekly SST and Global NWP Predictors (Petty 1997b; Petty and Hobgood 1998).

Actual Intensity-change Variables from Best-Track Data	
Description of Dependent or Predicted Variable	Variable Name
Current intensity of tropical cyclone (m s^{-1})	VMAX
Future 12-hour intensity change (m s^{-1})	DVMAX12
Future 24-hour intensity change (m s^{-1})	DVMAX24
Future 36-hour intensity change (m s^{-1})	DVMAX36
Future 48-hour intensity change (m s^{-1})	DVMAX48
Future 60-hour intensity change (m s^{-1})	DVMAX60
Future 72-hour intensity change (m s^{-1})	DVMAX72

Table 5: Actual Intensity-change Variables from Best-Track Data.

3.2 DMSP Constellation of Satellites

A series of seven DMSP satellites (Block 5D-2) have been launched since 1987. These satellites included flight numbers (F-#): F-8, F-9, F-10, F-11, F-12, F-13, and F-14. All of these satellites were equipped with an SSM/I except for F-9. The SSM/I on F-12 failed to function properly shortly after launch. In January 1989, the F-8 experienced a partial failure of its SSM/I and the satellite mission was terminated in August 1991. Satellites F-10 and F-11 formed a two-SSM/I constellation for observations of tropical cyclones from late-1991 to 1994. The additional launch of F-13 in early-1995 created a three-SSM/I constellation for the 1995 to 1996 tropical cyclone seasons. F-14's launch in early-1997 completed a four-SSM/I constellation for the 1997 tropical cyclone season. Failure of F-10 in November 1997 left the currently operational DMSP constellation with three functioning SSM/I-equipped satellites.

Specific information about the orbits of the relevant DMSP satellites is contained in Table 6. DMSP satellite orbits are near-circular, near-polar, and Sun-synchronous (i.e., the satellite crosses the Equator at the same local time each day). Inclination of the satellite orbital plane is 98.8 degrees from the Equator resulting in a retrograde orbit. The period for an orbit is 102 minutes, which yields 14.1 orbits per day. One satellite, F-10, did not reach its desired orbit. Therefore, its Equator-crossing time changed at a highly substantial rate before its failure. All of the SSM/I-equipped satellites listed in Table 6 are currently functioning properly and within specification limits, except as noted.

Flight Number	Launch Date	Equator-Crossing Times Upon Launch [Local Standard Time]		Equator-Crossing Times as of May 1998 [Local Standard Time]		Maximum Altitude (km)	Minimum Altitude (km)
		ascend	descend	ascend	descend		
F-10*	1 Dec 90	1942	0742	----	----	861	726
F-11	28 Nov 91	1702	0502	1915	0715	878	836
F-13	24 Mar 95	1743	0543	1745	0545	877	840
F-14	4 Apr 97	2039	0839	2045	0845	877	843

Table 6: DMSP Orbital Characteristics. * F-10 failed on 14 November 1997.

3.3 SSM/I Instrument Specifications

The SSM/I is a seven-channel, four-frequency, linearly polarized, passive-microwave radiometer (Hollinger *et al.* 1990). Spectral channels include vertically and

horizontally polarized electromagnetic radiation at 19.4, 37.0, and 85.5 GHz. Only vertically polarized radiation is measured at 22.2 GHz. Resolution of the channels is displayed in Table 7 (Hollinger *et al.* 1990; Poe 1997; Bauer and Grody 1995). Absolute accuracy of the SSM/I-measured brightness temperatures compared to aircraft measurements is less than 3.0 K. Intercalibration of the brightness temperatures measured by the F-10, F-11, and F-13 SSM/I's is between 0.1 to 0.5 K (Wentz 1995; Poe 1997; Colton *et al.* 1996).

Channel Information		Spectral Resolution (GHz)	Radiometric Resolution (K)	Spatial Resolution (km)			Sampling Resolution (km)
Center Frequency (GHz)	Polarization			Along-Track	Along-Scan (IFOV)	Along-Scan (EFOV)	
19.4±0.13	Vertical	0.24	≤ 0.50	69	43	70	25.0
19.4±0.13	Horizontal	0.24	≤ 0.48	69	43	70	25.0
22.2±0.13	Vertical	0.24	≤ 0.55	60	40	65	25.0
37.0±0.55	Vertical	0.90	≤ 0.37	37	28	55	25.0
37.0±0.55	Horizontal	0.90	≤ 0.37	37	29	55	25.0
85.5±0.80	Vertical	1.40	≤ 0.58	15	13	14	12.5
85.5±0.80	Horizontal	1.40	≤ 0.57	15	13	14	12.5

Table 7: SSM/I-channel Resolution Information. IFOV means instantaneous field of view (FOV) and EFOV means effective FOV.

SSM/I scanning characteristics and the resulting geometry are portrayed in Figures 4 through 7. The SSM/I is a conically scanning imager with an active scan angle

of 102.4 degrees limited by the body of the spacecraft. Depression and look angles of 45 degrees and a nominal orbital altitude of 833 km yield an incidence or zenith angle of 53.1 degrees. The conical scan, active scan angle, and orbital altitude result in a ground swath of about 1394 km. The satellite travels with a speed of 6.58 m s^{-1} and the scan period is 1.899 s. Therefore, the satellite ground track is 12.5 km per scan, which nearly equals the spatial resolution of the 85.5-GHz channels. At a sampling interval of 4.22 ms, 128 samples are recorded on every clockwise (i.e., left-to-right) scan for the 85.5-GHz channels. The remaining channels are sampled on every other scan at a 8.44-ms interval resulting in 64 samples.

During each scan, the SSM/I is calibrated with a cold target (i.e., a mirrored reflection of deep space, which has a brightness temperature of about 2.7 K) and a warm target with a brightness temperature near 300 K obtained by three precision thermistors. The conically scanning nature of the SSM/I yields a constant incidence angle (i.e., 53.1 degrees) and sensor-to-ground distance throughout each scan. This constant incidence angle allows for invariable planes of polarization and a large fixed polarization difference. Also, the constant sensor-to-ground distance results in uniform spatial resolutions and a consistent pathlength along each scan. Therefore, the limb-darkening problem common to cross-track scanners is avoided.

3.4 SSM/I-related Data

Data measured by the SSM/I are stored onboard the satellite until transmitted to ground receiving and processing stations. During initial processing, these raw data are

quality controlled. That is, the data are decommutated, deinterleaved, bit-flipped, and restructured into properly ordered orbits. Using scan calibration data, satellite ephemeris, and attitude corrections, a geolocated antenna temperature file called a Temperature Data Record (TDR) is created containing data from all seven channels. The geolocation (i.e., ground navigation data) accuracy of each SSM/I sample is less than 6 km (Hollinger 1991). This 6-km accuracy is obtained by applying roll, yaw, and pitch geometric corrections contained in the TDR. Without these geometric corrections, the geolocation errors would be 30 to 40 km. A correction for spill-over, cross-polarization coupling, and antenna pattern effects caused by the parabolic reflector used in the SSM/I is required. Therefore, an antenna pattern correction is applied to the TDR to produce a brightness temperature, T_B , file called a Sensor Data Record (SDR). Through the use of scientifically developed algorithms, the SDR can be converted into a file containing geophysical parameter data (e.g., rainfall) called an Environmental Data Record (EDR).

SSM/I TDR data for DMSP satellite flight numbers F-10 and F-11 can be obtained for the late-1991 to late-1997 tropical cyclone seasons. In addition, F-13 data are available for the 1995 to 1997 seasons and F-14 data exist for the 1997 season. It should be noted that due to SSM/I problems on F-8 and F-12 during the period of interest, data from these specific radiometers were not available for this research. The specific SSM/I dataset used in this research is maintained by the Naval Research Laboratory (NRL) in two locations: Washington, District of Columbia (DC), and Stennis Space Center (SSC), Mississippi. Unfortunately, it is not a contiguous dataset. That is, not all of the data from SSM/I orbits from 1991 to 1997 are contained in the NRL library.

The available constellation of radiometers virtually assured at least one coincidental SSM/I observation during a tropical cyclone per day (Velden *et al.* 1989). The probability of at least two observations per day was greater than or equal to 0.89. Spatial and temporal coverage characteristics of SSM/I orbits are graphically summarized in Figures 8 through 10.

3.5 Querying Data Library for SSM/I Orbits with Coverage of Tropical Cyclones

Using best-track tropical cyclone positions as input, a computer program developed by the NRL in DC determined orbits with adequate coincidental SSM/I coverage. The computer program used actual radar-tracked DMSP orbital ephemeris and SSM/I scanning characteristics to perform the required calculations. Output of this program was input to a Corel® Quattro® Pro 7.0 spreadsheet database. Using database functions, orbits were selected from those available in the SSM/I library of the NRL in DC and SSC. In addition, SSM/I orbits of tropical cyclones located west of 140 degrees West longitude and after or near (i.e., within 55.5 km of a coastline) landfall were excluded from consideration. Determinations of distance to landfall were performed using the best-track positions and coastline positions as input to a computer program used at the NHC that was developed by Kaplan (1992) based upon previous research by Merrill (1987). Additional cases with corresponding best-track intensities less than 15 m s^{-1} (i.e., 30 knots or Dvorak (1990) Current Intensity Number 2.0) were also eliminated. SSM/I-based tropical cyclone center of circulation determinations (see Section 3.7 for

more details) are not feasible for these weaker tropical cyclone intensities (Hawkins, personal communication, 1997; Miller, personal communication, 1997).

3.6 Processing SSM/I Orbits with Coincidental Coverage of Tropical Cyclones

A computer software system developed by the NRL in MRY called TROPX was used to process data from SSM/I orbits with coincidental coverage of tropical cyclones. This tropical cyclone satellite data processing system is a component of the Naval Research Laboratory [NRL] Satellite Image Processing System (NSIPS). TROPX contains display and analysis software tools specifically tailored to conduct multispectral satellite remote sensing studies of tropical cyclones (Helveston *et al.* 1996). TROPX interfaces with Precision Visuals~Workstation Analysis and Visualization Environment (PV~WAVE®) software produced by Visual Numerics®, Incorporated. The combination of TROPX and PV~WAVE® allows SSM/I data to be processed from the raw data format found in the NRL's archive to TDR, SDR, and EDR products.

SSM/I data identified as containing coincidental coverage were extracted from the archive and transferred to a disk storage device attached to a UNIX workstation at the NRL in MRY. Further processing and database functions were performed by TROPX on the same workstation. TROPX can be controlled locally or remotely using an Internet telnet connection. Therefore, this research was conducted in both California and Ohio.

3.7 Locating the Tropical Cyclone Center

The 85.5-GHz horizontally polarized channel (i.e., an SDR product) on the SSM/I provides the necessary spatial resolution and radiometric response to accurately determine the center of tropical cyclones (i.e., to center fix) (Melton 1994; Zhao 1994; Alliss *et al.* 1993 and 1992; Rappaport 1991; Glass and Felde 1989 and 1990; Rhudy 1989; Velden *et al.* 1989). See Figure 11 for an example of a 85.5-GHz horizontally polarized T_B image created by the TROPX center-fixing tool that was useful for this task. The latitude and longitude of the center of circulation were recorded to the nearest 0.1 degree. Scan time of the center of circulation was recorded to the nearest minute. This information and linearly interpolated best-track data were used to assess the accuracy of tropical cyclone center fixes using SSM/I data. Figures 12 to 20 are 35-panel 85.5-GHz horizontally polarized T_B images produced by TROPX of the 315 SSM/I orbits identified for use in this present research.

3.8 Determining if SSM/I Coverage is Adequate

Once an accurate tropical cyclone center fix was accomplished, only an orbit with adequate coverage was further processed from a brightness-temperature (i.e., SDR) to a rain-rate (i.e., EDR) image. Swath-width considerations and bad or missing data can prevent adequate coverage by a coincidental SSM/I orbit. Adequate orbital coverage was defined as at least half coverage over the ocean of a circular area within 444.4 km of a tropical cyclone center 111.1 km or more from land. These criteria ensured adequate rainfall measurements over water and minimize effects due to landfall (Merrill 1987).

3.9 Applying the Operational Rainfall Algorithm

The rainfall algorithm (Ferraro *et al.* 1996) used in this study was selected for two reasons. First, it has the capability to measure both convective and stratiform rainfall over the ocean. Second, it is the current operational EDR rainfall algorithm (Colton and Poe 1994). See the figures from the case studies discussed in Section 4.6 for examples of rain-rate images produced by the NESDIS/ORA rainfall algorithm using TROPX.

3.10 Examining Rainfall and Intensity-change Correlations

Using Statistical Package for Social Sciences (SPSS®) Base Statistics 7.0 for Windows™ software, descriptive statistics and data analysis tools (e.g., scatter-diagrams, histograms, and regression [Glahn 1985]) were generated. The current and time tendency of convective or intense (i.e., greater than or equal to 3 mm h⁻¹) rainfall parameters for regions within 444.4 km of the tropical cyclone center were correlated with current intensity and ensuing 12- to 72-hour intensity changes calculated from the best-track data. Each SSM/I observation was assigned to the closest best-track time interval within six hours of 0000, 0600, 1200, or 1800 UTC. If more than one SSM/I observation corresponded to the same record, the observation closer in time and/or with better coverage was used. Every effort was made to maximize temporal coverage by the available SSM/I observations.

Regions were designated as *central core* (i.e., 0 to 55.5 km), *inner core* (i.e., 0 to 111.1 km), *core* (i.e., 0 to 222.2 km), and *total* (i.e., 0 to 444.4 km). These regions are depicted in Figure 21. Three convective rainfall parameters were calculated for these four

regions. The percentage of convective pixels (PCP) was calculated by dividing the number of pixels with rain rates greater than or equal to 3 mm h^{-1} by the total number of pixels in the region of interest. This PCP parameter contains information about the areal coverage of convective rainfall within the region of interest. The average of convective pixels (ACP) was calculated by summing the rain rates of those pixels greater than or equal to 3 mm h^{-1} and dividing by the number of those pixels. This ACP parameter gives information about the intensity of convective rainfall areas within the region of interest. A third parameter was created by multiplying ACP by PCP, which created an areally weighted ACP (WACP). Additionally, the prior 12-hour time tendencies of the three convective rainfall parameters described above were calculated. To maximize the number of cases for use in regression model training, some prior 18- and 6-hour trends were substituted for missing 12-hour time tendencies. The resulting number of candidate convective rainfall parameters was 24. These 24 parameters and their SPSS® variable names are summarized in Table 8 below.

Current			12-hour Tendency (Current - 12 hours prior)		
Percentage of Convective Pixels	Average of Convective Pixels	Weighted Average of Convective Pixels	Percentage of Convective Pixels	Average of Convective Pixels	Weighted Average of Convective Pixels
central: PCPH inner: PCP1 core: PCP2 total: PCP4	central: ACPH inner: ACP1 core: ACP2 total: ACP4	central: WACPH inner: WACP1 core: WACP2 total: WACP4	central: DPCPH inner: DPCP1 core: DPCP2 total: DPCP4	central: DACPH inner: DACP1 core: DACP2 total: DACP4	central: DWACPH inner: DWACP1 core: DWACP2 total: DWACP4

Table 8: Candidate Rainfall Parameters.

Stratifications were used to determine possible factors affecting significant convective rainfall parameter and intensity-change correlations. These stratifications included: current intensity, prior 12-hour rate of intensity change, season, location, SST, vertical shear of the horizontal wind, translation speed, and landfall status. Intensity stratifications were tropical depression (i.e., less than 17 m s^{-1}), tropical storm (i.e., 17 to 32 m s^{-1}), hurricane (i.e., 33 to 49 m s^{-1}), or strong hurricane (i.e., greater than or equal to 50 m s^{-1}). Rate of intensity change classes were previous 12-hour change in intensity greater than 10 m s^{-1} (i.e., rapid strengthening), 10 to -10 m s^{-1} (i.e., moderate), or less than -10 m s^{-1} (i.e., rapid weakening). Seasonal categories were peak (i.e., August and September), early (i.e., before August), and late (i.e., after September). Location categories were north or south of 18 degrees North latitude and east or west of 110 degrees West longitude. SST classes were less than 26°C or greater than or equal to 26°C . Vertical shear of the zonal component of the horizontal wind between 200 and 850 mb classes were weak (i.e., absolute value less than 8.5 m s^{-1}) or strong (i.e., absolute value greater than or equal to 8.5 m s^{-1}). The stratification categories for prior 12-hour average translation speed were slow (i.e., less than or equal to 5 m s^{-1}) or fast (i.e., greater than 5 m s^{-1}). Landfall stratification was whether or not the tropical cyclone made landfall during its existence.

3.11 Developing Rainfall Parameter and Intensity-change Prediction Model

Given the limited number of SSM/I observations of tropical cyclones that were available and a need to maximize the number of cases used to develop a multiple-linear-

regression prediction model, the minimum number of independent cases needed to conduct meaningful one-tailed paired t tests of forecast-error means for the various forecast methods was determined. Hinkle *et al.* (1988) developed an equation useful for this purpose:

$$n = \frac{\sigma^2(z_\beta - z_\alpha)^2}{(ES)^2} \quad (16)$$

where n is the minimum number of cases required, σ is the standard deviation, z_β and z_α are normal-probability standard scores for β and α , respectively, and ES is the effect size. The statistical significance is determined by α . As with other statistical tests in this research, the value of α used to calculate n was 0.05. Hinkle *et al.* (1988) stated that β ought to be in 4:1 ratio with α . Therefore, in this research β was 0.20. A medium effect size of 0.5σ suggested by Hinkle *et al.* (1988) was used to determine n for this research. Applying these assumptions and using a table of normal-probability standard scores, Equation 16 was solved as below:

$$n = 4 [0.842 - (-1.645)]^2 = 24.7 \approx 25 \quad (17)$$

Previous research (Hobgood 1998a; Petty 1997a and b) calculated forecast errors using independent cases from the 1994 tropical cyclone season. Consequently, the intention was to use independent cases from the same 1994 season for comparison purposes. However, the data available from 1994 for this research did not include at least 25 cases with future 72-hour intensity-change variables corresponding to the SSM/I

observations. Therefore, the first tropical cyclone from 1995 with the required number of cases to increase the number of cases with future 72-hour intensity-change values to 25 was selected and added to the independent or model testing dataset. Thus, Flossie (1995) was combined with the tropical cyclones from 1994 to create the model testing dataset. Tracks of all tropical cyclones studied in this research, those in the model development or training dataset, and those in the model testing or evaluation dataset are plotted in Figures 22 to 24. Table 9 summarizes which tropical cyclones were used in each dataset and the corresponding number of SSM/I observations used in this research.

Year	Tropical Cyclone Name	SSM/I observations for center-fix accuracy study	SSM/I observations for model development	SSM/I observations for model testing	Dead and missing persons*	Landfall during existence indicated by a X
1991	Kevin	12	12	-		
1992	Celia	10	8	-		
	Darby	7	7	-	7	
	Estelle	8	7	-		
	Frank	5	5	-		
	Georgette	7	7	-		
	Tina	30	24	-		
1993	Calvin	1	1	-	34	X
	Eugene	2	2	-		
	Greg	4	3	-		
	Hilary	1	1	-		X
	Jova	2	2	-		
	Kenneth	3	3	-		
	Lidia	2	2	-	2	X
1994	Aletta	2	-	2		
	Bud	1	-	1		
	Carlotta	1	-	1		
	Gilma	1	-	1		
	John	2	-	2		
	Kristy	2	-	2		
	Lane	6	-	6		
	Miriam	3	-	3		
	Norman	4	-	4		
	Olivia	12	-	12		
	Paul	3	-	3		
	Rosa	3	-	3	9	X

(to be continued)

Table 9: Summary of SSM/I orbits and tropical cyclone datasets used in this research.

Table 9 (continued)

Year	Tropical Cyclone Name	SSM/I observations for center-fix accuracy study	SSM/I observations for model development	SSM/I observations for model testing	Dead and missing persons*	Landfall during existence indicated by a X
1995	Adolph	7	7	-		
	Barbara	18	18	-		
	Cosme	3	3	-		
	Dalila	10	10	-		
	Erick	6	6	-		
	Flossie	6	-	6	7	
	Gil	9	9	-		
	Henriette	7	7	-		X
	Ismael	7	7	-	105	X
	Juliette	13	13	-		
1996	Alma	5	4	-	20	X
	Boris	3	3	-	10	X
	Christina	4	4	-	24	X
	Douglas	12	12	-		
	Elida	14	14	-		
	Fausto	7	7	-	1	X
	Genevieve	23	22	-		
	Hernan	7	3	-		X
1997	Linda	20	18	-		
Total		315	251	46	219	11

Table 9: Summary of SSM/I orbits and tropical cyclone datasets used in this research.

* Obtained from seasonal summaries: Rappaport and Mayfield (1992), Lawrence and Rappaport (1994), Avila and Mayfield (1995), Pasch and Mayfield (1996), Avila and Rappaport (1996), Rappaport and Mayfield (1997), and Lawrence (1998).

Tables of correlations (not shown) between the 24 candidate rainfall variables and 6 future intensity-change variables were created by SPSS®. Those candidate rainfall parameters found to be significantly correlated with future intensity changes at the 0.95 level were rank ordered by correlation coefficient as potential predictors for use in the multiple-linear-regression model development. Hinkle *et al.* (1988) provided guidelines for interpreting the meaning of correlation coefficients. These guidelines are summarized in Table 10 below:

Absolute value of correlation coefficient	Interpretation
0.9 to 1.0	Very high correlation
0.7 to 0.9	High correlation
0.5 to 0.7	Moderate correlation
0.3 to 0.5	Low correlation
0.0 to 0.3	Little, if any, correlation

Table 10: Guidelines for Interpreting Correlation Coefficients (Hinkle *et al.* 1988).

Rainfall parameters with at least a low correlation coefficient (i.e., $r \geq 0.3$) with future 12-, 24-, 36-, 48-, 60-, and 72-hour intensity changes were selected for further screening. To prevent multicollinearity (i.e, a violation of the assumption required for multiple linear regression that the predictors be independent of each other), correlation coefficients between predictors were calculated for screening purposes. Multicollinearity was assumed to exist between predictors with at least a moderate correlation with each other

(i.e., $r > 0.5$). The predictor with the higher correlation coefficient with future intensity change was chosen and the other rejected. Therefore, some potential predictors were screened out and others were selected for further regression analysis.

The selected potential predictors (i.e., independent variables) and dependent variables (i.e., actual 12- to 72-hour intensity changes) for the model development dataset (i.e., 1991 to 1997) were standardized. That is, all variables had the model-development-dataset mean for that variable subtracted from it and the resulting difference was divided by the standard deviation for the model development dataset. This allowed for nondimensional comparisons of the resulting standardized regression coefficients between predictors and across dependent variables (i.e., intensity changes for the different forecast time periods). Via the SPSS® stepwise multiple-linear-regression model development tool, a prediction model based solely upon rainfall parameters was constructed for reference purposes. The statistical significance level for entry into the regression model was 0.95 and 0.90 to remain.

Additionally, rainfall parameters were correlated with current intensity to identify quantitative satellite-derived variable(s) useful for tropical cyclone current intensity specification. The present operational method (Dvorak 1990) is qualitative and subject to the skill and experience of the analyst and the analyst's interpretation and application of its decision-tree and rule-based methodology.

3.12 Combining Rainfall Parameters with Hobgood and Petty Prediction Models

To evaluate the impact of rainfall parameters on other intensity-change prediction models under development for the eastern North Pacific (Hobgood 1998a; Petty and Hobgood 1998), two combined multiple-linear-regression models were constructed in the same manner as the rainfall-parameter model described in Section 3.11. Predictors described by Hobgood (1998a) were computed for the six-hour interval best-track data records that corresponded to observations of the rainfall parameters selected using the same model-development dataset as Section 3.11. Hobgood's (1998a) climatic and persistence predictors and the rainfall-parameter predictors selected in Section 3.11 were screened and input as predictor candidates into the SPSS® multiple-linear-regression model development tool in the same manner as described in Section 3.11. To combine the rainfall-parameter predictors with predictors from the Petty (1997a and b) and Petty and Hobgood (1998) models, it must be noted that the rainfall parameters were adjusted to correspond with 0000, 0600, 1200, or 1800 UTC. Those rainfall parameters derived from F-11 and F-13 SSM/I orbits were normally within three hours of either 0000 or 1200 UTC. F-14 orbits tended to observe eastern North Pacific tropical cyclones within two hours of 0600 or 1800 UTC. However, F-10 orbits were generally close to 0600 or 1800 UTC. The synoptic-scale environmental-forcing predictors were calculated from global-ECMWF-model data available only at 0000 and 1200 UTC. Therefore, to maximize the number of cases for regression model development, global-NWP-model predictors were interpolated to 0600 or 1800 UTC as required to correspond with the adjusted time of rainfall-parameter observations. The interpolation of NWP-model data is not uncommon

in real-time forecasting of tropical cyclones. The difference between interpolations in this research and real-time forecasting is that the interpolations in real-time forecasting involve forecasted model fields. In this research, the interpolations were between current analysis model fields.

3.13 Evaluating Intensity-change Prediction Models

The predictive skill of the two forecast models developed in Section 3.12 were evaluated by examining the intensity-change forecast errors they produced on a testing or evaluation dataset (i.e., 1994 and 1995) that was independent of the dataset used to create the models. Also, these errors were homogeneously compared to those produced by the following methods: Hobgood (1998a), Petty and Hobgood (1998), official NHC forecast advisories, and currently operational statistical intensity-change forecast guidance (e.g., SHIFOR). Three types of forecast errors were examined for each forecast interval from 12 to 72 hours. Mean intensity-change forecast error (i.e., bias in units of m s^{-1}) was the average value of the differences between the forecasted intensity changes and the intensity changes that actually occurred. Willmott (1982) termed this error *mean bias error* (MBE). Mean absolute intensity-change forecast error (i.e., accuracy in units of m s^{-1}) was the average absolute value of the differences between the forecasted intensity changes and the intensity changes that actually occurred. Willmott (1982) termed this error *mean absolute error* (MAE). A third forecast-error measurement was calculated by dividing MAE by the mean absolute intensity change (MAIC) for the forecast interval of interest. This type of forecast error was termed *mean relative absolute error* (MRAE).

MRAE was useful for comparing the forecast skill of each method and across forecast intervals.

To evaluate the regression-based forecast models, the predictor variables for the model evaluation dataset (i.e., 1994 and 1995) were standardized using the mean and standard deviation from the model development dataset (i.e., 1991 to 1997). These standardized values were input to the regression-based models. The output were converted from standardized values to forecasted intensity changes for comparison purposes. The forecast errors described above were calculated for all the previously discussed forecast methods at the 12- to 72-hour forecast periods. Forecast errors for the methods were graphically displayed using Quattro® Pro. To understand how well each method performed in various situations, forecast errors were stratified by the current intensity categories described in Section 1.1. The statistical significance of differences between mean forecast errors produced at each forecast period by the different methods was assessed by performing one-tailed paired *t* tests at the 0.95 level.

3.14 Conducting Case Studies

Tropical cyclones with particularly good spatial and temporal coverage by SSM/I orbits were candidates for in-depth case studies. Also, strong hurricanes with maximum intensities greater than or equal to 50 m s^{-1} were significant cases that could be insightful upon close examination. Additionally, those cases exhibiting rapid intensity changes or the concentric eyewall cycle could provide interesting examples of forecast model skill and operational implementation issues for challenging situations. Tropical cyclones Tina

(1992), Olivia (1994), and Linda (1997) were strong hurricanes and subjects of aerial reconnaissance research missions. Therefore, they were chosen for case studies. An additional tropical cyclone with relatively low intensities throughout its existence was also chosen for a case study. Genevieve (1996) had excellent temporal and spatial coverage by SSM/I orbits. However, this long-lasting tropical cyclone's maximum intensity was only that of a tropical storm. By studying a weaker tropical cyclone, one might learn why it did **not** intensify.

3.15 Surveying Rainfall Characteristics of Eastern North Pacific Tropical Cyclones

Descriptive statistics of convective-rainfall-coverage parameters for the regions shown in Figure 21 were computed for the intensity categories defined in Section 1.1. Calculations used all available SSM/I observations from 1991 to 1997. These calculations were further stratified by time of day in an effort to detect a diurnal cycle of rainfall.

3.16 Analyzing Tropical Cyclone Center-position Differences Using the SSM/I

Statistics describing the distance differences between SSM/I-determined tropical cyclone centers of circulation (see Section 3.7) and interpolated best-track locations were calculated for all SSM/I observations. Differences were stratified by intensity categories of tropical depression, tropical storm, and hurricane.

Previous research by Velden *et al.* (1989) evaluated the accuracy of 20 center fixes using F-8 SSM/I observations of tropical cyclones that were of at least tropical

storm intensity. The mean distance error compared to aerial-reconnaissance center fixes was about 34 km. Of the 20 center fixes, 12 were for tropical storms. For tropical storms, the mean distance error increased to about 42 km.

Gaby *et al.* (1980) stated the limit of tropical cyclone center-fixing accuracy by satellite platforms is three times the spatial resolution of the sensor. Therefore, in the case of the SSM/I 85.5-GHz horizontally polarized channel, the accuracy limit would be 37.5 km (i.e., 3×12.5 km). Sources of error when comparing SSM/I center fixes with linearized postanalysis best-track positions include the trochoidal path of tropical cyclone centers of circulation (i.e., average 28-km width) and the geolocation accuracy of the SSM/I data (i.e., 6 km). Martin and Gray (1993) postulated that satellite center-fix errors are a combination of satellite navigation errors and the analyst's inability to accurately determine the exact center of circulation in an often ambiguous satellite image.

Sheets and McAdie (1988) conducted a study of tropical cyclone center-fix accuracy by comparing visible and infrared geostationary satellite center fixes with best-track locations for the 1986 eastern North Pacific tropical cyclone season. Stratification by current intensity yielded the following mean distance differences: tropical depression--87 km, tropical storm--72 km, and hurricane--50 km. The usual appearance of an eye at hurricane intensity was suggested as a reason for the lower errors associated with center fixes of hurricanes.

CHAPTER 4

RESULTS AND DISCUSSION

4.1 Statistics Concerning Independent and Dependent Variables

Before detailing the accomplishments related to the specific research goals enumerated in Section 1.4, descriptive statistics concerning the independent and dependent variables used in this research are presented. This statistical description is divided between the regression model training and testing datasets. Tables 11 to 13 contain statistics for the model-training-dataset independent variables chosen as predictors by the multiple-linear-regression model development tool to be discussed in the following Section 4.4. The dependent variables for the model training dataset are statistically described in Table 14. The same independent and dependent variables for the model testing dataset are summarized in Tables 15 to 18, in a similar manner as the model training dataset. Climatic and persistence; weekly SST and global-NWP-model; and, convective rainfall independent variables are grouped onto separate tables. A discussion of the descriptive statistical results for the two datasets follows the tables below.

Descriptive Statistics for Significant Climatic and Persistence Predictors for Model Training Dataset					
Variable Name	Mean	Minimum	Maximum	Standard Deviation	Number of Cases
LAT (°N)	17.5	9.2	25.7	3.4	251
VMAX (m s ⁻¹)	33.0	10.0	82.0	15.8	251
PVMAX12 (m s ⁻¹)	0.1	-15.3	23.0	6.4	251
LON (°W)	-114.4	-142.7	-89.4	10.0	251

Table 11: Descriptive Statistics for Significant Climatic and Persistence Predictors for Model Training Dataset.

Descriptive Statistics for Significant Weekly SST and Global-NWP Predictors for Model Training Dataset					
Variable Name	Mean	Minimum	Maximum	Standard Deviation	Number of Cases
POT (m s ⁻¹)	32.3	0.4	62.3	16.2	225
U2_8 (m s ⁻¹)	2.8	-7.5	16.8	4.3	225
DT_E7 (K)	-0.8	-6.3	7.5	2.4	225
V2_5 (m s ⁻¹)	0.2	-4.9	8.7	2.5	225
RAM ($\times 10^{14}$ m ⁴ s ⁻¹)	5.0	-2.5	13.0	3.0	225
T_E8 (K)	337.1	316.6	349.1	6.1	225

Table 12: Descriptive Statistics for Significant Weekly SST and Global-NWP Predictors for Model Training Dataset.

Descriptive Statistics for Significant Convective Rainfall Predictors for Model Training Dataset					
Variable Name	Mean	Minimum	Maximum	Standard Deviation	Number of Cases
PCPH (%)	44.1	0.0	100.0	32.0	251
DWACPH (mm h ⁻¹)	-0.6	-10.8	8.2	3.4	174
PCP1 (%)	37.6	0.0	95.5	24.8	251
WACP4 (mm h ⁻¹)	0.7	0.0	3.3	0.7	251

Table 13: Descriptive Statistics for Significant Convective Rainfall Predictors for Model Training Dataset.

Descriptive Statistics for Actual Intensity-change Variables for Model Training Dataset					
Variable Name	Mean	Minimum	Maximum	Standard Deviation	Number of Cases
DVMAX12 (m s ⁻¹)	-0.1	-21	23	6.8	248
DVMAX24 (m s ⁻¹)	-0.4	-28	41	12.3	241
DVMAX36 (m s ⁻¹)	-0.8	-36	54	16.8	227
DVMAX48 (m s ⁻¹)	-1.8	-44	62	20.8	210
DVMAX60 (m s ⁻¹)	-2.6	-49	67	22.7	191
DVMAX72 (m s ⁻¹)	-3.8	-51	62	23.9	173

Table 14: Descriptive Statistics for Actual Intensity-change Variables for Model Training Dataset.

Descriptive Statistics for Significant Climatic and Persistence Predictors for Model Testing Dataset					
Variable Name	Mean	Minimum	Maximum	Standard Deviation	Number of Cases
LAT (°N)	18.1	11.9	23.5	2.9	46
VMAX (m s ⁻¹)	27.7	12.8	64.1	13.8	46
PVMAX12 (m s ⁻¹)	-0.3	-18.0	15.4	5.8	46
LON (°W)	-120.0	-136.6	-106.5	8.9	46

Table 15: Descriptive Statistics for Significant Climatic and Persistence Predictors for Model Testing Dataset.

Descriptive Statistics for Significant Weekly SST and Global-NWP Predictors for Model Testing Dataset					
Variable Name	Mean	Minimum	Maximum	Standard Deviation	Number of Cases
POT (m s ⁻¹)	37.9	6.2	57.6	14.9	42
U2_8 (m s ⁻¹)	7.2	-10.1	16.4	7.4	42
DT_E7 (K)	-2.0	-12.4	4.0	3.7	42
V2_5 (m s ⁻¹)	1.0	-5.2	10.7	3.5	42
RAM ($\times 10^{14}$ m ⁴ s ⁻¹)	3.0	-4.8	11.0	4.0	42
T_E8 (K)	336.6	324.8	347.8	5.5	42

Table 16: Descriptive Statistics for Significant Weekly SST and Global-NWP Predictors for Model Testing Dataset.

Descriptive Statistics for Significant Convective Rainfall Predictors for Model Testing Dataset					
Variable Name	Mean	Minimum	Maximum	Standard Deviation	Number of Cases
PCPH (%)	35.7	0.0	99.2	30.0	46
DWACPH (mm h ⁻¹)	-0.4	-11.3	12.0	4.7	28
PCPI (%)	28.9	0.0	75.1	20.6	46
WACP4 (mm h ⁻¹)	0.6	0.0	2.7	0.7	46

Table 17: Descriptive Statistics for Significant Convective Rainfall Predictors for Model Testing Dataset.

Descriptive Statistics for Actual Intensity-change Variables for Model Testing Dataset					
Variable Name	Mean	Minimum	Maximum	Standard Deviation	Number of Cases
DVMAX12 (m s ⁻¹)	-1.1	-23	13	7.0	45
DVMAX24 (m s ⁻¹)	-1.4	-26	33	12.8	43
DVMAX36 (m s ⁻¹)	-2.2	-33	36	17.4	39
DVMAX48 (m s ⁻¹)	-2.0	-41	41	22.9	33
DVMAX60 (m s ⁻¹)	-4.1	-46	38	25.1	29
DVMAX72 (m s ⁻¹)	-3.3	-46	51	27.8	25

Table 18: Descriptive Statistics for Actual Intensity-change Variables for Model Testing Dataset.

Climatic and persistence variables were comparable between the two datasets. A difference between the two datasets was that the average current intensity (i.e., VMAX) of the cases used for testing was about 5 m s^{-1} less than the cases used for model development. Also, the range of current intensities for the testing cases was about 20 m s^{-1} less than the training dataset. These differences were attributed to the use of cases from intensity-record-breaking Hurricane Linda (1997) in the model training dataset.

Weekly SST and global-NWP-model predictors were also comparable between the two datasets. There were two differences worth noting. The average potential intensity change (i.e., POT) was about 5 m s^{-1} more for the testing cases than the model training cases. This was due to the lower average VMAX for the testing cases that was noted above, because $\text{POT} = \text{MPI} - \text{VMAX}$. Average MPI for both datasets was about 67 m s^{-1} . Average vertical shear of the zonal horizontal wind between 200 and 850 mb (i.e., U2_8) was about 4 m s^{-1} more for the testing cases than the training cases.

Average convective-rainfall-coverage variables (i.e., PCPH and PCP1) were nearly 9 percent greater for the model training dataset than the testing cases. The range of PCP1 was about 20 percent less for the testing cases than the training cases. Averages of dependent variables were comparable between the datasets. Given the above-noted minor differences between independent variables and the similarities between dependent variables for the two datasets, it was reasonable to expect a meaningful evaluation of forecast errors on the testing cases using models developed from the training dataset.

4.2 Accomplishment of Primary Goal 1: Rainfall and Intensity Correlations

This and following sections document the accomplishment of several goals of this research listed in Section 1.4. Primary Goal 1 was to determine if statistically significant correlations between rainfall parameters and current intensity and future intensity change existed. Using all available cases, tables of correlations (not shown) between candidate rainfall parameters (see Table 8) and dependent intensity variables (see Table 5) were created. Those rainfall variables with at least a low correlation (i.e., $r \geq 0.3$, significant at the 0.95 level) with intensity variables were selected for further screening. Many of the selected rainfall variables had very high correlation coefficients with other rainfall variables. Averages of convective pixels over the four regions (i.e., ACP variables) were often highly correlated with percentages of convective pixels (i.e., PCP variables) for the same region. PCP variables were more correlated with intensity variables than ACP variables. Therefore, to prevent confounding effects due to multicollinearity, ACP variables were disregarded from further study. The threshold for multicollinearity between independent variables was a moderate correlation (i.e., $r > 0.5$, significant at the 0.95 level) between the two variables. The statistically significant correlation coefficients between dependent intensity variables and rainfall variables that survived this screening procedure are listed in Table 19.

Most of the rainfall variables in Table 19 had a low, though significant, correlation with intensity variables. The exception was inner-core PCP, which had a moderate correlation (i.e., $r = 0.6$) with current intensity. This correlation was of similar sign and magnitude as relevant studies discussed in Section 2.5 (cf. Rhudy 1989; Rodgers

and Adler 1981; Felde and Glass 1991). Areally weighted average of convective pixels and prior 12-hour trend of these averages (e.g., WACP4 and DWACPH) dominated the variables in Table 19. Thus, Primary Goal 1 was accomplished.

Statistically Significant Rainfall and Intensity Variable Correlations			
Dependent Intensity Variable	Independent Rainfall Variables	Correlation Coefficient*	Number of Cases
VMAX	PCP1	0.6	297
DVMAX12	PCPH	0.4	293
	WACP4	0.4	293
	DWACPH	0.4	198
DVMAX24	WACP4	0.4	284
	DWACPH	0.4	190
DVMAX36	WACP4	0.4	266
	DWACPH	0.4	175
DVMAX48	WACP4	0.4	243
	DWACPH	0.4	159
DVMAX60	WACP4	0.3	220
	DWACPH	0.3	143
DVMAX72	WACP4	0.3	198

Table 19: Statistically Significant Rainfall and Intensity Variable Correlations.

* Correlation coefficients are all significant at the 0.95 level.

4.3 Accomplishment of Primary Goal 2: Stratified Rainfall and Intensity Correlations

The second primary goal was to examine significant rainfall and intensity correlations via stratified statistical analysis using various categories listed in Section 3.10. Stratified statistical analysis of correlation coefficients between significant rainfall and intensity variables for all 297 cases is contained in Table 20. The effects of stratifications on correlations between rainfall and intensity are discussed below.

As current intensity increased, the following correlations increased: inner-core PCP and current intensity; prior 12-hour trend in central-core WACP and future 12-hour intensity change; and, prior 12-hour trend in central-core WACP and future 24-hour intensity change. This result was similar to that found in SSM/I studies of tropical cyclones in the Atlantic and western North Pacific by Rodgers *et al.* (1994b) and Rodgers and Pierce (1995a), respectively. Also, this result supported a computational study by van Delden (1989) that found the deepening of tropical cyclones via diabatic heating by latent heat release within 111.1 km was increasingly effective as tropical cyclone intensity increased. The correlation between total WACP and future 36-hour intensity change decreased with increasing current intensity. This differential effect was probably due to the area over which the rainfall parameter was calculated and the stage of tropical cyclone development. Convection within the large 444.4-km radius appeared to be more important to future 36-hour intensity change in weaker tropical cyclones. This result confirmed a one- to three-day lag time between latent heat release within 444.4 km and future tropical cyclone development demonstrated in earlier numerical tropical cyclone prediction model studies by Kurihara and Tuleya (1974) and Rosenthal (1978).

Stratification	Category	Correlation Coefficients Between Intensity and Rainfall			
		VMAX	DVMAX12	DVMAX24	DVMAX36
		PCP1	DWACPH	DWACPH	WACP4
Current Intensity	$< 17 \text{ m s}^{-1}$	0.3	0.1	-0.0	0.7
	$17 - 32 \text{ m s}^{-1}$	0.3	0.3	0.3	0.6
	$33 - 49 \text{ m s}^{-1}$	0.3	0.4	0.5	0.4
	$\geq 50 \text{ m s}^{-1}$	0.4	0.5	0.5	0.1
Prior 12-h Intensity Trend	$< -10 \text{ m s}^{-1}$	0.9	0.4	0.4	-0.0
	$-10 - 10 \text{ m s}^{-1}$	0.7	0.3	0.4	0.3
	$> 10 \text{ m s}^{-1}$	0.4	0.5	0.4	-0.1
Time of Season	Early	0.4	0.4	0.4	0.5
	Peak	0.7	0.4	0.4	0.4
	Late	0.9	-0.2	0.5	-0.6
Location Within Basin	Northwest	0.8	0.4	0.4	-0.3
	Northeast	0.1	-0.3	0.1	-0.0
	Southeast	0.6	0.1	0.1	-0.1
	Southwest	0.7	0.4	0.5	0.5
SST	$< 26 \text{ }^{\circ}\text{C}$	0.7	0.3	0.3	-0.5
	$\geq 26 \text{ }^{\circ}\text{C}$	0.6	0.3	0.4	0.3
Absolute Value of Zonal Vertical Shear (200-850 mb)	$< 8.5 \text{ m s}^{-1}$	0.6	0.4	0.4	0.3
	$\geq 8.5 \text{ m s}^{-1}$	0.8	0.2	0.5	0.5
Prior 12-h Translation Speed	$\leq 5 \text{ m s}^{-1}$	0.7	0.3	0.4	0.4
	$> 5 \text{ m s}^{-1}$	0.6	0.5	0.5	0.4
Landfall During Existence	Yes	0.4	-0.1	0.2	0.2
	No	0.7	0.5	0.4	0.5
Overall		0.6	0.4	0.4	0.4

Table 20: Stratified Correlation Coefficients Between Intensity and Rainfall Parameters. Only those coefficients significant at the 0.95 level are bolded.

The overwhelming majority of cases in this research did not involve rapid intensity changes. Therefore, most correlations between rainfall and future intensity changes were not statistically significant for rapid intensity-change categories. There were two exceptions. Rapidly weakening tropical cyclones in this present study exhibited a very high correlation (i.e., $r = 0.9$) between inner-core PCP and current intensity. The areal coverage of inner-core convection appeared to be an important factor during rapid weakening. However, the direction of causality cannot be directly inferred from this very high correlation. That is, one cannot determine if rapid weakening caused areal coverage of inner-core convection to increase or *vice versa*. Nonetheless, the very high correlation indicated that inner-core PCP was a good specifier of current intensity during rapid weakening. A second exception was the correlation between the prior 12-hour trend in central-core WACP and future 12-hour intensity change for rapid intensifiers. For this category, the correlation was greater than other categories of prior intensity trend. This increased correlation for rapid intensifiers suggested that the trend in central-core convective rainfall was better related to future 12-hour intensity change when tropical cyclones underwent rapid intensification.

The correlations between convective rainfall and intensity differed significantly according to when the tropical cyclone occurred during the season. The correlation between current intensity and inner-core coverage by convective rainfall increased from early to late in the season. However, the correlation between total WACP reversed sign from early to late in the season. These results were most likely due to the common scenario that tropical cyclones in the late part of the season were: weaker by an average of

6 m s⁻¹; dissipating over cooler water; and, experiencing higher vertical wind shear than those in the early and peak portions of the season. Despite increased convective rainfall this decay could not be countered.

The variation of correlation coefficients according to location stratification was due mainly to the tracks of the tropical cyclones used in this present study. Most tracks went through the southern and western portions of the basin. Those tracks in the southwestern portion of the basin were over warmer water where increases in convective rainfall ought to have been associated with intensification. Based upon climatic knowledge of this ocean basin, cases over the northwestern portion of the basin typically experienced cooler water and higher environmental vertical wind shear. Therefore, as shown above, decreases in convection and decreases in current intensity tended to occur together (i.e., high positive correlation). The negative correlation for total WACP in the northwestern region was most likely due to a decoupling of the tropical cyclone from the lower boundary. This type of decoupling can occur when a tropical cyclone tracks over cool water and into high vertical wind shear. Therefore, convection that might have still been occurring could not effectively aid intensification of these generally recurving and dissipating tropical cyclones over the northwestern portion of the basin. The converse scenario might also be true. Convection could have been reduced in a decoupled tropical cyclone, while intensity remained high until the circulation spun down over cool water. Not enough cases over the eastern portion of the basin were available for statistically significant correlations to be calculated.

The SST stratification results can be explained in a similar manner as the aforementioned categories of late in the season and location in the northwestern portion of the basin. Movement of a tropical cyclone over cool water would normally result in weakening, despite the strength of its convective precipitation. In this category, total tropical cyclone convection could not overcome the negative influence of a cool SST (i.e., $< 26^{\circ}\text{C}$) on future intensity change.

Stratification results for categories of the absolute value of zonal tropospheric vertical wind shear were not as expected. Tropical cyclones that experienced strong values of vertical wind shear exhibited higher correlations between rainfall and intensity than those that experienced weak values of vertical shear. The average current intensities (i.e., VMAX) for both vertical wind shear stratifications were very similar (i.e., weak-- 34 m s^{-1} and strong-- 32 m s^{-1}). Consequently, the difference in correlation was not due to more intense tropical cyclones possibly being better able to maintain a positive relationship between rainfall and intensity despite strong vertical wind shear. The prior trends of intensity change for tropical cyclones in the strong vertical wind shear category were almost all negative--many were rapidly negative. Therefore, the correlation difference was similar to that found for rapidly weakening versus normal intensity-change categories. Decreasing intensity due to strong vertical wind shear was more highly correlated with decreasing convective rainfall than increasing intensity with increasing rainfall in a weak vertical wind shear.

Translation speed stratification did not appear to be significant. However, whether or not a tropical cyclone made landfall during its existence was significant.

Those cases where a tropical cyclone eventually made landfall had a lower correlation between rainfall and intensity variables. This was due to the fewer cases involving landfall in the total dataset and the complex interactions between landfall and intensity change described by Merrill (1987). Table 20 documents the accomplishment of Primary Goal 2.

4.4 Accomplishment of Primary Goal 3: Forecast Model Development

Primary Goal 3 was to develop multiple-linear-regression-based future intensity-change models that combined significant rainfall predictors identified above with predictors developed in previous research by Hobgood (1998a) and Petty and Hobgood (1998). To demonstrate the maximum variance that a solely rainfall-based model could explain, Table 21 was constructed. In Table 21, rainfall predictors had standardized regression coefficients that ranged between 0.2 and 0.3 throughout the forecast periods. The explained variance (i.e., r^2) only ranged from 25 to 8 percent for future 12- to 72-hour intensity changes, respectively. Given the moderate to low amount of explained variance, a rainfall-only model would most likely not improve upon the current suite of intensity-change guidance products available to tropical cyclone forecasters. However, combining the moderate amount of explained variance by rainfall parameters at the 12- to 36-hour forecast periods with the explained variance by predictors from other forecast models could increase the amount of explained variance of future 12- to 36-hour intensity change.

After screening for multicollinearity, the rainfall predictors in Table 21 were combined with Hobgood's (1998a) model and Petty and Hobgood's (1998) model using stepwise multiple linear regression. A single example of the SPSS® output for this regression procedure for the future 24-hour intensity-change forecast model involving rainfall and Hobgood (1998a) predictors is included in the Appendix. The standardized regression coefficients and explained variance for the resulting two new models are listed in Tables 22 and 23. The major improvement of explained variance by the new regression models involving rainfall parameters was an increase of explained variance by about 15 to 10 percent for the 12- to 36-hour forecast periods over the models of Hobgood (1998a) and Petty and Hobgood (1998). However, it should be noted that the model development dataset used in this present research was different than those used in their previous studies.

The model formed by combining convective rainfall and Hobgood (1998a) predictors is referred to as the Rain and Hobgood model (see Table 22) in discussions below. Similarly, combining convective rainfall with Petty and Hobgood (1998) predictors produced a model that is called the Rain and Petty model (see Table 23). When discussing both models together, they are described as the rain-related models.

Standardized Regression Coefficients for the Forecast Model Including Rainfall Predictors						
Time (h)	12	24	36	48	60	72
DWACPH	0.24	0.29	0.27	0.25	0.26	-
WACP4	0.18	0.30	0.34	0.24	0.18	0.28
PCPH	0.23	-	-	-	-	-
r^2	0.25	0.23	0.25	0.17	0.13	0.08
Cases	171	165	154	142	128	173

Table 21: Standardized Regression Coefficients for the Forecast Model Including Rainfall Predictors. Only those coefficients significant at the 0.95 level are displayed.

Standardized Regression Coefficients for the Forecast Model Including Rainfall, Climatic, Persistence, and Weekly SST Predictors						
Time (h)	12	24	36	48	60	72
DWACPH	0.15	0.12	-	-	-	-
WACP4	-	-	0.16	-	-	-
LAT	-0.18	-0.18	-0.14	-0.17	-0.28	-0.26
LON	-	-	-	-	0.40	0.28
PVMAX12	0.63	0.48	0.36	0.36	-	-
POT	-	0.31	0.42	0.47	-	-
VMAX	-	-	-	-	-0.45	-0.51
r^2	0.63	0.63	0.60	0.58	0.63	0.63
Cases	162	157	147	135	128	173

Table 22: Standardized Regression Coefficients for the Forecast Model Including Rainfall, Climatic, Persistence, and Weekly SST Predictors. Only those coefficients significant at the 0.95 level are displayed.

Standardized Regression Coefficients for the Forecast Model Including Rainfall, Climatic, Persistence, Weekly SST, and Global-NWP Predictors						
Time (h)	12	24	36	48	60	72
DWACPH	0.15	-	-	-	-	-
WACP4	-	-	0.16	-	-	-
LAT	-0.18	-0.18	-	-0.14	-0.26	-
LON	-	-	-	-	0.50	0.45
PVMAX12	0.63	0.43	0.39	0.25	-	-
POT	-	0.33	0.45	0.46	-	-
VMAX	-	-	-	-	-0.52	-0.52
T_E8	-	0.15	-	0.19	-	-
DT_E7	-	-	0.15	-	-	-
RAM	-	-	-	-0.13	-0.14	-0.22
U2_8	-	-	-	-	0.26	-
V2_5	-	-	-	-	-0.15	-
r^2	0.63	0.63	0.61	0.61	0.68	0.58
Cases	162	157	147	135	128	153

Table 23: Standardized Regression Coefficients for the Forecast Model Including Rainfall, Climatic, Persistence, Weekly SST, and Global-NWP Predictors. Only those coefficients significant at the 0.95 level are displayed.

Both rain-related models contained the same predictors for the 12-hour forecast period. Persistence of the prior intensity-change trend (i.e., PVMAX12) was the most important predictor at the 12-hour forecast period and had the highest standardized regression coefficient across all forecast periods. Latitude (i.e., LAT) and trend in central-core convective rainfall (i.e., DWACPH) had similar magnitudes of standardized regression coefficients at this forecast period. At the 24-hour forecast period, POT entered both rain-related models. Also, at the 24-hour forecast period, 850-mb equivalent potential temperature (θ_e) (i.e., T_E8) was selected instead of DWACPH in the Rain and Petty model. WACP4 was the rainfall parameter selected by both rain-related models in place of DWACPH for the 36-hour forecast period. The Rain and Petty model selected the time tendency of 700-mb θ_e (i.e., DT_E7) at the 36-hour forecast period, while LAT and TE_8, which were significant at the 24-hour period, were not selected. Beyond the 36-hour forecast period, rainfall parameters were not selected for the Rain and Hobgood and Rain and Petty models. Judging by the standardized regression coefficients for the rain-related models, the selected rainfall predictors had similar importance in predicting future intensity change as latitude and several of the global-NWP-model predictors (e.g., T_E8, DT_E7, and RAM). By including rainfall in the development of new intensity-change forecast models, Primary Goal 3 was achieved.

4.5 Accomplishment of Primary Goal 4: Forecast Error Comparisons

Given the accomplishment of Primary Goal 3, Primary Goal 4 involved a homogeneous evaluation and comparison of the forecast performance of the newly

created rain-related forecast models with previous forecast methods. Descriptive statistics for forecast errors defined in Section 3.13 are summarized in Table 24 for the new models, official NHC forecast advisories, and existing forecast guidance products. Mean absolute errors (MAE) for the homogeneous testing sample are graphically summarized in Figure 25.

Both rain-related forecast models produced the lowest 12-hour MAE of 2.8 m s^{-1} . At the 24-hour forecast period, the lowest MAE was 5.0 m s^{-1} for the Rain and Hobgood model. SHIFOR's 7.7 m s^{-1} MAE was the lowest for the 48-hour forecast period. MAEs for Hobgood's (1998a) model bested all other forecast methods with 9.7 and 10.4 m s^{-1} at the 60- and 72-hour forecast periods, respectively. An interesting result was that at least one objective forecast guidance product performed better on the model testing dataset than official NHC forecast advisories across all forecast periods.

Comparing MAEs for the rain-related models with other guidance models via one-tailed paired t tests found that only the MAE at the 12-hour forecast period for the Rain and Hobgood model was significantly less than the MAE at the 12-hour forecast period for the Hobgood (1998a) model at the 0.95 level. Mean relative absolute error (MRAE) provided a measure of forecast skill and allowed for quantitative descriptions of the importance of MAE differences in relation to other forecast methods. For example, the Rain and Hobgood model MRAEs for 12- and 24-hour forecast periods were 3 and 14 percent less, respectively, than those for official NHC forecast advisories.

Stratifications of the forecast models' mean bias errors (MBE) by current intensity (not shown) found that all models tended to **underforecast** future intensity changes for

tropical **depressions** and tropical **storms**. MBEs became increasingly negative for these categories of tropical cyclones as forecast period increased. All models tended to **overforecast** future intensity changes for **hurricanes** and strong hurricanes. As forecast period increased, MBEs for these tropical cyclone categories became increasingly positive. There were not enough cases with rapid intensity changes in the testing dataset to conduct a meaningful stratification analysis of forecast errors for rapid intensity change categories. Table 24 and Figure 25 illustrate the accomplishment of Primary Goal 4.

Homogeneous Comparisons of Forecast Model Performance on Testing Dataset								
Forecast Method	Forecast Period (h)	Mean Bias Error (m s ⁻¹)	Mean Absolute Error (m s ⁻¹)	Mean Absolute Intensity Change (m s ⁻¹)	Mean Relative Absolute Error (%)	Minimum (m s ⁻¹)	Maximum (m s ⁻¹)	Number of Cases
Official NHC forecast advisories	12	0.6	2.9	5.2	56	-10.3	10.3	45
	24	1.1	6.4	10.0	64	-28.2	25.6	43
	36	1.2	8.0	13.9	58	-28.2	20.5	39
	48	-1.2	9.6	18.2	53	-28.2	15.4	33
	60	-	-	20.2	-	-	-	-
	72	1.3	12.4	21.3	58	-41.0	23.1	25
SHIFOR	12	-0.3	3.2	5.2	62	-10.3	19.5	45
	24	-1.4	5.9	10.0	59	-29.2	15.9	43
	36	-1.7	7.7	13.9	55	-31.3	12.3	39
	48	-3.0	9.6	18.2	53	-34.9	13.9	33
	60	-	-	20.2	-	-	-	-
	72	-2.0	12.0	21.3	56	-41.5	12.8	25
Rainfall, Climatic, Persistence, and Weekly SST Predictors	12	0.9	2.8	5.2	53	-6.0	23.2	27
	24	2.0	5.0	10.0	50	-13.2	17.8	25
	36	1.9	8.7	13.9	63	-26.0	25.5	35
	48	1.0	10.7	18.2	59	-28.6	18.7	30
	60	-4.3	12.0	20.2	59	-36.2	12.2	29
	72	-2.7	12.1	21.3	57	-40.2	14.4	25
Rainfall, Climatic, Persistence, Weekly SST, and Global-NWP Predictors	12	0.9	2.8	5.2	53	-6.0	23.2	27
	24	0.9	5.6	10.0	56	-20.7	19.8	39
	36	0.9	9.2	13.9	66	-26.3	27.2	35
	48	2.4	10.8	18.2	59	-27.8	19.6	30
	60	1.2	14.5	20.2	72	-33.4	30.6	27
	72	-0.1	14.5	21.3	68	-43.5	24.2	25

(to be continued)

Table 24: Homogeneous Comparisons of Forecast Model Performance on Testing Dataset.

Table 24 (continued)

Forecast Method	Forecast Period (h)	Mean Bias Error (m s ⁻¹)	Mean Absolute Error (m s ⁻¹)	Mean Absolute Intensity Change (m s ⁻¹)	Mean Relative Absolute Error (%)	Minimum (m s ⁻¹)	Maximum (m s ⁻¹)	Number of Cases
Hobgood (1998a)	12	-0.9	3.9	5.2	75	-13.4	22.0	41
	24	0.6	5.8	10.0	58	-25.9	15.9	39
	36	0.7	8.0	13.9	58	-27.8	18.6	35
	48	0.5	10.3	18.2	57	-32.2	21.2	30
	60	1.9	9.7	20.2	48	-25.8	20.8	27
	72	2.3	10.4	21.3	49	-32.8	17.9	25
Petty and Hobgood (1998)	12	0.4	2.9	5.2	56	-6.8	19.5	41
	24	-0.2	5.3	10.0	53	-22.9	13.0	39
	36	0.5	7.6	13.9	54	-27.4	17.7	35
	48	1.1	10.4	18.2	57	-32.9	18.6	30
	60	4.2	10.7	20.2	53	-26.0	19.4	27
	72	5.0	11.1	21.3	52	-30.6	19.5	25

Table 24: Homogeneous Comparisons of Forecast Model Performance on Testing Dataset.

4.6 Accomplishment of Primary Goal 5: Case Studies

Case studies on Hurricane Tina (1992), Hurricane Olivia (1994), Tropical Storm Genevieve (1996), and Hurricane Linda (1997) were chosen to address Primary Goal 5. Each case study contains at least: a plot of the tropical cyclone's track; images of SSM/I-based rain-rate images; time series of intensity and significant variables (e.g., PCP1, TE_8, and absolute value of U2_8); and, homogeneous MAEs of forecast models discussed in Section 4.5 for 12- to 72-hour forecast periods. Of the cases studies, only Hurricane Olivia (1994) was independent of the model development dataset. Therefore,

the other tropical cyclone case studies were simply a stratification based upon a single tropical cyclone. However, real-time operational intensity and location information were input to the forecast models instead of best-track data to allow for more realistic homogeneous comparisons of forecast errors.

4.6.1 Case Study of Hurricane Tina (1992)

The track of Hurricane Tina (1992) is plotted in Figure 26. Figures 27 and 28 depict rainfall obtained from SSM/I observations from 20 September to 10 October. The rain-rate images show a convective ring cycle that occurred from 27 to 29 September. A chart of temporal variations of convective rainfall and intensity is in Figure 29. Increases of intensity were preceded by increases of coverage by inner-core convective rainfall (i.e., PCP1) on both 27 and 28 September. As an inner eyewall was supplanted by an outer convective ring on 28 September (as seen in Figures 27 and 28 and indicated by a fluctuation of PCP1 in Figure 29), the rate of intensity change was reduced. As the new eyewall contracted, the intensity increased until 1 October. The temporal changes of MPI and T_E8 are shown in Figure 30. After 1 October, T_E8 and MPI decreased along with intensity. That is, Tina encountered relatively drier air and cooler SST (i.e., lower MPI) as its intensity decreased. Rapid weakening of intensity occurred along with large decreases of PCP1. Absolute value of U2_8 is plotted along with intensity in Figure 31. Strong values of vertical wind shear coincided with rapid weakening after 3 October.

Evaluation of the MAEs for forecast methods applied to Tina found that they were, in general terms, slightly greater at the 48- to 72-hour forecast periods than for the 1994 and 1995 testing dataset. The rain-related models outperformed the other forecast

models at all forecast periods, except the 12-hour period. At the 12-hour forecast period the Petty and Hobgood (1998) performed the best.

4.6.2 Case Study of Hurricane Olivia (1994)

Hurricane Olivia's (1994) track is plotted in Figure 33. Rain-rate images from 22 to 29 September are depicted in Figure 34. Close-up rain-rate images from SSM/I observations of Olivia on 24 and 26 September are shown in Figure 35. Radar rain-rate/reflectivity images included in Figure 36 were obtained from NOAA WP-3D hurricane research aircraft that were nearly contemporaneous (i.e., within about two hours) with the SSM/I observations in Figure 35. Figures 35 and 36 allow for qualitative comparisons. Highly similar patterns of rainfall were apparent between the images obtained from two different observational platforms. Figure 37 depicts the relationship between inner-core convective rainfall and current intensity. The peak value of PCP1 in Figure 37 preceded maximum intensity by approximately one day. The lag time between PCP1 and VMAX in Figure 37 was consistently about one day. Slight decreases of T_E8 and MPI coincided with decreases of intensity after 26 September, as Figure 38 illustrates. Extreme values of vertical wind shear, shown in Figure 39, preceded and persisted beyond the rapid decrease of intensity after 26 September.

Forecast model evaluation for Olivia is in Figure 40. The method of Petty and Hobgood (1998) outperformed the other models for all forecast periods, except the 24-hour period. At the 24-hour forecast period, the official NHC forecast advisory was superior. Overall, model forecast errors for Olivia were fairly similar to those on the regression model testing dataset for the 12- to 36-hour forecast periods. Model errors

widely diverged for the 48- to 72-hour forecast periods. The Petty and Hobgood (1998) and Hobgood (1998a) models clearly outperformed the rest of the models at the later forecast periods.

4.6.3 Case Study of Tropical Storm Genevieve (1996)

Tropical Storm Genevieve's (1996) track is plotted in Figure 41. The SSM/I rain-rate images from 29 September to 9 October are illustrated in Figures 42 and 43. These rain-rate images showed no organized convective rings, no eyewall, and only spotty coverage by intense convection. The variations of convective rainfall and intensity were relatively flat, as Figure 44 depicts. Changes in convective rainfall and intensity did not appear to be related. Given the low intensities, the MPI values plotted in Figure 45 were surprisingly high. Relatively dry and cool low-level air (i.e., low T_E8 values) impinged on Genevieve after 3 October and may have negatively affected intensification. Denney (1976) proposed that the inflow of cool and dry low-level air is a major factor to be considered when forecasting eastern North Pacific tropical cyclone intensity. Vertical wind shear values charted in Figure 46 were relatively low. The low vertical wind shear values could reflect a low amount of internal vertical wind shear associated with a weaker tropical cyclone. Winds throughout the troposphere were light as Genevieve's track meandered in two loops between 30 September and 8 October. Relatively warm SSTs, which are reflected by higher MPI values, and low vertical wind shear are considered necessary, but not sufficient, conditions for tropical cyclone development. In the case of Genevieve, low inner-core convection and inflow of dry and cool low-level air might

explain why intensification did not occur, despite warm water and low vertical wind shear.

Figure 47 demonstrates that official NHC and SHIFOR forecasts outperformed the other widely divergent models, except at the 60- and 72-hour forecast periods where the Rain and Petty model's performance was the best. When the MAEs for model forecasts of Genevieve were compared to those on the testing dataset, Genevieve's MAEs were found to be more divergent at all forecast periods. The Rain and Petty model was most accurate at the 72-hour forecast period. MBEs of all guidance models (not shown) were highly positive. This result indicated a tendency for forecast guidance products to overforecast future intensity change for this tropical cyclone.

4.6.4 Case Study of Hurricane Linda (1997)

The track of Hurricane Linda (1997) is plotted in Figure 48. Rain-rate images of SSM/I observations from 9 to 17 September are displayed in Figures 49 and 50. A worldwide-record-breaking 24-hour rapid intensity increase on 11 September was preceded about a day earlier by a rapid increase of inner-core convective rainfall. A convective ring cycle occurred from 11 to 13 September. As the outer convective ring surrounded an inner eyewall late on 12 September, intensity reached a plateau above 80 m s^{-1} . The inner eyewall dissipated on 13 September.

A moderate decrease of MPI and T_E8 (i.e., cooler SST and drier air, respectively) began on 13 September, as Figure 52 indicates. Figure 53 demonstrates the strong vertical wind shear Linda encountered on 14 September. The combination of dry air, cool water, and strong vertical wind shear caused Linda to rapidly weaken on and

after 14 September. Rapid PCP1 decreases coincided with rapid intensity decreases on and after 13 September.

This author was onboard an Air Force Reserve Command WC-130H aircraft when it performed an aerial reconnaissance mission in and around Linda on 14 September. From 1811 to 2307 UTC, four center fixes were performed. A comparison of the differences between the aircraft center fixes and linearly interpolated best-track location data found differences of less than 1 km for all four center fixes. By comparison, a center fix from the temporally closest observation by the SSM/I onboard F-10 at 1824 UTC differed from the linearly interpolated best-track location data by 21 km.

Forecast model performance was evaluated using MAEs in Figure 54. The MAEs for Linda were much larger than the model testing dataset. Beyond the 24-hour forecast period, the errors were widely divergent. Official NHC forecast advisories and SHIFOR were outperformed at every forecast period by other forecast guidance, except for the superior performance of official NHC forecast advisories at the 12-hour forecast period. Rain-related models outperformed the other models at the 24-, 60-, and 72-hour forecast periods. The Petty and Hobgood (1998) model was best for the 36- and 48-hour forecast periods. Analysis of MBEs (not shown) for Linda found they were highly negative for all methods. That is, all forecast methods, including official NHC forecast advisories, tended to greatly underforecast Linda's future intensity change. For example, SHIFOR had a -17 m s^{-1} MBE at the 48-hour forecast period.

The results and discussion of this case study and the three previous case studies in this section demonstrate the accomplishment of Primary Goal 5.

4.7 Accomplishment of Secondary Goal 1: Convective Ring Cycle Analysis

Determination of the convective ring cycle via rainfall parameters was the first secondary goal. Qualitative analysis of the convective ring cycle was accomplished by observing and noting the temporal changes of patterns on rain-rate images, plots of inner-core convective rainfall, and contemporaneous variation of intensity in the aforementioned case studies of Hurricane Tina (1992) and Hurricane Linda (1997) in Section 4.6.

Some limitations on the use of the SSM/I to monitor the convective ring cycle in near real time were found to exist. Temporal resolution of SSM/I observations of tropical cyclones is a function of the number of nominally operating SSM/I-equipped satellites in orbit, the limited SSM/I swath width, and the location of the tropical cyclone of interest. Even if an orbit passes directly overhead a tropical cyclone, observations of the tropical cyclone are sometimes fouled by missing and/or bad data caused by data transmission and processing problems, scan-line dropouts, and other errors (Rappaport 1991). Despite these moderate limitations, SSM/I observations can provide substantial information concerning the temporal evolution of convective rainfall during tropical cyclones in the data-sparse eastern North Pacific basin.

4.8 Accomplishment of Secondary Goal 2: Coverage by Convective Rainfall

Documentation of coverage by convective rainfall (i.e., PCP) stratified by regions and current intensity was accomplished via Figures 55 to 58. These calculations used all of the 297 SSM/I observations eastern North Pacific tropical cyclone used in forecast

model training and testing. The rightmost bars for the “All times” category in Figures 55 to 58 indicated that as tropical cyclone intensity increased so did the average value of PCP for all regions, except one. That minor exception occurred for the total region (i.e., within 444.4 km), where the average PCP was just slightly higher for hurricanes than strong hurricanes. Also, the bar charts demonstrated that as the radius of the region increased, the average PCP decreased across all intensity categories. This result was due to the overwhelming effect of increasing the size of the denominator (i.e., total number of pixels in the region of interest) in the calculation of PCP. Average values of PCP ranged from 5 percent for the total region of a tropical depression to 76 percent for the central-core region of a strong hurricane.

4.9 Accomplishment of Secondary Goal 3: SSM/I Center-fix Study

The comparison of differences between SSM/I and linearly interpolated best-track locations of tropical cyclone centers of circulation was the third secondary goal of this research. The results related to this goal are stratified by current intensity and charted in Figure 59. As Martin and Gray (1993) and Sheets and McAdie (1988) found, the differences between satellite center-fix locations and a measure of “ground truth” (i.e., accuracy) in this present research decreased (accuracy increased) as the current intensity increased. Figure 59 shows that more intense tropical cyclones had smaller SSM/I center-fix differences. The overall average center-fix difference was 31 km. This result was slightly better than the 37.5-km limit of accuracy implied by Gaby *et al.* (1980). The results of this present study of 315 SSM/I center fixes found differences for tropical storm

and hurricane center fixes that were about 10 km better than the study of 20 SSM/I observations by Velden *et al.* (1989). The center-fix differences found in this present study were over 50 percent better at all intensity categories when compared to the study involving visible and infrared center fixes of eastern North Pacific tropical cyclones by Sheets and McAdie (1988).

In some cases where a tropical cyclone eye does not exist or is obscured by cold cirrus clouds, the analyst is often presented with an ambiguous infrared satellite image. Center fixes using visible satellite images in these situations are somewhat less ambiguous than infrared center fixes. However, visible images are only available to conduct center fixes during periods of daylight. The ability of an SSM/I observation to “penetrate” the cold cirrus clouds in the outflow of tropical cyclones to resolve the underlying structure of precipitation is key to its usefulness as a center-fixing tool. Additionally, the availability and accuracy of SSM/I center fixes is independent of the time of day. However, the limitations mentioned in Section 4.7 also apply to the use of SSM/I observations to center fix tropical cyclones.

4.10 Accomplishment of Secondary Goal 4: Diurnal Cycle of Convection

The fourth secondary goal was to stratify SSM/I observations of PCP within all four regions by time of day to ascertain if a diurnal variation of convective rainfall coverage could be detected. Additionally, intensity categories were examined to determine if current intensity affected a diurnal variation. The results of this analysis are contained in Figures 55 to 58. For weaker tropical cyclones (i.e., tropical depressions and

tropical storms), a peak in PCP occurred at 1200 UTC (i.e., 0300-0500 local standard time [LST]). Hurricane PCP values were relatively flat throughout the day with a slight dip at 0000 UTC (i.e., 1500-1700 LST). Values of PCP for strong hurricanes were relatively flat at all time periods. These diurnal variations were dampened out as the radius of interest increased.

The results of this present study of eastern North Pacific tropical cyclones confirmed with observations from satellite passive-microwave radiometers the results of a study by Hobgood (1986) using a numerical tropical cyclone prediction model. Rodgers and Pierce (1995a) found similar results for SSM/I rainfall within 444.4 km of the center of western North Pacific tropical cyclones.

4.11 Accomplishment of Secondary Goal 5: Comparison of Regression Coefficients

By comparing standardized regression coefficients of predictors in the forecast models developed for the eastern North Pacific basin using different tropical cyclone seasons, the fifth secondary goal was to determine the stability of such predictors. When the Rain and Petty model's standardized regression coefficients were compared to those of the Petty and Hobgood (1998) model, coefficients for variables that were selected for both models and at the same forecast periods compared quite well. The coefficients all had the same signs and nearly identical magnitudes. This result was probably due to the overlapping years used to develop both regression models. The Rain and Petty model used cases from 1991 to 1997 and the Petty and Hobgood (1998) model used cases from 1989 to 1995.

A comparison of standardized regression coefficients between the Rain and Hobgood and Hobgood (1998a) models yielded some differences in magnitude for three variables: LAT, POT, and PVMAX12 (i.e., prior 12-hour intensity change). LAT was more important in the Hobgood (1998a) model, with coefficients of -0.3 to -0.4 compared to -0.1 to -0.3 in the Rain and Hobgood model. In the Hobgood (1998a) model, POT's coefficients were about 0.1. While in the Rain and Hobgood model, coefficients for POT were much greater (i.e., between 0.4 and 0.5). This major difference was most likely caused by the use of weekly SSTs to calculate MPI in the Rain and Hobgood model and the use of climatic SSTs to calculate MPI in the Hobgood (1998a) model. PVMAX12 was more important in the Rain and Hobgood model with standardized regression coefficients between 0.4 and 0.6. In Hobgood's (1998a) model, the coefficients for PVMAX12 ranged from 0.2 to 0.5. In addition to the use of different SSTs, the differences in standardized regression coefficients between the Hobgood (1998a) and Rain and Hobgood models were most likely due to the different seasons used for regression model development. The Hobgood (1998a) regression seasons used in this comparison were 1988 to 1993 and had less overlap with the Rain and Hobgood model than the overlap of the two other models compared above. Therefore, standardized regression coefficients were somewhat sensitive to the seasons used to develop the regression model.

4.12 Accomplishment of Secondary Goal 6: Contribute to NRL Research Efforts

The 315 SSM/I observations of eastern North Pacific tropical cyclones used in this present research were identified, center-fixed, and processed from the raw data format (i.e., TDR) in the NRL DC and SSC dataset library to the rainfall images (i.e., EDR) maintained in the TROPX database at NRL MRY. The same data processed during this research contributed to other data currently being used by researchers in the NRL Marine Meteorology Division to develop a neural-network-based tropical cyclone intensity specification technique. Given the moderate correlation between inner-core convective rainfall and current intensity, rainfall is a variable now being used to train the neural network.

4.13 Accomplishment of Secondary Goal 7: Present Research in Scholarly Formats

In its proposed form, this research was presented orally at the 22nd Conference on Hurricanes and Tropical Meteorology (West 1997). Preliminary results were presented by poster at the Symposium on Tropical Cyclone Intensity Change (West 1998). The findings of this research will be submitted to the appropriate peer-reviewed journals and presented at the 23rd Conference on Hurricanes and Tropical Meteorology to be held in January 1999.

CHAPTER 5

CONCLUSIONS AND RECOMMENDATIONS FOR FUTURE RESEARCH

5.1 Satellite-measured Convective Rainfall is Related to Tropical Cyclone Intensity

Rainfall measured from passive-microwave radiometers observing eastern North Pacific tropical cyclones from satellites provided useful information for the specification of current intensity and prediction of intensity changes 12 to 36 hours into the future. The areal coverage of the inner core by convective precipitation was found to be moderately correlated with current intensity. This information could aid the development of objective tropical cyclone intensity specification techniques. The trend in central-core areally weighted convective rain rates was found to have a low, but significant, correlation with future 12- to 24-hour intensity changes. Also, the areally weighted average of convective rain rates within 444.4 km was shown to have a low, but significant, correlation with future 36-hour intensity change.

5.2 Relationships Between Rainfall and Intensity Are Affected by Other Factors

Stratified analysis of correlations between rainfall parameters and other factors illustrated that many correlations differed according to the categories used in the

stratifications. Also, case studies highlighted the negative impacts of high vertical wind shear, cool SST, and low-level inflow of cool dry air on convective rainfall and intensity relationships. In the unfavorable regime common during the dissipation of eastern North Pacific tropical cyclones, the otherwise positive relationship between future 36-hour intensity change and the total intensity and coverage of convective rainfall became negative. Simply stated, weakening occurred in the presence of negative factors, regardless of the latent heat released by rainfall. When these negative factors did not exist, changes in convective rainfall tended to precede intensity changes by about a day. In the presence of these negative factors, decreasing intensity and decreasing convective rainfall occurred concomitantly. Therefore, during periods of development and strengthening under favorable environmental conditions, convective rainfall played a positive role that preceded future intensification. During periods of weakening and dissipation under unfavorable conditions, convective rainfall diminished concurrently with wind speed. In other words, certain thresholds exist for negative factors beyond which the positive influence of latent heat release on future intensification is overwhelmed.

5.3 Rainfall Parameters Can Improve Statistical Intensity Forecast Guidance

Despite low correlation coefficients between convective rainfall parameters and future intensity changes, some of these parameters were selected by stepwise multiple linear regression for inclusion into forecast models using other predictors developed by Hobgood (1998a) and Petty and Hobgood (1998). The rainfall parameters improved the

explained variance of 12- to 36-hour intensity change over the models without rainfall information. The resulting rain-related forecast models outperformed all other forecast methods at the 12-hour forecast period in a homogeneous test. Mean relative absolute error (MRAE) for the 12-hour rain-related forecasts was 3 percent less than official NHC forecast advisories. MAE for the Rain and Hobgood model was the lowest of the forecast methods for the 24-hour forecast period. When compared to official NHC 24-hour forecast advisories, MRAE for the Rain and Hobgood model was 14 percent less. This improved performance might have been expected given the lag time between latent heat release and intensity change shown by previous numerical model and satellite observational studies. However, this present research is the first to use SSM/I-measured rainfall to actually demonstrate, via a homogeneous comparison of forecast errors, that rainfall information could improve operational tropical cyclone forecasting.

The finding that quantitative information from satellites could improve operational forecasting is significant. Using numerous forecast error studies, Ramage (1993) revealed that for forecasts out to 24 hours the combination of persistence and climatology outperformed operational forecasts based upon numerical weather prediction models or other methods. He lamented that, despite decades of improving computer resources and observations by satellites, the scientifically crude method of forecasting by persistence and climatology was still superior. While the Rain and Hobgood model contains persistence and climatic variables, the satellite-derived rainfall parameter was of similar importance as the climatic variable of latitude. The superior forecast performance of the Rain and Hobgood model at 12 and 24 hours slightly countered the conclusion of

Ramage (1993). A satellite-derived rainfall parameter could improve operational forecasting. Therefore, SSM/I-observed rainfall might point to an important physical process that needs better understanding. Better understanding of that process could lead to more accurate numerical tropical cyclone prediction modeling methods. Because of the complex interactions involved in tropical cyclone intensity change, the ultimate solution for operational forecasting of intensity change would be an accurate numerical tropical cyclone prediction model initialized with readily available and accurate observational data. Until that solution is available, statistically based forecasting techniques using appropriate predictors will continue to be the best guidance available to operational tropical cyclone forecasters.

5.4 SSM/I-derived Information has Utility for Observing Tropical Cyclones

In addition to the intensity-change forecasting implications of SSM/I-derived information, the DMSP constellation of SSM/I-equipped satellites makes important contributions to operationally observing tropical cyclones. Case studies in this present research showed that with some limitations the convective ring cycle was clearly observed using these satellites. Additionally, the finding concerning center-fix differences in this study was significant. When compared to studies using other satellite platforms, the much lower SSM/I center-fix differences demonstrated that they were superior in a basin without regular aircraft reconnaissance.

Real-world applications of the SSM/I system ought to be fully exploited despite some minor limitations noted in Chapter 4. The US government spends \$60 million (\$42

million on operations and maintenance and \$18 million for research and development) per year on the DMSP constellation of satellites (Tsugawa *et al.* 1997). Exploitation of SSM/I data to decrease intensity-change forecast errors and increase the accuracy of center fixes could in some ways help reduce the loss of life (see Table 9) and enable a better allocation of the resources required for adequate preparation, response, and mitigation involved with these dangerous tropical cyclones. By applying SSM/I data to this important problem, some of the \$60 million spent per year might be better justified.

Additionally, the ability to better center fix tropical cyclones could improve related NWP efforts. Increased center-fix accuracy would improve the location of bogus tropical cyclone circulations inserted into NWP models. The resulting improved bogus locations could reduce tropical cyclone track and intensity errors produced by NWP models.

5.5 Recommendations for Future Research

SSM/I-equipped DMSP satellites have been operational for 11 years. Lessons learned from this present research demonstrate some of the positive impacts that data from them could have on the future of tropical cyclone forecasting. Given the positive results obtained in the eastern North Pacific Ocean basin, future research should attempt to extrapolate and confirm these results in other basins. Through such research, other basins without aerial reconnaissance would be able to better exploit satellite information to improve intensity specification and prediction techniques. In the Atlantic Ocean basin,

intensity and rainfall relationships could be more accurately studied due to the regular availability of high-quality *in situ* intensity data from aircraft.

It is the author's hope that real-time operational testing of the statistical rain-related forecast models developed in this present research will be conducted. Additional lessons could be learned from such future research applications. In that research, operational forecasters would be able to test and critically evaluate forecast guidance products that objectively quantify important satellite-derived information. Weaknesses of the rain-related forecast models would be exposed and new directions for future research suggested.

The forecast performance of statistical intensity-change guidance products developed at The Ohio State University and elsewhere is degraded for those tropical cyclones undergoing rapid intensity changes. This degradation of performance is an artifact of the statistical methodology used to develop the forecast models. For example, only 14 percent of the cases used to develop the regression models in this present study involved rapid intensity increases or decreases. Therefore, the forecast equations were not designed to handle rapid intensity changes. Future research might develop forecast models based upon regressions using only those cases undergoing rapid intensity change. Once identified as a rapidly strengthening or weakening tropical cyclone, the appropriate model would then be used instead of the standard model. Another stratification of cases for statistical forecast model development could involve current intensity. One of the results of this present research was that for all forecast methods discussed in Section 4.5 forecast errors differed with current intensity (i.e., underforecasts for weaker and

overforecasts for stronger tropical cyclones). Therefore, in a manner similar to that discussed above for rapid intensity changes, forecast models could be developed and used based upon current intensity.

Some thresholds used in this present research could be changed to see if they would have a significant impact on the findings. For example, the threshold chosen for stratified analysis of tropospheric vertical wind shear was 8.5 m s^{-1} in this current study. While, Zehr (1992) proposed a higher threshold at 12.5 m s^{-1} that was rejected in favor of 8.5 m s^{-1} as suggested by Fitzpatrick (1997). Perhaps, a new study using the higher threshold could be conducted. A study of that kind might help in understanding exactly how much vertical wind shear is detrimental to intensity and rainfall correlations given the related results in Table 20. A second threshold that could be reexamined is that for convective precipitation. Perhaps, the higher 6 mm h^{-1} threshold would produce significantly different results.

Additionally, a substantial modification of the TROPX software would enable the calculation of regionally averaged rain rates without a convective threshold. That is, the sum of the rain rates (including zero) in a region would be divided by the number of pixels in the region of interest. This type of rainfall parameter would have units of mm h^{-1} instead of % and would include the impact of both rainfall types (i.e., stratiform and convective). Also related to TROPX, as more SSM/I observations for the 1997 and 1998 eastern North Pacific tropical cyclone seasons become available for processing they could be used to increase the number of cases available for future regression model training and testing efforts.

LIST OF REFERENCES

- Adler, R.F., and E.B. Rodgers, 1977: Satellite-observed latent heat release in a tropical cyclone. *Mon. Wea. Rev.*, **105**, 956-963.
- Alliss, R.J., G.D. Sandlin, S.W. Chang, and S. Raman, 1993: Applications of SSM/I data in the analysis of Hurricane Florence (1988). *J. Appl. Meteor.*, **32**, 1581-1591.
- , S. Raman, and S.W. Chang, 1992: Special Sensor Microwave/Imager (SSM/I) observations of Hurricane Hugo (1989). *Mon. Wea. Rev.*, **120**, 2723-2737.
- AMS, 1993: Policy Statement. Hurricane detection, tracking and forecasting. *Bull. Amer. Meteor. Soc.*, **74** (7), 1377-1380.
- Anthes, R.A., 1974: The dynamics and energetics of mature tropical cyclones. *Rev. Geophys. Space Phys.*, **12** (3), 495-522.
- Atlas, D., and O.W. Thiele, 1981: *Precipitation Measurements from Space*. Workshop Report, 28 April-1 May 1981, NASA GSFC, Greenbelt, MD.
- Avila, L.A., 1998: Forecasting tropical cyclone intensity changes: An operational challenge. *Preprints, Symp. on Trop. Cyclone Intensity Change*, 11-16 January 1998, Phoenix, AZ, Amer. Meteor. Soc., 1.1, 1-3.
- , and E.N. Rappaport, 1996: Eastern Pacific hurricanes. *Weather of 1995*. *Weatherwise*, **49** (1), 42-43.
- , and M. Mayfield, 1995: Eastern North Pacific hurricane season of 1993. *Mon. Wea. Rev.*, **123**, 897-906.
- Barbor, K., 1997: *Impact of the 1996 Hurricane Season on Atlantic Fleet Operations*. Presentation at the 51st Interdepartmental Hurricane Conference, 25-28 March 1997, Miami, FL, OFCM.
- Barrett, E.C., and M.J. Beaumont, 1994: Satellite rainfall monitoring: An overview. *Remote Sensing Reviews*, **11**, 23-48.

- Bauer, P., and N.C. Grody, 1995: The potential of combining SSM/I and SSM/T2 measurements to improve the identification of snow cover and precipitation. *IEEE Trans. Geosci. Remote Sens.*, **33** (2), 252-261.
- Cecil, D.J., 1997: Basin to basin differences in the relationship between ice scattering signature and future tropical cyclone intensity. *Preprints, 22nd Conf. on Hurr. and Trop. Meteor.*, 19-23 May 1997, Fort Collins, CO, Amer. Meteor. Soc., 3a.4, 31-32.
- Colton, M.C., and G.A. Poe, 1994: Meeting Review. Shared Processing Program, Defense Meteorological Satellite Program, Special Sensor Microwave/Imager Algorithm Symposium, 8-10 June 1993. *Bull. Amer. Meteor. Soc.*, **75** (9), 1663-1669.
- , and -----, E.A. Uliana, R.W. Conway, and B. Gardiner, 1996: Intersensor calibration of DMSP SSM/I'S F8 - F13, 1987-1995. *Preprints, 8th Conf. on Sat. Meteor. and Oceanogr.*, 28 January-2 February 1996, Atlanta, GA, Amer. Meteor. Soc., 185-187.
- Davis, M.A.S., G.M. Brown, and P.W. Leftwich, 1984: *A Tropical Cyclone Data Tape for the Eastern and Central North Pacific Basins, 1949-1983: Contents, Limitations and Uses*. NOAA Technical Memorandum NWS NHC 25. National Hurricane Center, Miami, FL, 16 pp.
- DeMaria, M., and J. Kaplan, 1994: A statistical hurricane intensity prediction system (SHIPS) for the Atlantic basin. *Wea. Forecasting*, **9**, 209-220.
- Denney, W.J., 1976: *Cool Inflow as a Weakening Influence on Eastern North Pacific Tropical Cyclones*. NOAA Technical Memorandum NWS WR 110. Redwood City, CA, 4 pp.
- Dvorak, V.F., 1990: *A Workbook on Tropical Clouds and Cloud Systems Observed in Satellite Imagery, Volume II*. NAVEDTRA 40971. US Navy, Stennis Space Center, MS.
- Economist, 1998: The season of El Niño. The Americas. *The Economist*, **347**(8067), 35-38.
- Elsberry, R.L., 1998: Thoughts on why statistical tropical cyclone intensity forecasts have so little skill. *Preprints, Symp. on Trop. Cyclone Intensity Change*, 11-16 January 1998, Phoenix, AZ, Amer. Meteor. Soc., 1.3, 4-10.
- , G.J. Holland, H. Gerrish, M. DeMaria, C.P. Guard, and K. Emanuel, 1992: Is there

- any hope for tropical cyclone intensity prediction?--A panel discussion. *Bull. Amer. Meteor. Soc.*, **73** (3), 264-275.
- Felde, G.W., and M. Glass, 1991: SSM/I brightness temperature analysis of tropical cyclones. *Preprints, 19th Conf. on Hurr. and Trop. Meteor.*, 6-10 May 1991, Miami, FL, Amer. Meteor. Soc., 400-404.
- Ferraro, R.R., and G.F. Marks, 1995: The development of SSM/I rain-rate retrieval algorithms using ground-based radar measurements. *J. Atmos. Oceanic Technol.*, **12**, 755-770.
- , F. Weng, N.C. Grody, and A. Basist, 1996: An eight year (1987-1994) time series of rainfall, clouds, water vapor, snow cover, and sea ice derived from SSM/I measurements. *Bull. Amer. Meteor. Soc.*, **77** (5), 891-905.
- , N.C. Grody, and G.F. Marks, 1994: Effects of surface conditions on rain identification using the SSM/I. *Remote Sensing Reviews*, **11**, 195-209.
- Fitzpatrick, P.J., 1997: Understanding and forecasting tropical cyclone intensity change with the typhoon intensity prediction scheme (TIPS), *Wea. Forecasting*, **12**, 826-846.
- , 1996: *Understanding and Forecasting Tropical Cyclone Intensity Change*. Ph.D. Dissertation. Department of Atmospheric Science Paper No. 598. Colorado State University, 346 pp.
- Frank, N.L., and C.L. Jordan, 1960: Climatological Aspects of the Intensity of Typhoons. *Geophys. Mag.*, **30** (1), 131-148.
- Gaby, D.C., J.B. Lushine, B.M. Mayfield, S.C. Pearce, and F.E. Torres, 1980: Satellite classifications of Atlantic tropical and subtropical cyclones: A review of eight years of classifications at Miami. *Mon. Wea. Rev.*, **108**, 587-595.
- Glahn, H.R., 1985: Chapter 8. Statistical weather forecasting. *Probability, Statistics, and Decision Making in the Atmospheric Sciences*. Eds. A.H. Murphy, and R.W. Katz. Westview Press, Boulder, CO, 289-335.
- Glass, M., and G. W. Felde, 1992: Intensity estimation of tropical cyclones using SSM/I brightness temperatures. *Preprints, Joint Session of the Sympos. on Wea. Forecasting and 6th Conf. on Sat. Meteor. and Oceanogr.*, 5-10 January, 1992, Atlanta, GA, Amer. Meteor. Soc., J8-J10.
- , and -----, 1990: Tropical storm structure analysis using SSM/I and OLS data.

Preprints, 5th Conf. on Sat. Meteor. and Oceanogr., 3-7 September 1990, London, England, Amer. Meteor. Soc., 432-437.

-----, and -----, 1989: Structure of tropical cyclones and surrounding regions as determined from OLS and SSM/I imagery analysis. *Preprints, 4th Conf. on Sat. Meteor. and Oceanogr.*, 16-19 May 1989, San Diego, CA, Amer. Meteor. Soc., 35-38.

Gray, W.M., 1968: Global view of the origin of tropical disturbances and storms. *Mon. Wea. Rev.*, **96** (10), 669-700.

Grody, N.C., 1997: Remote sensing from satellites using microwave radiometry. *Short Course on Passive Microwave Satellite Radiometry*, 2 February 1997, Long Beach, CA, Amer. Meteor. Soc.

-----, 1991: Classification of snow cover and precipitation using the Special Sensor Microwave/Imager (SSM/I). *J. Geophys. Res.*, **96**, 7423-7435.

Gross, J.M., and M.B. Lawrence, 1996: 1995 National Hurricane Center forecast verification. *Minutes of the 50th Interdepartmental Hurricane Conference*, 26-29 March 1996, Miami, FL, OFCM, B10-B50.

Hawkins, J.D., 1997: Personal communication. Electronic mail message (hawkins@nrlmry.navy.mil), 1 May 1997. Naval Research Laboratory, Marine Meteorology Division, Monterey, CA.

-----, J. Sandidge, R. Holyer, D.A. May, and G. Poe, 1996: Tropical cyclone characterization via satellite remotely sensed techniques. *Preprints, 8th Conf. on Sat. Meteor. and Oceanogr.*, 28 January-2 February 1996, Atlanta, GA, Amer. Meteor. Soc., 200-203.

Helveston, M.J., J.D. Hawkins, D.A. May, G.A. Poe, and G. Sandlin, 1996: Processing system for tropical cyclone multi-sensor satellite data sets. *Preprints, 12th International Conf. on IIPS for Meteor., Oceanogr., and Hydrology*, 28 January-2 February, 1996, Atlanta, GA, Amer. Meteor. Soc., 476-478.

Hinkle, D.E., W. Wiersma, and S.G. Jurs, 1988: *Applied Statistics for the Behavioral Sciences*, 2nd Edition. Houghton Mifflin Company, Boston, MA, 682 pp.

Hobgood, J.S., 1998a: The effects of climatological and persistence variables on the intensities of tropical cyclones over the eastern North Pacific Ocean. *Wea. Forecasting* (in press).

- , 1998b: A comparison of the thermodynamic and empirical maximum potential intensities over the eastern North Pacific Ocean. *Preprints, Symp. on Tropical Cyclone Intensity Change*, 11-16 January 1998, Phoenix, AZ, Amer. Meteor. Soc., P1.25, 129-130.
- , 1997: The effects of climatological factors on the intensities of tropical cyclones over the eastern North Pacific Ocean. *Preprints, 22nd Conf. on Hurr. and Trop. Meteor.*, 19-23 May 1997, Fort Collins, CO, Amer. Meteor. Soc., 8a.4, 282-283.
- , 1986: A possible mechanism for the diurnal oscillations of tropical cyclones. *J. Atmos. Sci.*, **43** (23), 2901-2922.
- Holland G. J., 1997: The maximum potential intensity of tropical cyclones. *J. Atmos. Sci.*, **54**, 2519-2541.
- , 1993: Chapter 9. Ready reckoner. *Global Guide to Tropical Cyclone Forecasting*. World Meteorological Organization Technical Document Number 560, Tropical Cyclone Program Report Number 31, Geneva, Switzerland.
- Hollinger, J.P., 1991: *DMSP Special Sensor Microwave/Imager Calibration/Validation*. Final Report Volume II, Naval Research Laboratory, Washington, DC.
- , 1989: *DMSP Special Sensor Microwave/Imager Calibration/Validation*. Final Report Volume I, Naval Research Laboratory, Washington, DC.
- , J.L. Peirce, and G.A. Poe, 1990: SSM/I instrument evaluation. *IEEE Trans. Geosci. Remote Sens.*, **28** (5), 781-790.
- Houze, R.A., 1993: *Cloud Dynamics*. Academic Press, 573 pp.
- Hughes, L.A., 1952: On the low-level wind structure of tropical storms. *J. Meteor.*, **9**, 422-428.
- Hunter, H.E., E.B. Rodgers, and W.E. Shenk, 1981: An objective method for forecasting tropical cyclone intensity using Nimbus-5 Electrically Scanning Microwave Radiometer measurements. *J. Appl. Meteor.*, **20**, 137-145.
- Jarvinen, B.R., and C.J. Neumann, 1979: *Statistical Forecasts of Tropical Cyclone Intensity for the North Atlantic Basin*. NOAA Technical Memorandum NWS NHC 10. National Hurricane Center, Miami, FL, 22 pp.
- Johnson, R.H., and P.J. Hamilton, 1988: The relationship of surface features to the precipitation and air flow structure of an intense midlatitude squall line. *Mon.*

Wea. Rev., **116**, 1444-1472.

- Jorgensen, D.P., 1984: Mesoscale and convective-scale characteristics of mature hurricanes. Part I: General observations by research aircraft. *J. Atmos. Sci.*, **41** (8), 1268-1285.
- , and P.T. Willis, 1982: A Z-R relationship for hurricanes. *J. Appl. Meteor.*, **21**, 356-366.
- Kaplan, J., 1992: Computer subroutine ALAND written in FORTRAN 77 code.
- Khrgian, A.K., 1959: *Meteorology: A Historical Survey*, Volume 1, 2nd Edition, Revised. Edited by K.P. Pogosyan, Translated from Russian by R. Hardin in 1970. Keter Press, Jerusalem, 387 pp.
- Kidder, S.Q., and T.H. Vonder Haar, 1995: *Satellite Meteorology: An Introduction*. Academic Press, San Diego, CA, 466 pp.
- Kurihara, Y., and R.E. Tuleya, 1974: Structure of a tropical cyclone developed in a three-dimensional numerical simulation model. *J. Atmos. Sci.*, **31**, 893-919.
- Lawrence, M.B., 1998: Eastern North Pacific Hurricanes. *Weatherwise*, **51**(2), 40-42.
- , and E.N. Rappaport, 1994: Eastern North Pacific hurricane season of 1992. *Mon. Wea. Rev.*, **122**, 549-558.
- MacArthur, P.D., 1991: *Microwave Derived Rainrates in Typhoons and Their Use in the Diagnosis and Prediction of Typhoon Intensity*. Master's Thesis, Saint Louis University, 70 pp.
- Marks, F.D., 1990: Radar observations of tropical weather systems. *Radar in Meteorology: Battan Memorial and 40th Anniversary Radar Meteorology Conference*, Boston, MA, Amer. Meteor. Soc., 401-425.
- Martin, J.D., and W.M. Gray, 1993: Tropical cyclone observation and forecasting with and without aircraft reconnaissance. *Wea. Forecasting*, **8**, 519-532.
- McBride, J.L., 1995: Chapter 3. Tropical cyclone formation. *Global Perspectives on Tropical Cyclones*. World Meteorological Organization Technical Document Number 693, Tropical Cyclone Program Report Number 38, Geneva, Switzerland.
- McCoy, J.H., 1991: *Tropical Cyclone Asymmetries as Revealed by Recent Satellite Brightness Temperatures*. Master's Thesis, Saint Louis University, 133 pp.

- Melton, E.C., 1994: *Analysis of the Structural Characteristics and Intensity Evolution of Super Typhoon Flo (1990) in Special Sensor Microwave/Imager (SSM/I) Data*. Master's Thesis, North Carolina State University, 112 pp.
- Merrill, R.T., 1987: *An Experiment in Statistical Prediction of Tropical Cyclone Intensity Change*. NOAA Technical Memorandum NWS NHC 34. National Hurricane Center, Miami, FL, 34 pp.
- Middleton, W.E.K., 1965: *A History of the Theories of Rain and Other Forms of Precipitation*. Franklin Watts, Incorporated, New York, NY, 223 pp.
- Miller, D., 1997: Personal communication. Electronic mail message (miller@npmocw.navy.mil), 7 May 1997. TSgt, USAF, Joint Typhoon Warning Center, Nimitz Hill, Guam.
- Molinari, J., D. Vollaro, and F. Robasky, 1992: Use of ECMWF operational analyses for studies of the tropical environment. *Meteor. Atmos. Phys.*, **47**, 127-144.
- Mundell, D.B., 1991: Tropical cyclone intensification. *Preprints, 19th Conf. on Hurr. and Trop. Meteor.*, May 6-10, 1991, Miami, FL, Amer. Meteor. Soc., 511-515.
- , 1990: *Prediction of Tropical Cyclone Rapid Intensification Events*. Master's Thesis, Colorado State University, 186 pp.
- Neumann, C.J., 1993: Chapter 1. Global overview. *Global Guide to Tropical Cyclone Forecasting*. World Meteorological Organization Technical Document Number 560, Tropical Cyclone Program Report Number 31, Geneva, Switzerland.
- OFCM, 1998: *National Hurricane Operations Plan*. Office of the Federal Coordinator for Meteorological Services and Supporting Research, FCM-P12-1998, Washington, DC, May 1998.
- , 1997: *National Plan for Tropical Cyclone Research and Reconnaissance (1997-2002)*. Office of the Federal Coordinator for Meteorological Services and Supporting Research, FCM-P25-1997, Washington, DC.
- Palmén, E., 1948: On the formation and structure of tropical hurricanes. *Geophysica*, **3**, 26-38.
- Pasch, R.J., and M. Mayfield, 1996: Eastern North Pacific hurricane season of 1994. *Mon. Wea. Rev.*, **124**, 1579-1590.
- Petty, K.R., 1997a: The effects of synoptic factors on the intensities of tropical cyclones

- over the eastern North Pacific Ocean. *Preprints, 22nd Conf. on Hurr. and Trop. Meteor.*, 19-23 May 1997, Fort Collins, CO, Amer. Meteor. Soc., 8a.2, 278-279.
- , 1997b: *The Effects of Synoptic Factors on the Intensities of Tropical Cyclones Over the Eastern North Pacific Ocean*. Ph.D. Dissertation, The Ohio State University, 154 pp.
- , and J.S. Hobgood, 1998: On improving hurricane intensity guidance in the eastern North Pacific. *Wea. Forecasting* (submitted).
- Poe, G.A., 1997: Review of satellites-Historical perspective. *Short Course on Passive Microwave Satellite Radiometry*, 2 February 1997, Long Beach, CA, Amer. Meteor. Soc.
- Ramage, C.S., 1993: Forecasting in Meteorology. *Bull. Amer. Meteor. Soc.*, **74**(10), 1863-1871.
- Rao, G.V., and P.D. MacArthur, 1994: The SSM/I estimated rainfall amounts of tropical cyclones and their potential in predicting the cyclone intensity changes. *Mon. Wea. Rev.*, **122**, 1568-1574.
- , -----, and J.H. McCoy, 1991: The latent heat release and brightness temperature anomalies associated with tropical cyclones and their utility in predicting the intensity changes of tropical storms. *Preprints, 19th Conf. on Hurr. and Trop. Meteor.*, 6-10 May 1991, Miami, FL, Amer. Meteor. Soc., 175-178.
- Rao, K.P., S.J. Holmes, R.K. Anderson, J.S. Winston, P.E. Lehr, 1990: *Weather Satellites: Systems, Data, and Environmental Applications*. Amer. Meteor. Soc., Boston, MA.
- Rappaport, E.N., 1991: *Preprints, 19th Conf. on Hurr. and Trop. Meteor.*, 6-10 May 1991, Miami, FL, Amer. Meteor. Soc.
- , and M. Mayfield, 1997: Eastern Pacific hurricane season: A quiet year. 1996 U.S. highlights. *Weatherwise*, **50** (1), 42-43.
- , and -----, 1992: Eastern North Pacific hurricane season of 1991. *Mon. Wea. Rev.*, **120**, 2697-2708.
- Reynolds, R.W., and T.M. Smith, 1994: Improved global sea surface temperature analyses using optimal interpolation. *J. Climate*, **7**, 929-948.
- Rhudy, D.K., 1989: *Applications of Microwave Radiometric Measurements to Infer*

Tropical Cyclone Intensity and Strength. Master's Thesis, Saint Louis University, 91 pp.

Riehl, H., 1954: *Tropical Meteorology*. McGraw-Hill Book Company, New York, 392 pp.

Rodgers, E.B., and H.F. Pierce, 1995a: A satellite observational study of precipitation characteristics in western North Pacific tropical cyclones. *J. Appl. Meteor.*, **34**, 2587-2599.

-----, and -----, 1995b: Environmental influence on Typhoon Bobbie's precipitation distribution. *J. Appl. Meteor.*, **34**, 2513-2532.

-----, and R.F. Adler, 1981: Tropical cyclone rainfall characteristics as determined from a satellite passive microwave radiometer. *Mon. Wea. Rev.*, **109** (3), 506-521.

-----, W.S. Olson, V.M. Karyampudi, and H.F. Pierce, 1997: The response of Opal's (1995) intensity to its satellite observed latent heat distribution. *Preprints, 22nd Conf. on Hurr. and Trop. Meteor.*, 19-23 May 1997, Fort Collins, CO, Amer. Meteor. Soc., 3a.3, 29-30.

-----, J.-J. Baik, and H.F. Pierce, 1994a: The environmental influence on tropical cyclone precipitation. *J. Appl. Meteor.*, **33**, 573-593.

-----, S.W. Chang, and -----, 1994b: A satellite observational and numerical study of precipitation characteristics in western North Atlantic tropical cyclones. *J. Appl. Meteor.*, **33**, 129-139.

Rosenthal, L., 1978: Numerical simulation of tropical cyclone development with latent heat release by the resolvable scales. Part 1. Model description and preliminary results. *J. Atmos. Sci.*, **35**, 258-271.

Sampson, C.R., R.A. Jeffries, J-H. Chu, and C.J. Neumann, 1995: *Tropical Cyclone Forecasters Reference Guide. 6. Tropical Cyclone Intensity*. NRL/PU/7541--95-0012. Naval Research Laboratory, Monterey, CA.

Shapiro, L.J., and H.E. Willoughby, 1982: The response of balanced hurricanes to local sources of heat and momentum. *J. Atmos. Sci.*, **39**, 378-394.

Sheets, R.C., 1990: The National Hurricane Center--Past, present and future. *Wea. Forecasting*, **5** (2), 185-232.

-----, and C. McAdie, 1988: Preliminary results of a study of the accuracy of satellite-

based tropical cyclone position and intensity estimates. *National Hurricane Operations Plan*. Office of the Federal Coordinator for Meteorological Services and Supporting Research, FCM-P12-1988, Washington, DC.

Simpson, R.H., and H. Riehl, 1981: *The Hurricane and Its Impact*. Louisiana State University Press, Baton Rouge, LA, 398 pp.

Skou, N., 1989: *Microwave Radiometer Systems: Design and Analysis*. Artech House, Norwood, MA.

Spencer, R.W., H.M. Goodman, and R.E. Hood, 1989: Precipitation retrieval over land and ocean with the SSM/I: Identification and characteristics of the scattering signal. *J. Atmos. Oceanic Technol.*, **6**, 254-273.

Tai, K.-S., and Y. Ogura, 1987: An observational study of easterly waves over the eastern Pacific in the northern summer using FGGE data. *J. Atmos. Sci.*, **44** (2), 339-361.

Titley, D., 1995: Hurricane Gordon: Evasion at sea. *Minutes of the 49th Interdepartmental Hurricane Conference*, 14-17 February 1995, Miami, FL, OFCM, B73-B89.

Tokay, A., and D.A. Short, 1996: Evidence from tropical raindrop spectra of the origin of rain from stratiform versus convective clouds. *J. Appl. Meteor.*, **35**, 355-371.

Tsugawa, B., R. Dumont, and K. Barnett, 1997: *The Federal Plan for Meteorological Services and Supporting Research: Fiscal Year 1998*. Office of the Federal Coordinator for Meteorological Services and Supporting Research. FCM P1-1997, Washington, DC, June 1997.

US Navy, 1956: *Fourth Research Report, Task 12: Intensification of tropical cyclones Atlantic and Pacific areas*. Project AROWA, Norfolk NAS, VA.

van Delden, A., 1989: On the deepening and filling of balanced cyclones by diabatic heating. *Meteor. and Atmos. Phys.*, **41**, 127-145.

Velden, C.S., W.S. Olson, and B.A. Roth, 1989: Tropical cyclone center-fixing using DMSP SSM/I data. *Preprints, 4th Conf. on Sat. Meteor. and Oceanogr.*, 16-19 May 1989, San Diego, CA, Amer. Meteor. Soc., J36-J39.

Weng, F., and N.C. Grody, 1994: Retrieval of cloud liquid water using the Special Sensor Microwave/Imager (SSM/I). *J. Geophys. Res.*, **99**, 25535-25551.

Wentz, F.J., 1995: *Deriving Earth Science Products from SSM/I: Progress Report for Contract NASW-4714*, August 1993 Through January 1995. Remote Sensing

- West, D.A., 1998: The use of SSM/I rainfall to predict eastern North Pacific tropical cyclone intensity change. *Preprints, Symp. on Tropical Cyclone Intensity Change*, 11-16 January 1998, Phoenix, AZ, Amer. Meteor. Soc., P1.5, 49-50.
- , 1997: The effects of rainfall on the intensity change of tropical cyclones over the eastern North Pacific Ocean. *Preprints, 22nd Conf. on Hurr. and Trop. Meteor.*, 19-23 May 1997, Fort Collins, CO, Amer. Meteor. Soc., 3a.5, 33-34.
- , 1993a: Environmental influencing of Tropical Cyclone Freda's precipitation. *Preprints, 20th Conf. on Hurr. and Trop. Meteor.*, 10-14 May 1993, San Antonio, TX, Amer. Meteor. Soc., 181-184.
- , 1993b: *Spatial and Temporal Variations of Satellite Microwave Measurements of Latent Heat Release in Tropical Cyclones Due to Environmental Forcing Obtained from a Numerical Model*. Master's Thesis, The Ohio State University, 115 pp.
- Whitney, L.D., 1995: *The Relationship Between Sea Surface Temperature and Maximum Intensity of Tropical Cyclones in the Eastern North Pacific Ocean*. Master's Thesis, The Ohio State University, 86 pp.
- , and J.S. Hobgood, 1997: The relationship between sea surface temperatures and maximum intensities of tropical cyclones in the eastern North Pacific Ocean. *J. Climate*, **10**, 2921-2930.
- Wilheit, T., R. Adler, S. Avery, E. Barrett, P. Bauer, W. Berg, A. Chang, J. Ferriday, N. Grody, S. Goodman, C. Kidd, D. Kniveton, C. Kummerow, A. Mugnai, W. Olson, G. Petty, A. Shibata, and E. Smith, 1994: Algorithms for the retrieval of rainfall from passive microwave measurements. *Remote Sensing Reviews*, **11**, 163-194.
- Willmott, C.J., 1982: Some comments on the evaluation of model performance. *Bull. Amer. Meteor. Soc.*, **63**(11), 1309-1313.
- Willoughby, H.E., 1990: Temporal changes of the primary circulation in tropical cyclones. *J. Atmos. Sci.*, **47** (2), 242-264.
- , 1988: The dynamics of the tropical cyclone core. *Aust. Meteor. Mag.*, **36**, 183-191.
- , F.D. Marks, and R.J. Feinberg, 1984: Stationary and moving convective bands in hurricanes. *J. Atmos. Sci.*, **41** (22), 3189-3211.

- , J.A. Clos, and M.G. Shoreibah, 1982: Concentric eye walls, secondary wind maxima, and the evolution of the hurricane vortex. *J. Atmos. Sci.*, **39**, 395-411.
- Zehr, R.M., 1992: *Tropical Cyclogenesis in the Western North Pacific*. NOAA Technical Report NESDIS 61. Washington, DC, 181 pp.
- Zhao, H., 1994: *Analysis of Tropical Cyclones Using Microwave Data from the Special Sensor Microwave/Imager*. Master's Thesis, University of Washington, 82 pp.

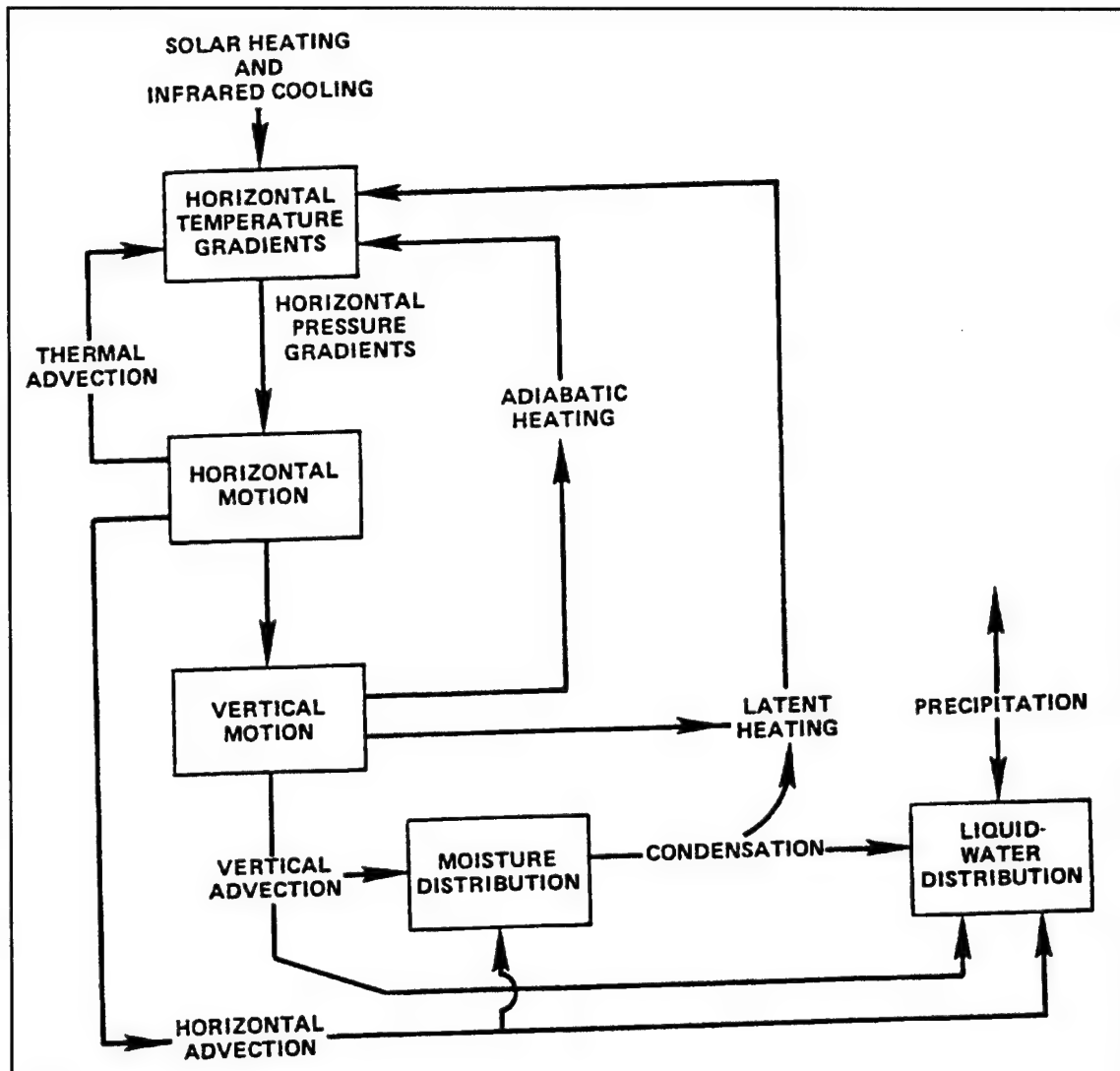


Figure 1: Interactions of synoptic-scale water and motion fields (Atlas and Thiele 1981).

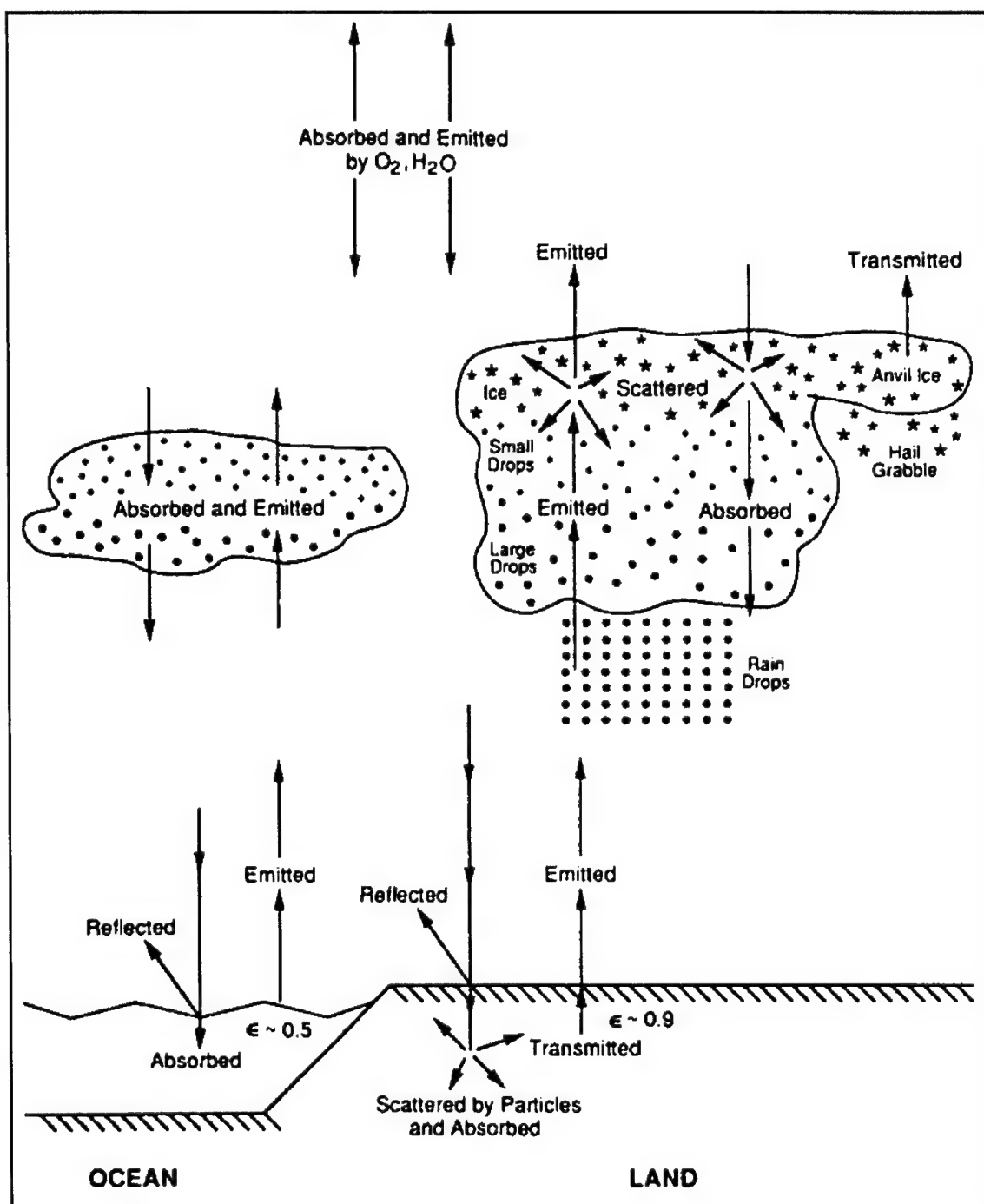


Figure 2: Interactions involving microwave radiation (Rao *et al.* 1990).

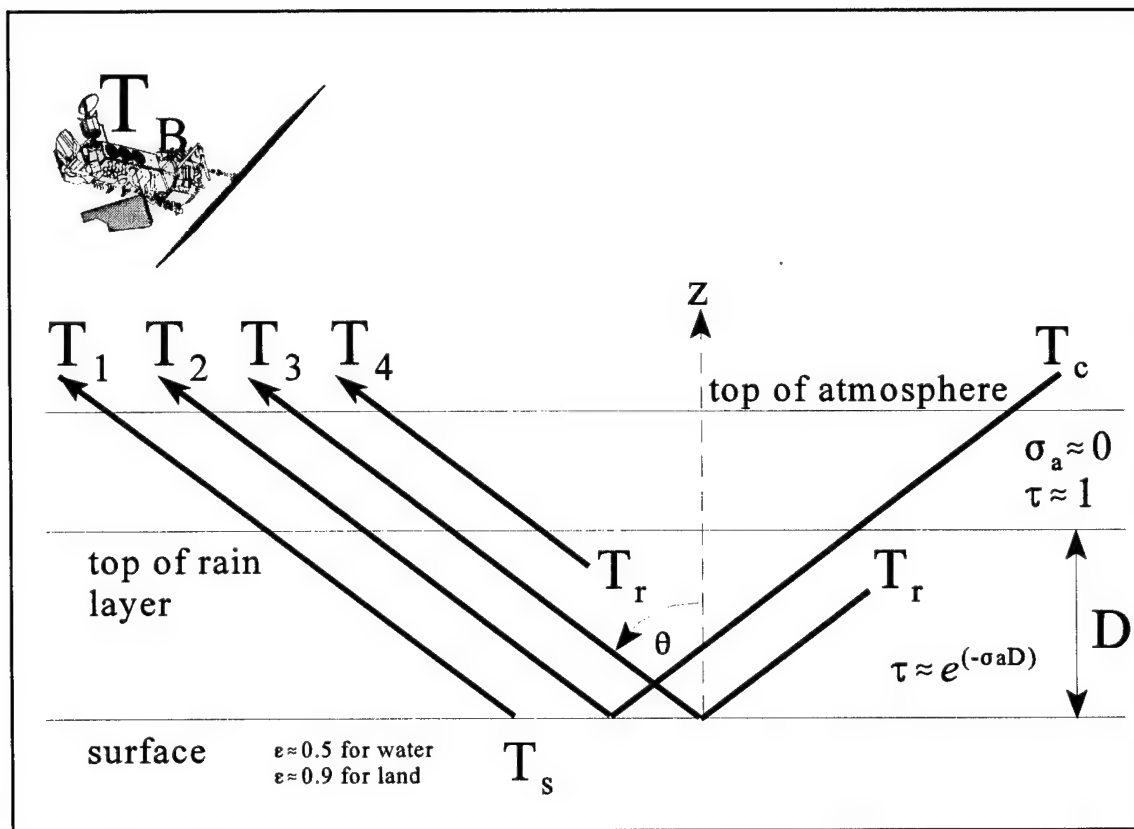


Figure 3: Geometry describing microwave radiative transfer involving rainfall.

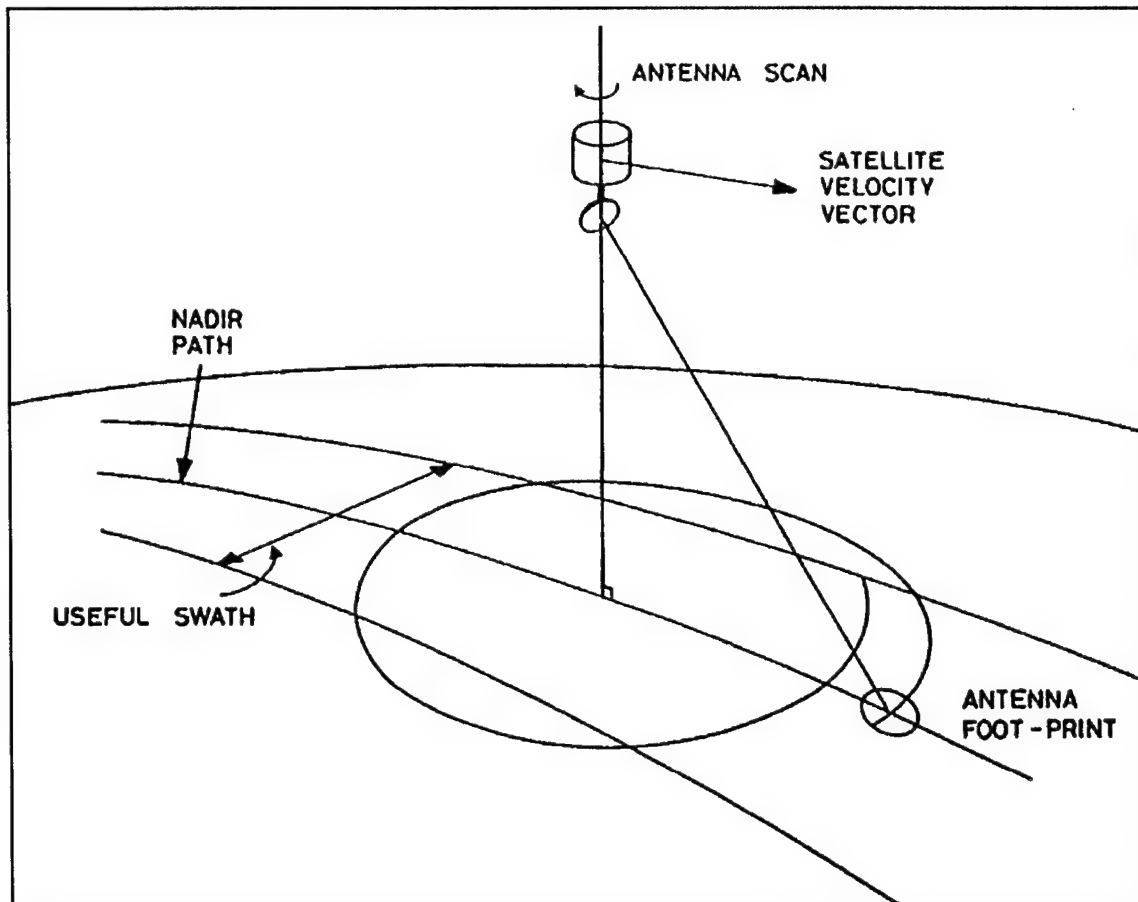


Figure 4: Conical-scanning radiometer (Skou 1989).

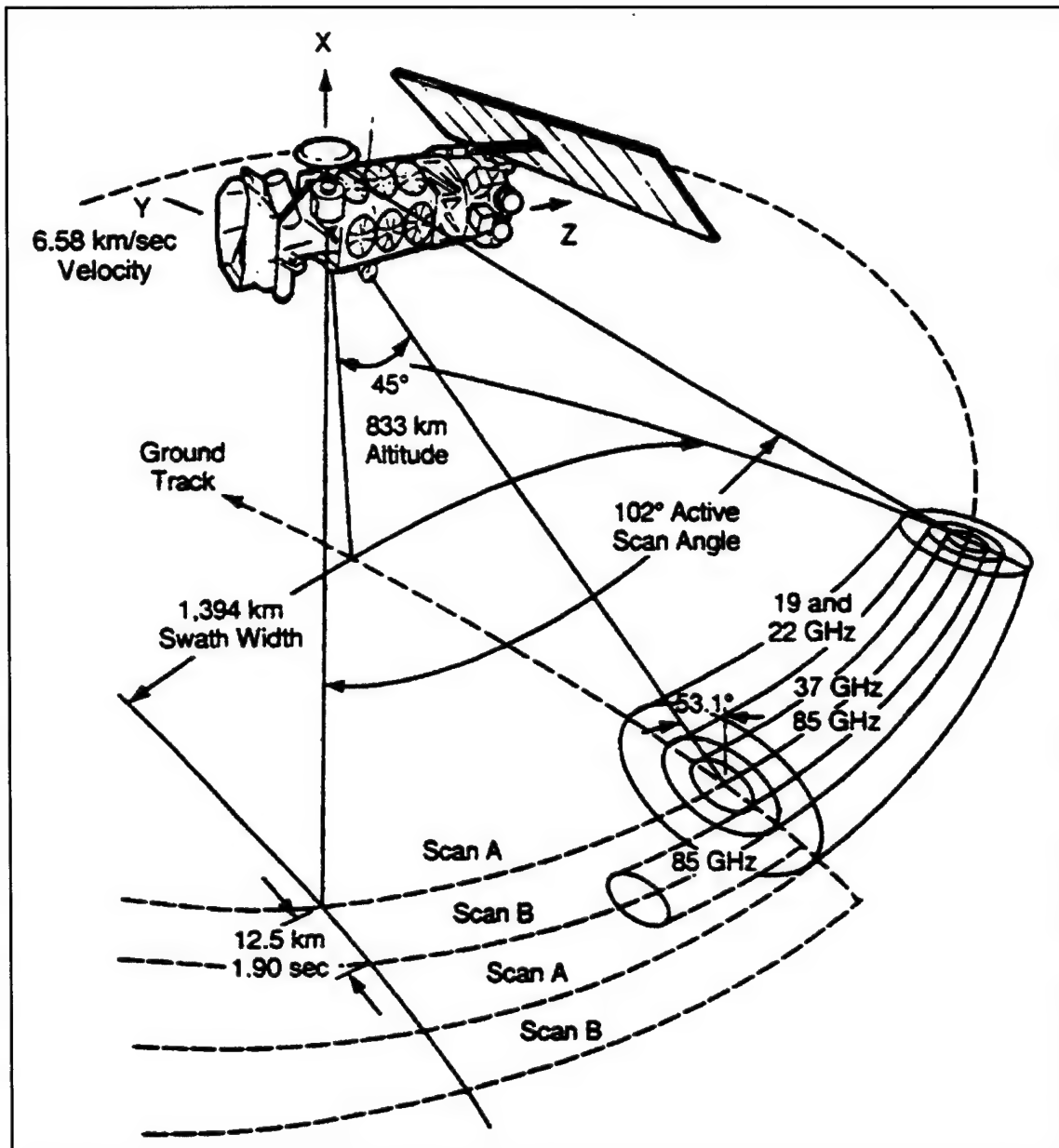


Figure 5: SSM/I scan geometry (Hollinger *et al.* 1990).

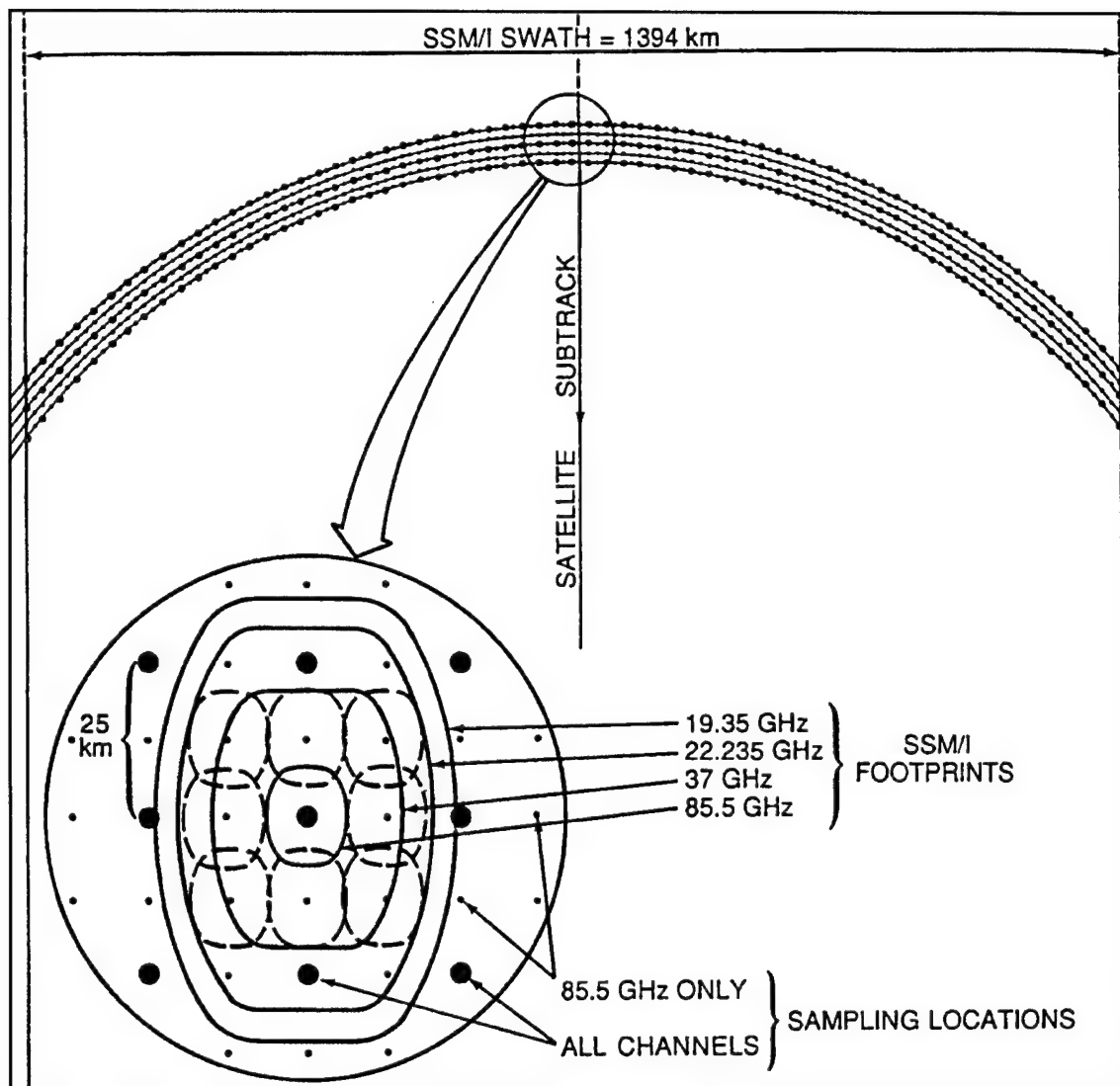


Figure 6: SSM/I scan characteristics (Spencer *et al.* 1989).

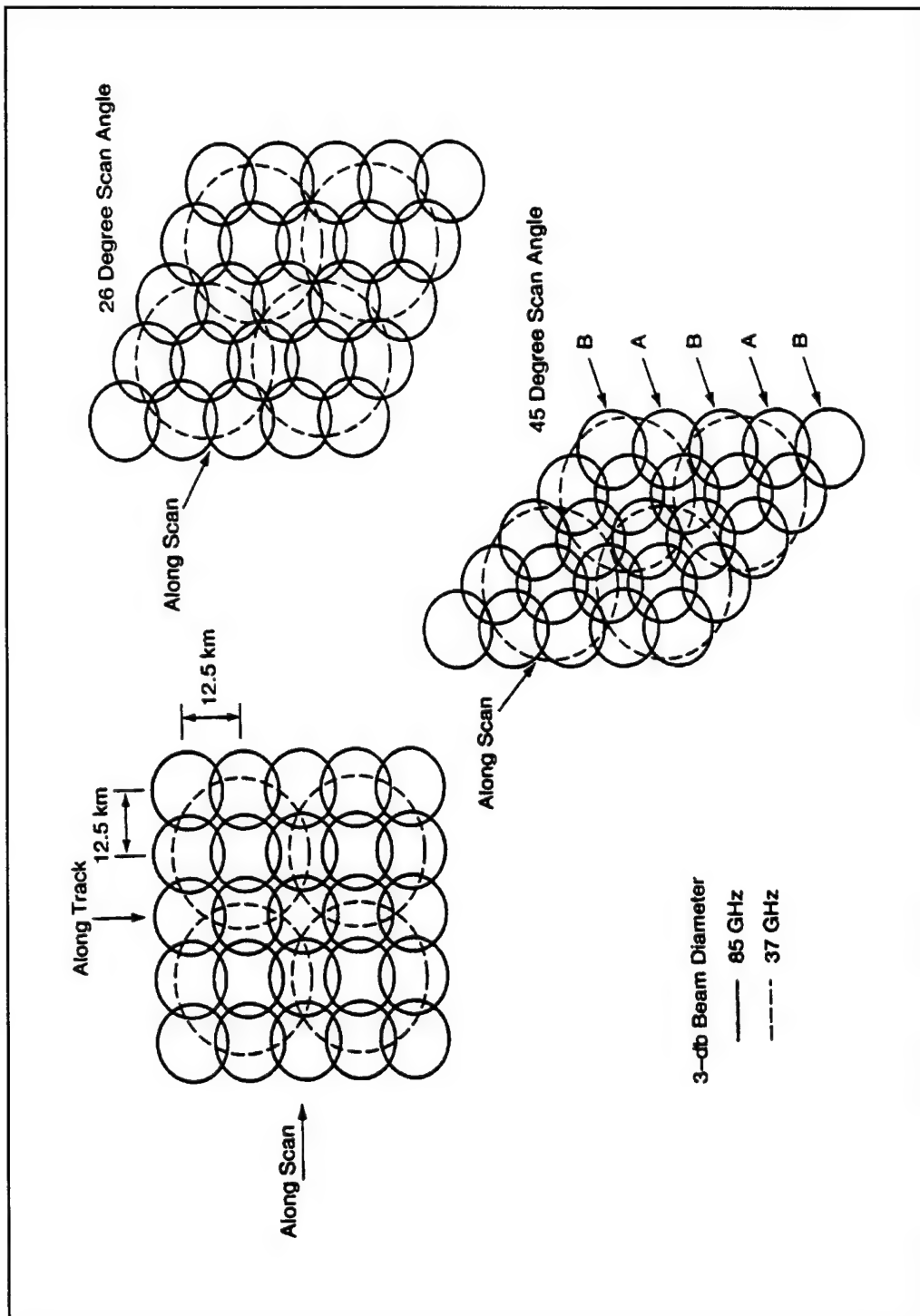


Figure 7: SSM/I spatial sampling illustrating along-scan changes (Hollinger 1989).

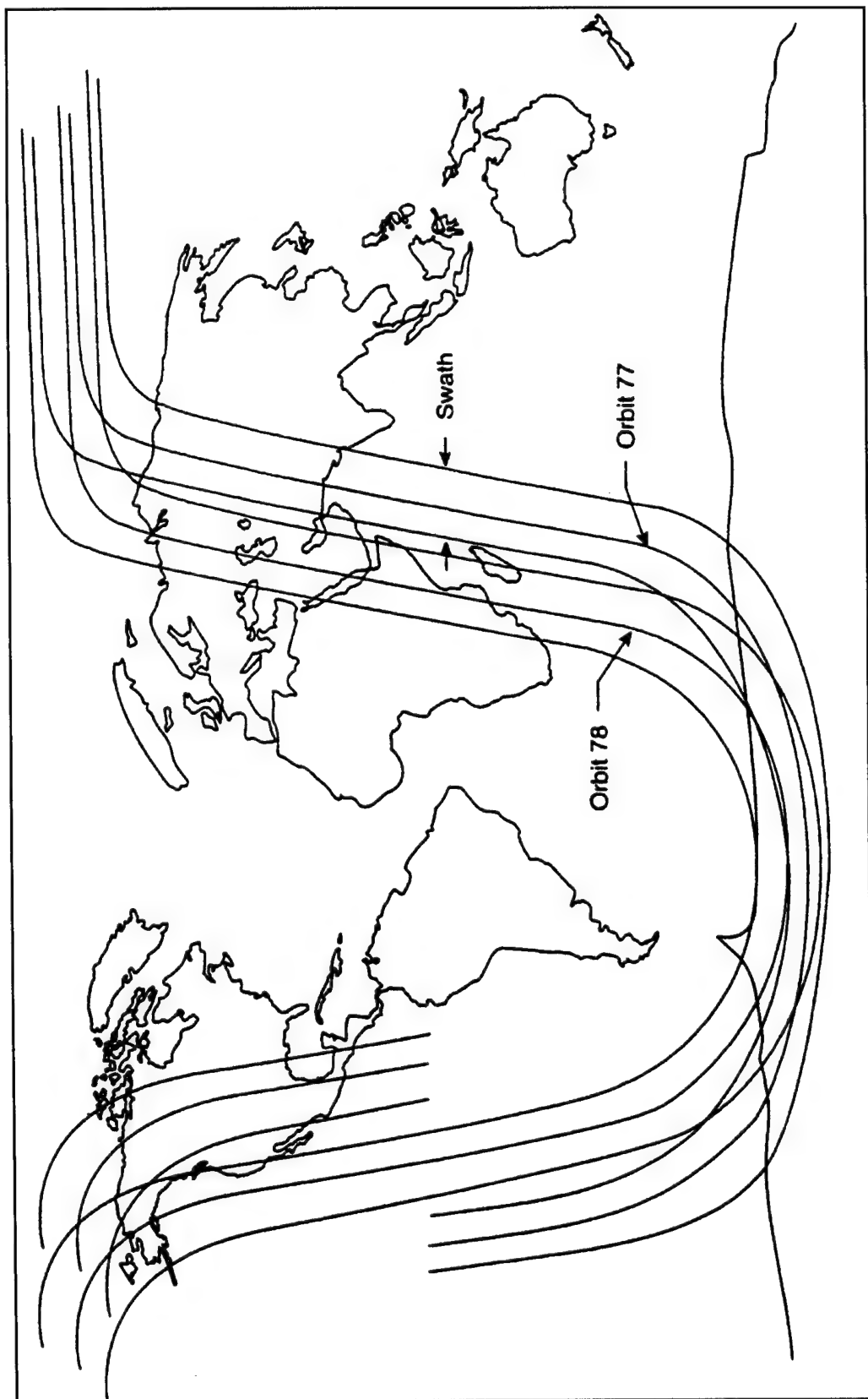


Figure 8: Equatorial view of successive SSM/I orbits with swath widths (Hollinger 1989).

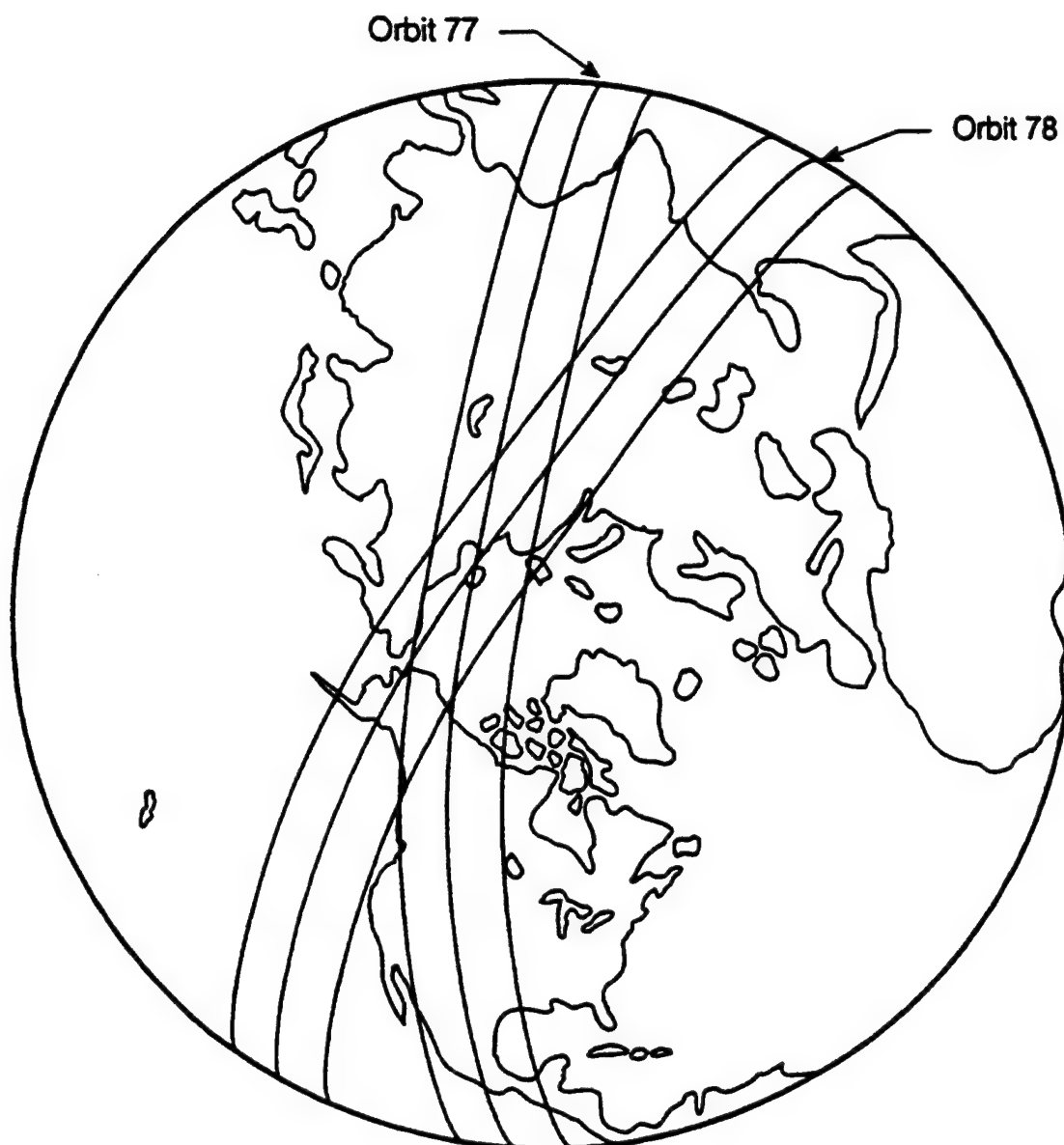
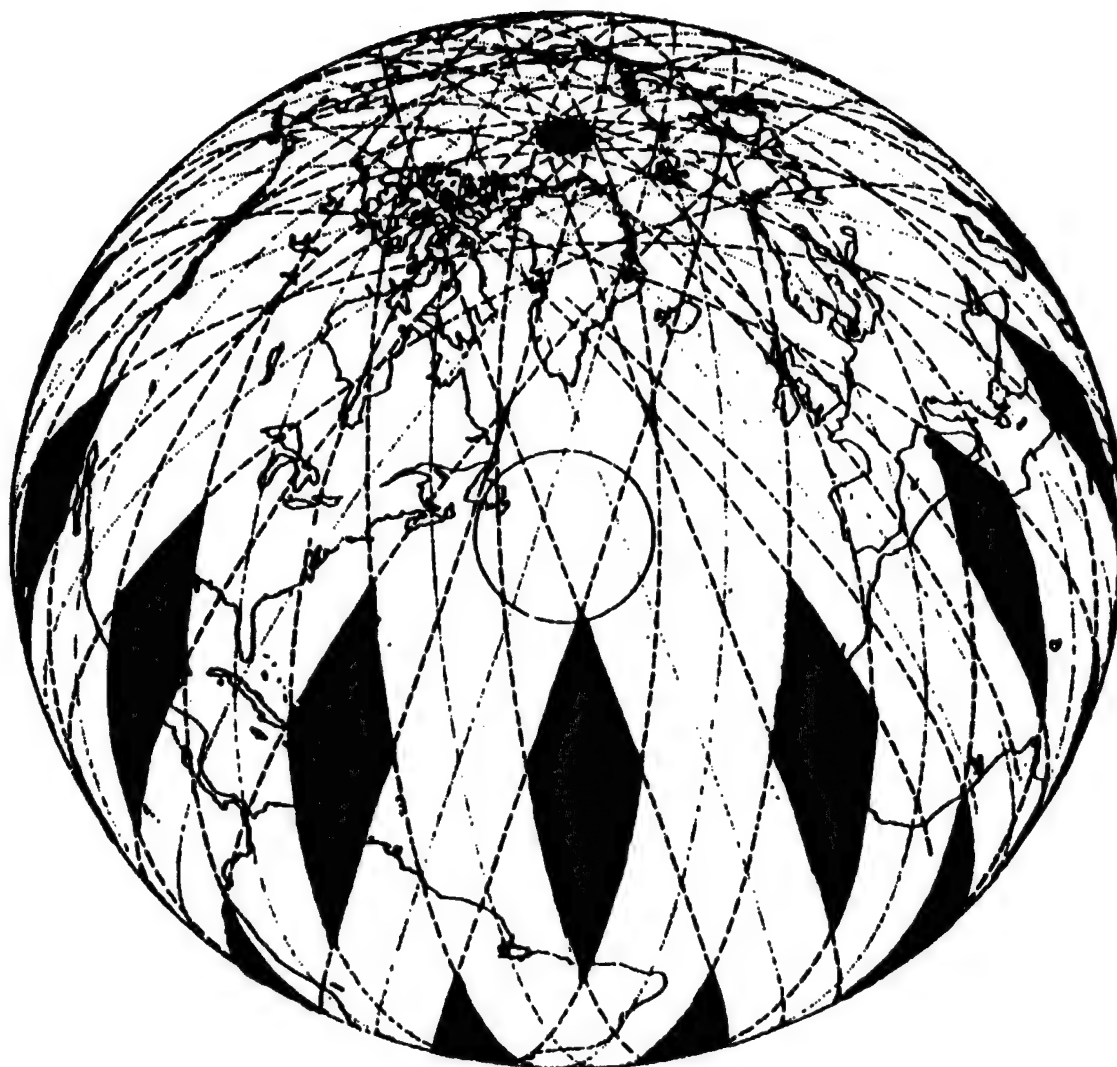


Figure 9: Polar view of successive SSM/I orbits with swath widths (Hollinger 1989).



1400 km Swath

Figure 10: Coverage by one SSM/I in 24 hours. Dark areas indicate data gaps (Hollinger 1989).

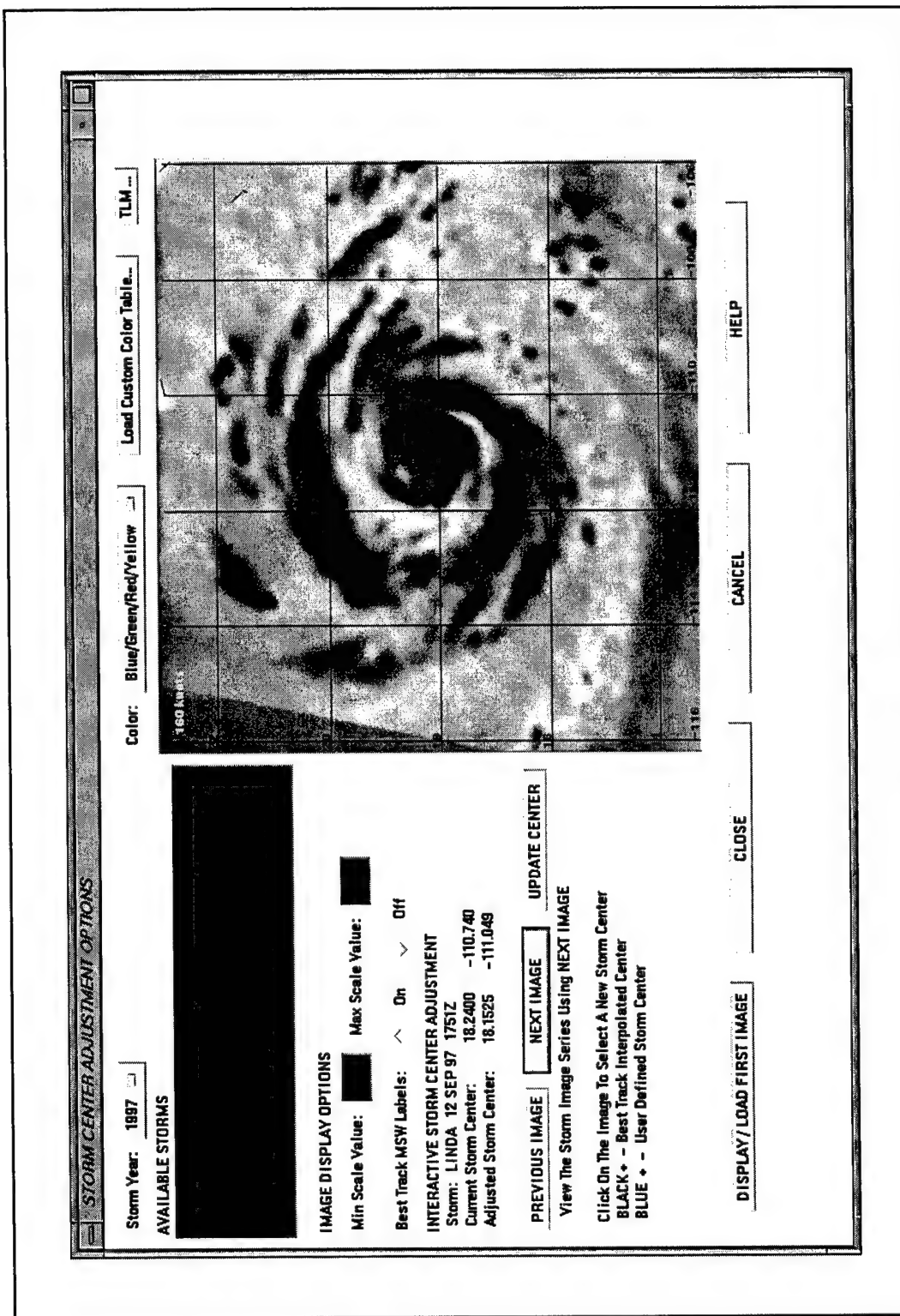


Figure 11: Center-fixing tool in TROPX depicting 85.5-GHz horizontally polarized T_B image of Hurricane Linda (1997).

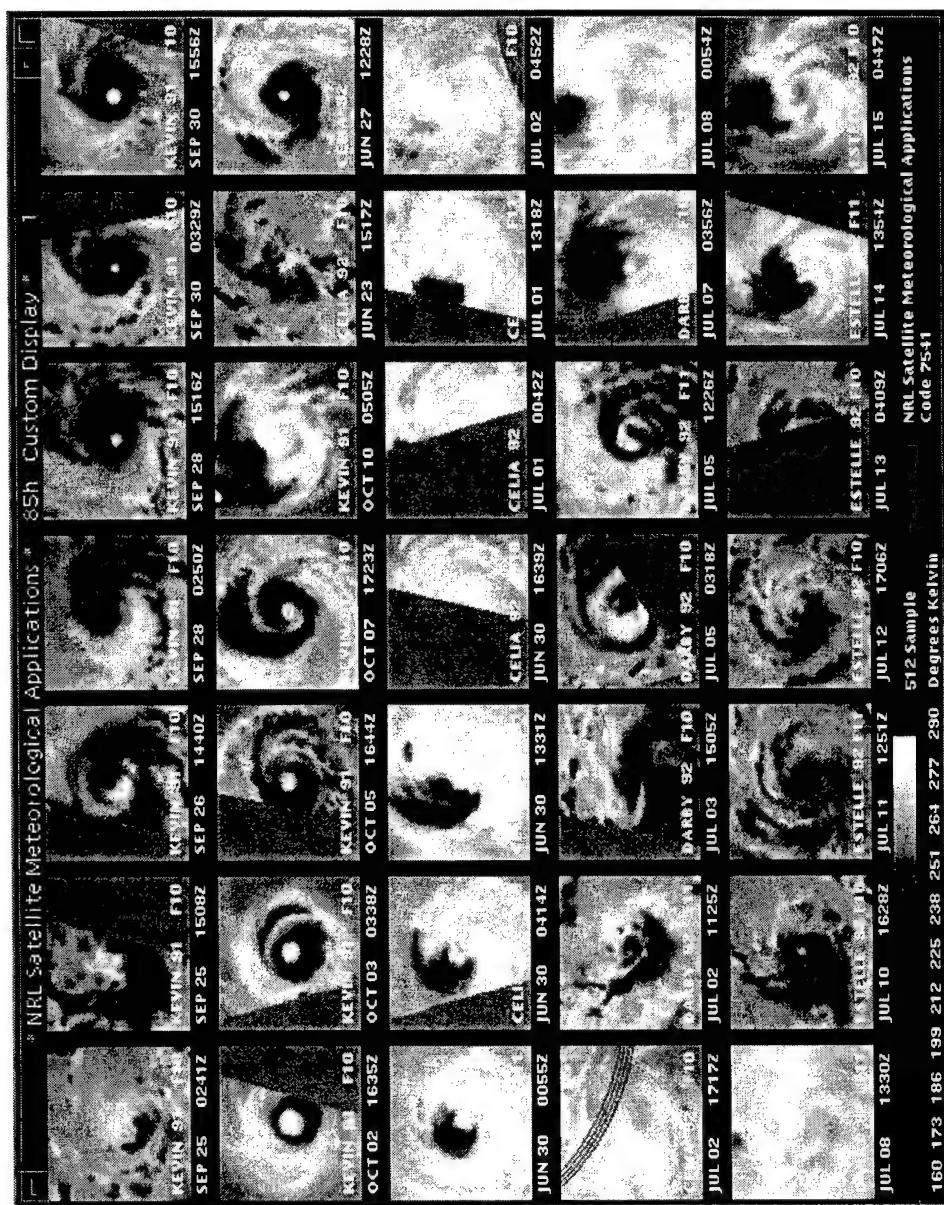


Figure 12: 35-panel TROPX display showing 85.5-GHz horizontally polarized T_B images of tropical cyclones observed by SSM/I and used in this present research (observations 1-35).

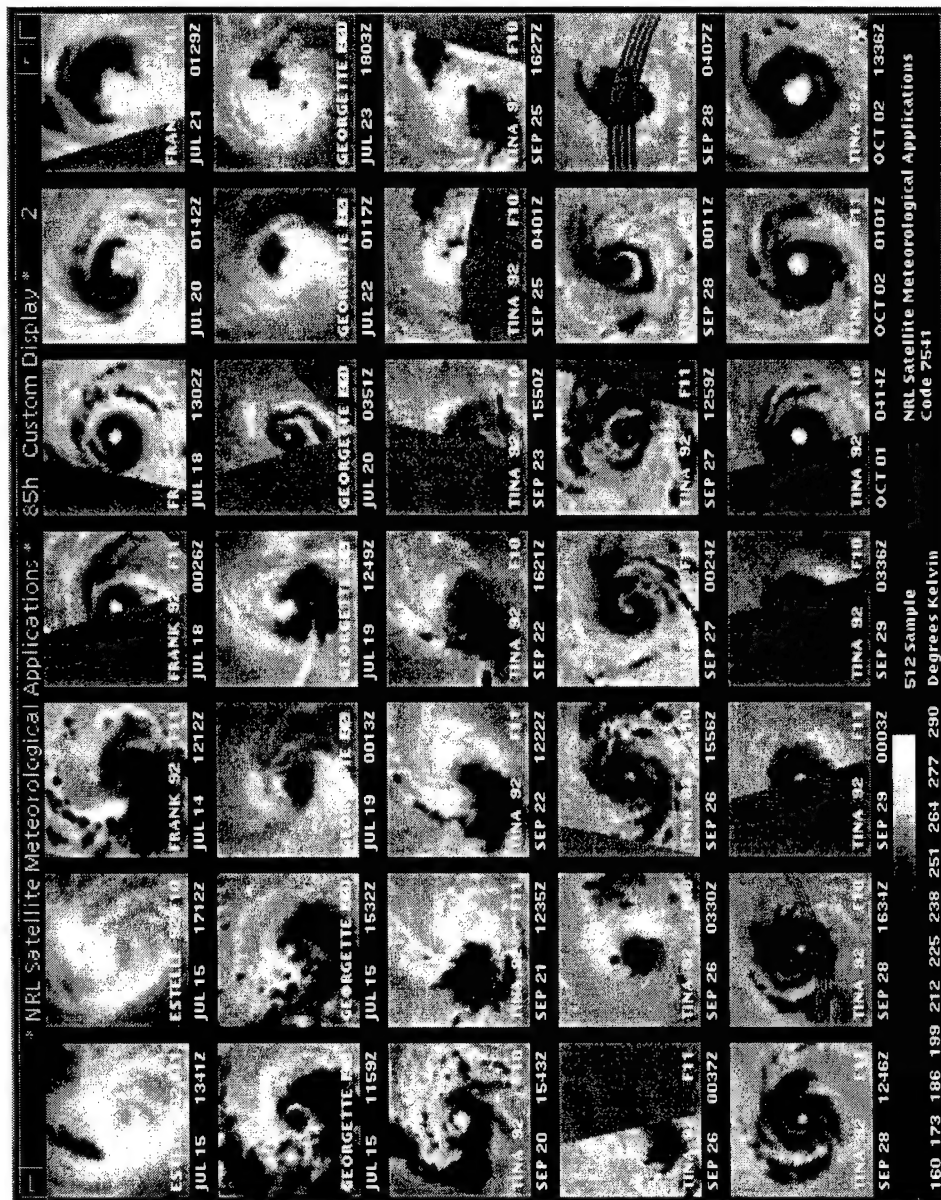


Figure 13: 35-panel TROPX display showing 85.5-GHz horizontally polarized T_B images of tropical cyclones observed by SSM/I and used in this present research (observations 36-70).

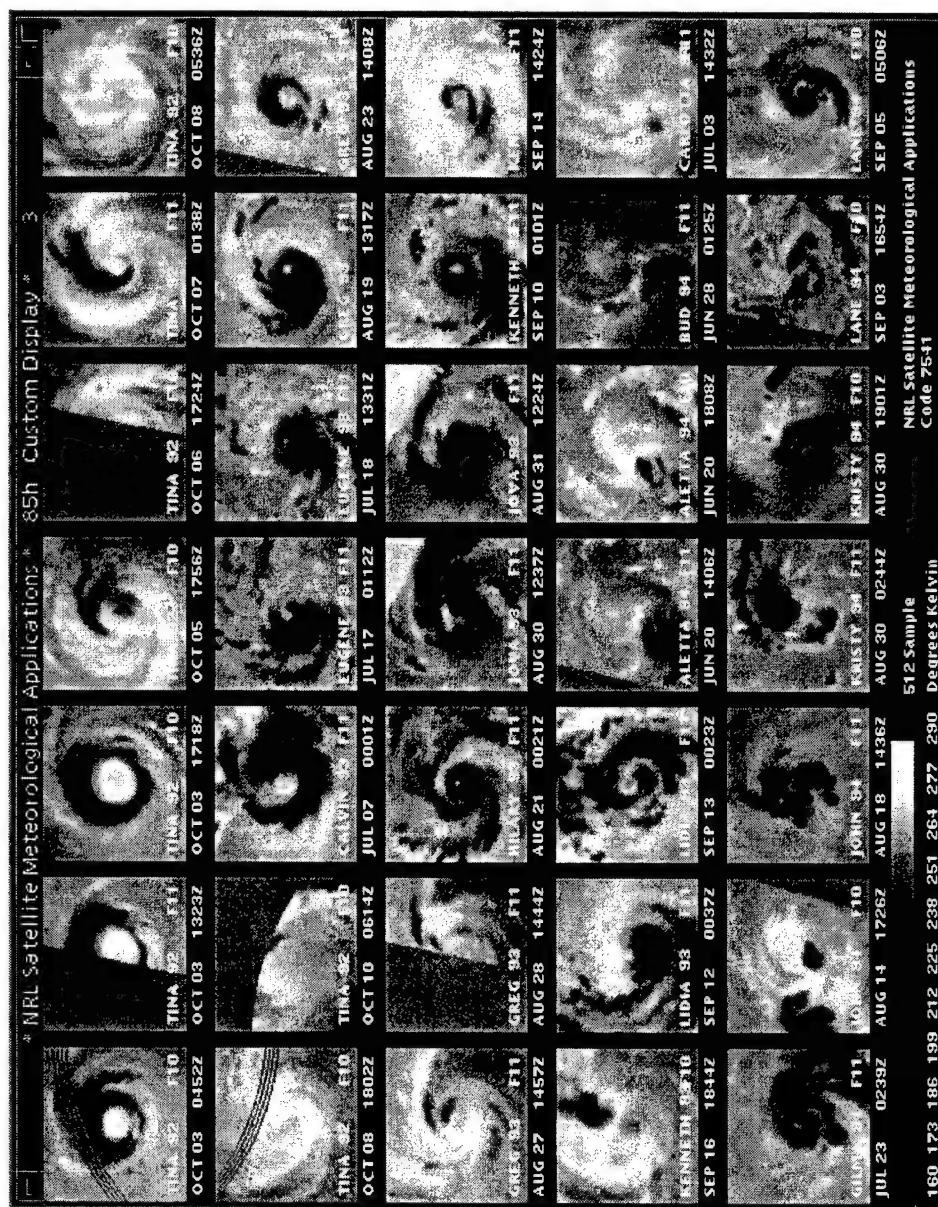


Figure 14: 35-panel TROPX display showing 85.5-GHz horizontally polarized T_B images of tropical cyclones observed by SSM/I and used in this present research (observations 71-105).

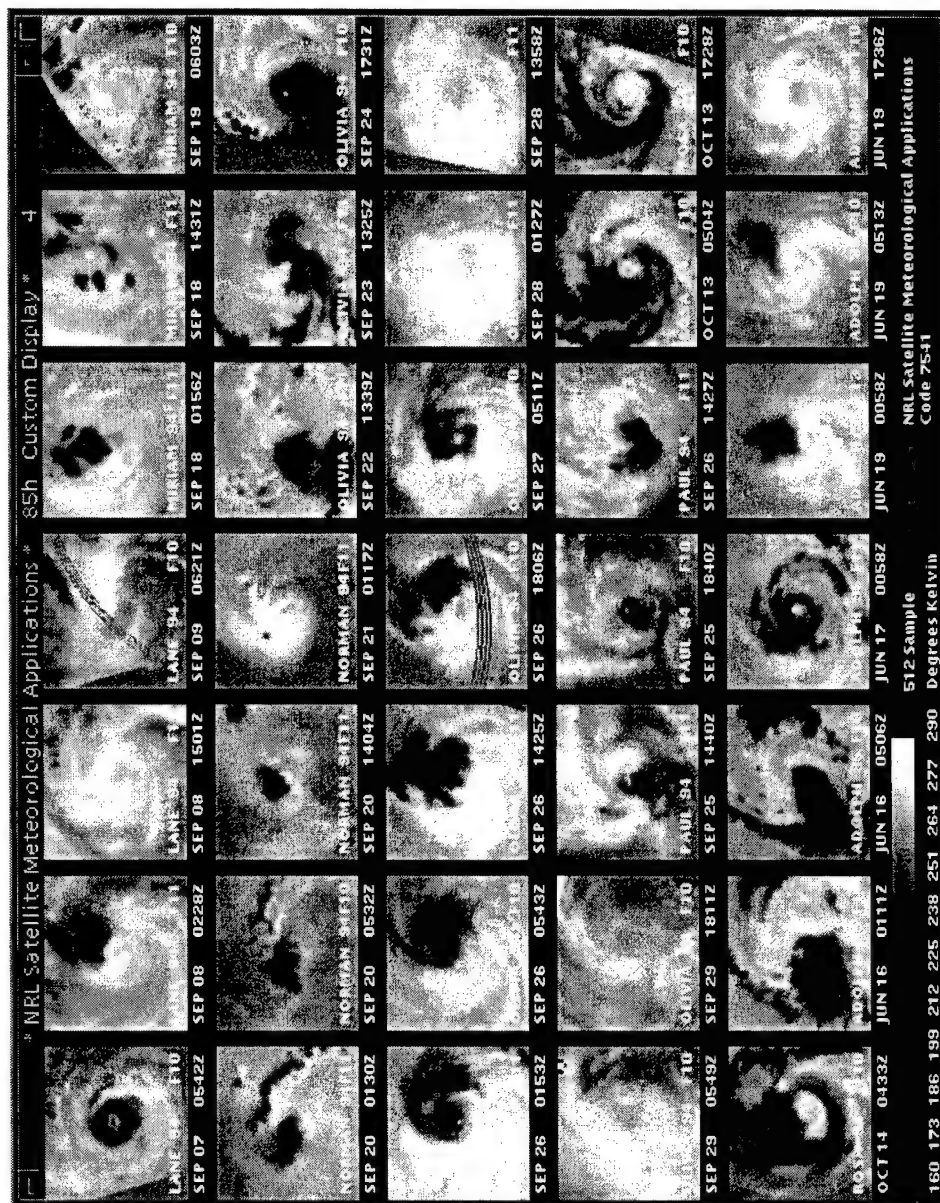


Figure 15: 35-panel TROPX display showing 85.5-GHz horizontally polarized T_B images of tropical cyclones observed by SSM/I and used in this present research (observations 106-140).

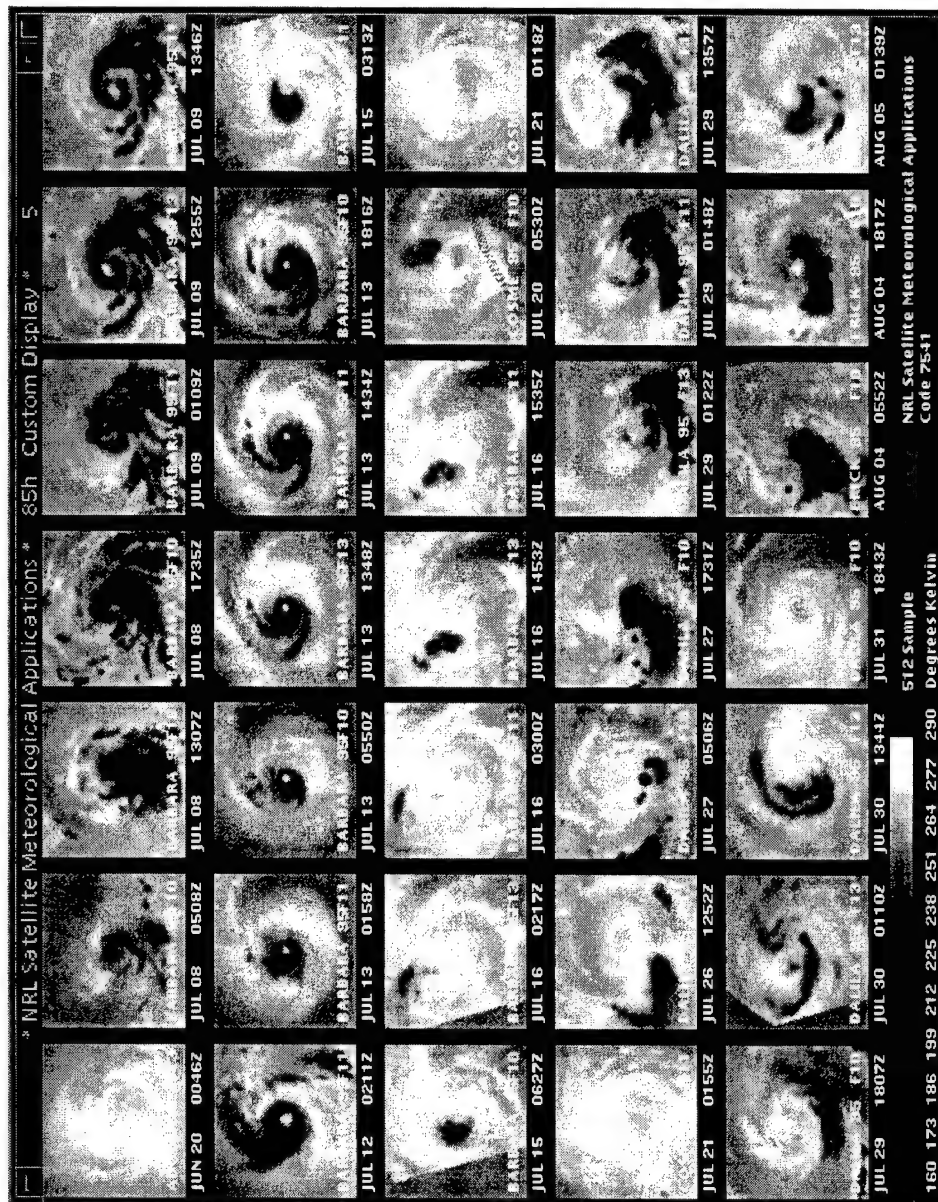


Figure 16: 35-panel TROPX display showing 85.5-GHz horizontally polarized T_B images of tropical cyclones observed by SSM/I and used in this present research (observations 141-175).

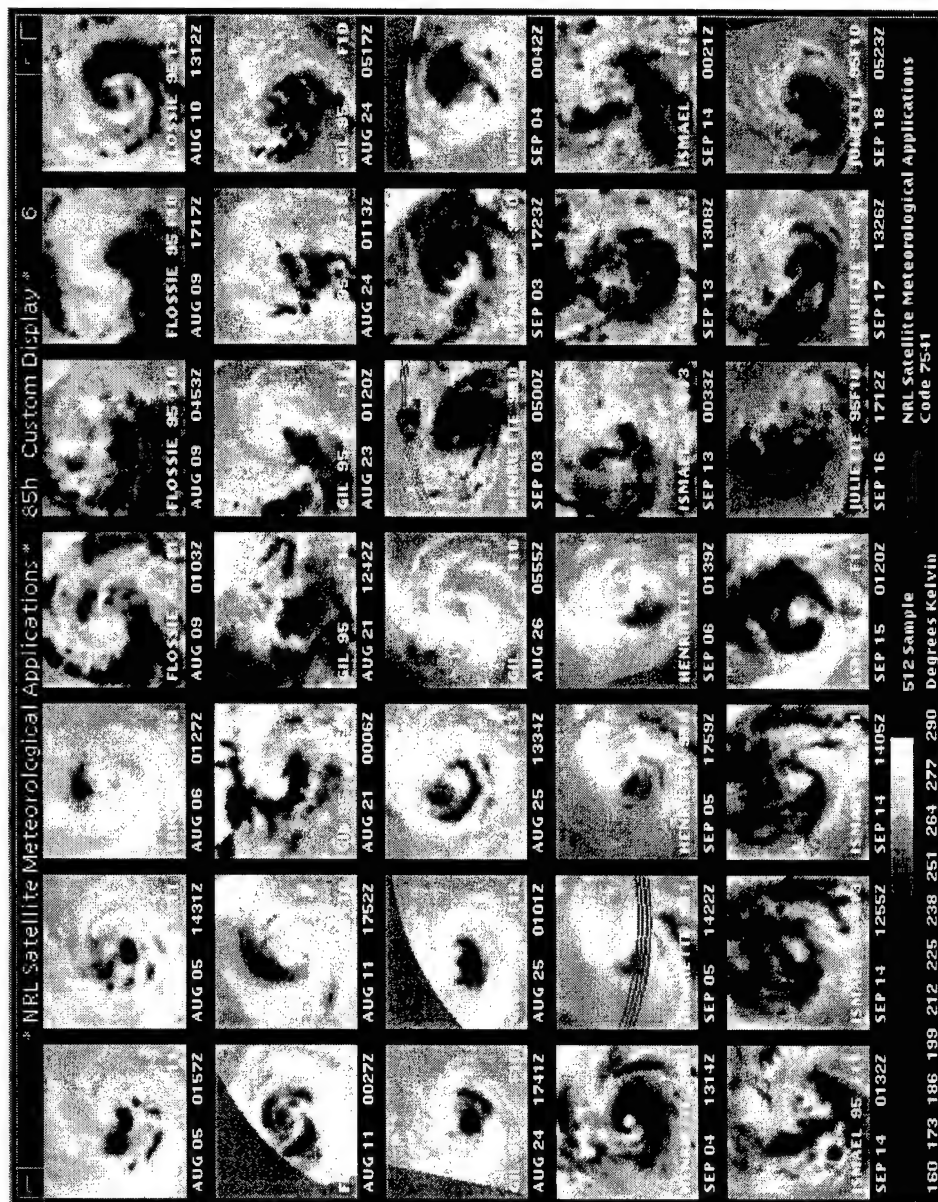


Figure 17: 35-panel TROPX display showing 85.5-GHz horizontally polarized T_B images of tropical cyclones observed by SSM/I and used in this present research (observations 176-210).

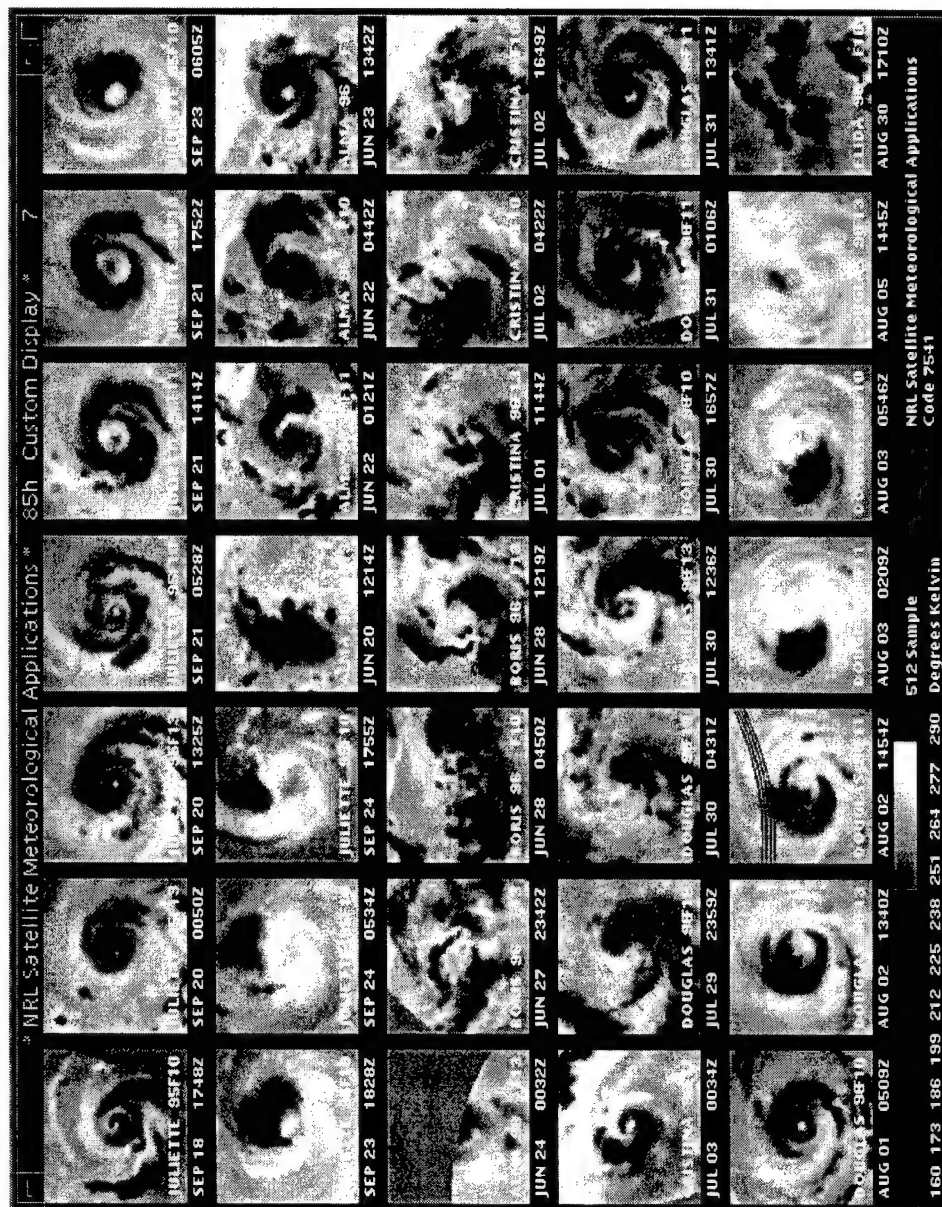


Figure 18: 35-panel TROPX display showing 85.5-GHz horizontally polarized T_b images of tropical cyclones observed by SSM/I and used in this present research (observations 211-245).

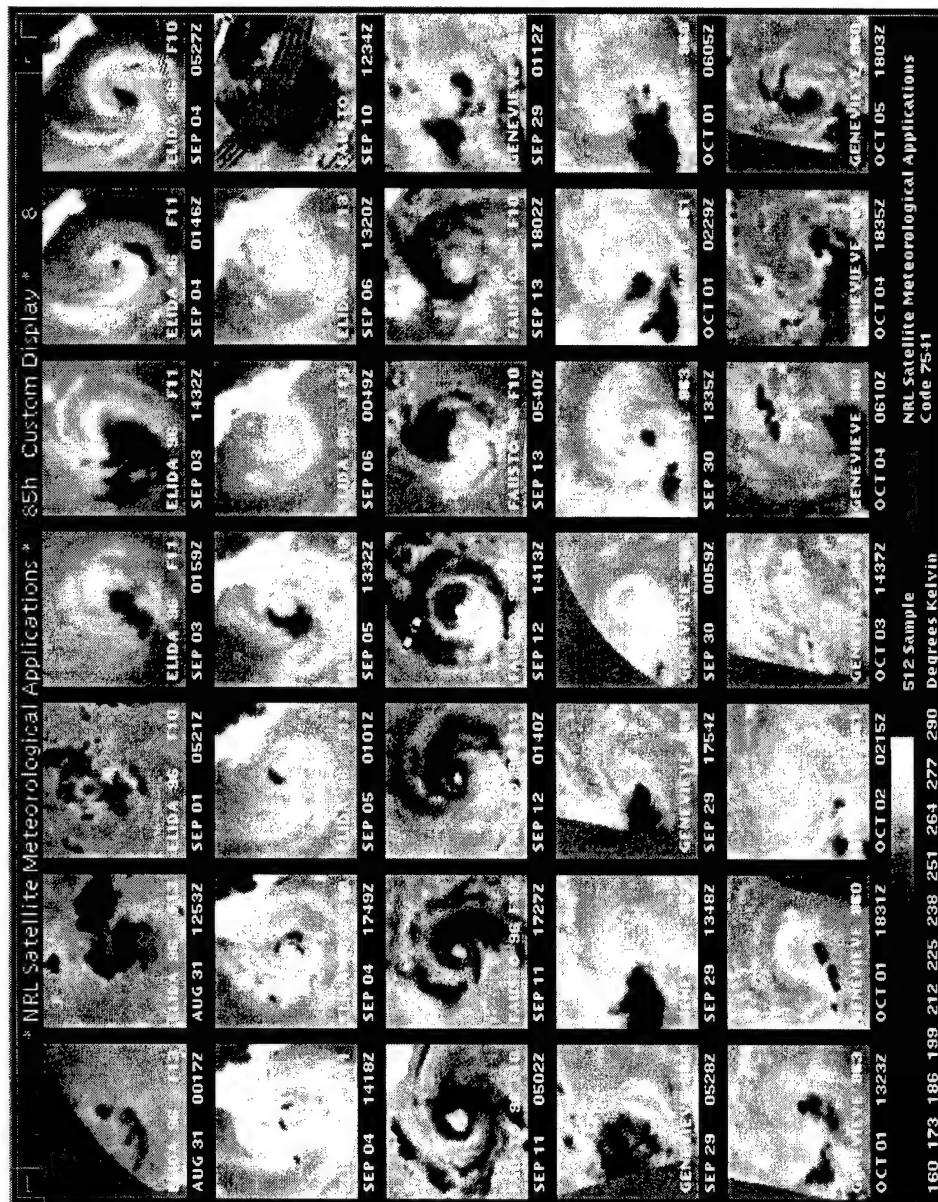


Figure 19: 35-panel TROPX display showing 85.5-GHz horizontally polarized T_B images of tropical cyclones observed by SSM/I and used in this present research (observations 246-280).

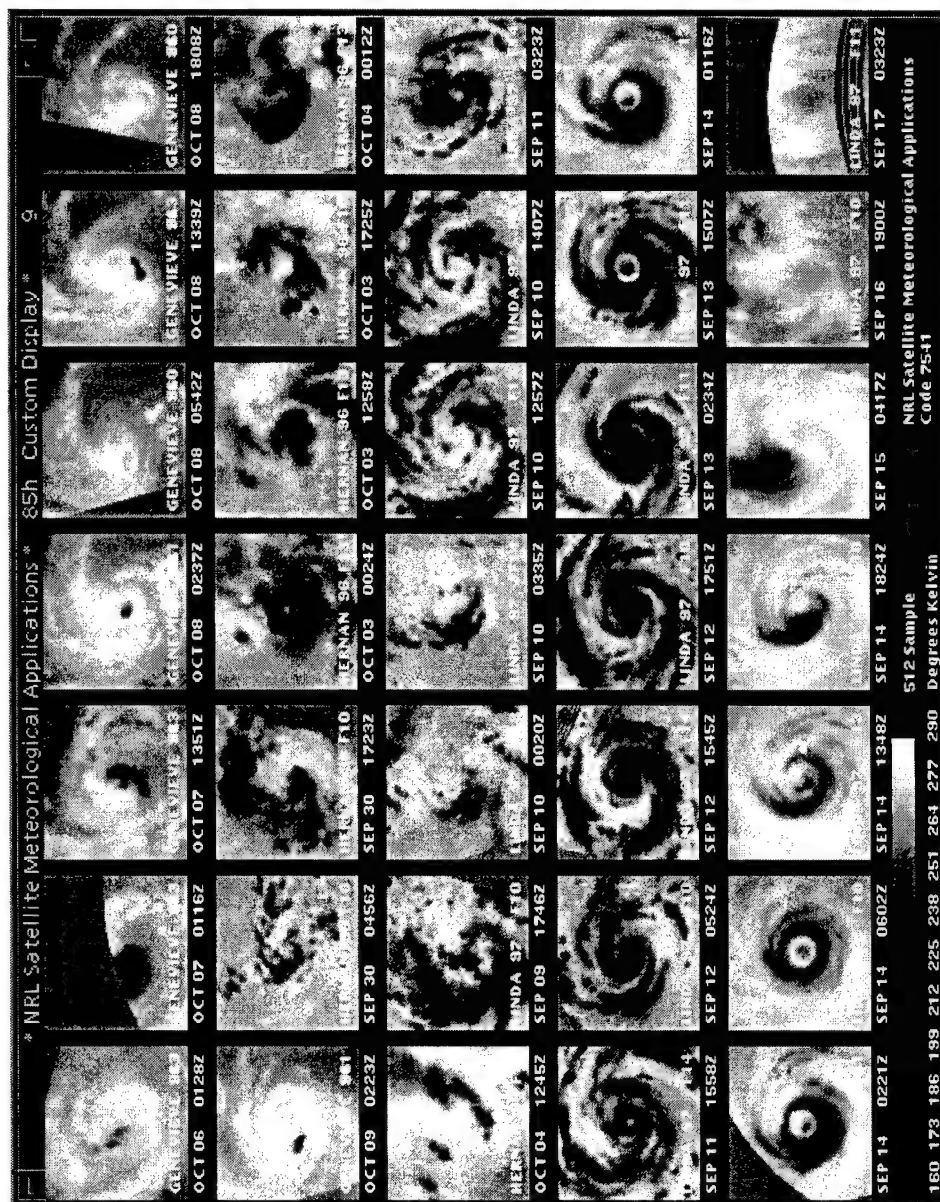


Figure 20: 35-panel TROPX display showing 85.5-GHz horizontally polarized T_B images of tropical cyclones observed by SSM/I and used in this present research (observations 281-315).

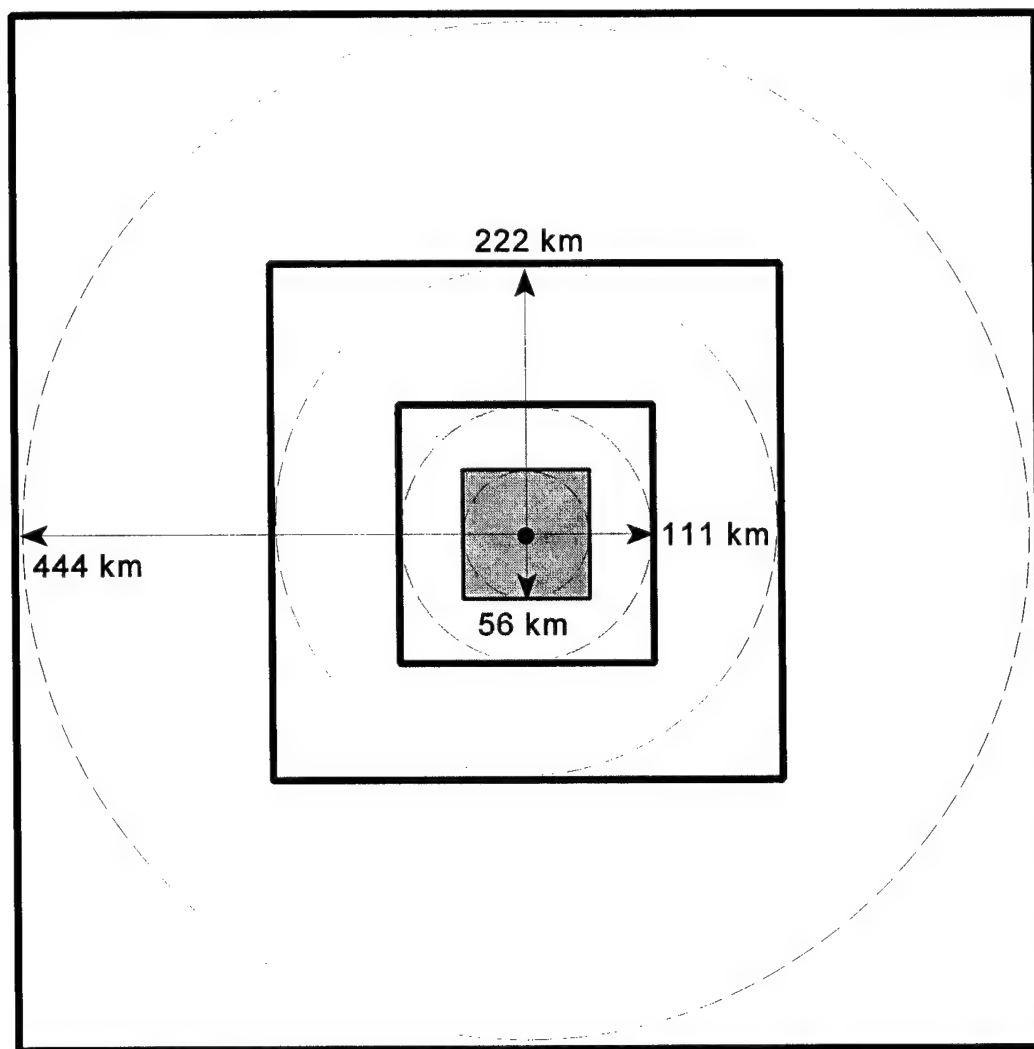


Figure 21: Regions used to calculate rainfall parameters. Radial distance for each region is indicated near the radii arrowheads. The 444-, 222-, 111-, and 56-km radii correspond to the total, core, inner-core, and central-core regions of the tropical cyclone, respectively.

1991–1997 Tropical Cyclone Tracks

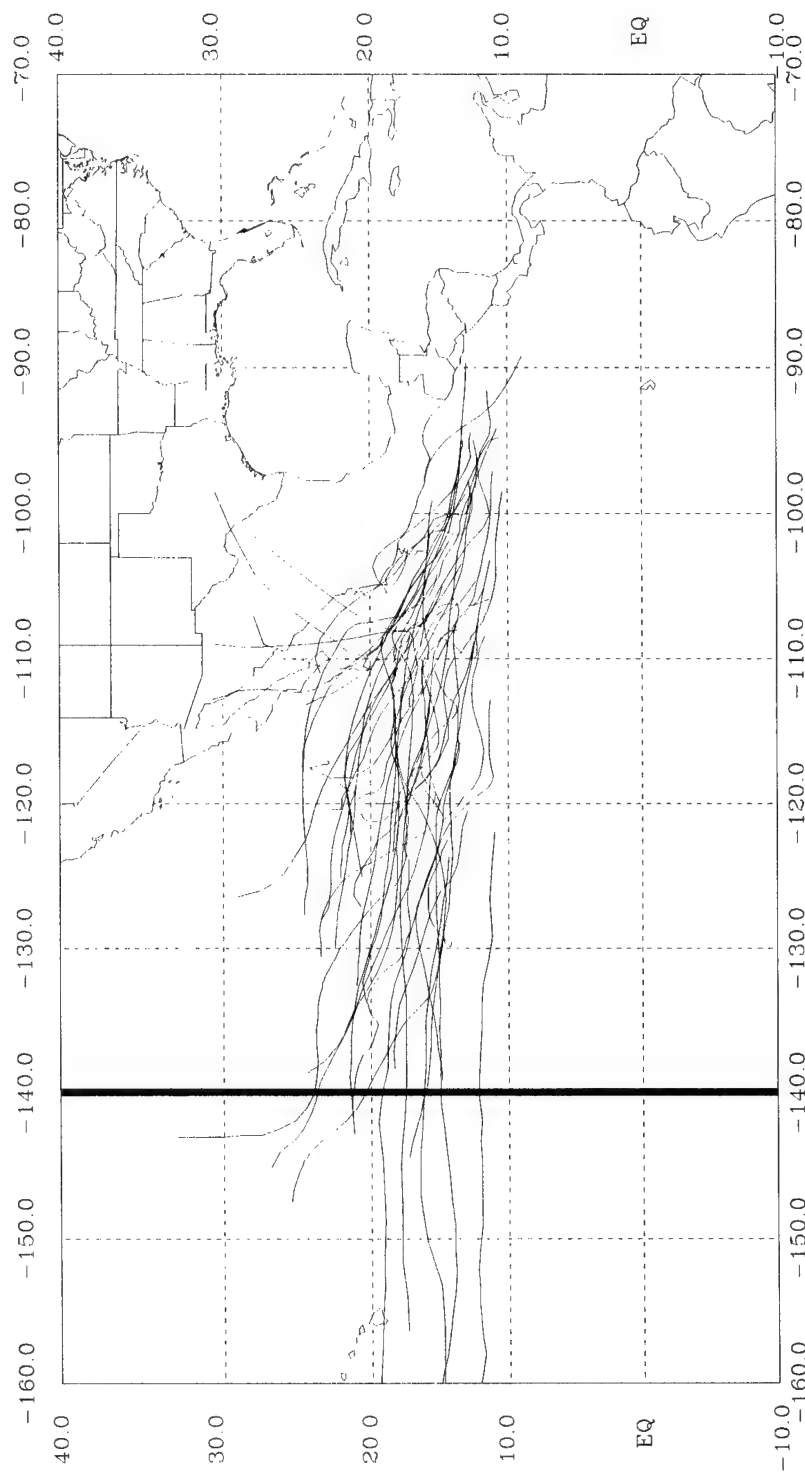


Figure 22: Plotted tracks of tropical cyclones from 1991 to 1997 studied in this research. Bold vertical line indicates western boundary of eastern North Pacific Ocean basin (140 °W).

Tropical Cyclone Tracks for Model Training

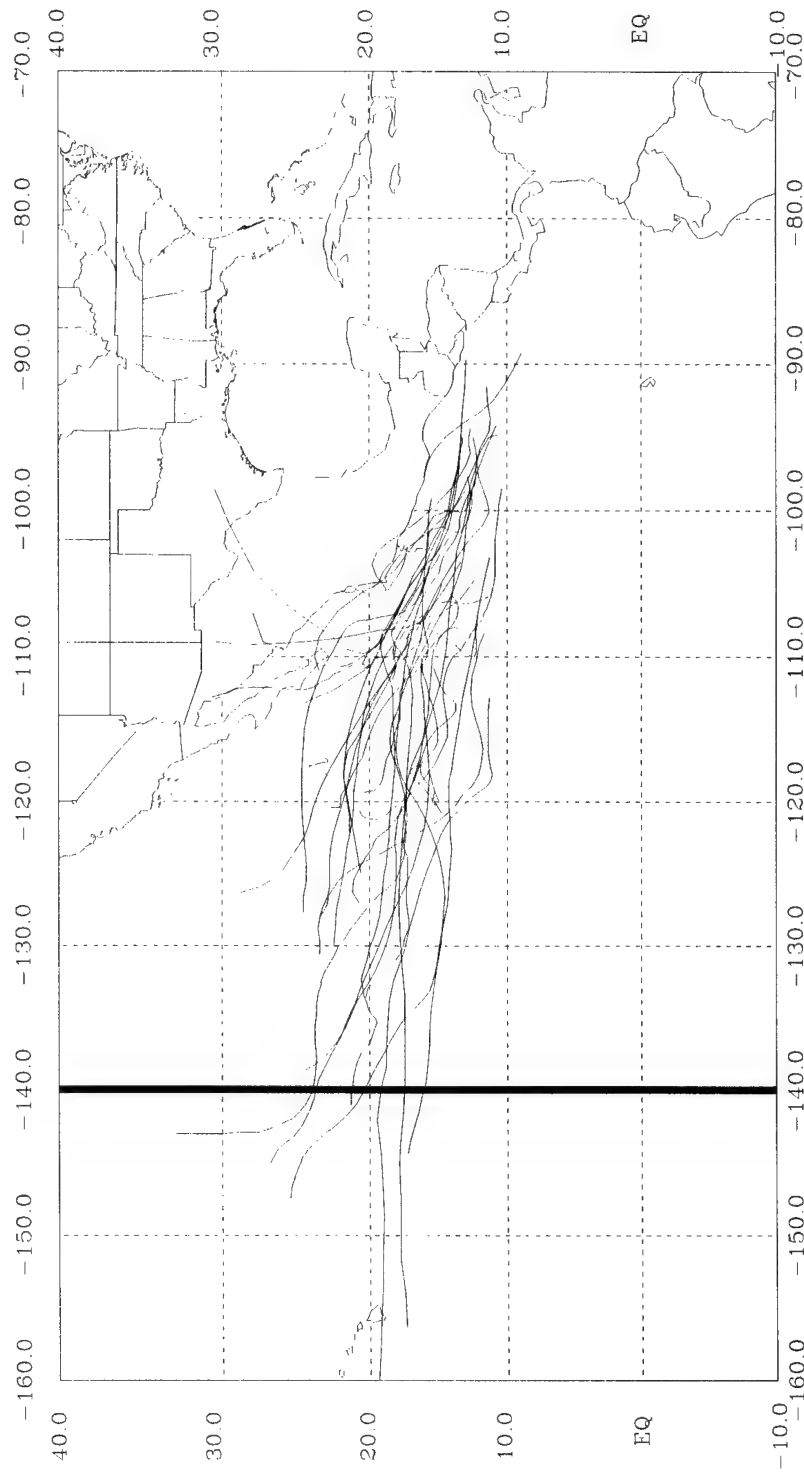


Figure 23: Plotted tracks of tropical cyclones from 1991 to 1997 used to develop regression models for this research. Bold vertical line indicates western boundary of eastern North Pacific Ocean basin (140°W).

Tropical Cyclone Tracks for Model Testing

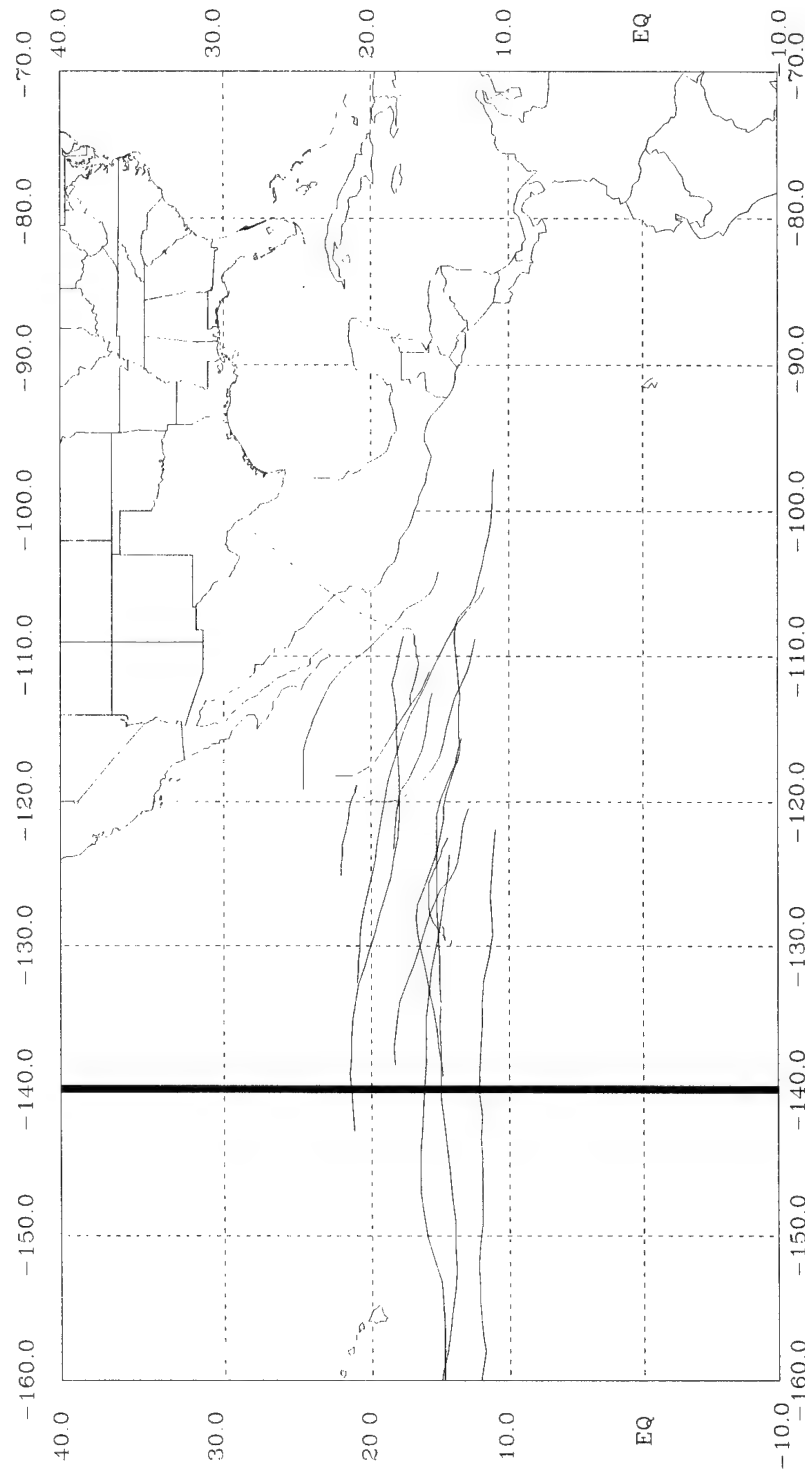


Figure 24: Plotted tracks of tropical cyclones from 1994 and 1995 used to evaluate regression models for this research. Bold vertical line indicates western boundary of eastern North Pacific Ocean basin (140°W).

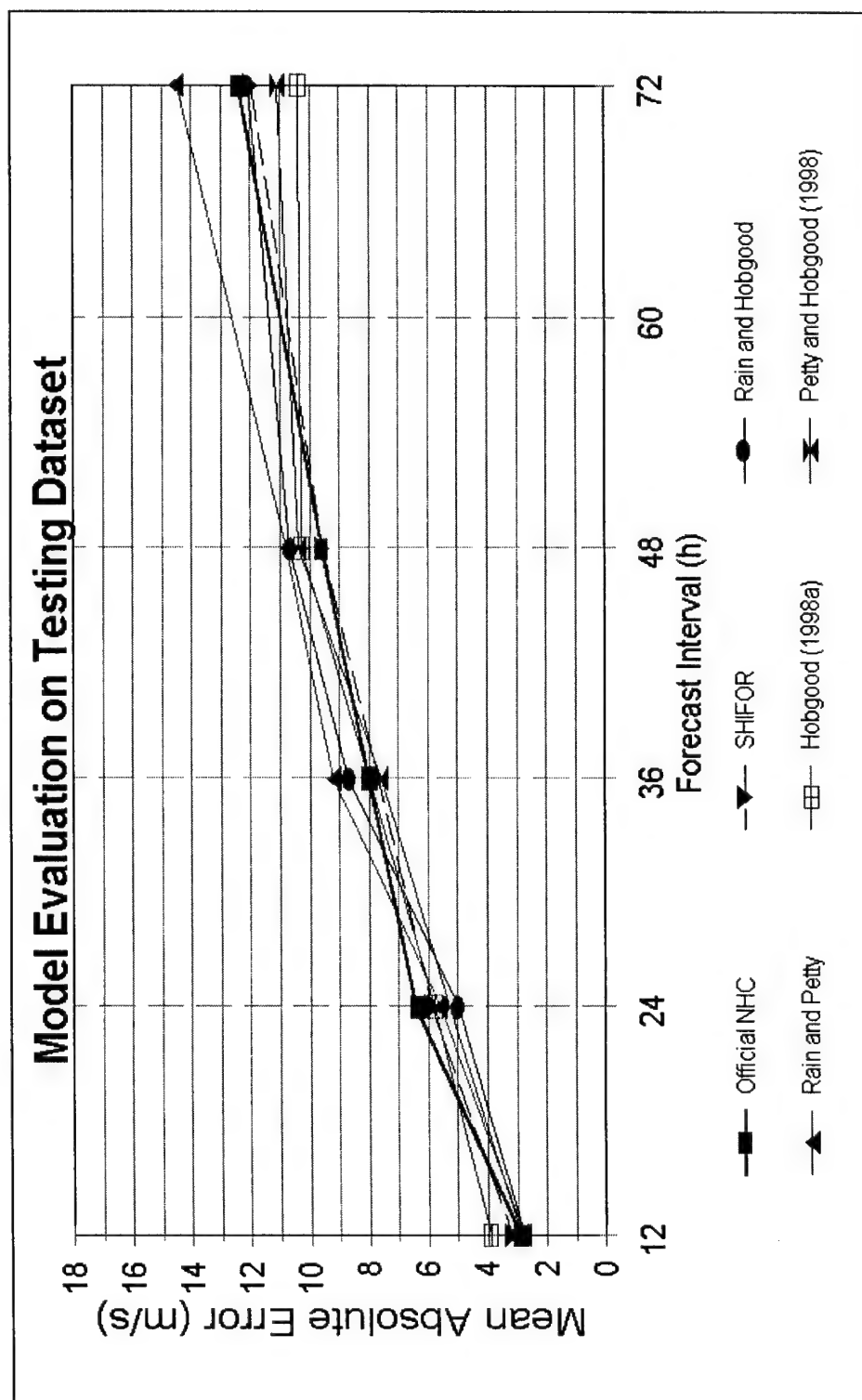


Figure 25: Homogeneous evaluation of forecast methods on testing dataset.

Tina (1992) Track

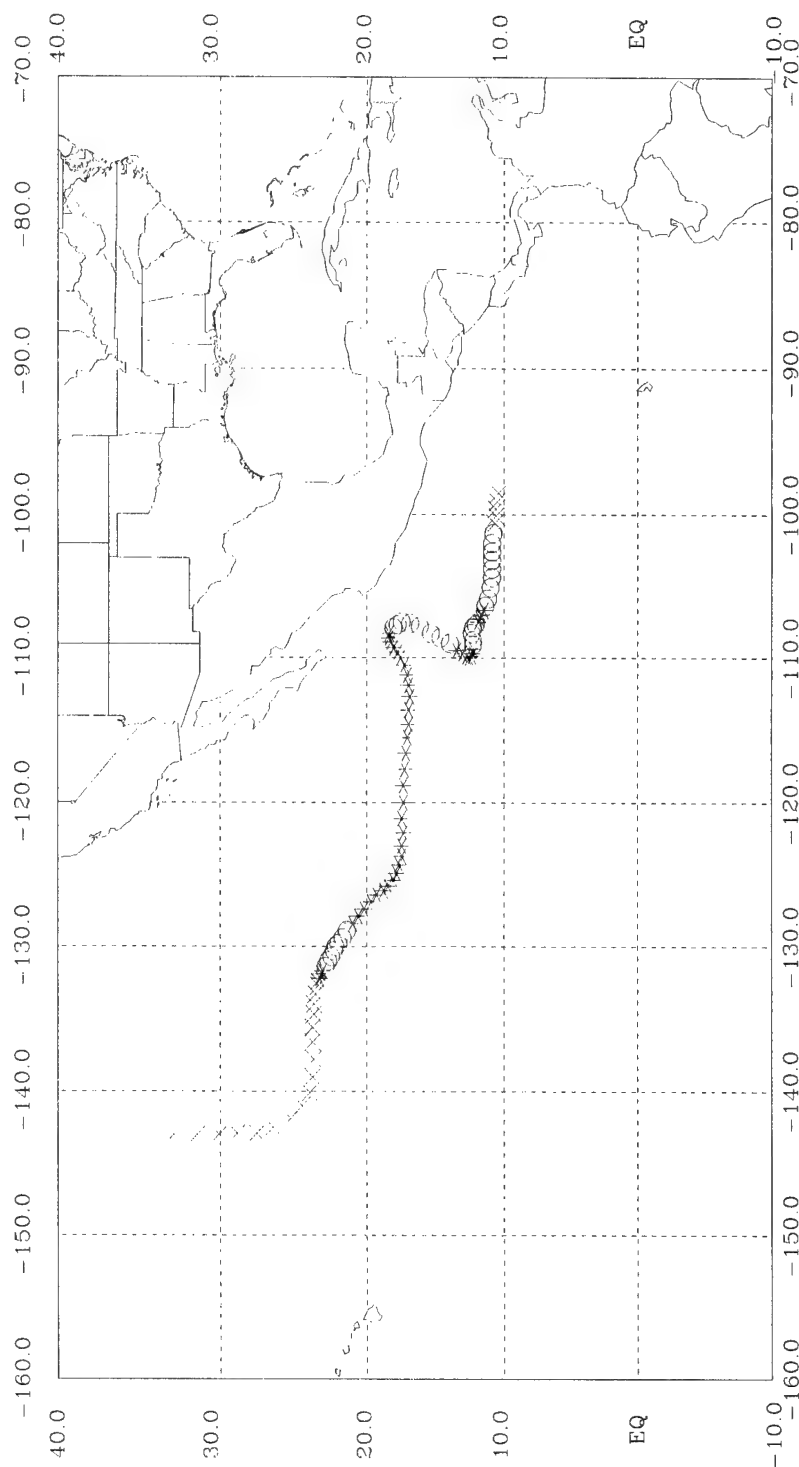


Figure 26: Plotted track of Hurricane Tina (1992). Tropical depression, tropical storm, and hurricane intensity stages are indicated by x, o, and *, respectively.

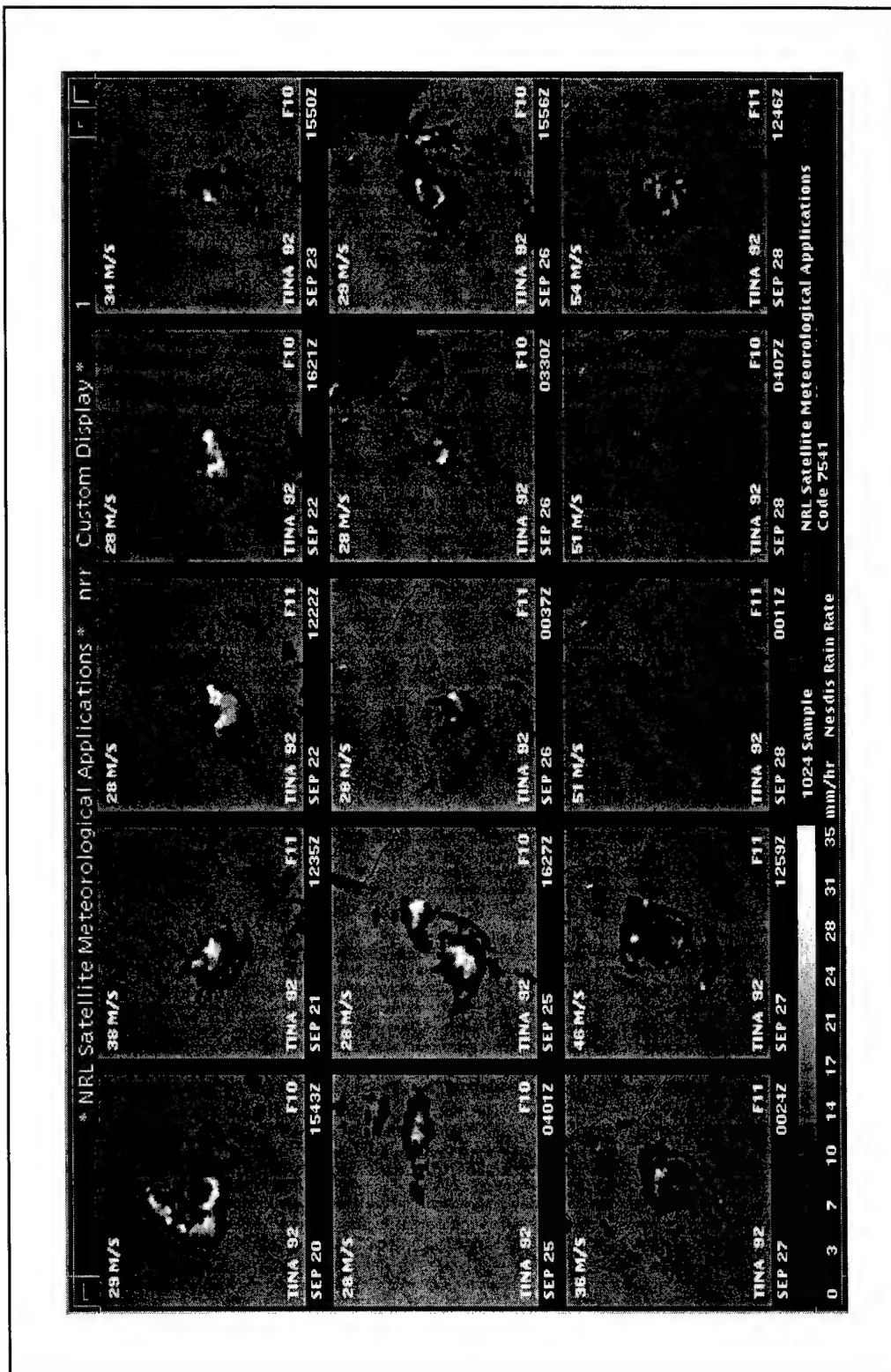


Figure 27: 15-panel TROPX display showing NESDIS/ORA rainfall algorithm applied to SSM/I observations of Hurricane Tina (1992) during 20-28 September. Current interpolated intensity is indicated in the upper-left of each panel. Satellite flight number is depicted in the lower-right of each panel.

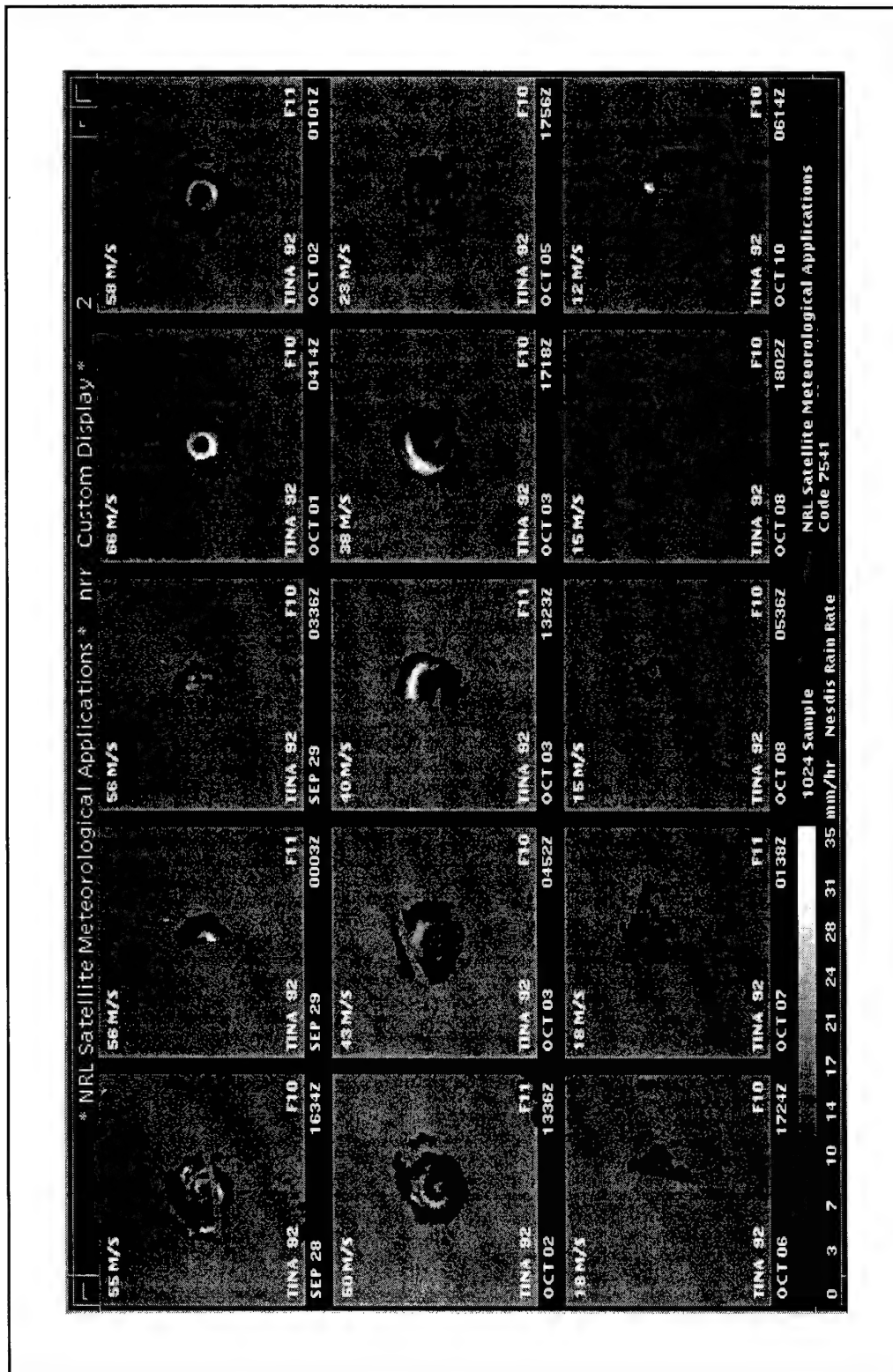


Figure 28: 15-panel TROPX display showing NESDIS/ORA rainfall algorithm applied to SSM/I observations of Hurricane Tina (1992) during 28 September-10 October. Current interpolated intensity is indicated in the upper-left of each panel. Satellite flight number is depicted in the lower-right of each panel.

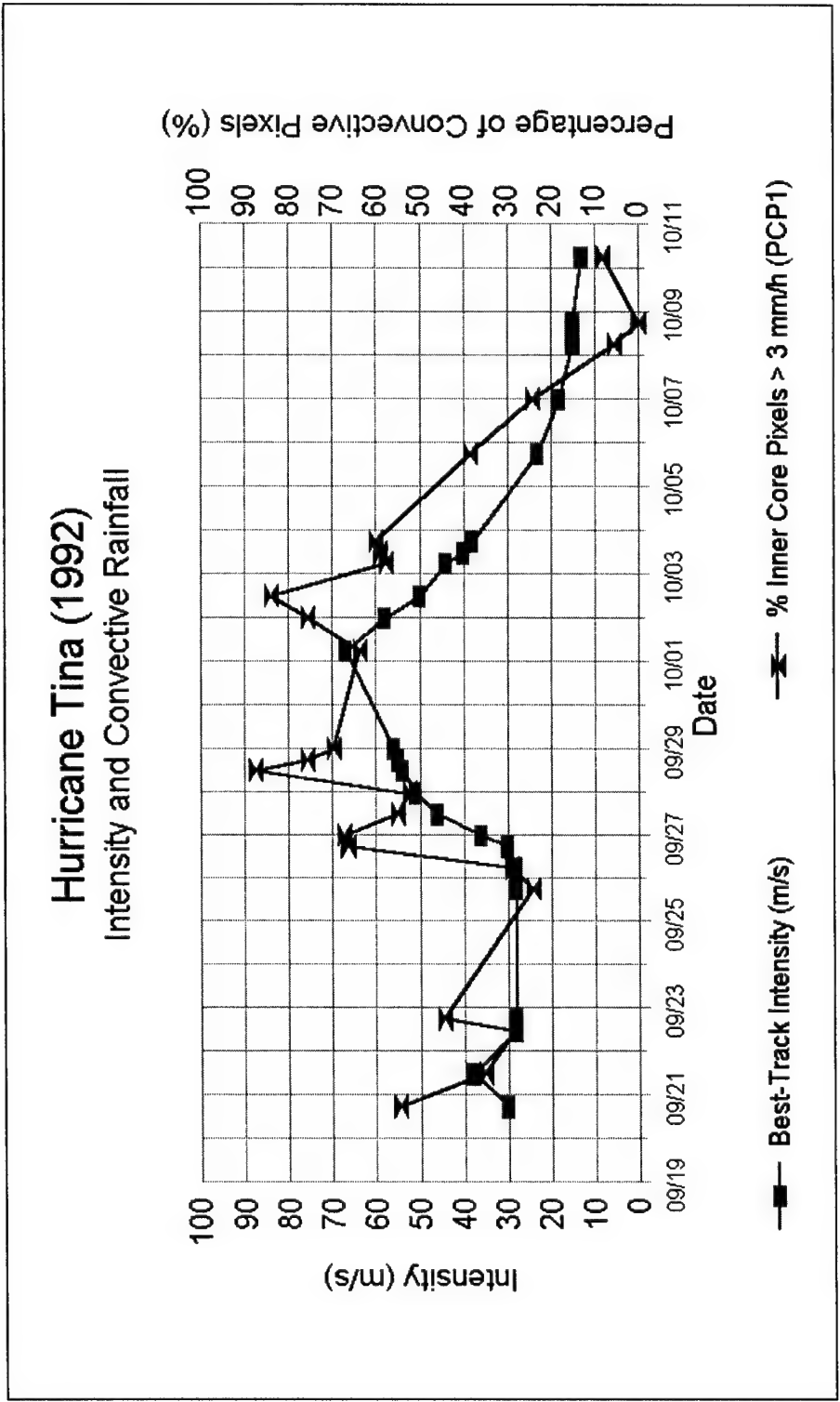


Figure 29: Temporal variation of current intensity and convective rainfall (PCP1) for SSM/I observations of Hurricane Tina (1992).

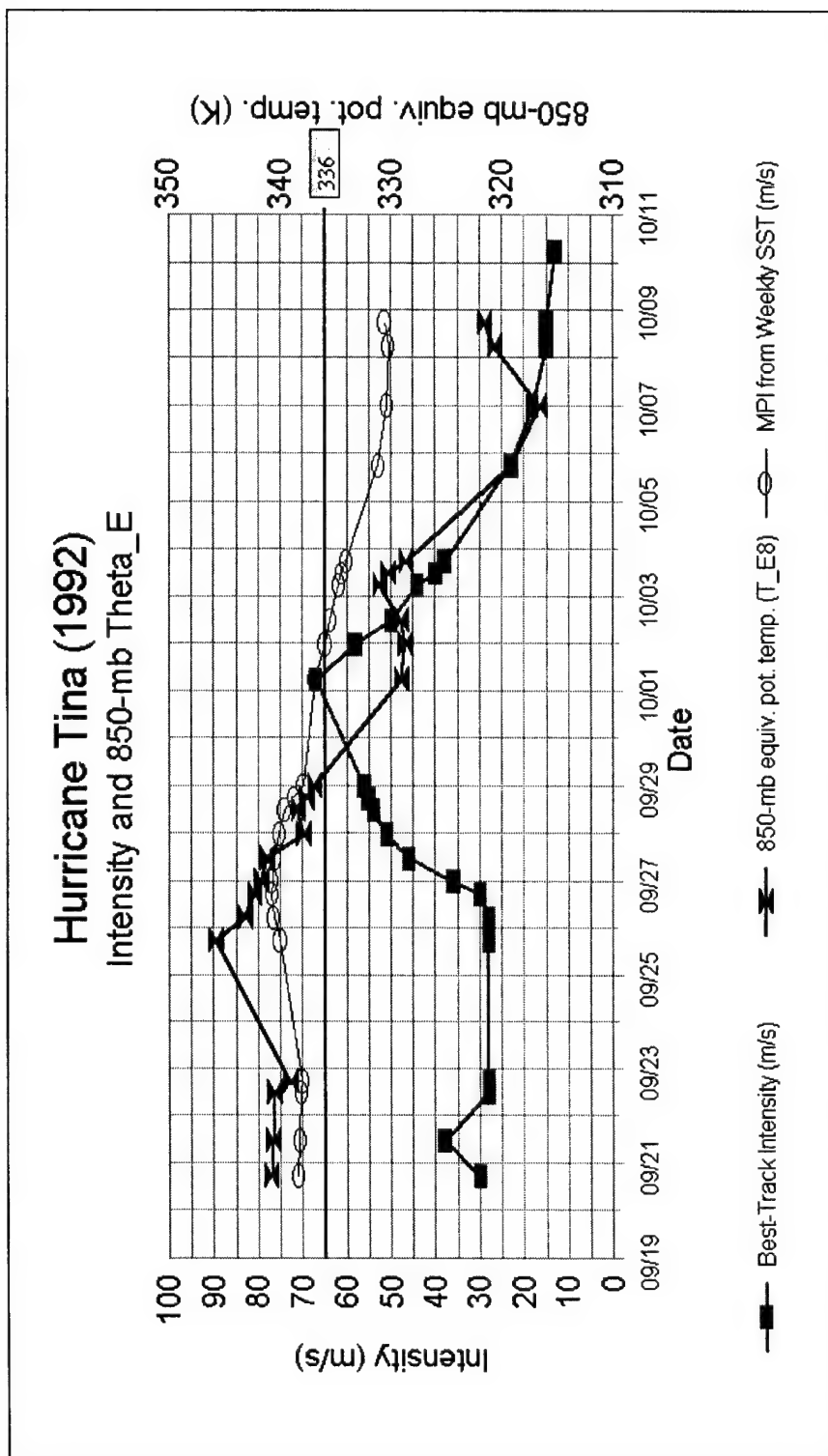


Figure 30: Temporal variation of current intensity and 850-mb equivalent potential temperature (θ_e) for Hurricane Tina (1992). MPI is included for comparison to current intensity. A reference line at 336 K is provided as a threshold between high and low values of 850-mb θ_e .

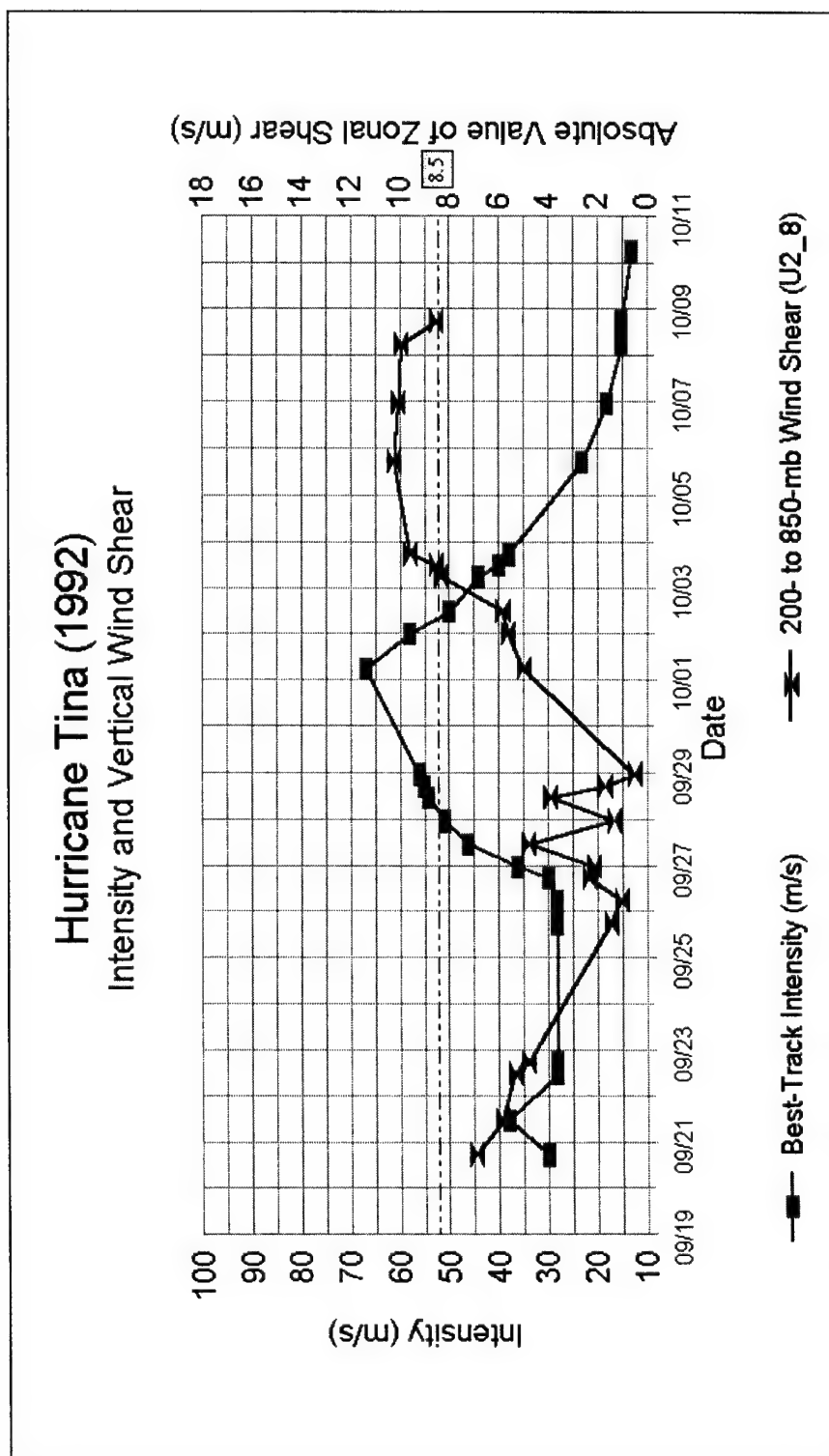


Figure 31: Temporal variation of current intensity and absolute value of 200- to 850-mb vertical shear of the zonal horizontal wind (U2_8) for Hurricane Tina (1992). A reference line at 8.5 m s⁻¹ is provided as a threshold between high and low values of vertical shear.

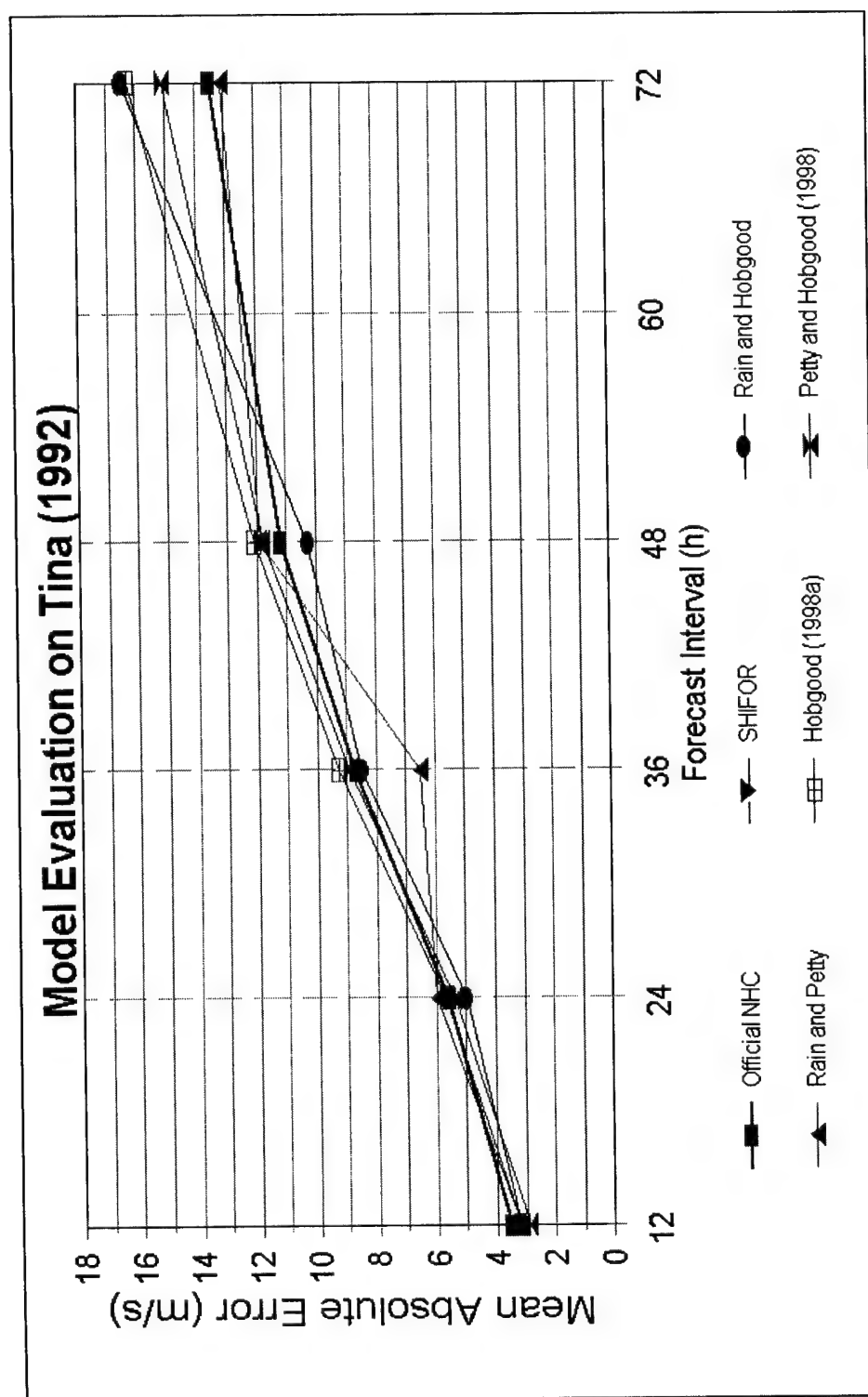


Figure 32: Homogeneous evaluation of forecast methods on Hurricane Tina (1992). Data not available for SHIFOR.

Olivia (1994) Track

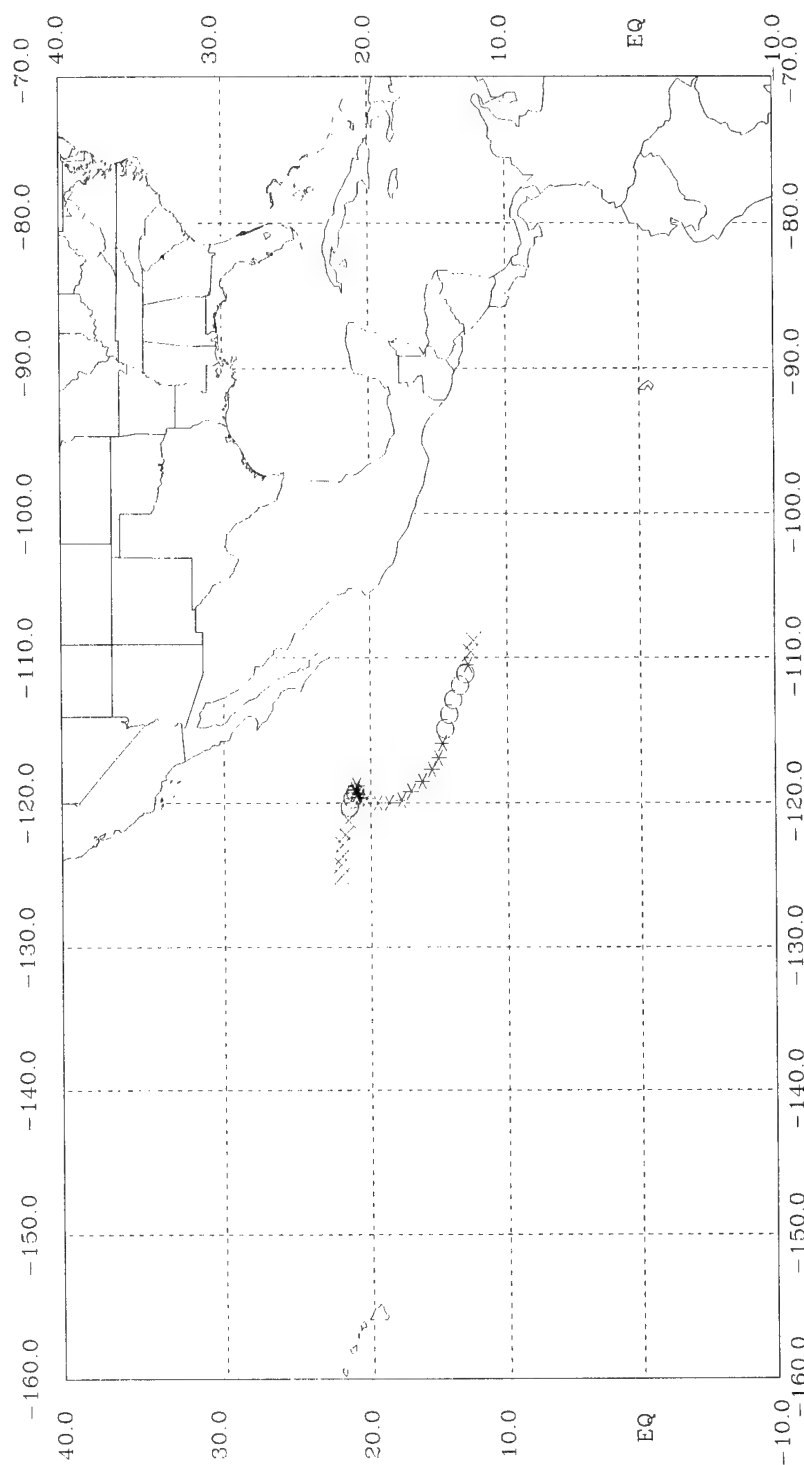


Figure 33: Plotted track of Hurricane Olivia (1994). Tropical depression, tropical storm, and hurricane intensity stages are indicated by x, o, and *, respectively.

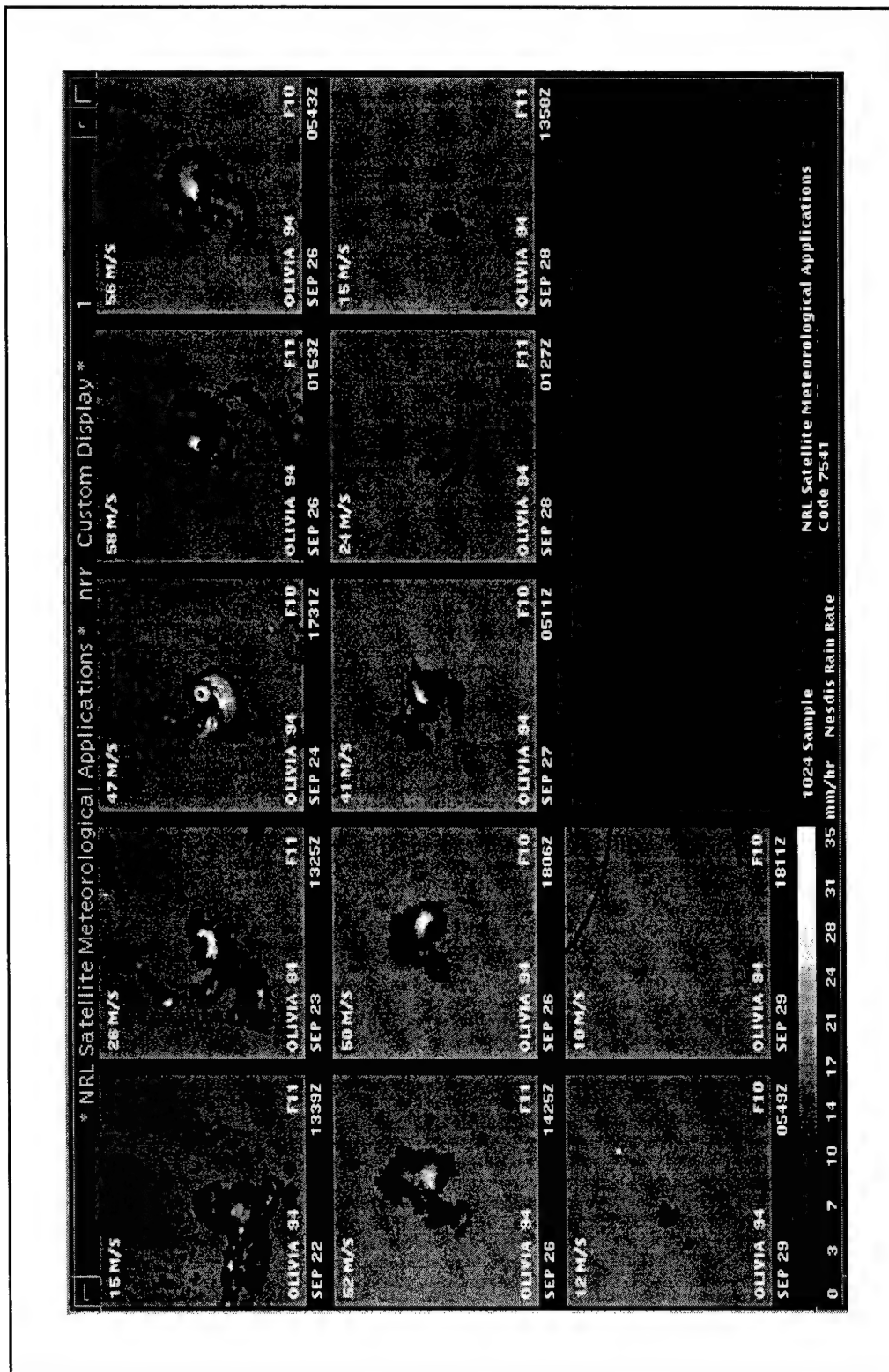


Figure 34: 15-panel TROPX display showing NESDIS/ORA rainfall algorithm applied to SSM/I observations of Hurricane Olivia (1994) during 22-29 September. Current interpolated intensity is indicated in the upper-left of each panel. Satellite flight number is depicted in the lower-right of each panel.

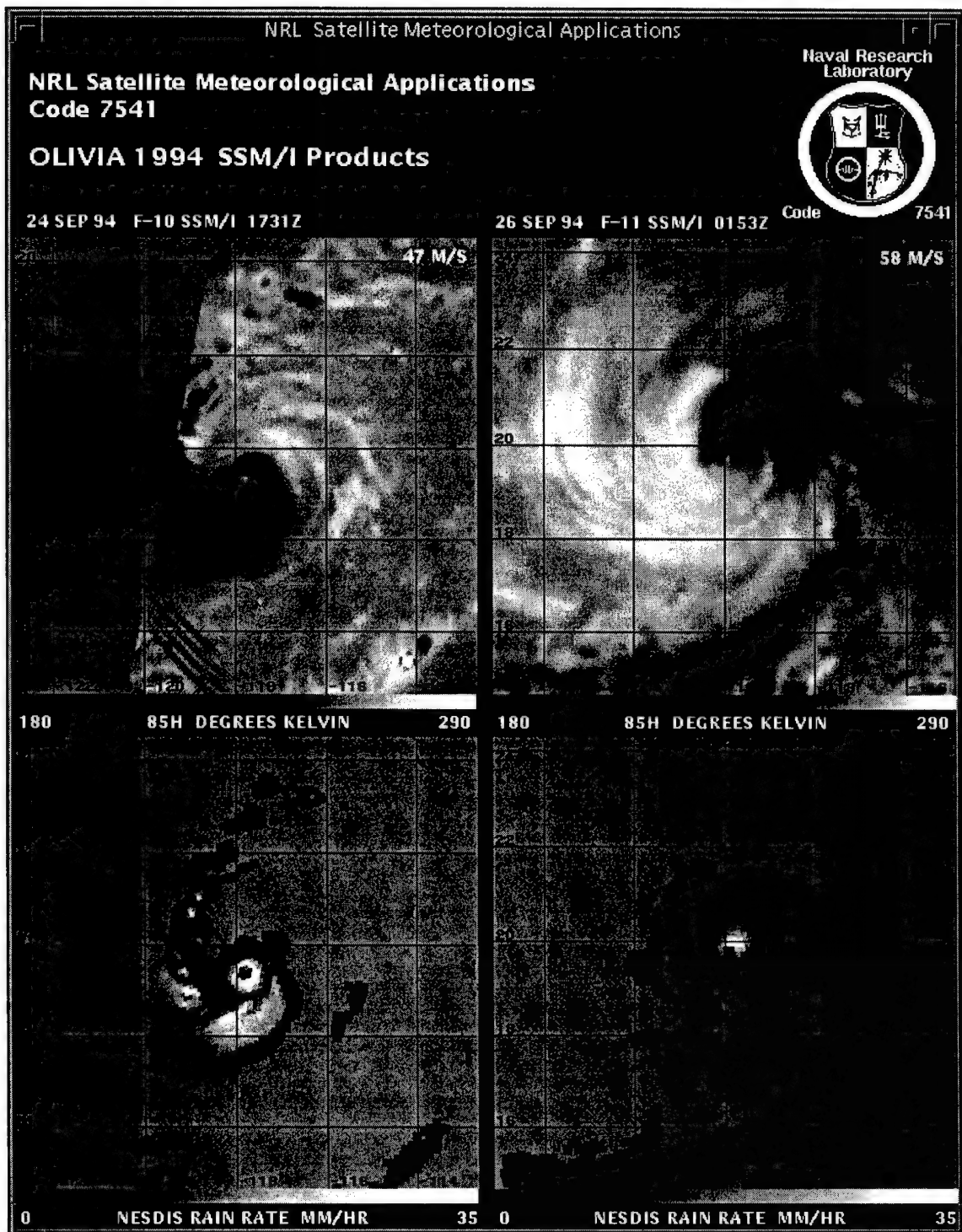


Figure 35: 4-panel TROPX display showing two SSM/I observations of Hurricane Olivia (1994) on 24 and 26 September. Top panels are 85.5-GHz horizontally polarized T_B images. Bottom panels are NESDIS/ORA rainfall images.

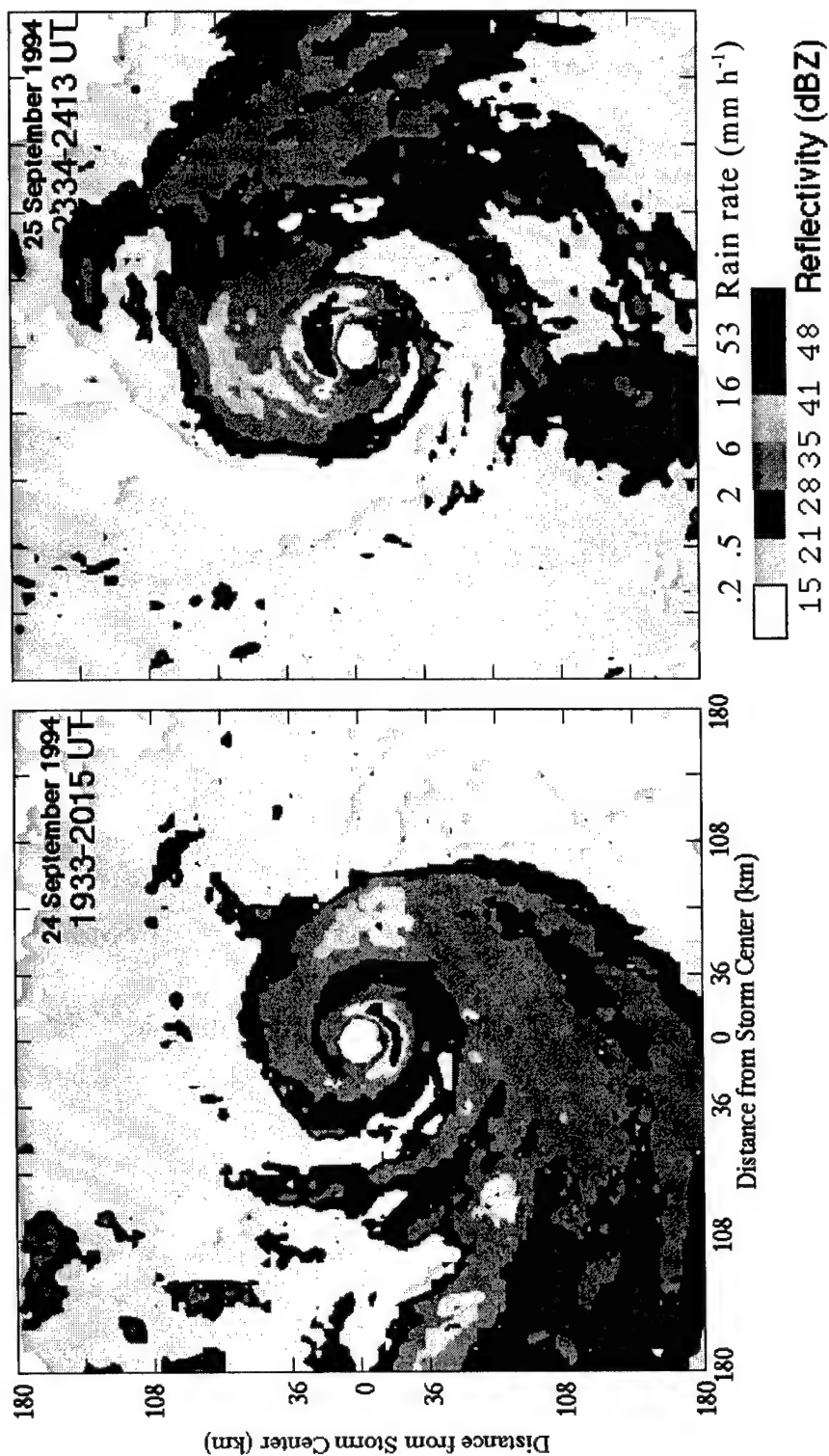


Figure 36: 2-panel graphic of composites obtained from radar onboard NOAA WP-3D aircraft flights into Hurricane Olivia (1994) during 24 to 26 September. Distance and reflectivity scales apply to both panels. Graphic adapted from image file located at http://www.aoml.noaa.gov/hrd/graphics/OlivLF_2days.GIF.

Hurricane Olivia (1994)

Intensity and Convective Rainfall

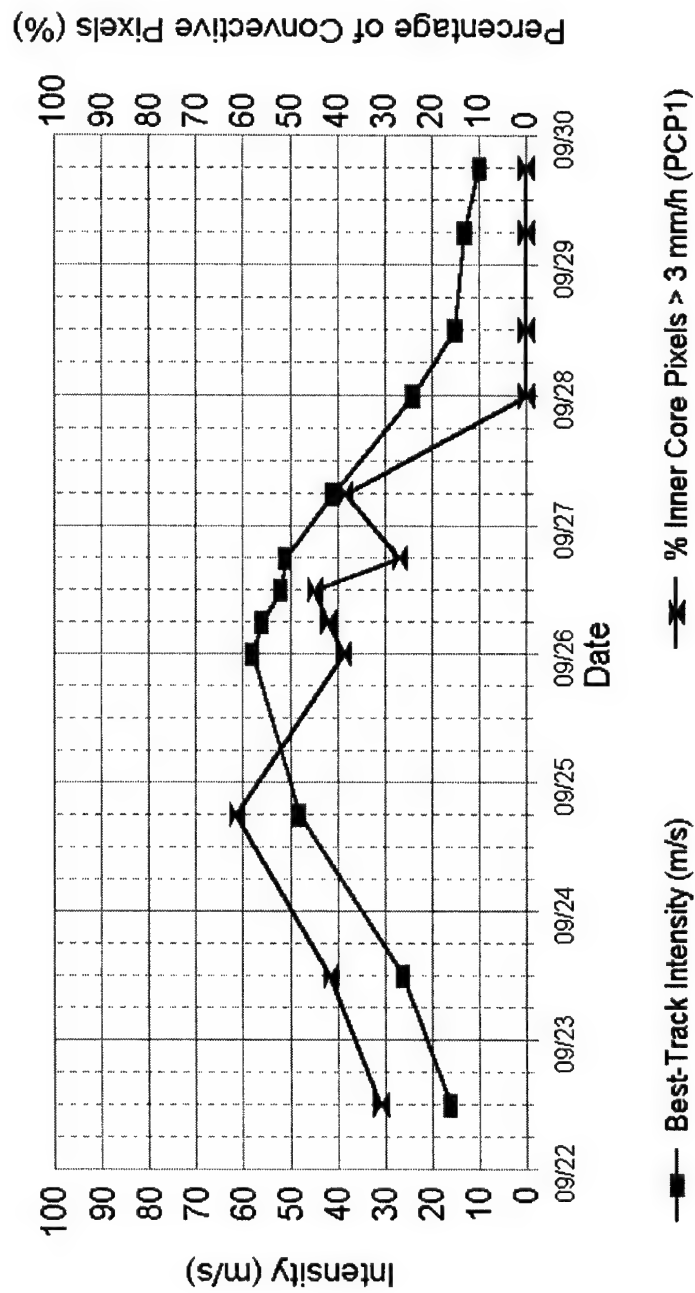


Figure 37: Temporal variation of current intensity and convective rainfall (PCP1) for SSM/I observations of Hurricane Olivia (1994).

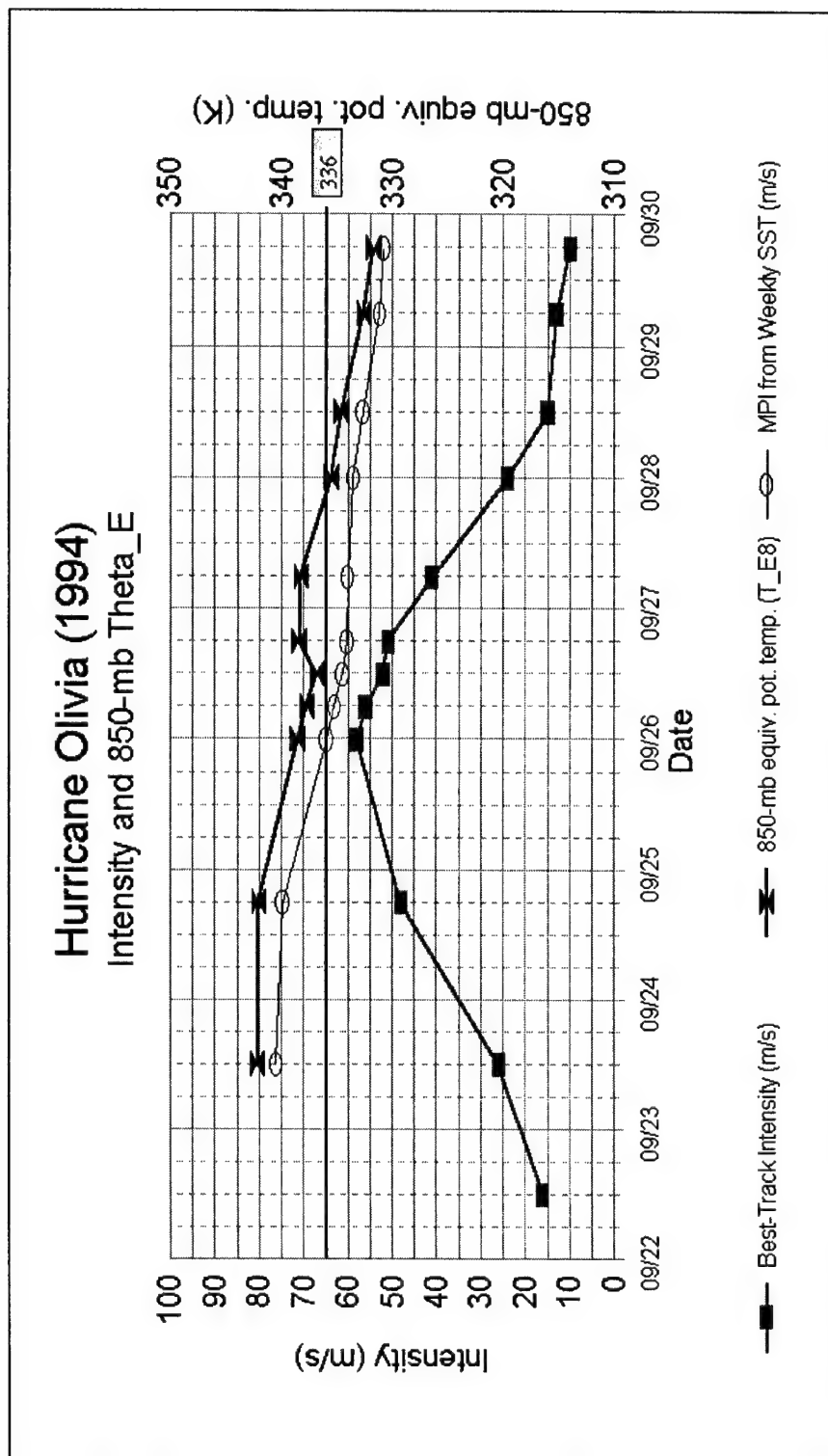


Figure 38: Temporal variation of current intensity and 850-mb equivalent potential temperature (θ_e) for Hurricane Olivia (1994). MPI is included for comparison to current intensity. A reference line at 336 K is provided as a threshold between high and low values of 850-mb θ_e .

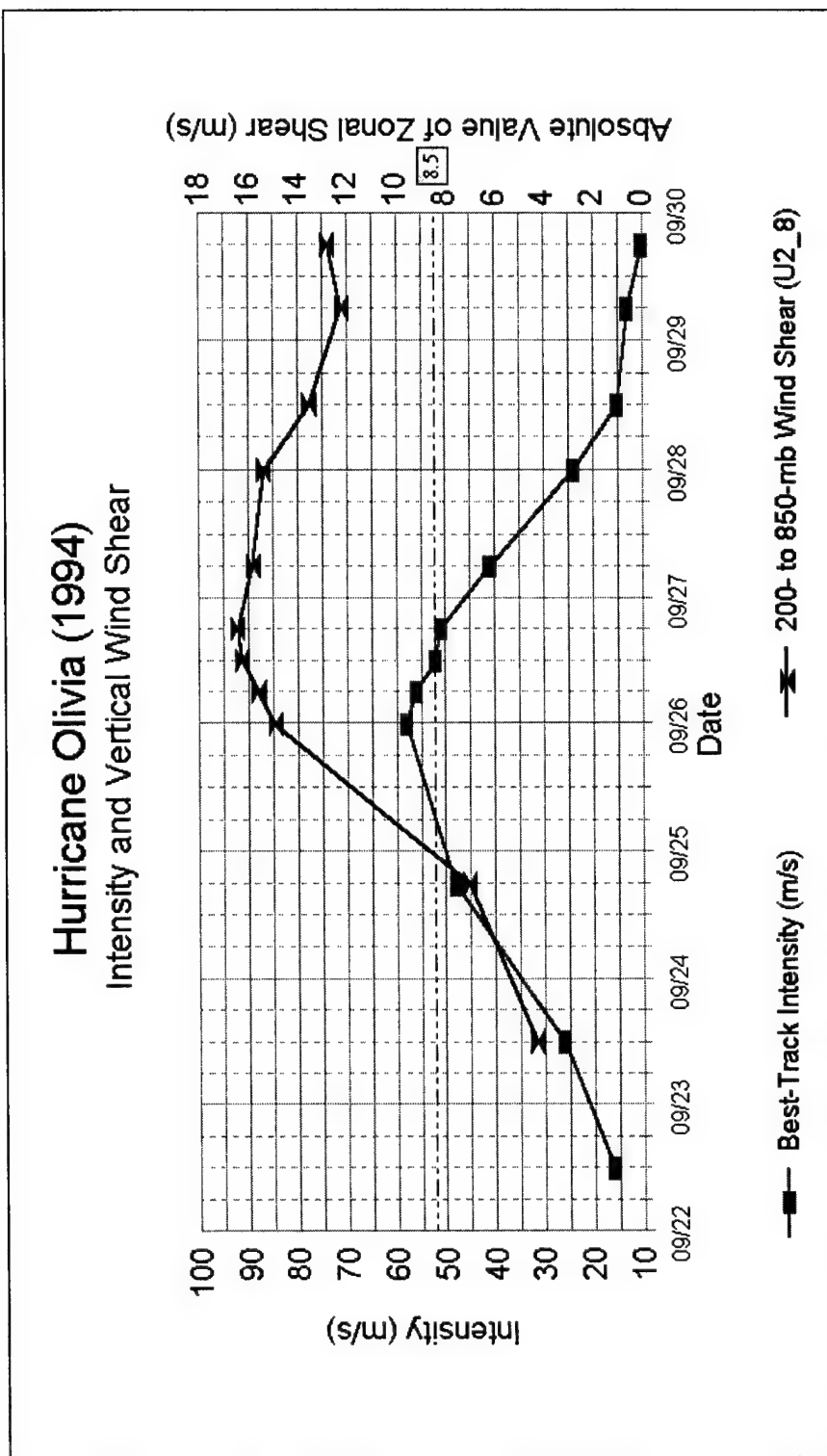


Figure 39: Temporal variation of current intensity and absolute value of 200- to 850-mb vertical shear of the zonal horizontal wind (U2_8) for Hurricane Olivia (1994). A reference line at 8.5 m s⁻¹ is provided as a threshold between high and low values of vertical shear.

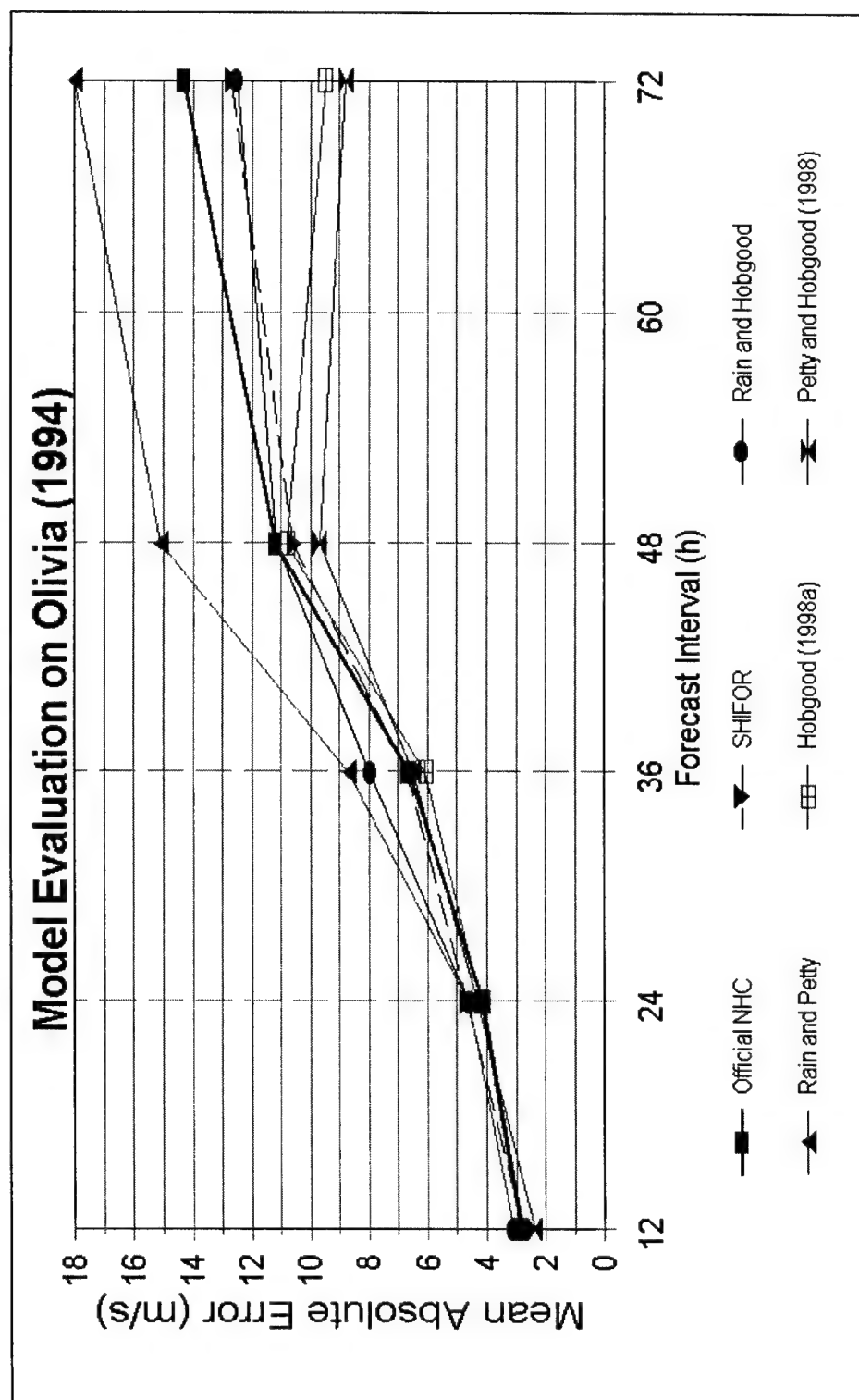


Figure 40: Homogeneous evaluation of forecast methods on Hurricane Olivia (1994).

Genevieve (1996) Track

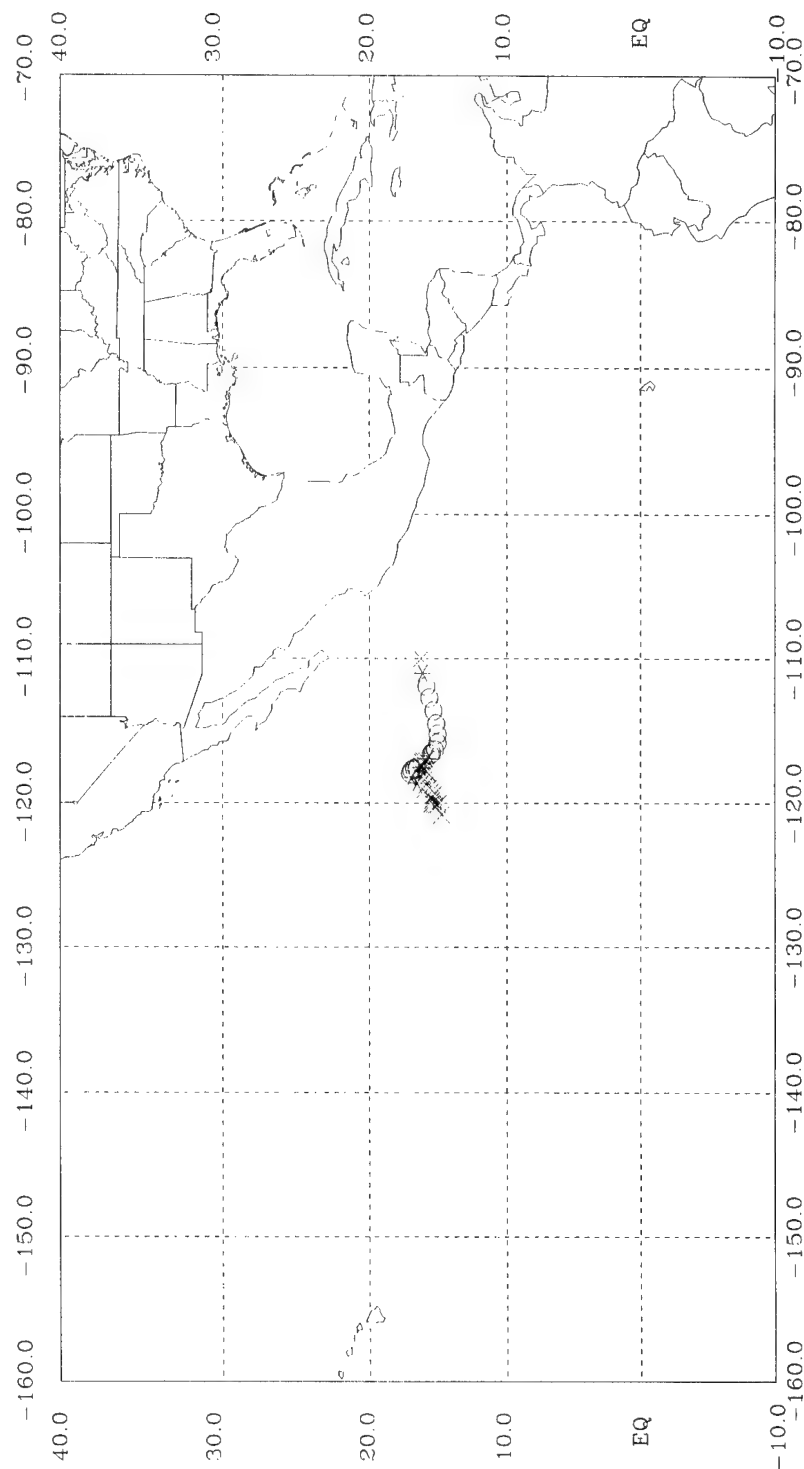


Figure 41: Plotted track of Tropical Storm Genevieve (1996). Tropical depression, tropical storm, and hurricane intensity stages are indicated by x, o, and *, respectively.

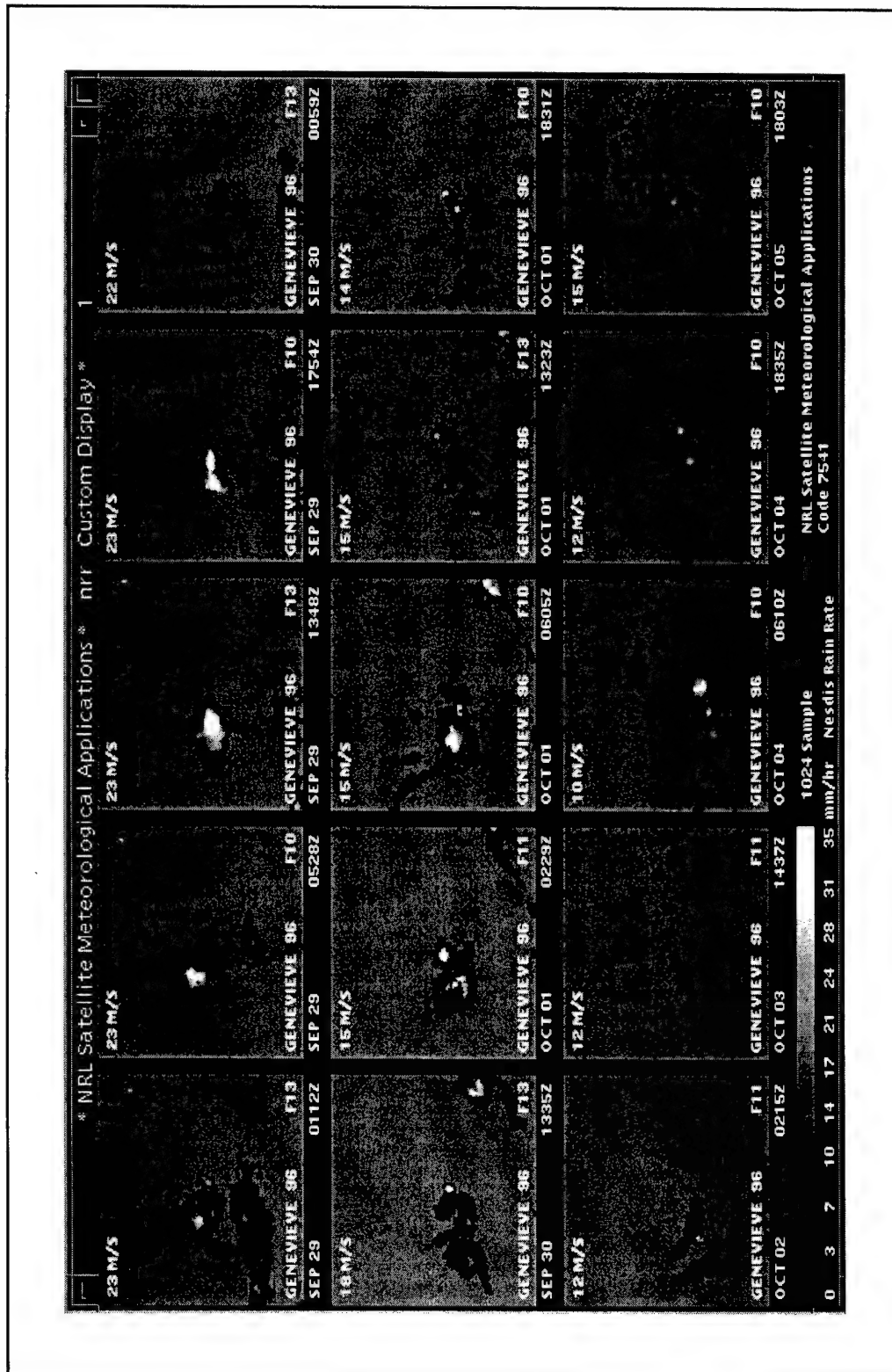


Figure 42: 15-panel TROPX display showing NESDIS/ORA rainfall algorithm applied to SSM/I observations of Tropical Storm Genevieve (1996) during 29 September-5 October. Current interpolated intensity is indicated in the upper-left of each panel. Satellite flight number is depicted in the lower-right of each panel.

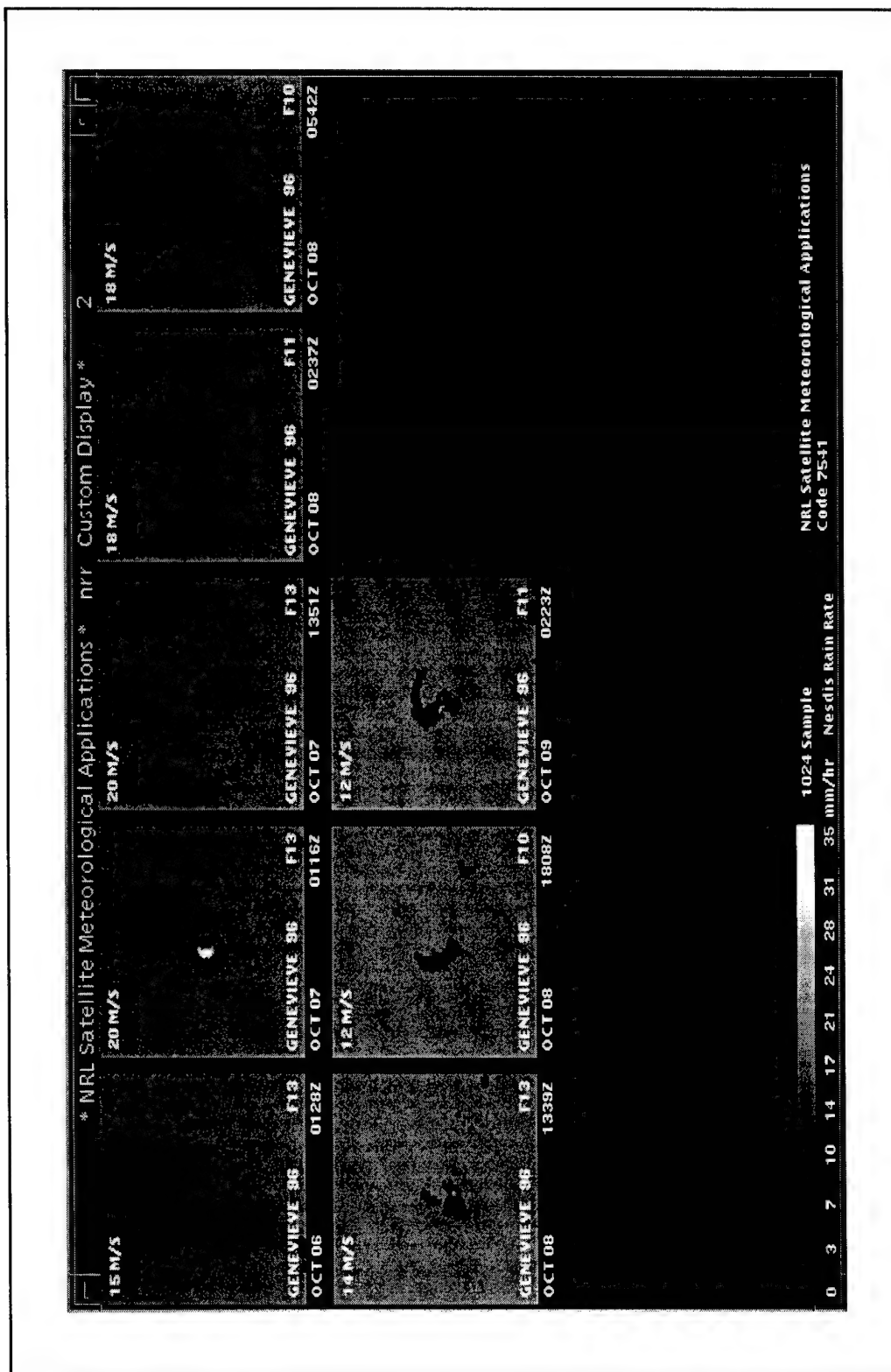


Figure 43: 15-panel TROPX display showing NESDIS/ORA rainfall algorithm applied to SSM/I observations of Tropical Storm Genevieve (1996) during 6-9 October. Current interpolated intensity is indicated in the upper-left of each panel. Satellite flight number is depicted in the lower-right of each panel.

Tropical Storm Genevieve (1996) Intensity and Convective Rainfall

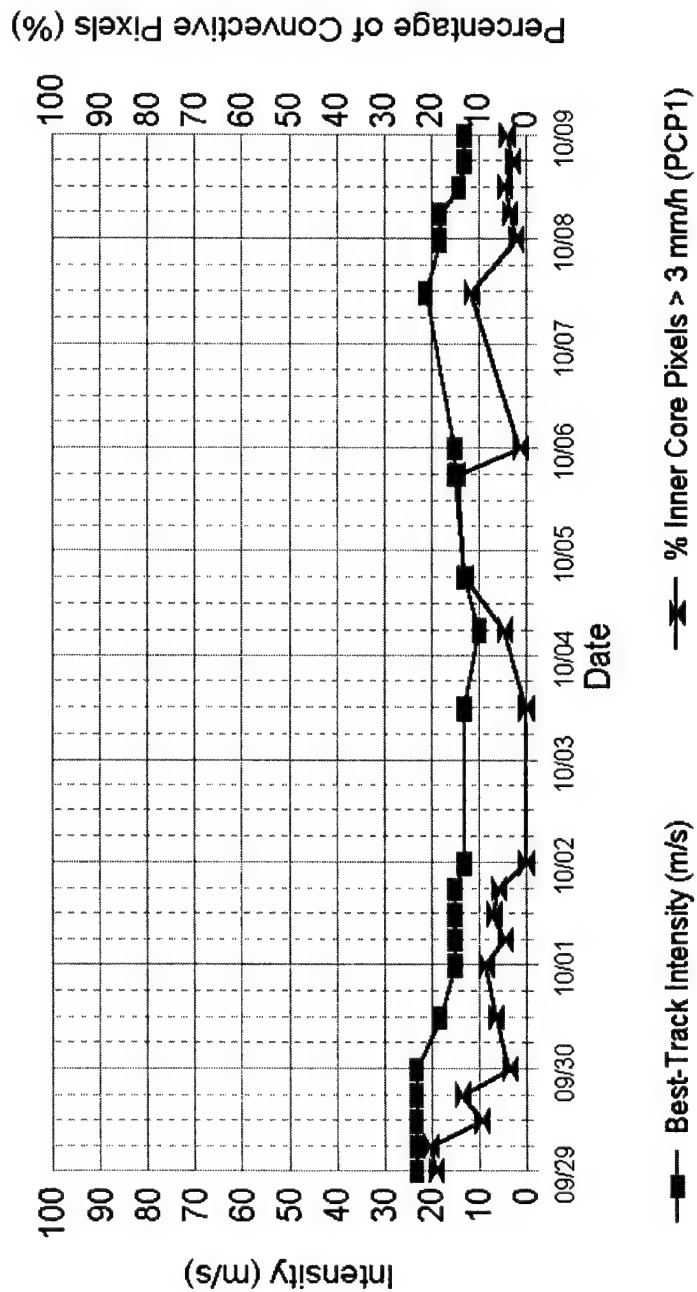


Figure 44: Temporal variation of current intensity and convective rainfall (PCP1) for SSM/I observations of Tropical Storm Genevieve (1996).

Tropical Storm Genevieve (1996) Intensity and 850-mb Theta_E

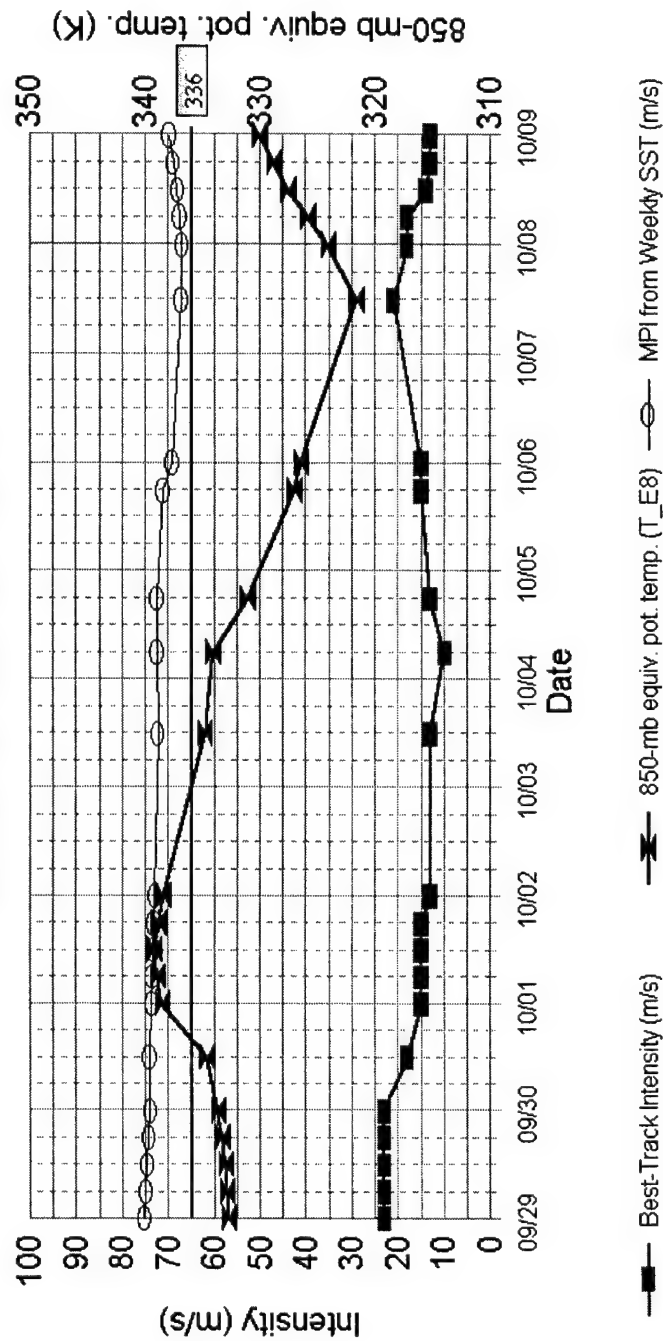


Figure 45: Temporal variation of current intensity and 850-mb equivalent potential temperature (θ_e) for Tropical Storm Genevieve (1996). MPI is included for comparison to current intensity. A reference line at 336 K is provided as a threshold between high and low values of 850-mb θ_e .

Tropical Storm Genevieve (1996) Intensity and Vertical Wind Shear

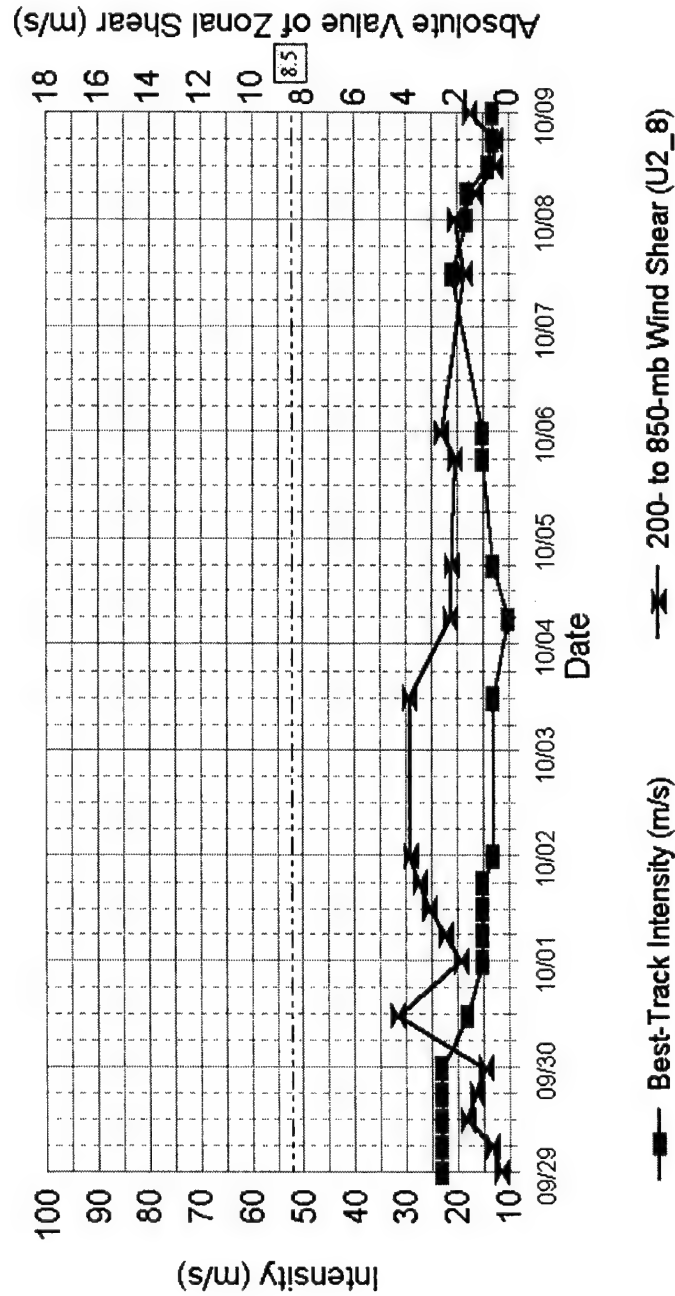


Figure 46: Temporal variation of current intensity and absolute value of 200- to 850-mb vertical shear of the zonal horizontal wind (U2_8) for Tropical Storm Genevieve (1996). A reference line at 8.5 m s⁻¹ is provided as a threshold between high and low values of vertical shear.

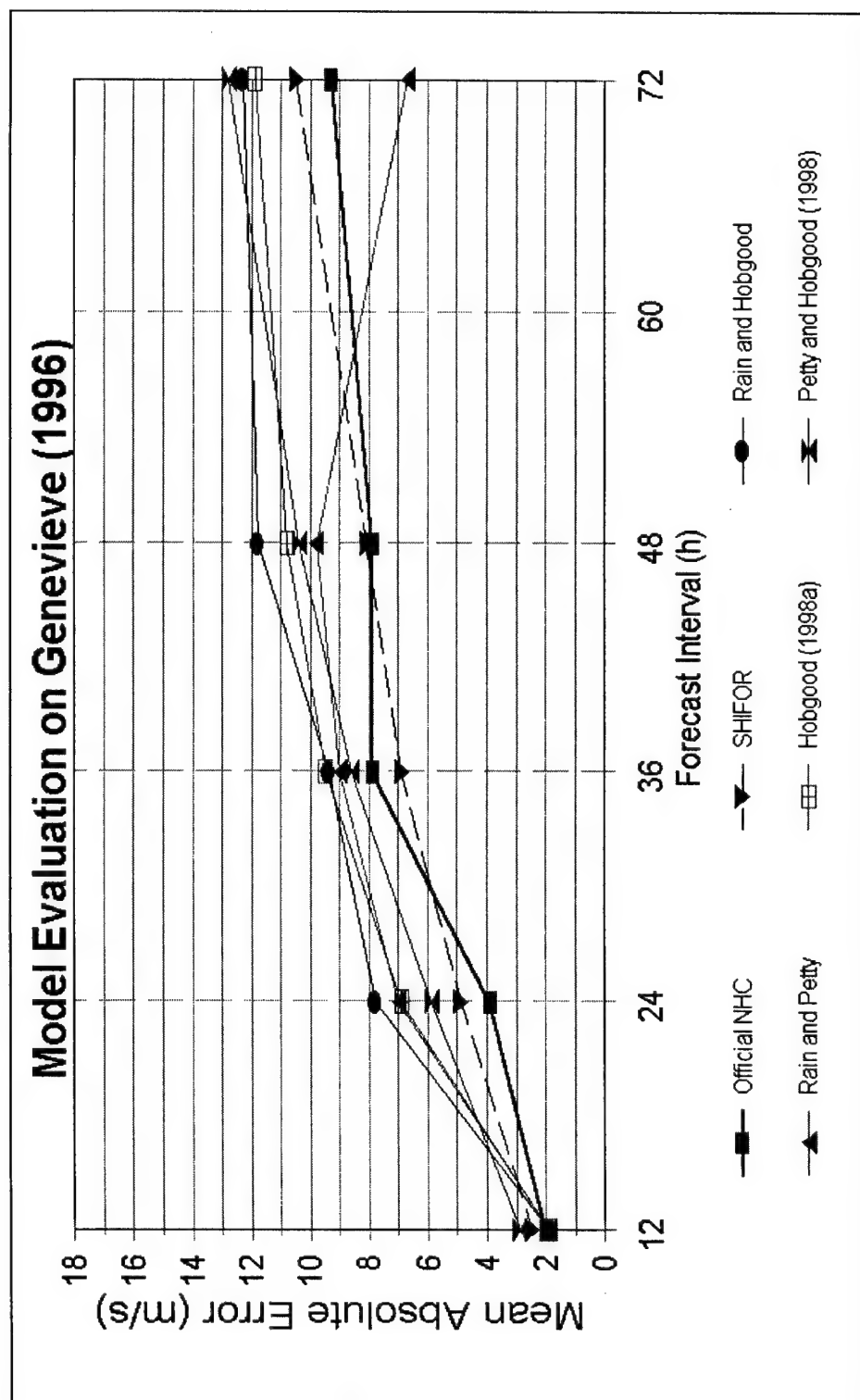


Figure 47: Homogeneous evaluation of forecast methods on Tropical Storm Genevieve (1996).

Linda (1997) Track

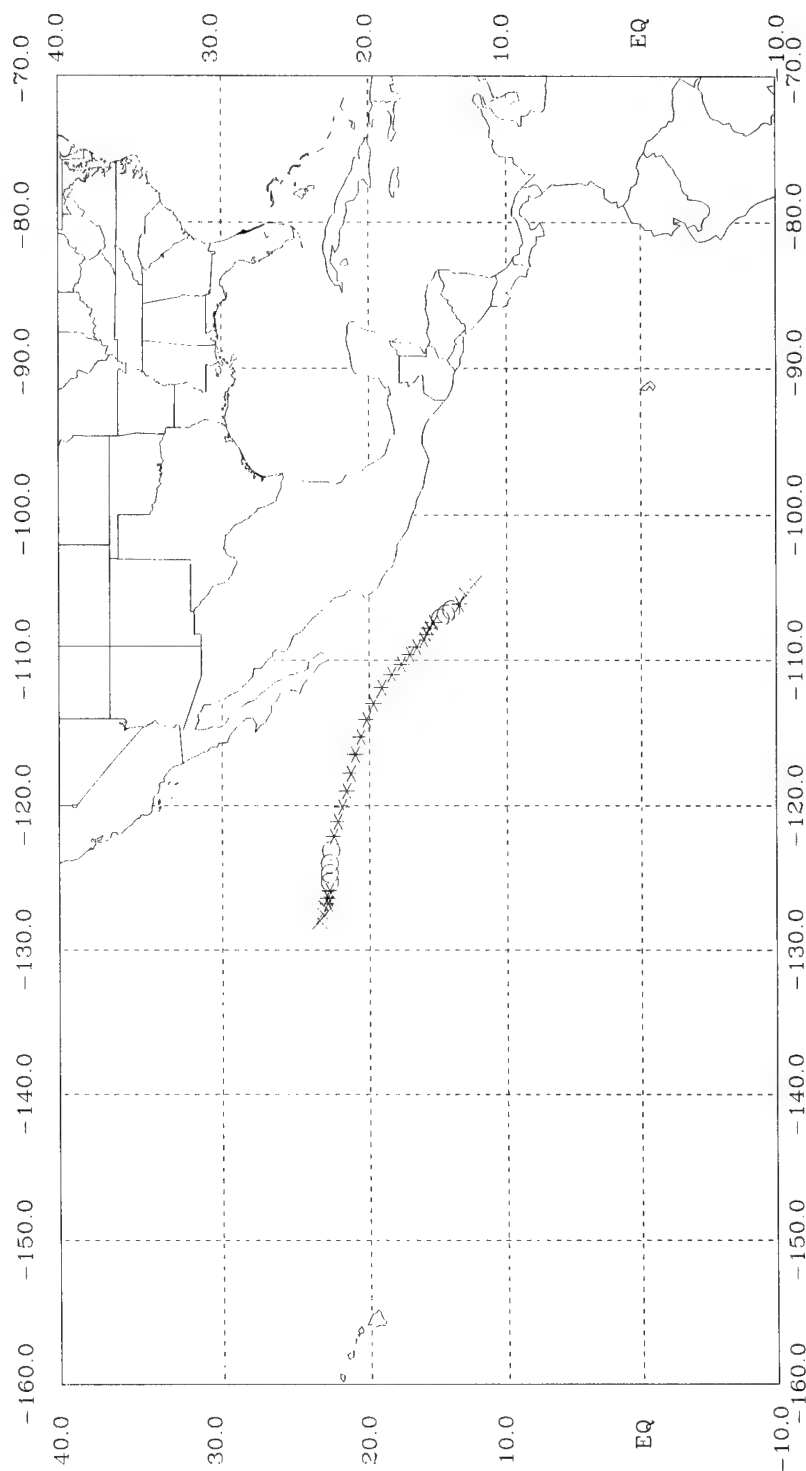


Figure 48: Plotted track of Hurricane Linda (1997). Tropical depression, tropical storm, and hurricane intensity stages are indicated by x, O, and *, respectively.

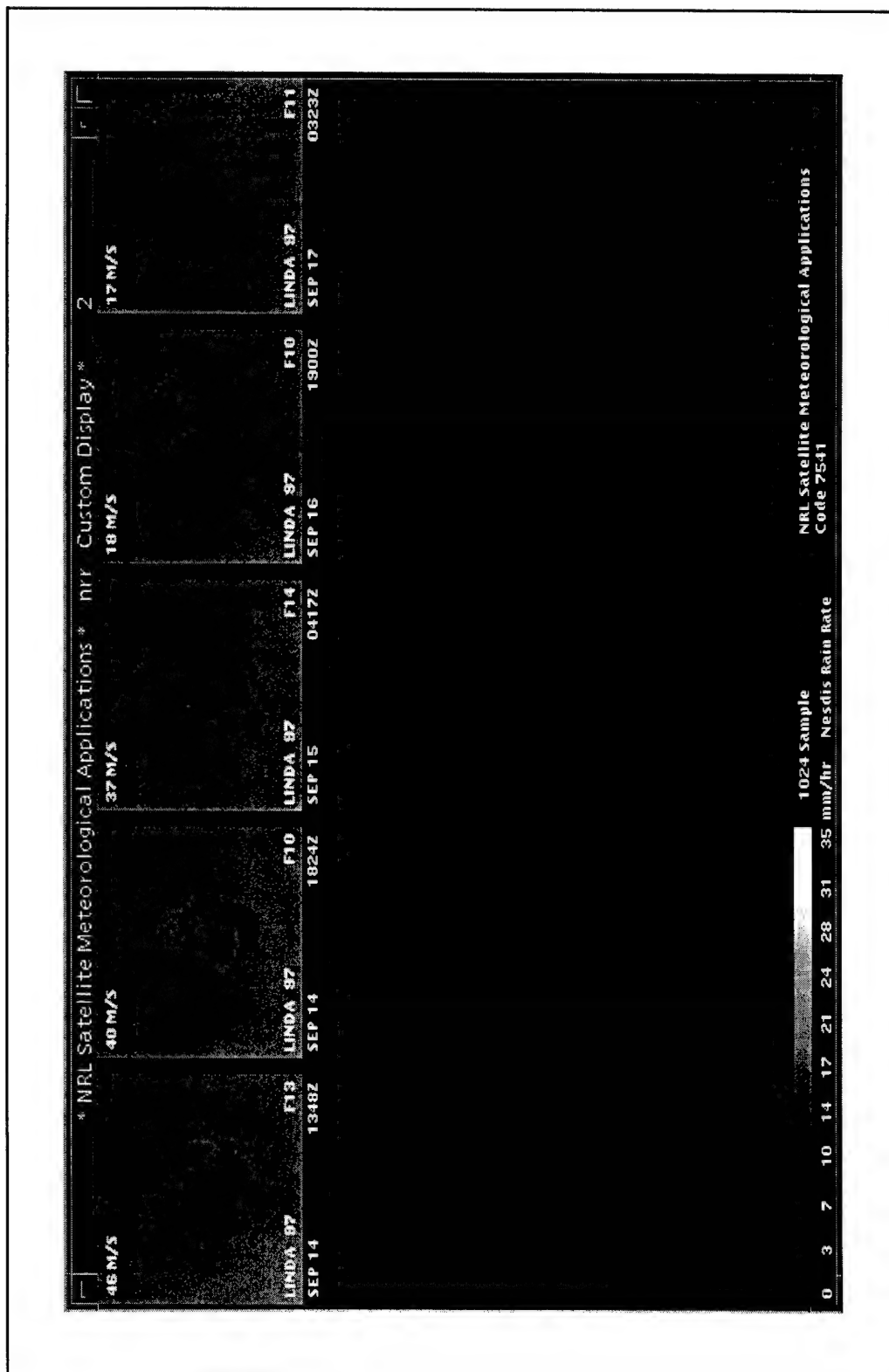


Figure 50: 15-panel TROPX display showing NESDIS/ORA rainfall algorithm applied to SSM/I observations of Hurricane Linda (1997) during 14-17 September. Current interpolated intensity is indicated in the upper-left of each panel. Satellite flight number is depicted in the lower-right of each panel.

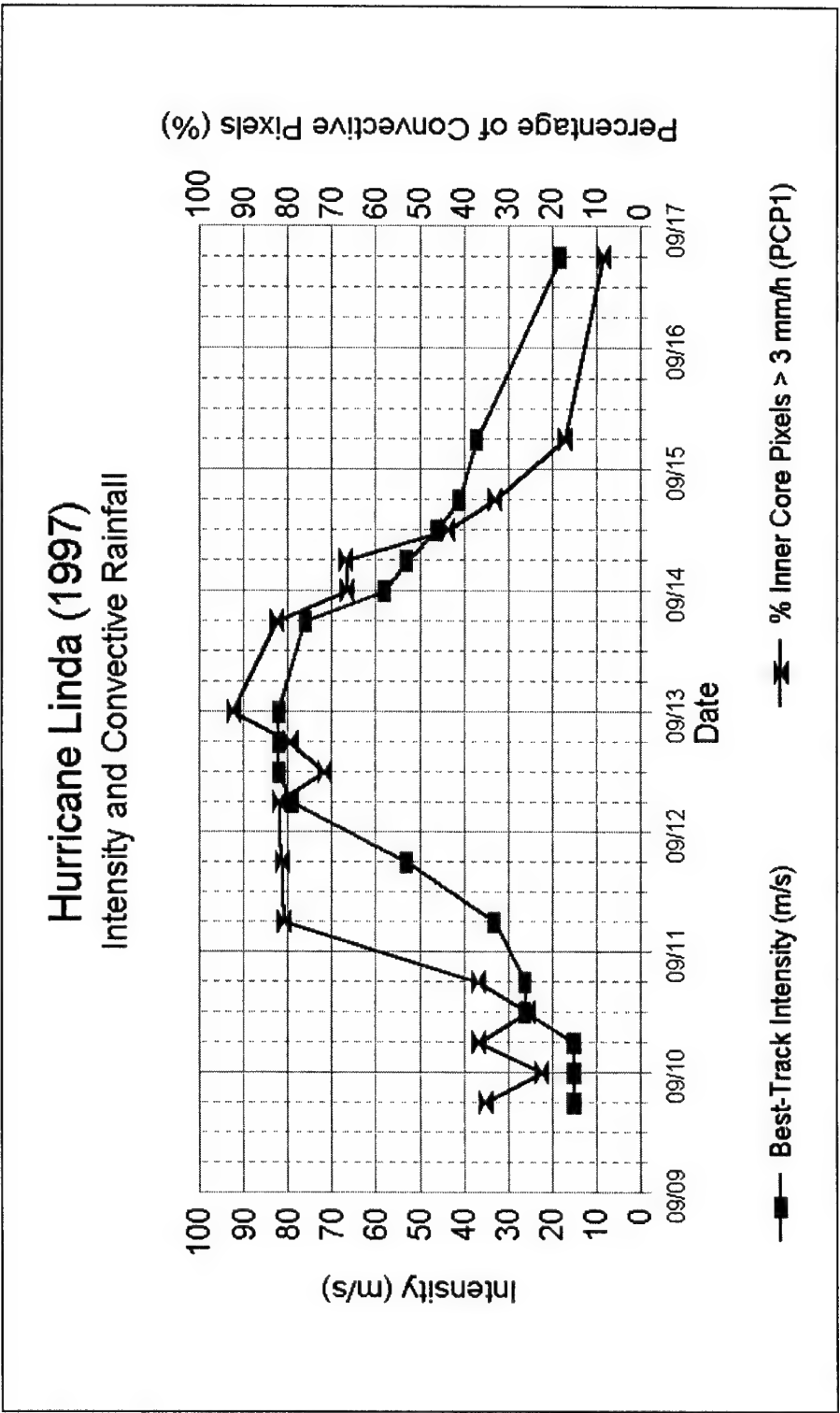


Figure 51: Temporal variation of current intensity and convective rainfall (PCP1) for SSM/I observations of Hurricane Linda (1997).

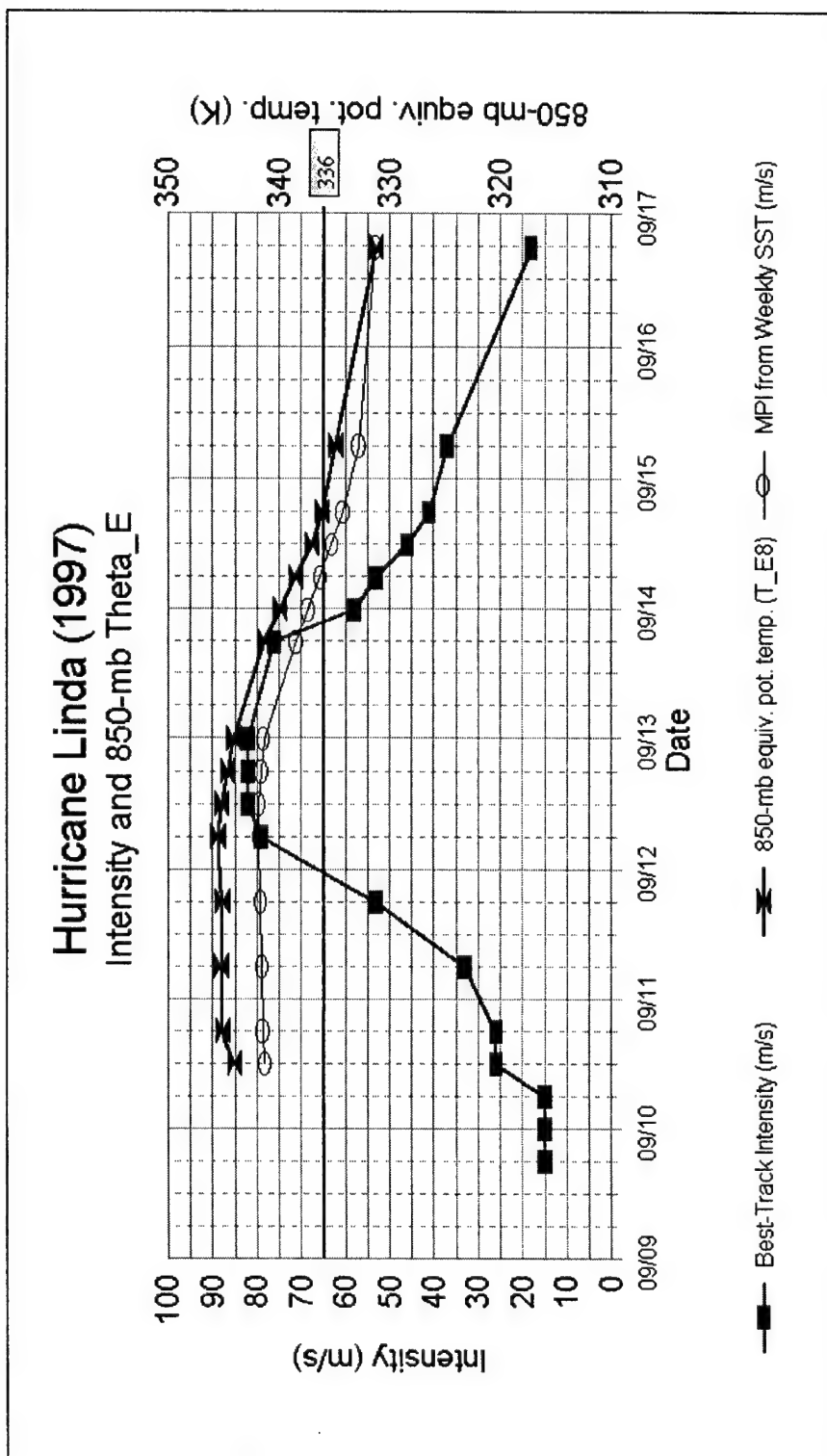


Figure 52: Temporal variation of current intensity and 850-mb equivalent potential temperature (θ_e) for Hurricane Linda (1997). MPI is included for comparison to current intensity. A reference line at 336 K is provided as a threshold between high and low values of 850-mb θ_e .

Hurricane Linda (1997)

Intensity and Vertical Wind Shear

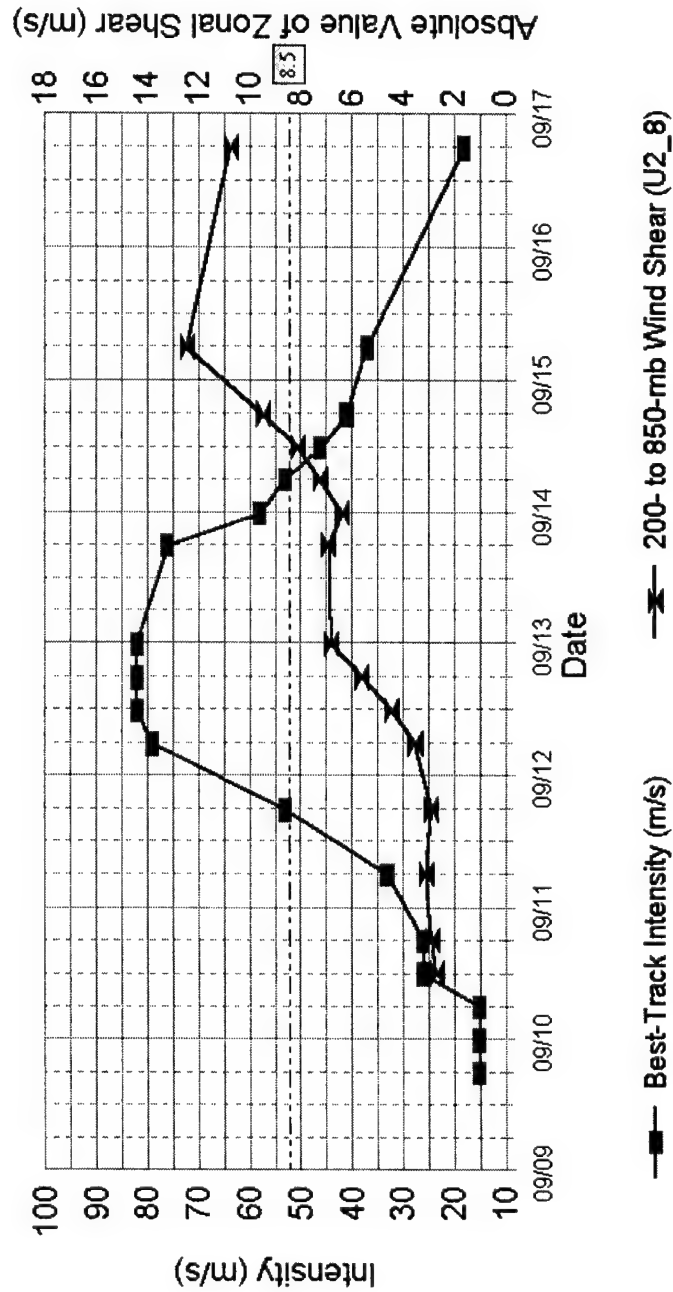


Figure 53: Temporal variation of current intensity and absolute value of 200- to 850-mb vertical shear of the zonal horizontal wind (U2_8) for Hurricane Linda (1997). A reference line at 8.5 m s⁻¹ is provided as a threshold between high and low values of vertical shear.

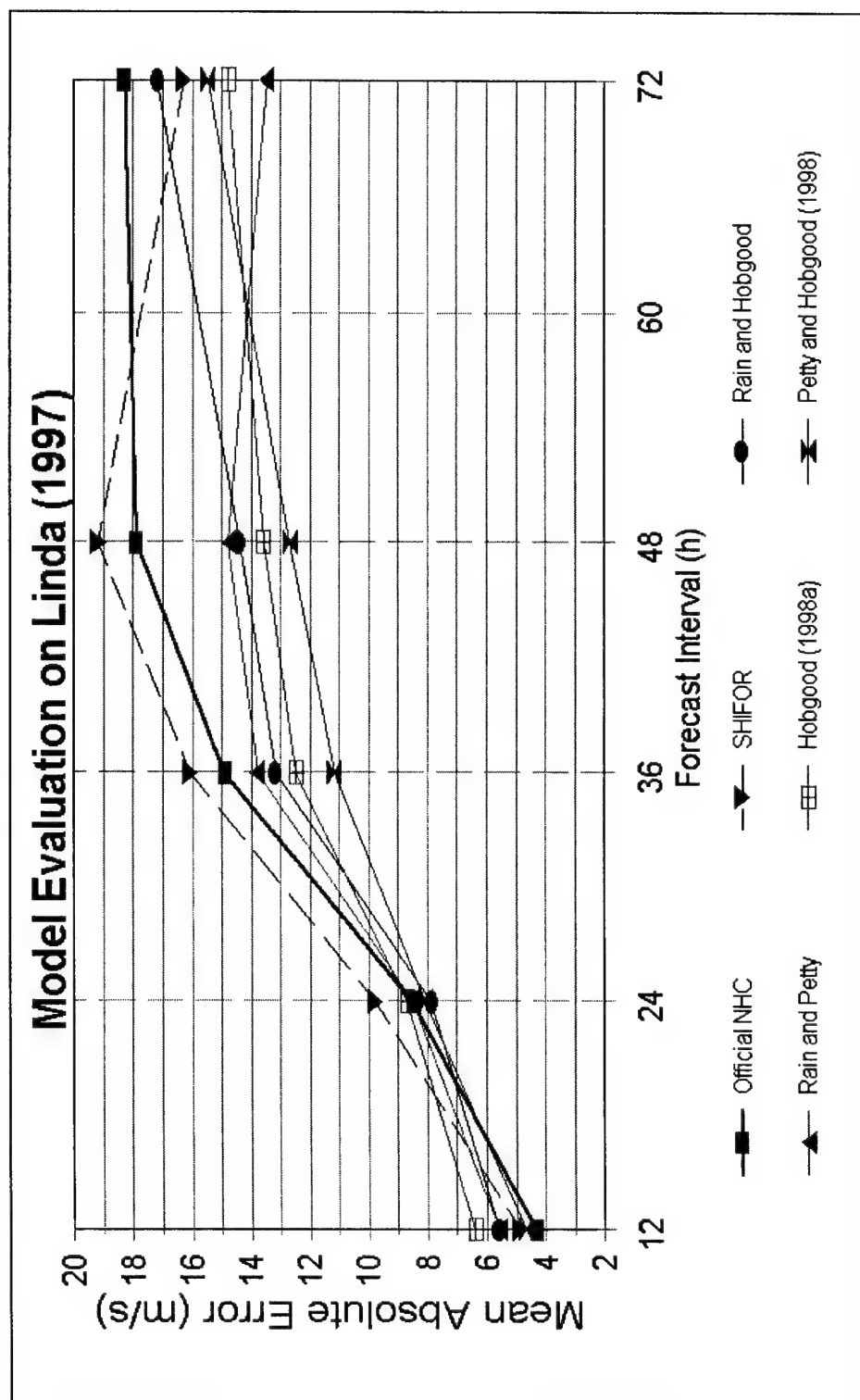


Figure 54: Homogeneous evaluation of forecast methods on Hurricane Linda (1997).

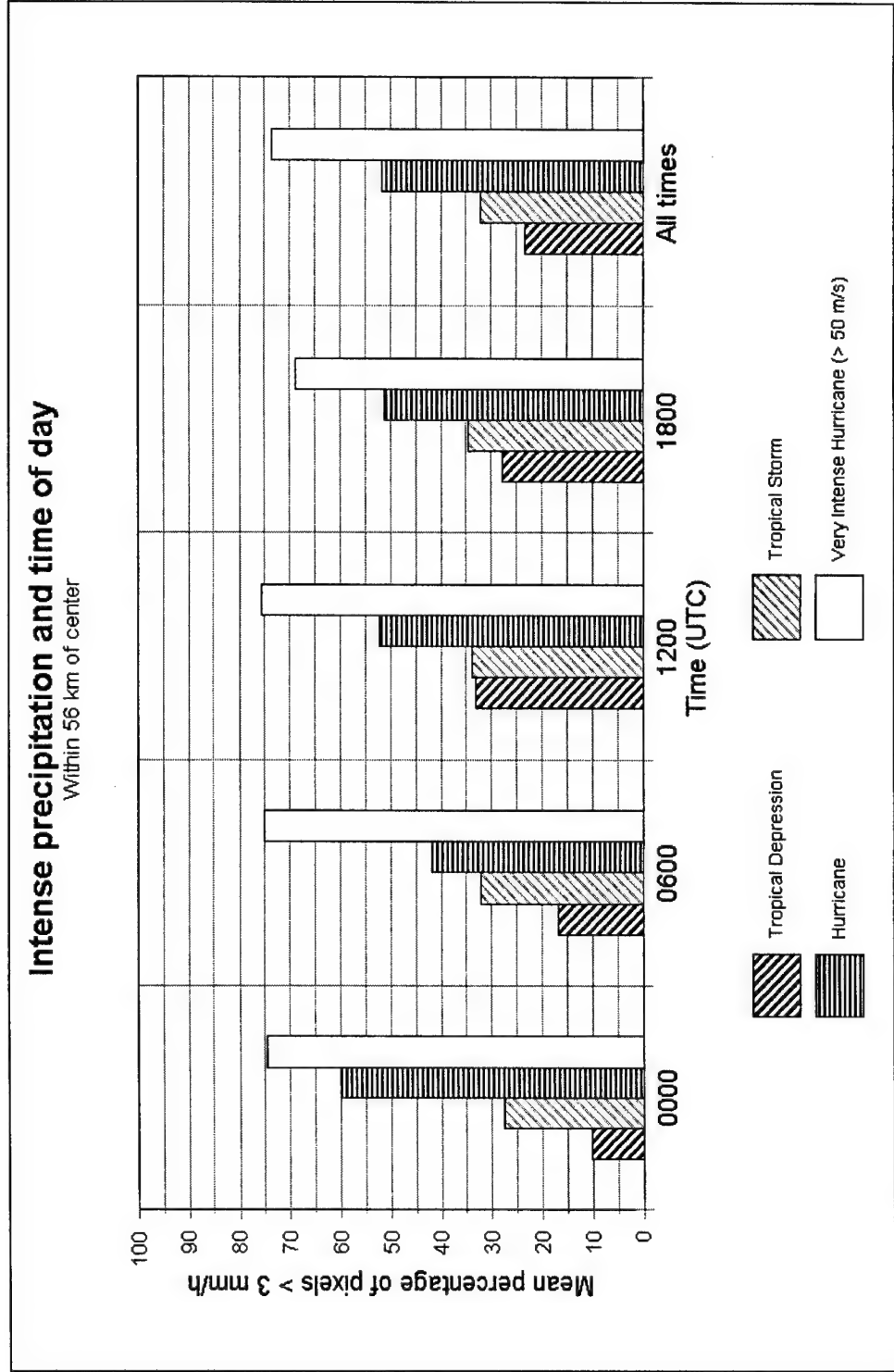


Figure 55: Central-core convective rainfall coverage stratified by time of day and tropical cyclone intensity.

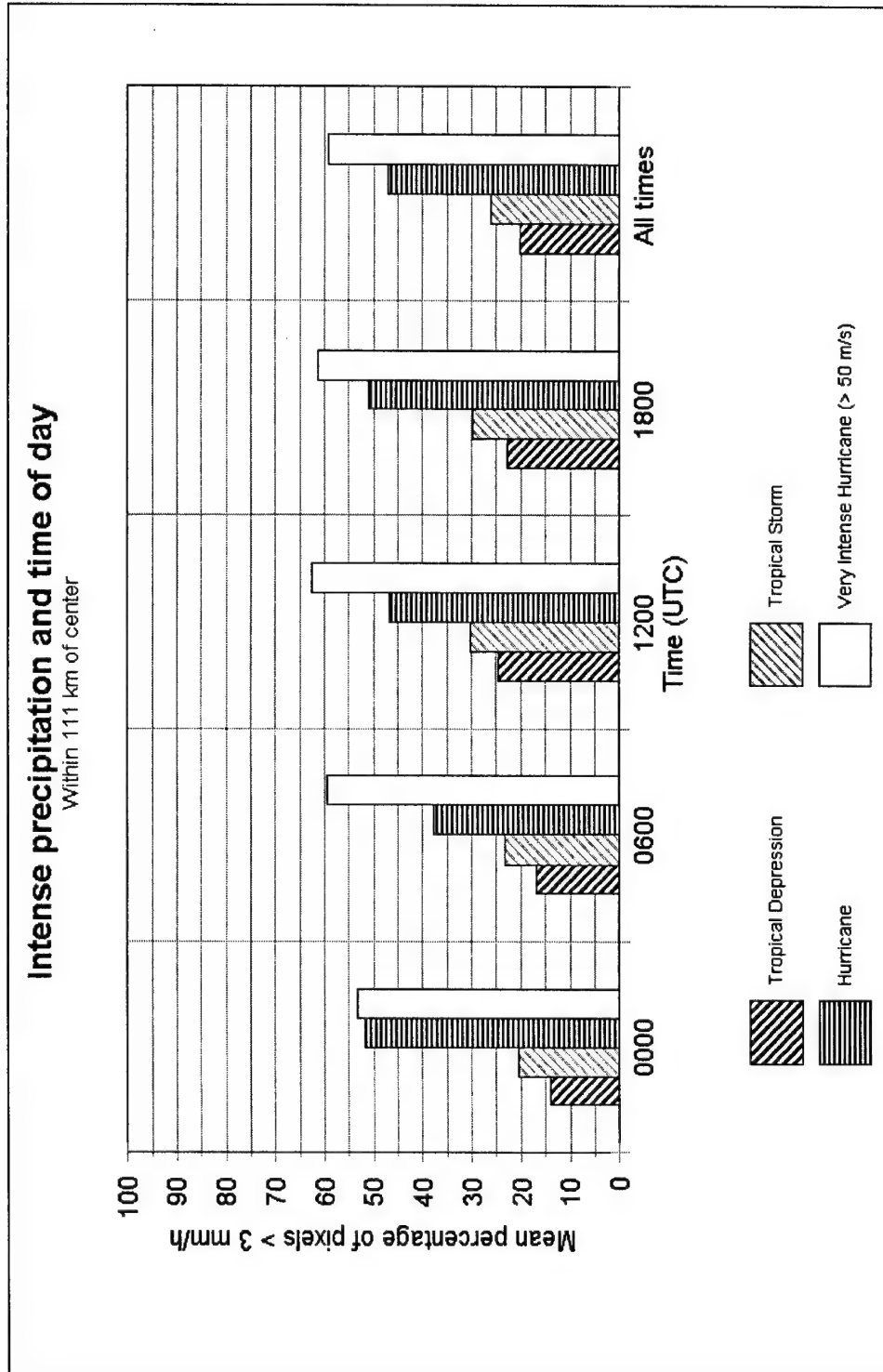


Figure 56: Inner-core convective rainfall coverage stratified by time of day and tropical cyclone intensity.

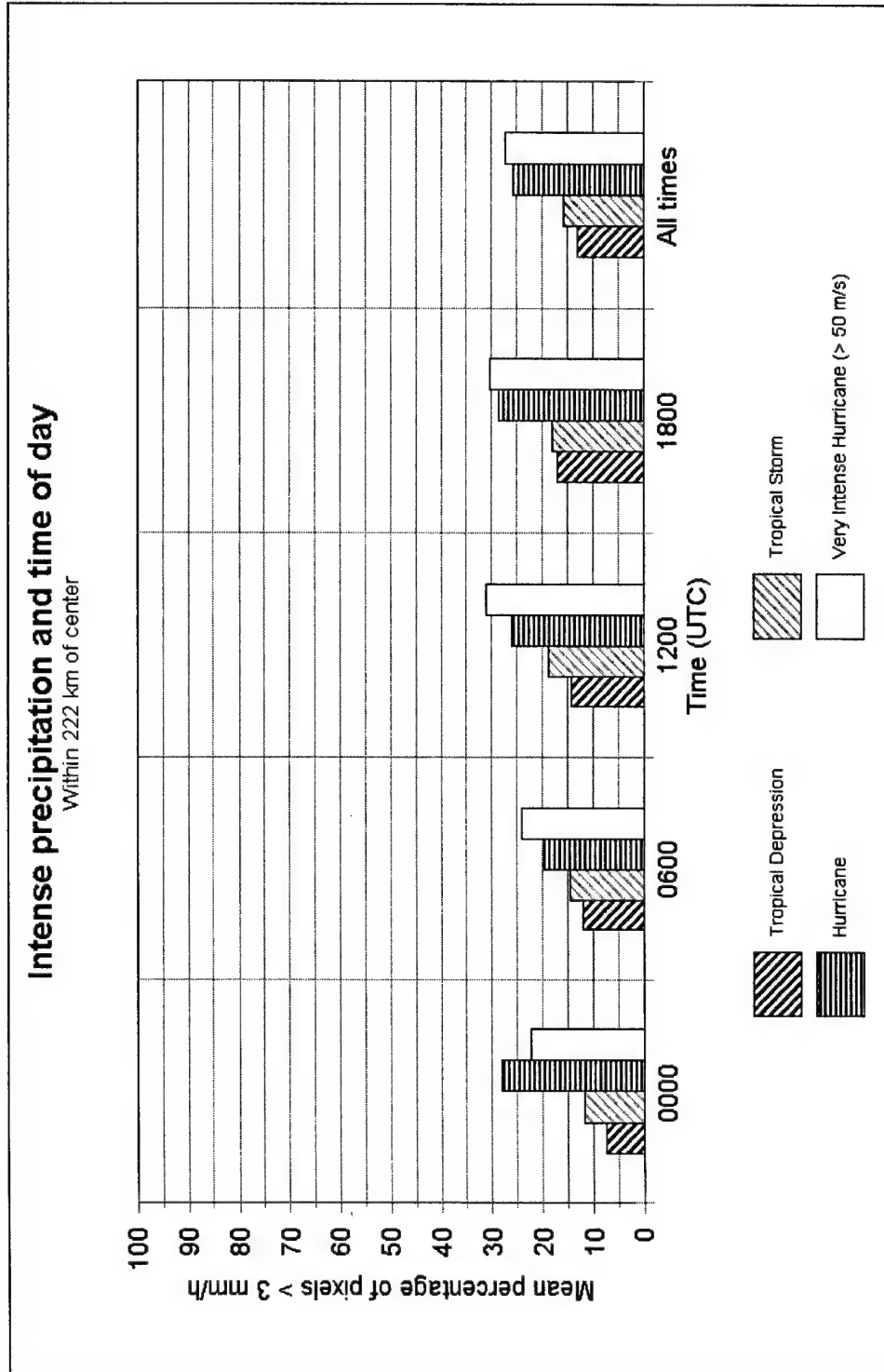


Figure 57: Core convective rainfall coverage stratified by time of day and tropical cyclone intensity.

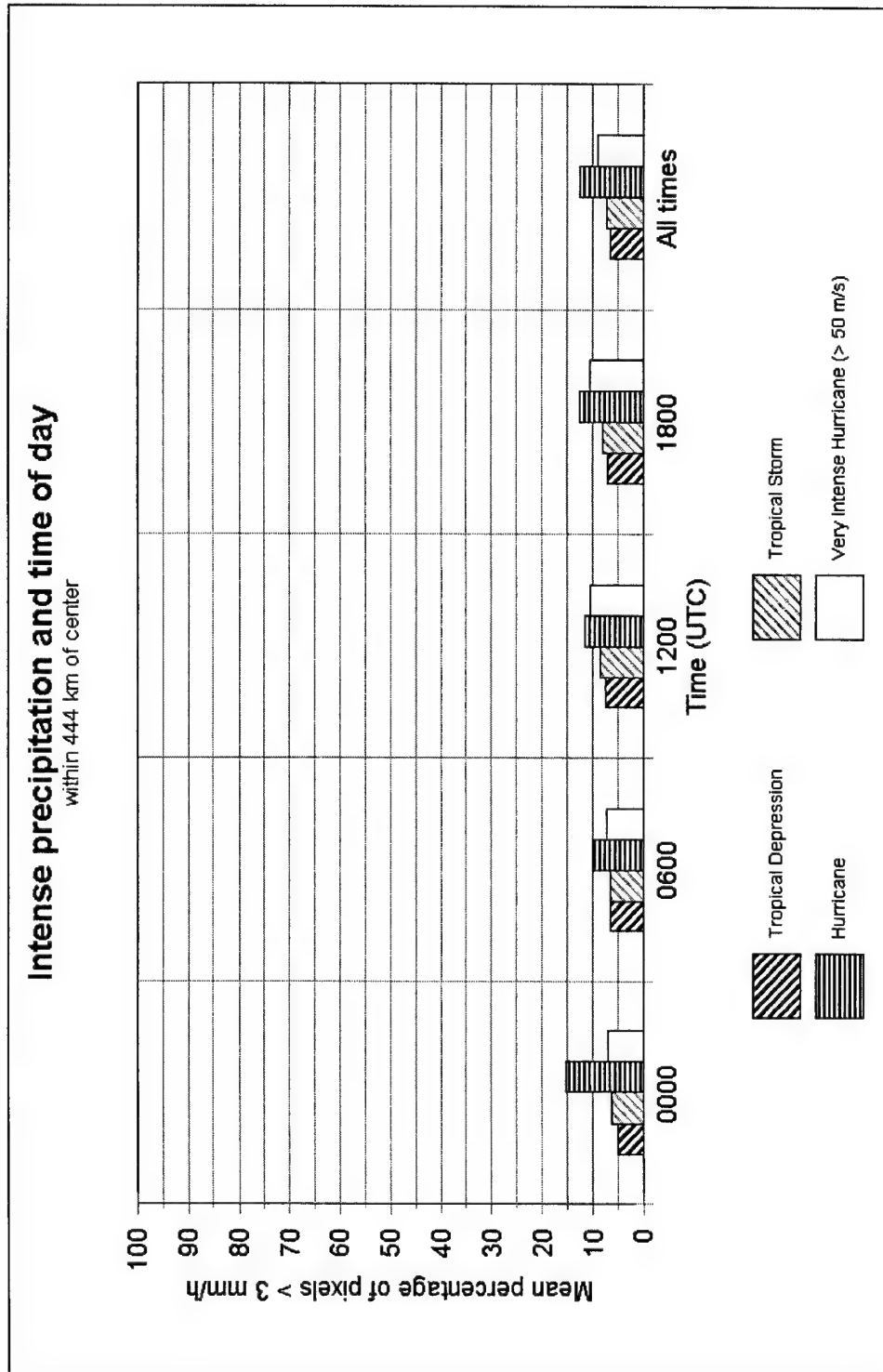


Figure 58: Total convective rainfall coverage stratified by time of day and tropical cyclone intensity.

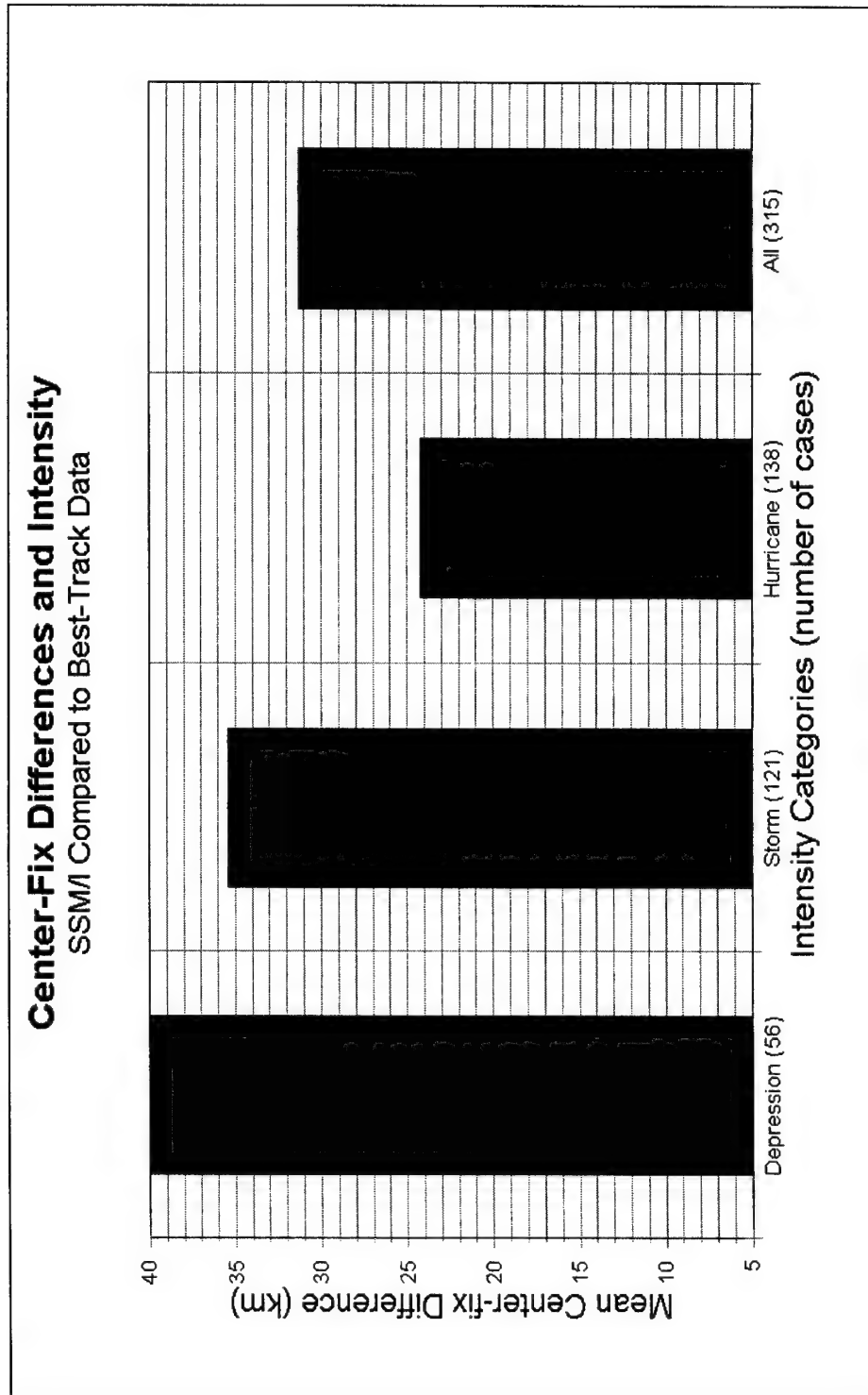


Figure 59: Mean center-fix differences when comparing SSM/I center fixes with linearly interpolated best-track data tropical cyclone locations.

APPENDIX

Example SPSS® Output

Regression

Descriptive Statistics

	Mean	Std. Deviation	N
DVMAX24	-1.68	12.43	157
DWACPH	-67.4706	343.1805	157
WACP4	62.4690	61.3055	157
PVMAX12	-2.43E-02	6.8706	157
LAT	17.8462	3.1521	157
POT	32.0627	16.1882	157

Correlations

		DVMAX24	DWACPH	WACP4	PVMAX12	LAT	POT
Pearson Correlation	DVMAX24	1.000	.391	.399	.669	-.552	.516
	DWACPH	.391	1.000	.306	.287	-.260	.267
	WACP4	.399	.306	1.000	.515	-.343	.049
	PVMAX12	.669	.287	.515	1.000	-.466	.221
	LAT	-.552	-.260	-.343	-.466	1.000	-.384
	POT	.516	.267	.049	.221	-.384	1.000
Sig. (1-tailed)	DVMAX24	.	.000	.000	.000	.000	.000
	DWACPH	.000	.	.000	.000	.000	.000
	WACP4	.000	.000	.	.000	.000	.270
	PVMAX12	.000	.000	.000	.	.000	.003
	LAT	.000	.000	.000	.000	.	.000
	POT	.000	.000	.270	.003	.000	.
N	DVMAX24	157	157	157	157	157	157
	DWACPH	157	157	157	157	157	157
	WACP4	157	157	157	157	157	157
	PVMAX12	157	157	157	157	157	157
	LAT	157	157	157	157	157	157
	POT	157	157	157	157	157	157

Model Summary^{a,b}

Model	Variables		R	R Square	Adjusted R Square	Std. Error of the Estimate
	Entered	Removed				
1	PVMAX12 ^c	.	.669	.448	.445	9.26
2	POT ^d	.	.769	.591	.585	8.00
3	LAT ^e	.	.784	.615	.608	7.78
4	DWACPH ^f	.	.793	.629	.619	7.67
5	DWACPH ^{f,g}	.	.793	.629	.619	7.67

a. Dependent Variable: DVMAX24

b. Method: Stepwise (Criteria: Probability-of-F-to-enter <= .050, Probability-of-F-to-remove >= .100).

c. Independent Variables: (Constant), PVMAX12

d. Independent Variables: (Constant), PVMAX12, POT

e. Independent Variables: (Constant), PVMAX12, POT, LAT

f. Independent Variables: (Constant), PVMAX12, POT, LAT, DWACPH

g. Probability of F-to-enter = .050 limits reached.

ANOVA^a

Model		Sum of Squares	df	Mean Square	F	Sig.
1	Regression	10795.480	1	10795.480	125.905	.000 ^b
	Residual	13290.166	155	85.743		
	Total	24085.646	156			
2	Regression	14225.409	2	7112.705	111.088	.000 ^c
	Residual	9860.237	154	64.028		
	Total	24085.646	156			
3	Regression	14819.211	3	4939.737	81.561	.000 ^d
	Residual	9266.435	153	60.565		
	Total	24085.646	156			
4	Regression	15142.064	4	3785.516	64.336	.000 ^e
	Residual	8943.582	152	58.839		
	Total	24085.646	156			
5	Regression	15142.064	4	3785.516	64.336	.000 ^e
	Residual	8943.582	152	58.839		
	Total	24085.646	156			

a. Dependent Variable: DVMAX24

b. Independent Variables: (Constant), PVMAX12

c. Independent Variables: (Constant), PVMAX12, POT

d. Independent Variables: (Constant), PVMAX12, POT, LAT

e. Independent Variables: (Constant), PVMAX12, POT, LAT, DWACPH

Coefficients^a

Model		Unstandardized Coefficients		Standardized Coefficients	t	Sig.	Collinearity Statistics
		B	Std. Error	Beta			Tolerance
1	(Constant)	-1.653	.739		-2.236	.027	
	PVMAX12	1.211	.108	.669	11.221	.000	1.000
2	(Constant)	-11.178	1.450		-7.711	.000	
	PVMAX12	1.056	.096	.584	11.049	.000	.951
	POT	.297	.041	.387	7.319	.000	.951
3	(Constant)	3.386	4.860		.697	.487	
	PVMAX12	.920	.103	.509	8.971	.000	.781
	POT	.254	.042	.331	6.094	.000	.850
	LAT	-.740	.236	-.188	-3.131	.002	.700
4	(Constant)	3.425	4.791		.715	.476	
	PVMAX12	.875	.103	.484	8.500	.000	.754
	POT	.237	.042	.308	5.657	.000	.822
	LAT	-.693	.234	-.176	-2.966	.004	.695
	DWACPH	4.500E-03	.002	.124	2.342	.020	.868
5	(Constant)	3.425	4.791		.715	.476	
	PVMAX12	.875	.103	.484	8.500	.000	.754
	POT	.237	.042	.308	5.657	.000	.822
	LAT	-.693	.234	-.176	-2.966	.004	.695
	DWACPH	4.500E-03	.002	.124	2.342	.020	.868

Coefficients^a

Model		Collinearity Statistics
		VIF
1	(Constant)	
	PVMAX12	1.000
2	(Constant)	
	PVMAX12	1.051
	POT	1.051
3	(Constant)	
	PVMAX12	1.280
	POT	1.176
	LAT	1.428
4	(Constant)	
	PVMAX12	1.327
	POT	1.216
	LAT	1.439
	DWACPH	1.152
5	(Constant)	
	PVMAX12	1.327
	POT	1.216
	LAT	1.439
	DWACPH	1.152

a. Dependent Variable: DVMAX24

Excluded Variables^a

Model		Beta In	t	Sig.	Partial Correlation	Collinearity Statistics	
						Tolerance	VIF
1	DWACPH	.217 ^b	3.617	.000	.280	.918	1.090
	WACP4	.073 ^b	1.050	.295	.084	.734	1.362
	LAT	-.307 ^b	-4.872	.000	-.365	.783	1.277
	POT	.387 ^b	7.319	.000	.508	.951	1.051
2	DWACPH	.138 ^c	2.540	.012	.201	.874	1.144
	WACP4	.108 ^c	1.798	.074	.144	.730	1.370
	LAT	-.188 ^c	-3.131	.002	-.245	.700	1.428
3	DWACPH	.124 ^d	2.342	.020	.187	.868	1.152
	WACP4	.079 ^d	1.322	.188	.107	.709	1.411
4	WACP4	.053 ^e	.876	.383	.071	.679	1.473
5	WACP4	.053 ^e	.876	.383	.071	.679	1.473

Excluded Variables^a

Model		Collinearity Statistics
		Minimum Tolerance
1	DWACPH	.918
	WACP4	.734
	LAT	.783
	POT	.951
2	DWACPH	.874
	WACP4	.696
	LAT	.700
3	DWACPH	.695
	WACP4	.633
4	WACP4	.629
5	WACP4	.629 ^f

a. Dependent Variable: DVMAX24

b. Independent Variables in the Model: (Constant), PVMAX12

c. Independent Variables in the Model: (Constant), PVMAX12, POT

d. Independent Variables in the Model: (Constant), PVMAX12, POT, LAT

e. Independent Variables in the Model: (Constant), PVMAX12, POT, LAT, DWACPH

f. This variable is not added to the model because PIN = .050 limits reached.

Collinearity Diagnostics^a

Model	Dimension	Eigenvalue	Condition Index	Variance Proportions		
				(Constant)	PVMAX12	POT
1	1	1.004	1.000	.50	.50	
	2	.996	1.004	.50	.50	
2	1	1.898	1.000	.05	.00	.05
	2	1.001	1.377	.00	.94	.00
	3	.101	4.330	.95	.06	.95
3	1	2.820	1.000	.00	.00	.02
	2	1.019	1.664	.00	.75	.00
	3	.152	4.307	.01	.10	.75
	4	9.265E-03	17.445	.99	.15	.23
4	1	2.863	1.000	.00	.00	.02
	2	1.287	1.492	.00	.31	.00
	3	.699	2.024	.00	.50	.00
	4	.142	4.493	.01	.05	.76
	5	9.257E-03	17.587	.99	.14	.22
5	1	2.863	1.000	.00	.00	.02
	2	1.287	1.492	.00	.31	.00
	3	.699	2.024	.00	.50	.00
	4	.142	4.493	.01	.05	.76
	5	9.257E-03	17.587	.99	.14	.22

Collinearity Diagnostics^a

Model	Dimension	Variance Proportions	
		LAT	DWACPH
1	1		
	2		
2	1		
	3		
3	1	.00	
	2	.00	
	3	.03	
	4	.97	
4	1	.00	.01
	2	.00	.28
	3	.00	.63
	4	.03	.08
	5	.96	.00
5	1	.00	.01
	2	.00	.28
	3	.00	.63
	4	.03	.08
	5	.96	.00

a. Dependent Variable: DVMAX24

Casewise Diagnostics^a

Case Number	Std. Residual	DVMAX24
238	3.279	36
239	3.277	41

a. Dependent Variable: DVMAX24

Residuals Statistics^a

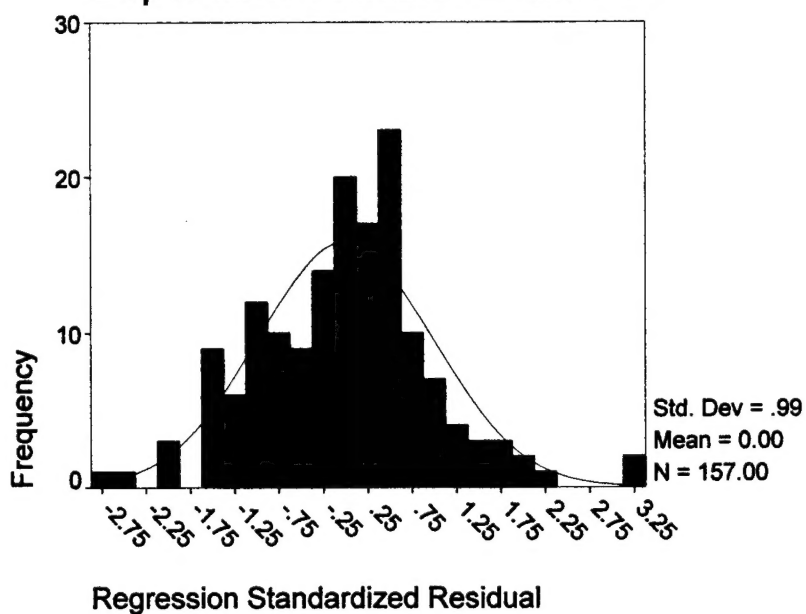
	Minimum	Maximum	Mean	Std. Deviation	N
Predicted Value	-23.62	17.89	-1.68	9.85	157
Residual	-20.78	25.15	-1.13E-16	7.57	157
Std. Predicted Value	-2.227	1.987	.000	1.000	157
Std. Residual	-2.710	3.279	.000	.987	157

a. Dependent Variable: DVMAX24

Charts

Histogram

Dependent Variable: DVMAX24



Scatterplot

Dependent Variable: DVMAX24

